

University of Southern Queensland  
Faculty of Engineering and Surveying

**Measurement of fracture toughness, mechanical and  
electrical loss tangents of calcium carbonate  
reinforced vinyl ester composites**

A dissertation Submitted by

**Mustapha Jamal Eddine**

in fulfilment of the requirements of

**Courses ENG4111 and 4112 Research Project**

towards the degree of

**Bachelor of Engineering (Mechanical)**

Submitted: October, 2009

## **Abstract**

*Vinyl ester resin was reinforced with calcium carbonate powder in an attempt to increase fracture toughness of the composites for structural applications. A considerable percentage by weight of calcium carbonate powder would be added to reduce the composite cost but at the same time the fracture toughness of it would be maintained. The composites were cast to shape and then cured in ambient conditions. After that, they were post-cured in a conventional oven. The composite specimens were then subjected to short bar tests to measure their fracture toughness. It was found that the toughest composite was made from pure resin. However, the fracture toughness had a sudden increase for the composite with 35% by weight of the filler but it was still much lower than that of pure resin. Scanning electron microscope (SEM) was also employed to analyse the failure modes of the specimens and it was found that the fractured surfaces examined correlated with the fracture toughness. As far as fracture toughness was concerned, calcium carbonate was not a suitable filler for vinyl ester resin. Moreover, dynamic mechanical analysis (DMA) and loss tangent measurements were conducted on the specimens. From these measurements, it was observed that the oven post-curing process increased the stiffness of the composites; but decreased their electrical loss tangent.*

**University of Southern Queensland**  
**Faculty of Engineering and Surveying**

<b>ENG4111 Research Project Part 1 &amp; ENG4112 Research Project Part 2</b>
--

## **Limitations of Use**

The Council of the University of Southern Queensland, its Faculty of Engineering and Surveying, and the staff of the University of Southern Queensland, does not accept any responsibility for the truth, accuracy or completeness of material contained within or associated with this dissertation.

Persons using all or any part of this material do so at their own risk, and not at the risk of the Council of the University of Southern Queensland, its Faculty of Engineering and Surveying or the staff of the University of Southern Queensland.

This dissertation reports an educational exercise and has no purpose or validity beyond this exercise. The sole purpose of the course pair entitled "Research Project" is to contribute to the overall education within the student's chosen degree program. This document, the associated hardware, software, drawings, and other material set out in the associated appendices should not be used for any other purpose: if they are so used, it is entirely at the risk of the user.



Professor Frank Bullen  
Dean  
Faculty of Engineering and Surveying

# Certification

I certify that the ideas, designs and experimental work, results, analysis and conclusions set out in this dissertation are entirely my own efforts, except where otherwise indicated and acknowledged.

I further certify that the work is original and has not been previously submitted for assessment in any other course or institution, except where specifically stated.

**Mustapha Jamal Eddine**

**Student Number: 0050060811**

A handwritten signature in red ink, appearing to read 'Mustapha', is written over a horizontal line.

Signature

29/10/2009

Date

## **Associated Publications**

Ku, H, Jamal Eddine, M and, Trada, M, Fracture Toughness of Calcium Carbonate Powder Reinforced Vinyl Ester Composites: Pilot Study, Journal of composite material, 2009, (submitted for publication).

Jamal Eddine, M, Ku, H, and Trada, M, Micrographs of the Fracture of Vinyl Ester Composites: Pilot Study, Journal of Applied Polymer Sciences, 2009, (submitted for publication).

# Acknowledgement

I would like to thank the people involved with this project or and anyone helped in guiding me throughout the issues I encountered.

First of all, I would like to thank my project supervisor Dr. Harry Ku for his guidance in this topic. Thank you for your patience and advice, it has been very effective in getting this project done correctly.

Also, I would like to thank the technician in this field, Mohan Trada. Thank you for your instruction and help during the construction and testing part of this report.

Furthermore, I would like to thank my friend Auc Fai Chan for spending his precious time in giving advice on my way in expressing ideas.

Finally I would like to thank the University of Southern Queensland for providing the equipment to fulfil the conducting of the tests.

# Table of Contents

<b>Abstract</b> .....	i
<b>Limitations of Use</b> .....	ii
<b>Certification</b> .....	iii
<b>Associated Publications</b> .....	iv
<b>Acknowledgement</b> .....	v
<b>Table of Contents</b> .....	vi
<b>Table of Figures</b> .....	xiv
<b>List of Tables</b> .....	xx
<b>Glossary of Terms</b> .....	xxiii
<b>Chapter 1 - Introduction</b> .....	1
1.1 Introduction .....	1
1.2 Project Background .....	1
1.3 Research Aims and Objectives .....	2
1.4 Justification .....	3
1.5 Scope .....	3
1.6 Concluding Remarks .....	4

<b>Chapter 2 - Literature Review</b> .....	5
2.1 Introduction to Composite Materials .....	5
2.2 Polymer Composites .....	6
2.2.1 Thermoplastic and Thermoset Polymers .....	6
2.3 Importance of Composite Materials .....	8
2.4 Materials Used .....	8
2.5 Background of Vinyl Ester .....	9
2.5.1 Chemical Structure .....	10
2.5.2 Vinyl Ester and Cross Linking .....	13
2.6 Catalysts.....	16
2.7 Fillers .....	17
2.7.1 Calcium Carbonate .....	17
2.8 Review of Previous Work.....	19
2.8.1 SLG Reinforced Phenolic Resin.....	19
2.8.2 Polystyrene Reinforced with White Cement .....	21
2.8.3 Vinyl Ester Reinforced with Rubber Modifiers.....	23
2.8.4 Liquid Rubber Modified Vinyl Ester Resins .....	24
<b>Chapter 3 – Experimental Methodology</b> .....	25
3.1 Specimen Design .....	25
3.2 Mould Design .....	25
3.3 Mould Preparation .....	27

3.4	Composite Preparation.....	29
3.5	Curing .....	33
3.6	Problems During Methodology .....	35
3.6.1	The Mould .....	35
3.6.2	Chevron Slots.....	36
<b>Chapter 4 - Consequential Effects of Project.....</b>		<b>38</b>
4.1	Sustainability .....	38
4.2	Ethical Responsibility.....	38
4.3	Risk Assessment .....	39
4.4	Risk Identification .....	39
4.4.1	Material Handling.....	40
4.5	Testing .....	42
4.6	Risk Control.....	42
<b>Chapter 5 - Fracture Mechanics .....</b>		<b>44</b>
5.1	Introduction to Fracture Mechanics.....	44
5.2	Categories of Fracture Mechanics .....	46
5.3	Fracture Toughness.....	46
5.3.1	Importance of Fracture Toughness .....	53
<b>Chapter 6 - Scanning Electron Microscope.....</b>		<b>54</b>
6.1	Background on Electron Microscopes.....	54

6.2	Basic Systems of SEM.....	55
6.2.1	The Illumination system .....	57
6.2.2	The Vacuum System.....	59
6.2.3	Sample Manipulation System .....	60
6.2.4	The Imaging System .....	60
<b>Chapter 7 - Dynamic Mechanical Analysis .....</b>		<b>61</b>
7.1	Theory of Dynamic Mechanical Analysis .....	61
7.1.1	Dynamic Oscillatory Test .....	62
7.2	Glass Transition Temperature.....	64
<b>Chapter 8 - Dielectric Properties.....</b>		<b>67</b>
8.1	Loss Tangent.....	67
8.2	Loss Tangent Measurements .....	70
8.2.1	Calculating Loss Tangent .....	71
8.2.2	Measuring Loss Tangent.....	73
<b>Chapter 9 – Fracture Toughness Tests and Measurements .....</b>		<b>74</b>
9.1	Fracture Toughness Tests .....	74
9.2	Standard Fracture Toughness Tests .....	74
9.2.1	Plane-Strain Fracture Toughness Test (ASTM E: 399).....	75
9.2.2	Other Fracture Toughness Tests .....	77
9.3	Non-Standard Fracture Toughness Tests.....	79

9.3.1 Charpy V-Notch Impact Test.....	79
9.3.2 Short Rod and Short Bar Test.....	81
9.4 Detailed Information on Short Rod and Short Bar Test .....	83
9.4.1 Introduction.....	83
9.4.2 Development of Short Bar Geometry .....	83
9.4.3 Thickness and Sharpness of the Chevron Slot.....	88
9.4.4 Short Bar Method Test and Sample Size.....	90
<b>Chapter 10 – Fracture Toughness Apparatus.....</b>	<b>93</b>
10.1 Test Configuration Requirements.....	93
10.1.1 Test Machine Stiffness .....	93
10.1.2 Load-Line Variation .....	94
10.1.3 Friction.....	95
10.1.4 Plastic Deformation .....	95
10.2 Short Rod and Bar Testing Methods .....	95
10.3 The MTS 810 Material Testing System.....	96
10.4 The MTS 810 Short Bar Testing .....	98
10.4.1 Gripper Design.....	99
10.4.2 Obtaining the Test Results.....	100
<b>Chapter 11 - DMA, SEM and Loss Tangent Specimens Preparation and Apparatus .....</b>	<b>102</b>
11.1 Specimens Preparation.....	102

11.1.1 SEM Specimens Preparation .....	102
11.1.2 DMA and Loss Tangent Specimens Preparation.....	105
11.2 Apparatus.....	106
11.2.1 Scanning Electron Microscope Apparatus.....	106
11.2.2 Dynamic Mechanical Analysis Apparatus.....	107
11.2.3 Loss Tangent Apparatus .....	108
<b>Chapter 12 - Results and Discussions .....</b>	<b>110</b>
12.1 Fracture Toughness.....	110
12.2 Dynamic Mechanical Analysis .....	115
12.2.1 For 5% by Weight Filler .....	115
12.2.2 For 10% by Weight Filler .....	118
12.2.3 For 15% by Weight Filler .....	120
12.2.4 DMA Measurement Summary.....	123
12.3 Microscopic Analysis .....	124
12.4 Loss Tangent Test.....	136
12.5 Concluding Remarks .....	140
12.5.1 Fracture Toughness.....	140
12.5.2 Dynamic Mechanical Analysis .....	140
12.5.3 Microscopic Analysis .....	141
12.5.4 Loss Tangent.....	141
12.6 Further Research.....	142

12.6.1 Predicting Fracture Toughness using FEA .....	143
12.6.2 Different Filler Concentrations .....	145
<b>References</b> .....	147
<b>Appendix A - Project Specification</b> .....	A-1
<b>Appendix B - Specimen Dimensions</b> .....	B-1
<b>Appendix C - Mixture Tables</b> .....	C-1
<b>Appendix D – Actual Specimen Measurements</b> .....	D-1
<b>Appendix E – Fracture Toughness Results</b> .....	E-1
<b>Appendix F – MTS 810 Testing System Data</b> .....	F-1
0% by Weight of Filler .....	F-1
5% by Weight of Filler .....	F-10
10% by Weight of Filler .....	F-18
15% by Weight of Filler .....	F-27
20% by Weight of Filler .....	F-36
25% by Weight of Filler .....	F-44
30% by Weight of Filler .....	F-53
35% by Weight of Filler .....	F-61
40% by Weight of Filler .....	F-70

<b>Appendix G – LCR Loss Tangent Measurements</b> .....	G-1
5% by weight of VE/CACO <sub>3</sub> (Ambient cured) .....	G-2
5% by weight of VE/CACO <sub>3</sub> (Ambient cured Plus Oven Post-cured) .....	G-3
10% by weight of VE/CACO <sub>3</sub> (Ambient cured) .....	G-4
10% by weight of VE/CACO <sub>3</sub> (Ambient cured Plus Oven Post-cured) .....	G-5
15% by weight of VE/CACO <sub>3</sub> (Ambient cured) .....	G-6
15% by weight of VE/CACO <sub>3</sub> (Ambient cured Plus Oven Post-cured) .....	G-7

# Table of Figures

Figure 2.1: Idealised chemical structure of a typical epoxy based vinyl ester .....	10
Figure 2.2: Schematic representation of uncured vinyl ester resin (uncured) .....	11
Figure 2.3: Schematic representation of polyester resin (uncured). .....	11
Figure 2.4: Schematic representation of cured vinyl ester resin.....	12
Figure 2.5: The structure of bishophenol A vinyl ester .....	12
Figure 2.6: Schematic of addition or free radical crosslinking of vinyl ester.....	15
Figure 2.7: Fracture toughness of PF/E-SPHERES.....	20
Figure 2.8: $K_{Ic}$ of polystyrene with different percentages of calcium carbonate.....	21
Figure 2.9: $K_{Ic}$ of polystyrene with different percentages of white cement .....	22
Figure 3.1: The two main assemblies used to create short bar test specimens.....	26
Figure 3.2: The mould assembly .....	27
Figure 3.3: Layout of the chevron slots drafted using SolidWorks. ....	28
Figure 3.4: The chevron slot glued to the notch component .....	28
Figure 3.5: The Assembled mould ready for pouring.....	29
Figure 3.6: Apparatus used in the composite preparation process. ....	33
Figure 3.7: The Steridium laboratory oven used for the post-curing process .....	34

Figure 3.8: Wax sealing applied around the mould edges to prevent leaking .....	36
Figure 3.9: Plastic tape is applied to the chevron slot. ....	37
Figure 4.1: Risk Identification and control chart.....	43
Figure 5.1: T-2 tanker, broken in two in fitting-out dock.....	45
Figure 5.2: Schematic drawing of fracture toughness specimens with (a) edge and (b) Internal flaws .....	47
Figure 5.3: (a) crack force lines (b) stress amplification at the flaw tips .....	48
Figure 5.4: Fracture modes, (a) opening mode (b) In-plane shear (c) out-of-plane shear.....	49
Figure 5.5: The relationship between fracture toughness and material thickness .....	51
Figure 6.1: Diagram of the electron optical column of a typical scanning electron microscope.....	56
Figure 6.2: Diagram of the vacuum system of a scanning electron microscope .....	59
Figure 7.1: Phase lag of 0° and 90° indicating purely elastic behaviour and purely viscous behaviour respectively .....	62
Figure 7.2: Method of calculating the complex modulus, the storage modulus, and the loss modulus .....	63
Figure 8.1: (a) parallel connection of C and G (b) Phasor diagram .....	71
Figure 9.1: Specimens types used in the $K_{Ic}$ test (ASTM E 399) .....	75

Figure 9.2: Specimens types used in other $K_{Ic}$ test (ASTM E 399).....	76
Figure 9.3: Standard Charpy-V notch specimen.....	80
Figure 9.4: Charpy V-notch impact test. ....	80
Figure 9.5: Short rod (a) and short bar (b) and testing specimen. ....	82
Figure 9.6: Short Bar Specimen with Straight Chevron Slots.....	84
Figure 9.7: Short Bar Specimen with Curved Chevron Slots.....	85
Figure 9.8: Curved and Straight Slots Tangent at $a_c$ .....	87
Figure 9.9: Chevron slot angle and initial crack length for curved chevron slots. ....	88
Figure 9.10: Variation of load versus crack length.....	90
Figure 9.11: Cross-section dimension of short bar specimen. ....	92
Figure 10.1: Stiff and soft machine characteristics.....	94
Figure 10.2: The MTS 810 Load Unit.....	96
Figure 10.3: The operating system layout of the MTS 810.....	97
Figure 10.4: A short bar specimen attached to the MTS 810.....	98
Figure 10.5: Gripper used in MTS 810 Material Testing System.....	99
Figure 10.6: Results printout from the MTS 810.....	100
Figure 10.7: Measurement of the test specimen using digital vernier callipers. ....	101
Figure 11.1: A sputter coater.....	103

Figure 11.2: Diagrammatic representation of a sputter coater .....	104
Figure 11.3: Two gold coated samples with the extra parts removed .....	104
Figure 11.4: The mould used to cast both DMA and the loss tangent specimens.....	105
Figure 11.5: Scanning Electron Microscope at QUT .....	106
Figure 11.6: (A) The Dynamic Mechanical Analyser (B) Test specimen positioned in the DMA dual cantilever clamp arrangement.....	107
Figure 11.7: Agilent 4263B LCR Meter.....	108
Figure 11.8: Two copper plates forming the parallel plate capacitor with a sample sandwiched between two copper plates .....	109
Figure 12.1: Fracture toughness of vinylester reinforced with calcium carbonate....	112
Figure 12.2: DMA results for ambiently cured VE/CaCO <sub>3</sub> (5%).....	115
Figure 12.3: DMA results for ambiently plus oven cured VE/CaCO <sub>3</sub> (5%). .....	116
Figure 12.4: DMA results for two VE/CaCO <sub>3</sub> (5%) samples.....	117
Figure 12.5: DMA results for ambiently cured VE/CaCO <sub>3</sub> (10%).....	118
Figure 12.6: DMA results for ambiently plus oven cured VE/CaCO <sub>3</sub> (10%). .....	119
Figure 12.7: DMA results for two VE/CaCO <sub>3</sub> (10%) specimens .....	120
Figure 12.8: DMA results for ambiently cured (15%) .....	121
Figure 12.9: DMA results for ambiently plus oven cured VE/CaCO <sub>3</sub> (15%). .....	121

Figure 12.10: DMA results for two VE/CaCO <sub>3</sub> (15%) specimens .....	122
Figure 12.11: Six samples of fractured specimens .....	124
Figure 12.12: Four critical points for the fractured surface to be analysed .....	125
Figure 12.13: Schematic illustration of a fracture surface .....	126
Figure 12.14: Fractured surface of neat vinyl ester showing typical unstable crack propagation. ....	127
Figure 12.15: The fractured surface of neat vinyl ester resin, illustrating striations followed by a turbulent flow pattern of the fracture zone. ....	128
Figure 12.16: Micrograph of area 2 is the stretched-zone, shows some micro voids and some scratches on the fractured surface .....	128
Figure 12.17: Micrograph of area 3 .....	129
Figure 12.18: Micrograph of area 4 .....	129
Figure 12.19: The fractured surface of VE/CaCO <sub>3</sub> (35%) where patches of calcium carbonate appear as second phase and strengthen the structure. ....	130
Figure 12.20: The micrograph of area 1, the CaCO <sub>3</sub> powder partially dissolves in the resin.....	131
Figure 12.21: The micrograph of area 2 shows brittle fracture lines and aggregated particles of CaCO <sub>3</sub> .....	131
Figure 12.22: The micrograph of area 3 shows different sizes of CaCO <sub>3</sub> aggregated particles.....	132

Figure 12.23: The micrograph of area 4 .....	132
Figure 12.24: The micrograph of area 1 shows large voids .....	133
Figure 12.25: The micrograph of area 2 shows that most of the fracture surface has been damaged .....	134
Figure 12.26: The micrograph of area 3 shows that some of the fracture lines initiated at the air voids.....	134
Figure 12.27: The micrograph of area 4 shows that air voids are shown to serve both as crack initiators and crack arrestors.....	135
Figure 12.28: Loss tangent of vinylester reinforced with 5% CaCO <sub>3</sub> by weight.....	136
Figure 12.29: Loss tangent of vinylester reinforced with 10% CaCO <sub>3</sub> by weight....	137
Figure 12.30: Loss tangent of vinylester reinforced with 15% CaCO <sub>3</sub> by weight....	138
Figure 12.31: The mesh of the model (random distribution of the particles).....	144
Figure 12.32: Simple geometry with three different percentages of the filler.....	146

## List of Tables

Table 2.1: Physical and chemical properties of CaCO <sub>3</sub> .....	18
Table 2.2: Fracture toughness of PF/E-SPHERES .....	20
Table 2.3: Fracture toughness of rubber modified vinyl ester.....	23
Table 3.1: Weight of materials required to make 1000 g of VE/CaCO <sub>3</sub> (10%). .....	31
Table 5.1: Plane strain fracture toughness and strength values for polymers.....	51
Table 8.1: Typical dissipation factor. ....	68
Table 9.1: Effect of chevron slot geometry .....	89
Table 12.1: The measured geometry of the 10% by weight filler specimen 1. ....	110
Table 12.2: fracture toughness for VE/CaCO <sub>3</sub> post-cured in oven.....	112
Table 12.3: DMA results for all the samples with different curing method and filler percentages. ....	123
Table 12.4: Result of the fracture toughness and other parameters for VE with different filler percentage .....	125
Table 12.5: Loss tangent values for different frequencies, curing methods and filler percentages. ....	139

## Appendix Figures

Figure B.1: The selected geometry of the specimens ..... B-2

Figure B.2: The standard dimensions of the short bar specimen for (B=50). ..... B-3

## Appendix Tables

Table C.1: Weight of materials required to make 1000 g of VE/CaCO<sub>3</sub> (0%). ..... C-1

Table C.2: Weight of materials required to make 1000 g of VE/CaCO<sub>3</sub> (5%). ..... C-1

Table C.3: Weight of materials required to make 1000 g of VE/CaCO<sub>3</sub> (10%). ..... C-1

Table C.4: Weight of materials required to make 1020 g of VE/CaCO<sub>3</sub> (15%). ..... C-1

Table C.5: Weight of materials required to make 1050 g of VE/CaCO<sub>3</sub> (20%). ..... C-2

Table C.6: Weight of materials required to make 1120 g of VE/CaCO<sub>3</sub> (25%). ..... C-2

Table C.7: Weight of materials required to make 1200 g of VE/CaCO<sub>3</sub> (30%). ..... C-2

Table C.8: Weight of materials required to make 1300 g of VE/CaCO<sub>3</sub> (35%). ..... C-2

Table C.9: Weight of materials required to make 1400 g of VE/CaCO<sub>3</sub> (40%). ..... C-3

Table D.1: specimens' geometrical measurements for 0 wt% of VE/CaCO<sub>3</sub>..... D-1

Table D.2: specimens' geometrical measurements for 10 wt% of VE/CaCO<sub>3</sub>..... D-1

Table D.3: specimens' geometrical measurements for 10 wt% of VE/CaCO<sub>3</sub>..... D-1

Table D.4: specimens' geometrical measurements for 15 wt% of VE/CaCO<sub>3</sub>..... D-2

Table D.5: specimens' geometrical measurements for 20 wt% of VE/CaCO <sub>3</sub> .....	D-2
Table D.6: specimens' geometrical measurements for 25 wt% of VE/CaCO <sub>3</sub> .....	D-2
Table D.7: specimens' geometrical measurements for 30 wt% of VE/CaCO <sub>3</sub> .....	D-3
Table D.8: specimens' geometrical measurements for 35 wt% of VE/CaCO <sub>3</sub> .....	D-3
Table D.9: specimens' geometrical measurements for 40 wt% of VE/CaCO <sub>3</sub> .....	D-3
Table E.1: Fracture toughness calculation for 0 wt% of CaCO <sub>3</sub> . ....	E-1
Table E.2: Fracture toughness calculation for 5 wt% of CaCO <sub>3</sub> . ....	E-1
Table E.3: Fracture toughness calculation for 10 wt% of CaCO <sub>3</sub> . ....	E-2
Table E.4: Fracture toughness calculation for 15 wt% of CaCO <sub>3</sub> . ....	E-2
Table E.5: Fracture toughness calculation for 20 wt% of CaCO <sub>3</sub> . ....	E-2
Table E.6: Fracture toughness calculation for 25 wt% of CaCO <sub>3</sub> . ....	E-3
Table E.7: Fracture toughness calculation for 30 wt% of CaCO <sub>3</sub> . ....	E-3
Table E.8: Fracture toughness calculation for 35 wt% of CaCO <sub>3</sub> . ....	E-3
Table E.9: Fracture toughness calculation for 40 wt% of CaCO <sub>3</sub> . ....	E-3

# Glossary of Terms

CMC = Ceramic Matrix Composites

DMA = Dynamic Mechanical Analysis

DMTA= Dynamic Mechanical Thermal Analysis

ISRM = International Society for Rock Mechanics

LCR meter = Inductance, Capacitance, and Resistance meter

LEFM = Linear Elastic Fracture Mechanics

MMC = Metal Matrix Composites

PMC = Polymer Matrix Composites

PVC = Poly-Vinyl Chloride

QUT = Queensland University of Technology

SEM = Scanning Electron Microscope

TEM = Transmission Electron Microscope

USQ = University of Southern Queensland

VE = Vinyl Ester

# Chapter 1 - Introduction

## 1.1 Introduction

This chapter gives an overview of the project outline along with the research objectives. The focus of this thesis is to investigate the filler-resin mixture and the catalyst used in order to optimise fracture toughness of the composite.

The official Project Topic is, “*Measurement of fracture toughness, mechanical and electrical loss tangents of calcium carbonate reinforced vinyl ester composites*”.

## 1.2 Project Background

The popularity of the composite materials is expected to grow exponentially since composite materials still offer numerous new possible applications. Composite materials have several advantages over traditional metal and alloy-based structures. Compared to these traditional structures, composites encompass superior strength-to-weight ratios, lower maintenance requirements and greater corrosion resistance. Moreover, composites exhibit a higher strength to weight ratio than steel or aluminium and can be engineered to provide a wide range of tensile, flexural, fracture and impact strength properties. For example, a composite’s strength per unit density is roughly two times that of aluminium and four times that of steel (Shelter 2003).

However, while composites offer significant potential for application in civil engineering structures, their acceptance into this industry continues to be discouraging due to their expensive manufacturing cost relative to the traditional building materials.

Furthermore, composites are difficult to repair since most composites use thermoset matrices that cannot be reshaped (Barbero 1998).

Nevertheless, with increased demand and applications for composites, pressure is being placed on developing less expensive composites with superior or comparable material properties. To make the composite more cost effective, cheap fillers are being used. Additionally, cost can be reduced further by improving the manufacturing techniques.

### **1.3 Research Aims and Objectives**

The broad aim of this project is to study the effects of different percentages of the filler, calcium carbonate, on the fracture toughness of the vinyl ester composites which are post cured in an oven.

Within this aim mentioned above, the following specific objectives are adopted:

1. Understand the methods and benefits of making the composites.
2. Study the effects of the filler on the fracture toughness of the composites by means of short bar tests and a Scanning Electron Microscope (SEM).
3. Measure the properties of the composite as they are deformed under periodic stress and compare the change in the mechanical properties between the oven and ambient cured samples at high temperatures using a Dynamic Mechanical Thermal Analyser (DMTA).
4. Measure the composite dielectric properties.

## **1.4 Justification**

Several fillers have been tested and their effects on the composite material are obtained. However, countless new fillers are still to be tested and in this project calcium carbonate is under consideration.

The justification of this project also stems from the author's desire to be part of the large ongoing research in the composite field, and to add valuable information to this ongoing research.

## **1.5 Scope**

Composites are increasingly being used in a wide range of structures such as aerospace, marine, transportation and civil engineering. Applications in aerospace, marine and transport are very much performance driven while civil engineering applications are largely cost driven. In order to reduce the cost of composites, a wide range of fillers are being used. These fillers do not only reduce the cost of the composites, but also have a significant influence on their final structural properties. In this project, calcium carbonate will be used as filler. This project will involve the production of a range of vinyl ester composite specimens with different percentages by weight of the filler. After preliminary curing, the specimens will be post-cured in ovens.

Short bar tests will be used to evaluate the fracture toughness. Additionally, a scanning electron microscope will be used to study the fractured surfaces produced as a result of the short bar tests. Furthermore, the change in the mechanical and electrical

properties of the composites will be measured by means of dynamic mechanical analyser and LCR meter, respectively. The findings will be analysed in detail.

## **1.6 Concluding Remarks**

This project aims to obtain the optimum mixture of the filler-resin and the catalyst being used on the mixture that maximises its fracture toughness. Furthermore, valuable information from this project will be added to the ongoing research in the composites field.

The literature review will provide the background for the methods used in the preparation and testing of the composites. It will also provide the basis for the limitations and expected outcomes of this project.

## Chapter 2- Literature Review

### 2.1 Introduction to Composite Materials

It is a very challenging exercise to define composite materials and agree upon a single, simple, and useful definition. There is no universally accepted definition for composite materials. Any definition is at best imprecise, and may or may not include materials considered by others to be composites (Lee 1989).

However, composite materials can generally be defined as multiphase materials formed from a combination of two or more different materials that have distinct properties. This combination consequently produces a material that has improved specific characteristics not available from any of the original components.

Generally, composites are famous for their structural properties; however they are also well known for their electrical, thermal and environmental applications (Zweben 1998). They contain a continuous matrix constituent that binds together and provides an array of a stronger, stiffer reinforcement constituent (Miracle & Donaldson 2003).

Composite materials are generally classified by the matrix material. For example, polymer matrix composites (PMCs), metal matrix composites (MMCs) and ceramic matrix composites (CMCs) (Mallick 1997).

## 2.2 Polymer Composites

Polymers are substances composed of a long chain of repeating molecules (Kenneth & Michael 2005). The molecular structure of polymers gives them unique material properties and great versatility in processing methods. Polymers are easy to manufacture and process. Traditional materials like metals and wood are a lot harder to work and form. However, polymers have a low density and can be shaped at relatively low temperatures. Components that have normally been made from wood, metal, ceramics, and glass are now constantly being redesigned using polymers (Osswald & Menges 1995).

The main constituent materials creating the reinforced polymer composites are polymer matrix resins. The addition of various fillers to the matrix resins gives a range of the required properties for a specific application (Davey 2006).

### 2.2.1 Thermoplastic and Thermoset Polymers

Polymer resins are classified into two main types, thermoplastic and thermoset. Both types are discussed in detail below.

#### **Thermoplastics:**

Thermoplastics are polymers that solidify as they cool, stopping the free movement of the long molecules. When they are heated, these materials regain their “flow” or viscosity as the molecules are able to slide past one another with ease. Thermoplastics are further divided into two classes: amorphous and semi-crystalline polymers. Amorphous thermoplastics have a random molecular structure as the molecules remain in disorder as it cools. Semi-crystalline thermoplastics solidify with a certain

order in their molecular structure and usually behave like leathery or rubbery materials at room temperature due to a sub-zero glass transition temperature (Davey 2006).

### **Thermosetting:**

Thermosetting polymers are chemically cured, causing the long macromolecules to crosslink with each other. This results in a network of molecules that cannot slide past one another. The crosslinking in these networks causes the material to lose its ability to regain viscousness or “flow” upon reheating. Thermosetting materials are stiff and brittle as a result of the high density of crosslinking.

One of the major advantages of thermosetting resins is that they can be liquid at room temperature when the moulding process commences. This allows fillers and other additives like colorants, reinforcements, and processing aids to be easily mixed by simply stirring through. The most commonly known and used thermosetting resins in composites today include phenolics, amino plastics, unsaturated polyesters, epoxies, vinyl ester, polyimides, and polyurethanes. Each group has different properties which make them more appealing in certain applications than others. An understanding of the formation and structure of the resin is vital for material selection and application.

The matrix resin materials considered in this current study are thermosetting polymer systems. These materials are typically two-part chemical systems which react when mixed to form the final thermoset polymer network. The primary matrix chemistry considered is that of vinyl esters, which feature an acrylated epoxy oligomer cross linked with styrene monomer.

## 2.3 Importance of Composite Materials

Materials played a huge role in human evolution. This can be observed from the naming of the ages which are the Stone, Iron and Bronze ages. Therefore, it can be predicted that our age will be named as 'The Age of Composites' or 'The Age of Engineered Materials' (Stuart 1989).

Composites are not always man-made, since some of them can occur naturally. Abalone shell, wood, bone and teeth are some typical natural composites (Askeland 1999).

Man [sic] learned to use composite materials over a very long time. Historic evidences are the Egyptian sarcophagi, fashioned from glued and laminated wood veneer and their cloth tape, soaked in resin for mummy embalming. In addition, the Mongolian warriors' high-performance, re-curved archery bows of bullock tendon and pine resin are 80 percent as strong as the modern fibreglass ones (Lee 1989).

None the less, there is a variety of materials available that can be combined together to form particular composite systems. This wide range gives engineers huge flexibility to achieve the optimum combination for specific applications. All of the alternative types of basic materials have their own unique properties that contribute to the characteristics of the resultant composites.

## 2.4 Materials Used

In this project vinyl ester resin (HETRON 922PAS) was used. This material was bought from Nupol Composite, a division of Nuplex Industries (Aust) Pty Ltd. Cost of the resin was \$7 per kilogram. The hardener used in the cross linking process was

Methyl Ethyl Ketone Peroxide-20 (MEKP-20). Additionally, calcium carbonate ( $\text{CaCO}_3$ ), bought from Biolab (Aust) Ltd was used as a filler in this project. The cost of the filler was \$8 per kilogram. All the materials used in this project will be discussed in detail in this chapter.

## **2.5 Background of Vinyl Ester**

In the late 1950s vinyl ester, or vinylester, resins were prepared only in laboratory-scale quantities. It was not until 1965 that they were commercially introduced by Shell Chemical Company under the trade name of EPOCRYL resins (Kulshreshtha & Vasile 2002).

Fundamentally, vinylester polymers were developed in an attempt to combine the fast and simple cross-linking of unsaturated polyesters with the mechanical and thermal properties of epoxies (Astrom 1997). This development was successful and ended up with the vinylester resins which combine superior chemical, thermal and mechanical resistance properties of epoxies with the rapid curing and ease of processing of unsaturated polyesters. Moreover, vinyl ester polymers can contain a high ratio of fillers of up to 70% by weight since they have low molecular weight compared with that of unsaturated polyesters (Kulshreshtha & Vasile 2002).

Vinylester polymers have long been known as the premium resin for corrosion resistance applications. However, they are becoming more preferable candidates for new structural composite applications as a result of their excellent elevated temperature performance, high elongation, and fatigue resistance (Blankenship et al. 1989).

### 2.5.1 Chemical Structure

Vinylesters (VE) are chemically similar to both epoxy and unsaturated polyesters resins. The chemical structure of vinyl ester resins is such that the reaction sites are at the end of each polymer chain, rather than along the chain length like polyesters. This structure results in a thermoset resin that has a lower cross-link density and exhibits greater toughness properties, such as interlaminar shear and impact strength (Sumerak 2003).

The vinyl ester molecule also features fewer ester groups. These ester groups are susceptible to water degradation by hydrolysis which means that vinyl esters exhibit better resistance to water and many other chemicals than their polyester counterparts, and are frequently found in applications such as pipelines and chemical storage tanks.

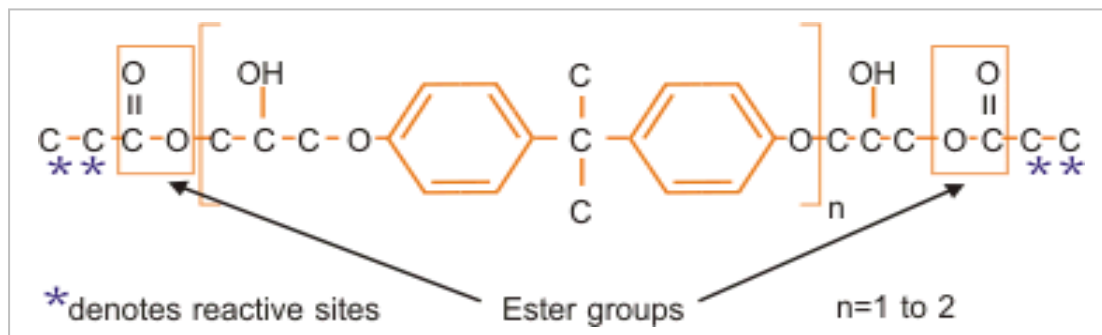
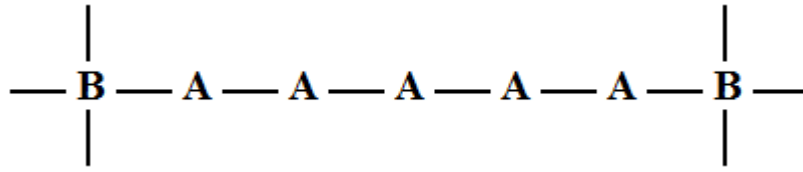


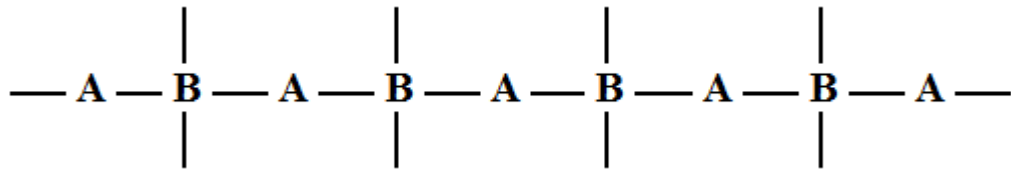
Figure 2.1: Idealised chemical structure of a typical epoxy based vinyl ester. (Source: Ku et al. 2009, p. 21)

Figure 2.1 shows the idealized chemical structure of a typical epoxy based vinyl ester. Note the positions of the ester groups and the reactive sites ( $C^* = C^*$ ) within the molecular chain.



**Figure 2.2: Schematic representation of uncured vinyl ester resin (uncured)**

The molecular chains of vinyl ester represented in Figure 2.2 can be compared to the schematic representation of polyester shown in Figure 2.3, where the difference in the location of the reactive sites can be clearly seen.



**Figure 2.3: Schematic representation of polyester resin (uncured).**

With the reduced number of ester groups in a vinyl ester when compared to polyester, the resin is less prone to damage by hydrolysis. The material is therefore sometimes used as a barrier or ‘skin’ coat for a polyester laminate that is to be immersed in water, such as in a boat hull. The cured molecular structure of the vinyl ester (Figure 2.4) shows that it tends to be tougher than a polyester, although to really achieve these properties the resin usually needs to have an elevated temperature post cure (Agarwal et al. 2006). This is why the specimens in this project are post-cured in an oven at elevated temperatures in three stages.

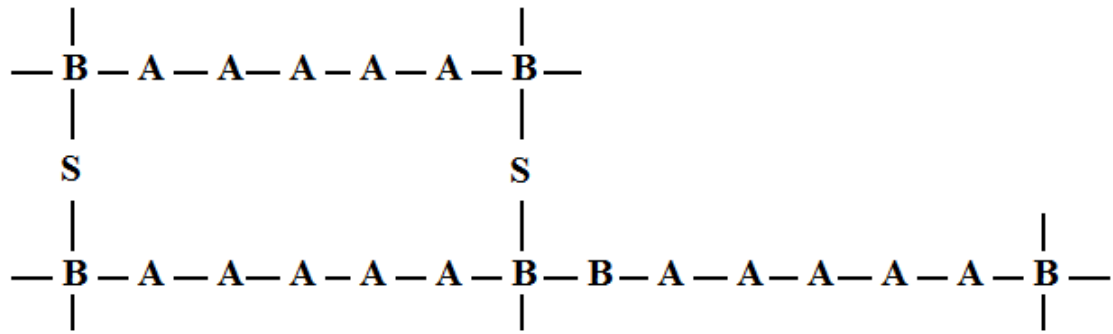


Figure 2.4: Schematic representation of cured vinyl ester resin.

Unsaturated resins such as polyesters and vinyl esters have ester groups in their structures. Esters are susceptible to hydrolysis and this process is accelerated and catalyzed by the presence of acids or bases. Vinyl esters contain substantially less ester molecules than polyesters. They contain only one at each end of the resin molecule. This is illustrated by the structure of bisphenol A vinyl ester in Figure 2.5. This means that vinyl esters, just like epoxies, have few possible crosslink sites per molecule. Vinyl esters of high molecular weight therefore have relatively low crosslink density and thus lower modulus, than if the starting point is a lower molecular-weight polymer.

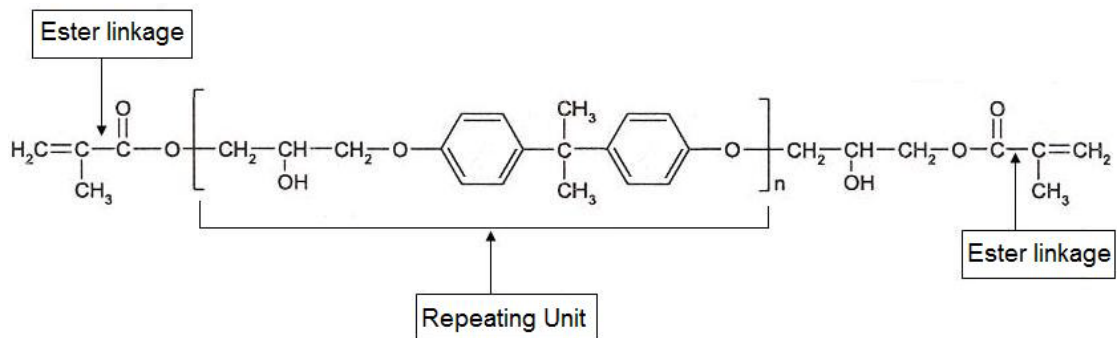


Figure 2.5: The structure of bisphenol A vinyl ester. (Source: Ku et al. 2002)

Vinyl esters crosslink in time frames and under the conditions similar to those of unsaturated polyesters, i.e. crosslinking occurs fairly quickly and often at room temperature (Astrom 1997). Methacrylic acid is used to manufacture the vinyl esters. This means that next to each ester linkage is a large methyl group. This group occupies a lot of space and hinders any molecule approaching the ester group by impeding their access. These two aspects of the design of the vinyl ester molecule combine to make them more chemically resistant than polyesters (Pritchard 1999). There are three families of vinyl esters. The most commonly used family is based on the reaction between methacrylic acid and diglycidylether of bisphenol A (DGEBA) as shown in Figure 2.5. This family of vinyl ester is used in this research.

The polymerization product between methacrylic acid and bisphenol A is vinyl ester, which can be a highly viscous liquid at room temperature or a low melting point solid, depending on the acid and bisphenol A used. For further processing, the polymer is dissolved in a low molecular monomer, or reactive diluent, usually styrene, the result is a low viscosity liquid referred to as resin. The resin used in this research has 50% by weight of styrene.

### **2.5.2 Vinyl Ester and Cross Linking**

With the addition of a small amount of initiator to the resin, the crosslinking reaction or curing is initiated. The initiator used is organic peroxide, Methyl Ethyl Ketone Peroxide (MEKP). The added amount is usually 1 to 2 percent by weight.

The initiator is a molecule that produces free radicals. The free radical attacks one of the double bonds of the ends of the polymer and binds to one of the carbon atoms, thus producing a new free radical at the other carbon atom; see the initiation step in

Figure 2.6. This newly created free radical is then free to react with another double bond. Since the small monomer molecules, the styrene molecules, move much more freely within the resin than the high molecular weight polymer molecules, this double bond very likely belongs to a styrene molecule.

The bridging step creates a new free radical on the styrene, which is free to react with another double bond and so on, as demonstrated in the bridging step in Figure 2.6. Obviously the styrene is not only used as solvent, but also actively takes part in the chemical reaction. Monomers are consequently called curing agents and initiators are called catalysts (Astrom 1997).

It is important here to note the difference between a resin changing from liquid to solid state and the attainment of full cure. The term “cured” refers to a state in which all possible network linkages have been formed through the conversion of unsaturation sites in the oligomer and reactive monomer. However, a resin typically changes from liquid to solid state when only a small portion of these bonds have been formed. The cure reaction must then continue within the new solid for full conversion to be achieved (Davey 2004).

For a crosslink to occur, it is necessary for two unsaturation points and two free radicals to be in sufficient proximity for the reaction to initiate. The mobility of the oligomer and reactive monomer significantly influence their ability to achieve the required proximity which is a determining factor in the progress of a given cure reaction. The mobility of the oligomer and reactive monomer is a function of their respective molecular weights and temperature (Davey 2004).

Figure 2.6 illustrates the whole crosslinking process showing the reactants, the initiation step, the bridging step and the resulted cross-linked polymer.

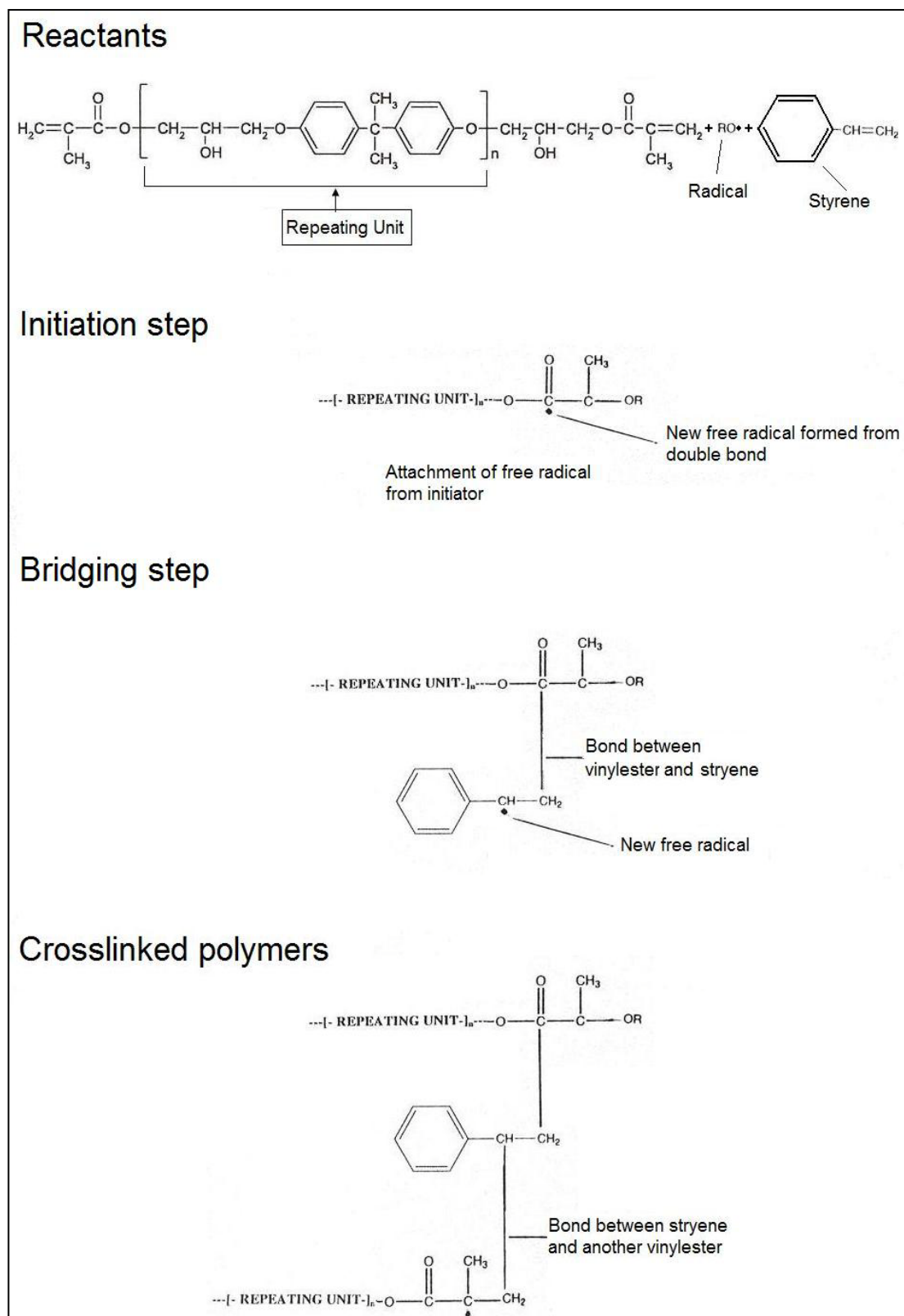


Figure 2.6: Schematic of addition or free radical crosslinking of vinyl ester (Source: Ku 2003, p. 2032)

The crosslinking of vinylester is identical to the crosslinking in unsaturated polyesters. Both, vinylester and polyester utilise a base oligomer and reactive monomer, in which both final thermoset polymer networks are formed by using a free-radical cross-linking cure mechanism. Additionally, just like unsaturated polyester, the crosslinking in vinylester forms relatively quick and occur at room temperature (Astrom 1997). However, unlike unsaturated polyester, vinylester, like epoxy has only few available crosslinking sites per molecule.

## 2.6 Catalysts

The catalytic system can be broken in to two parts. The first part is the initiator called ‘catalyst’ and the second part is the activator called ‘promoter’, each of them having a particular role in the curing reaction and being dependent.

The catalyst is peroxide; the choice of the peroxide catalysts is determined by the resin under consideration and the temperature at which the resin is to be cured. Usually, Methyl Ethyl Ketone Peroxide (MEKP) is used for room temperature curing and Benzoyl Peroxide (BPO) is intended for elevated temperature curing. MEKP is normally used with a concentration varying between 1 to 5 percentages by weight for room temperature curing.

The activator used in this project, is generally a cobalt salt (cobalt naphthenate or preferably cobalt octoate due to its higher purity) used with a concentration of 0.2-0.3 wt%. However, the commercial resin grades are often supplied with the option of being pre-promoted, thus containing the promoter. The advantage of these grades is that the resin is supplied in a condition that can be used immediately (Kulshreshtha & Vasile 2002).

## **2.7 Fillers**

Fillers are used for enhancing performance as well as economical reasons. The addition of the filler reduces cost considerably since less resin and catalyst is used. Moreover, fillers change the material properties in order to obtain the desired strength and heat characteristics as well as the electric conductivity of the composite (Katz & Milewski 1987). Some commonly used fillers are saw dust, glass powder, silica and hollow spheres.

Composites can be divided into two groups; those with high performance reinforcement, and those with low performance reinforcements. The high performance composites have the reinforcement placed in such a way that optimal mechanical behaviour is obtained. The low performance composites are those where the reinforcement is so small that it is sufficient to be dispersed into the material well enough to let the material to be processed in the same way as if it is without the filler (Schwartz 1996).

### **2.7.1 Calcium Carbonate**

Calcium carbonate is the most widely used extender availability. It provides a balance between manufacturing cost and mechanical properties.

The main industrial use of calcium carbonate is in the construction industry, either as a building material in its own right, for example, marble or limestone aggregate for road building, or as an ingredient of cement or as the starting material for the preparation of builder's lime by burning in a kiln. Calcium carbonate is also widely used as filler in plastics (Reade Advanced Materials 2006).

Precipitated calcium carbonate, pre-dispersed in slurry form, is also now widely used as filler material with the aim of achieving maximum saving in material and production costs (Arist Craft 2009). Calcium carbonate is referred as precipitated calcium carbonate (PCC) in industry (Solvay 2007).

The calcium carbonate powder being used is manufactured by LabServ and supplied by Biolab (Australia) Ltd. Its purity is 99% (assay 99.0%). The physical and chemical properties are listed in Table 2.1.

**Table 2.1: Physical and chemical properties of CaCO<sub>3</sub>. (Source: Reade Advanced Materials 2006)**

<b>Appearance</b>	White powder
<b>Odour</b>	Odourless
<b>Decomposition temperature</b>	825 °C
<b>Solubility in water</b>	Very soluble
<b>Solubility in organic solvents</b>	Not in alcohol but in acids
<b>Specific gravity</b>	2.7 – 2.95
<b>Particle size</b>	1.2 – 1.5 µm
<b>Flammability</b>	Non combustible
<b>Molecular weight</b>	100.09 g/mol
<b>Other information</b>	Tasteless

## 2.8 Review of Previous Work

The previous work in this field is shown in this section to provide results for comparison.

### 2.8.1 SLG Reinforced Phenolic Resin

In recent research reported by Cardona et al. (2007), the effect of filling phenol formaldehyde resin with ceramic-based fillers was examined. Figure 2.7 illustrates the fracture toughness of Borden J2027 specimens filled with varying weight percentages of SLG (E-spheres), post-cured conventionally and in microwaves. For the microwaves post-cured samples it was found that the fracture toughness is highest with neat resin (0 % by weight of SLG); its value is  $20.26 \text{ MPa}\sqrt{\text{m}}$ . The value dropped to a low of  $9.56 \text{ MPa}\sqrt{\text{m}}$  when the SLG by weight was 10%; after this the values varied from 12.74 to  $10.64 \text{ MPa}\sqrt{\text{m}}$  as the percentage by weight of SLG increased from 15 to 20%. All the values were within the three percent markers of  $9.56 \text{ MPa}\sqrt{\text{m}}$  (10% SLG). The fracture toughness increased back to  $14.26 \text{ MPa}\sqrt{\text{m}}$  when the percentage by weight of SLG was 35%.

It was also found that the values of fracture toughness, post-cured in microwaves, were generally higher than those post-cured conventionally. The difference is particularly obvious with neat resin; the difference in fracture toughness is 37%.

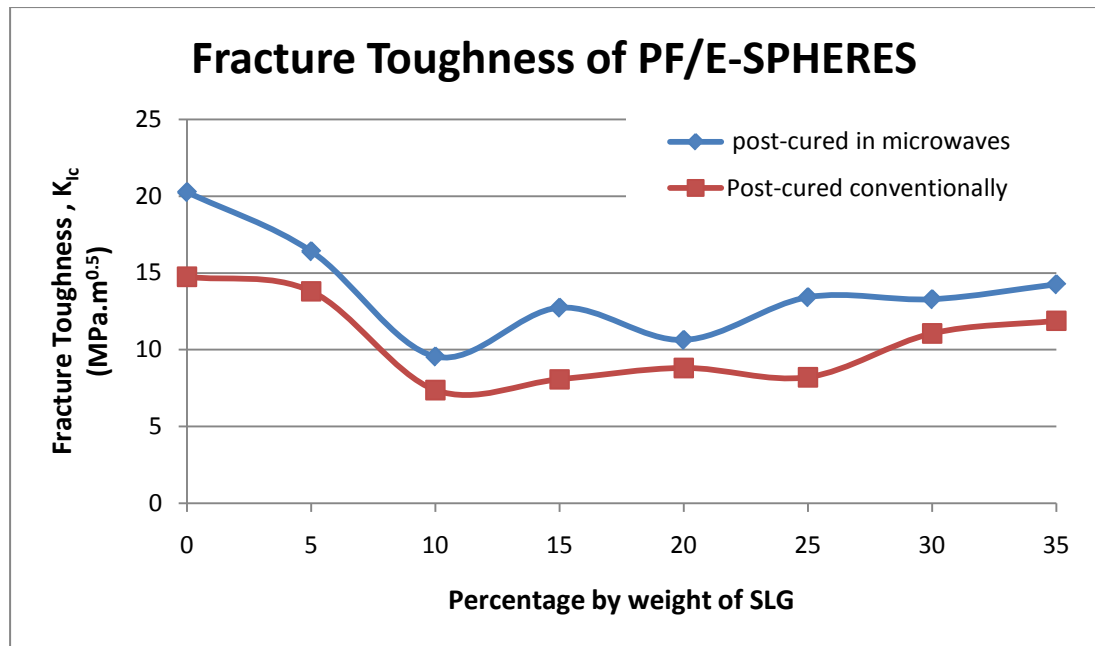


Figure 2.7: Fracture toughness of PF/E-SPHERES with varying percentage by weight of SLG post-cured conventionally and in microwaves respectively. (Source: Cardona et al. 2007)

Table 2.2 lists the numerical values of the fracture toughness of PF/E-SPHERES with varying percentages by weight of SLG, post-cured in microwaves, with the standard deviation given in brackets.

Table 2.2: Fracture toughness of different percentage by weight of SLG reinforced phenolic resin

Percentage By weight of SLG	Fracture toughness MPa $\sqrt{m}$	
	Cured by microwave	Cured conventionally
0	20.26 (0.981) <sup>#</sup>	14.75 (0.0603)
5	16.41 (1.721)	13.8 (1.007)
10	9.56 (0.632)	7.37 (0.424)
15	12.74 (0.204)	8.07 (0.516)
20	10.64 (0.531)	8.81 (0.333)
25	13.42 (1.058)	8.21 (0.277)
30	13.29 (0.581)	11.06 (0.708)
35	14.26 (0.900)	11.88 (0.524)

<sup>#</sup> Standard deviation (Source: Cardona et al. 2007)

### 2.8.2 Polystyrene Reinforced with White Cement

With the intention of developing polymer-matrix composites with high mechanical strength, Rai and Singh (2004) prepared composites by mixing 0.5% to 5.0% of either calcium carbonate or white cement, with polystyrene followed by casting them in an aluminium mould (Rai & Singh 2004).

The average fracture toughness of polystyrene containing 0.5% to 5.0% of calcium carbonate and white cement were shown in Figure 2.8 and Figure 2.9, respectively.

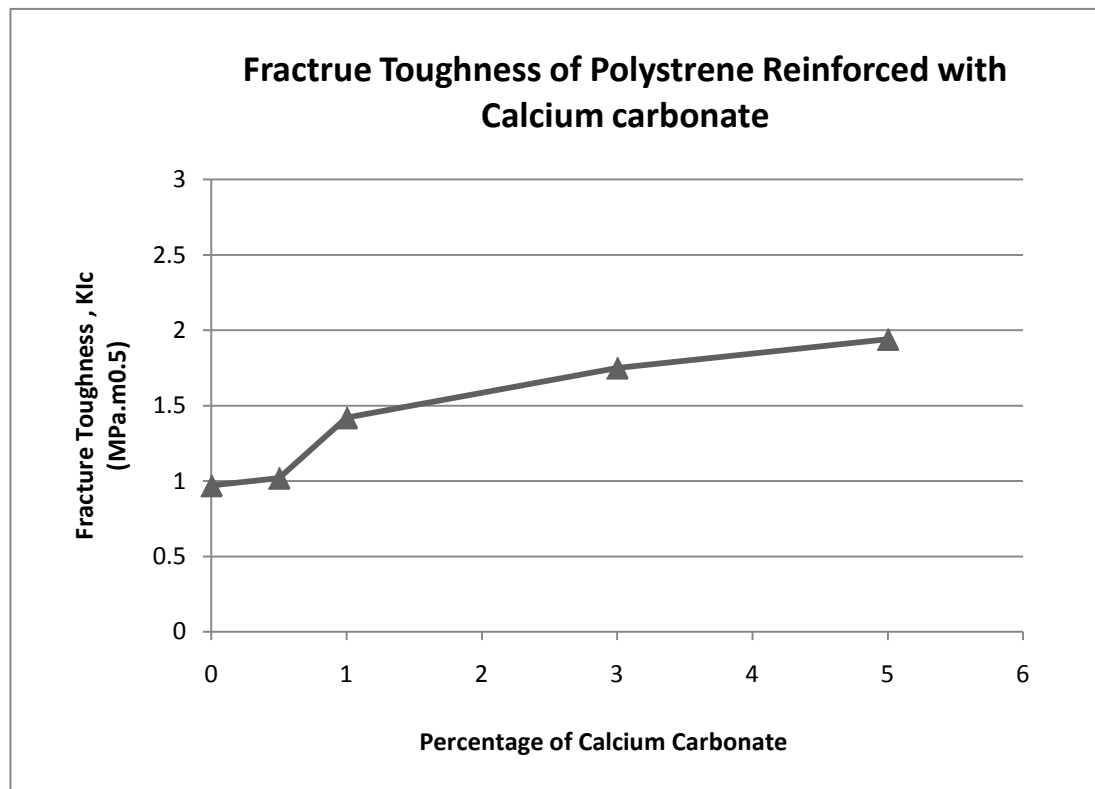
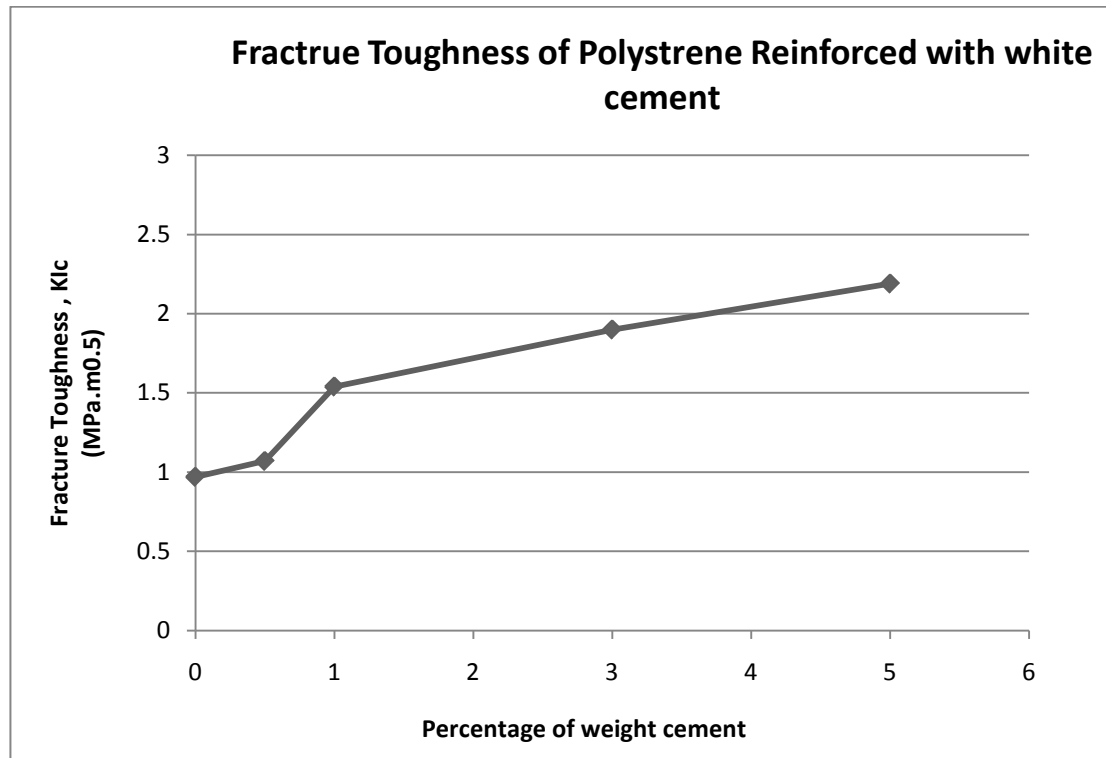


Figure 2.8: Fracture toughness ( $K_{Ic}$ ) of polystyrene with different percentages of calcium carbonate. (Source: Rai & Singh 2004)



**Figure 2.9: Fracture toughness ( $K_{Ic}$ ) of polystyrene with different percentages of white cement. (Source: Rai & Singh 2004)**

From Figure 2.8 and Figure 2.9, the fracture toughness ( $K_{Ic}$ ) of the cured neat polystyrene sample was  $0.97 \text{ MPa}\sqrt{\text{m}}$ . When the concentrations of calcium carbonate and white cement in polystyrene were increased from 0.5% to 5%, toughness values increased from 1.02 to  $1.94 \text{ MPa}\sqrt{\text{m}}$  and from 1.07 to  $2.19 \text{ MPa}\sqrt{\text{m}}$  respectively.

For a given percentage of additives, the values of fracture toughness of white cement were found to be higher than those of calcium carbonate (Rai & Singh 2004).

### 2.8.3 Vinyl Ester Reinforced with Rubber Modifiers

In another study, Robinette et al. (2004) added epoxy terminated rubber (ETBN) and vinyl terminated rubber (VTBN) to modified vinyl ester resins. All modified samples experienced a significant increase in fracture toughness with some degree of plasticization. ETBN yielded a higher toughness than VTBN due to the difference in rubber particle formation and morphology. Chemical linkage of VTBN to the vinyl ester matrix hindered complete phase separation, but helped to retain fracture toughness when VTBN was compared with ETBN (Robinette et al. 2004).

Table 2.3 shows the results obtained from the fracture toughness measurement of the rubber modified vinyl ester.

**Table 2.3: Fracture toughness of rubber modified vinyl ester. (Source: Robinette et al. 2004)**

<b>Resin</b>	<b>Percentage by weight of the filler</b>	<b>Filler material</b>	<b>Fracture toughness, <math>K_{Ic}</math>, (MPa <math>\sqrt{m}</math>)</b>
vinyl ester	0%	--	0.79±0.09
vinyl ester	4%	ETBN	1.44±0.07
vinyl ester	8%	ETBN	1.40±0.11
vinyl ester	4%	VTBN	1.14±0.12
vinyl ester	8%	VTBN	1.45±0.18

#### 2.8.4 Liquid Rubber Modified Vinyl Ester Resins

Vinyl ester resin cured with styrene was reinforced with two different liquid rubbers. The first reinforcer was un-reactive rubber called, “carboxyl terminated poly (butadiene-co-acrylonitrile)” or CTBN. As a result of adding CTBN, maximum in fracture toughness as a function of the additive content was achieved. Yet, CTBN suffered from rapid deterioration in toughness at higher concentrations. The second reinforcer was a reactive rubber called, “vinyl terminated poly (butadiene-co-acrylonitrile)” or VTBN. The addition of VTBN resulted in the reduction of fracture toughness with increasing reactive elastomer loading (Auad et al. 2001).

During crosslinking, it was observed that the system underwent a phase separation mechanism similar to that in unsaturated polyester resins (UPE) modified with a low profile additive (LPA). The process led to a sharp drop in density at high CTBN concentrations ( $\geq 10\%$  by weight) and the development of a co-continuous microstructure in the composites. On the other hand, the use of a reactive rubber, VTBN, led to a different morphology consisting of small rubber particles in the thermoset matrix (Auad et al. 2001).

## Chapter 3 – Experimental Methodology

### 3.1 Specimen Design

The short bar test was selected to measure the fracture toughness of the specimens in this project, refer to Chapter 9 for detailed information on different fracture toughness tests and for the justifications of using the short bar test.

The dimensions of specimens are accordingly modified to the geometrical recommendations of the International Society for Rock Mechanics (ISRM) (Matsuki et al. 1991). The standard ISRM short-rod test geometry has a specimen length to diameter (short rod) or length to breadth (short bar) ratio of  $L/D = 1.45$  (ISRM 1981a). The breadth dimension selected was 50 millimetres.

All the resulting dimensions of the specimen are shown in Appendix B,

Figure B.2. The selected size provides a practical specimen for testing because it is easy to handle and it also reduces the cost of the testing as mould and composite materials are reduced.

### 3.2 Mould Design

The mould used to create a sample of short bar test specimens is shown in Figure 3.1. The mould used in this project was designed and constructed by Davey (2006).

The mould is made from 6 millimetres of Poly Vinyl Chloride (PVC) sheets which is a hard thermoplastic polymer material. Two main assemblies are used to create the

short bar specimens. These are the cover and the mould assemblies shown in Figure 3.1. The cover assembly is made of the notch components and the notch holder. The notch components are fastened in a line along the 3mm thick PVC notch holder with 6mm spacing. The notches can be attached to the notch holder using metal screws, plastic screws or even glue. The notch components are used to create the grip grooves in the specimens.

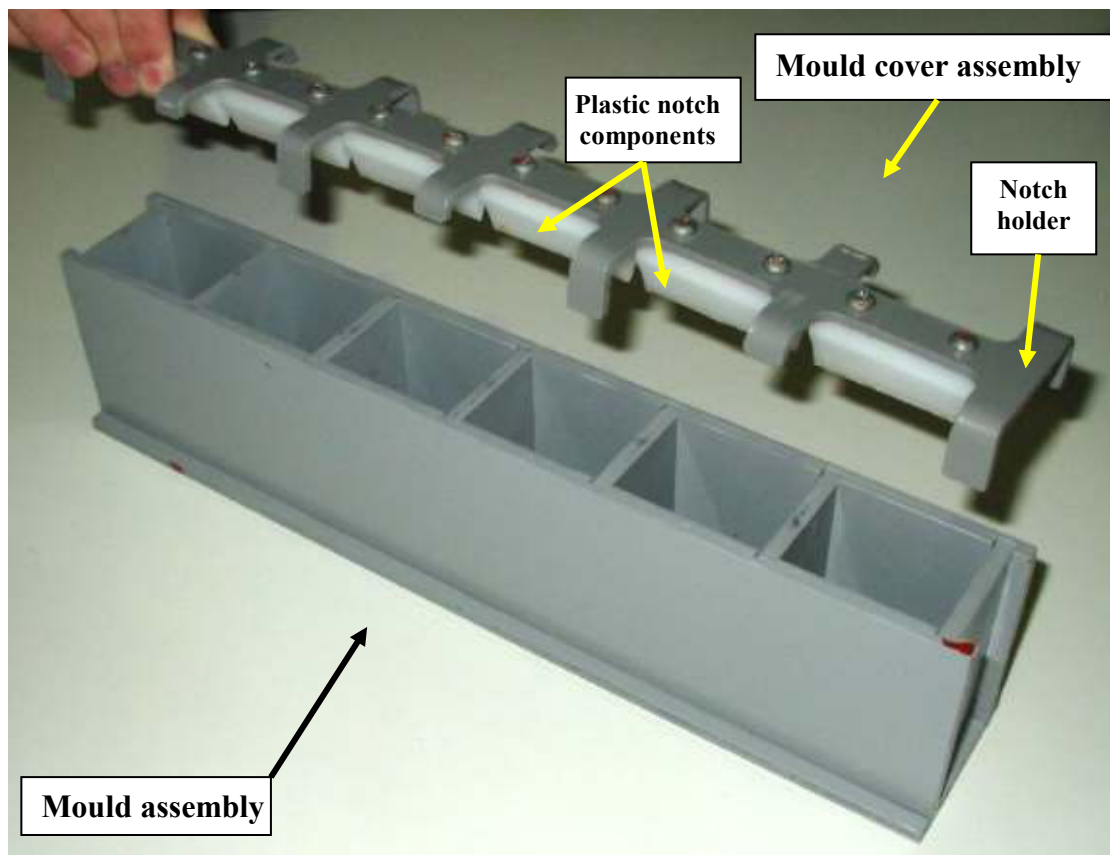


**Figure 3.1:** The two main assemblies used to create short bar test specimens. (Source: Davey 2006, p. 49)

The mould assembly is made of ten parts. These parts are a base component, two side components and seven division components, as shown in Figure 3.2. The base component contains machined grooves for the side components, and similarly the side components have grooves for the division components. All the parts fit nicely together using these grooves, as illustrated in Figure 3.2.

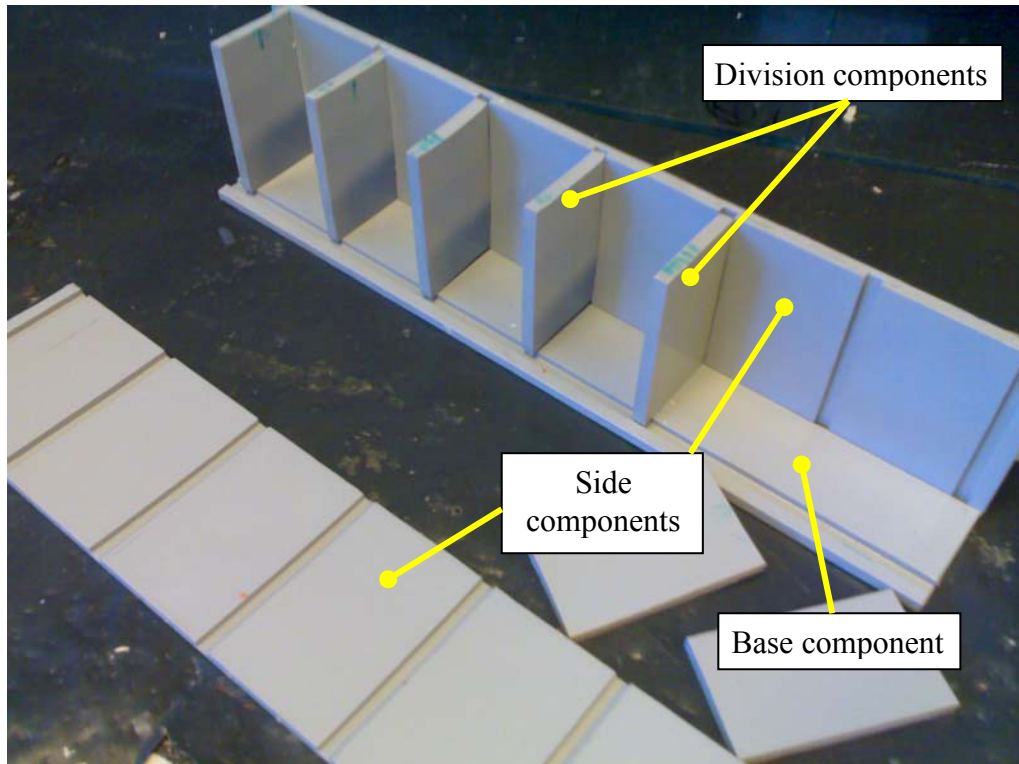


**Figure 3.2: The mould assembly**

### **3.3 Mould Preparation**

The preparation procedures are divided into two main parts: the preparation of the mould cover assembly and the preparation of the mould assembly (refer to Figure 3.1).

First of all, chevron slots were constructed from a cardstock sheet, since it had the desirable properties in terms of thickness and strength (refer to section 9.4.3). The chevron slots were drafted in SolidWorks 2008 to the standard dimension, as shown in Figure 3.3.

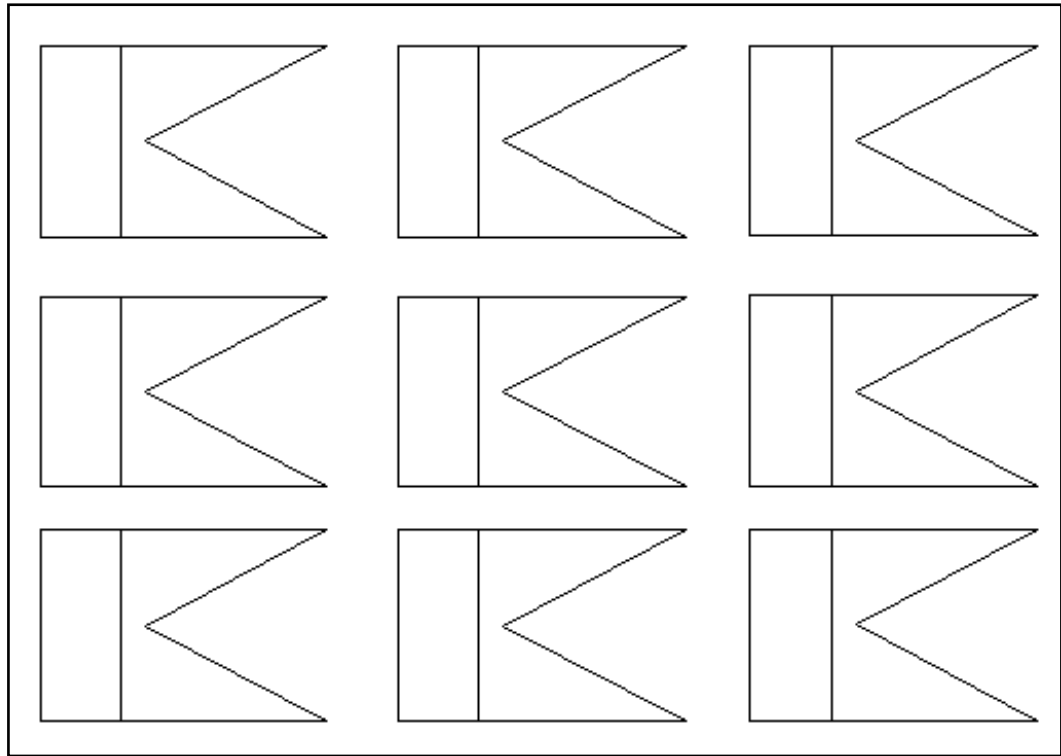


**Figure 3.3:** Layout of the chevron slots drafted using SolidWorks and printed on cardstock sheet.

Afterwards, they were printed out onto a cardstock sheet. The cardstock slots were then carefully cut using a pair of scissors and were glued to the notch component as illustrated in Figure 3.4. Finally, the notch components were attached to the notch holder using metal screws.

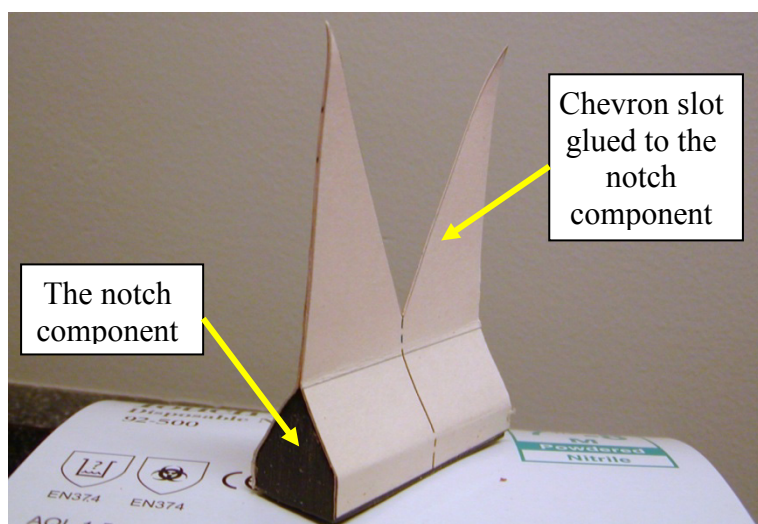


**Figure 3.4:** The chevron slot glued to the notch component

Secondly, the mould assembly was build up using a base component, two side components and seven division components, as shown in Figure 3.2. In preparing the mould it is essential to lubricate the parts and ensure that they fit together tightly to prevent any leaking. A well lubricated mould makes extracting the test specimen easy and it does not interfere with its chemical structure. The finished ready to use mould is shown in Figure 3.5.

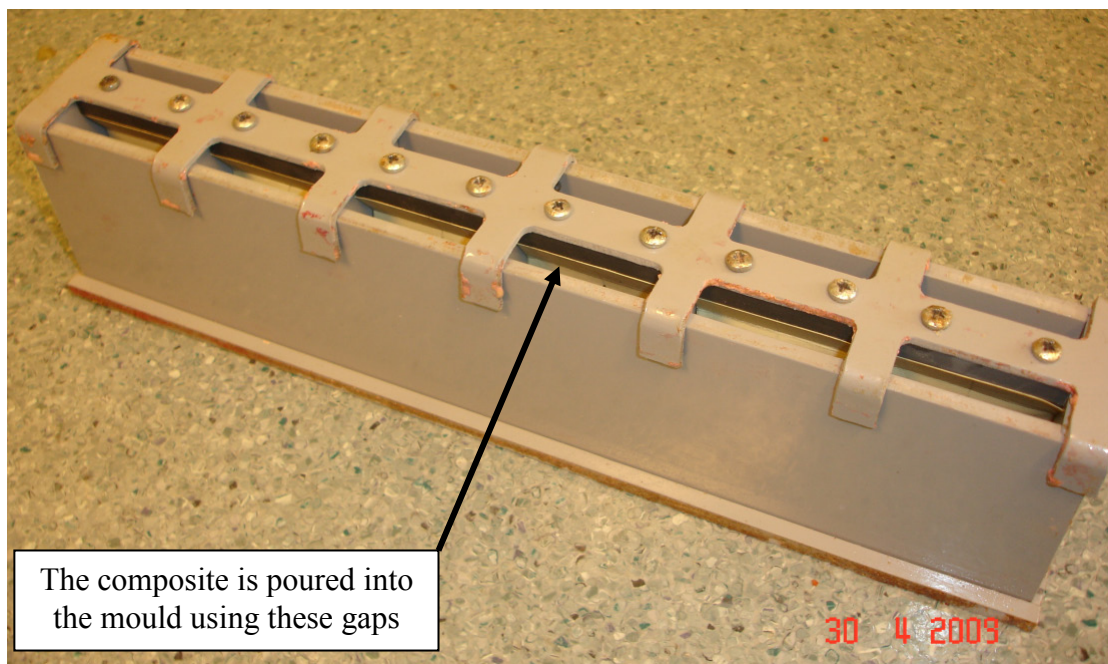


Figure 3.5: The Assembled mould ready for pouring.

### 3.4 Composite Preparation

An appropriate range of the filler percentages has to be selected. This range will depend on the ability of the filler, calcium carbonate, to mix with the resin. Therefore, a few test mixes were conducted. The mixing and pouring processes became extremely difficult at 45% by weight of the filler. Consequently, it was decided that the mixtures would be done up to 40% by weight of the filler, in steps of 5%.

The amounts of resin needed to be used in the mixes have to be estimated. It is more convenient to estimate the weight of the resin required, than estimating the volume of the resin required, since all the mixtures are calculated as percentage by weight. Therefore, the following formula was used to calculate the mass of the resin required based on the density of the resin and the volume of the specimens:

$$m = RD_{VE} \times \rho_{H_2O} \times V \times N \quad (3.1)$$

where  $m$  is the mass of the resin needed to be mixed (g);  
 $RD_{VE}$  is the relative density of vinyl ester resin (see Table 3.1);  
 $\rho_{H_2O}$  is the density of water (g/cm<sup>3</sup>);  
 $V$  is the volume of the specimen (cm<sup>3</sup>); and  
 $N$  is the number of specimens that the mould produces.

$RD_{VE}$  is listed in Table 3.1 and it is equal to 1.1. The density of water is 1 g/cm<sup>3</sup> at 20°C. The volume of the specimen,  $V$ , can be determined by two different methods. The first is calculating the specimen volume using the specimen dimensions provided in Appendix B,

Figure B.2. The second method is using a graduated cylinder. The graduated cylinder is filled half way and then the starting volume is recorded.

Afterwards, the specimen is inserted into the graduated cylinder and the finish volume is recorded. Finally, the volume of the specimen can be calculated by subtracting the final volume from the starting volume. The volume of the specimen was determined using the second method and was equal to 151.239 cm<sup>3</sup>.  $N$  is equal to six, since the mould can fit only six specimens.

Thus, using equation (3.1) the mass of the resin needed to be mixed is:

$$\begin{aligned}
 m &= RD_{VE} \times \rho_{H_2O} \times V \times N \\
 &= 1.1 \times 1 \frac{g}{cm^3} \times 151.239 \text{ cm}^3 \times 6 \\
 &= 998.177 \text{ g}
 \end{aligned}$$

Therefore, 1000 grams (g) of the resin mixture will be enough to fill the mould. After that, the mass of the constituent materials to produce the desired composition with the total adding up to 1000g can be determined. The resin hardener ratio used in the experiment was 98% resin by weight and 2% hardener by weight (Astrom 1997). Table 3.1 lists the mixture constituents derived for each mixture percentage, based on 10% by weight mixture. The tables for other mixtures are in Appendix C.

**Table 3.1: Weight of materials required to make 1000 g of VE/CaCO<sub>3</sub> (10%).**

<b>Parameters \ Materials</b>	<b>Resin (R)</b>	<b>Catalyst (C)</b>	<b>R+C</b>	<b>CaCO<sub>3</sub></b>	<b>VE/CaCO<sub>3</sub></b>
<b>Relative density</b>	1.1	1.0	--	2.85	---
<b>Percentage by weight of the resin and catalyst mixture</b>	98%	2%	100%	--	--
<b>Net percentage by weight in 1000g of VE/CaCO<sub>3</sub></b>	88.2%	1.8%	90%	10%	100%
<b>Weight of material in 1000g of VE/CaCO<sub>3</sub> (10%)</b>	882 (g)	18 (g)	900(g)	100 (g)	1000 (g)

It is essential to take all the safety precautions before handling the materials (refer to section 4.3). Fundamentally, personal protective equipment (PPE) is required during this process, such as fully covered shoes, a face mask, gloves and goggles. Additionally, all the mixing must be done in the exhaust cabinet to avoid exposure to toxic fumes.

With the compositions calculated, the three materials can be measured out. It is important that the materials are measured out accurately to ensure that the actual composition matches the quoted composition.

For ease of mixing and more accurate measuring, the resin and the filler are measured in separate containers. The calcium carbonate is then added to the resin and thoroughly mixed.

With the calcium carbonate completely mixed into the resin the catalyst is measured directly into the mixture by zeroing scales. This method is more accurate than if the catalyst is first measured into another container, because droplets of the catalyst would be left in that container which could be a significant percentage of the catalyst, since the total catalyst is only a few grams.

Once the catalyst is added, the composite mixture should be stirred until it becomes a consistent colour and texture.

After mixing is complete the mixture is poured into the moulds which should have been prepared prior to the mixing process. The composites are then left in the mould overnight to cure.

Finally, the specimens are carefully removed from the mould and labelled by designating a specimen number (1-6) and percentage of the filler.

Figure 3.6 shows the apparatus used in the composite preparation process.

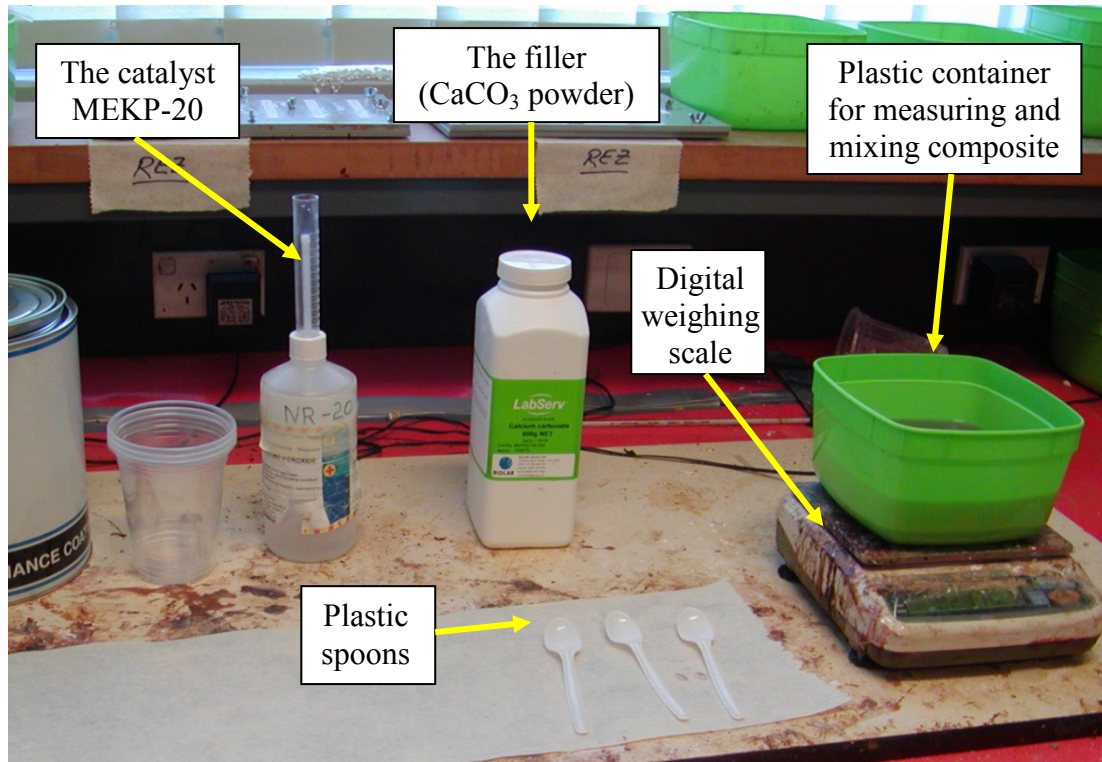


Figure 3.6: Apparatus used in the composite preparation process.

### 3.5 Curing

Initial curing of the specimens took approximately 12 hours at room temperature in the moulds. This allowed the specimens to harden and be removed with no deformation.

Once the specimens were removed they were post-cured using an oven, as shown in Figure 3.7. The oven model used is a Steridium laboratory oven.



**Figure 3.7: The Steridium laboratory oven used for the post-curing process of the specimens**

The post-curing process is done to ensure that the specimens are fully cured before testing, and explicitly to help fully cross-link the polymer chains. The oven curing involves three stages at different temperatures, these were;

- 4 hours at 50°C;
- 4 hours at 80°C; and
- 2 hours at 100°C.

It was observed that the specimens colour became darker after the ten hours post curing cycle. All the specimens were cleaned from any excess resin from the upper face of the test piece surface, where the composite would puddle as a result of the resin expanding slightly in the early stages of curing. The excess resin was simply

filed back using a normal file. It was also noted that the top surface of the specimen contained porosities, which was possibly caused by resin expansion. Finally, the specimens were then ready to be tested.

## **3.6 Problems During Methodology**

Various problems were encountered during the preparation of the specimens. These problems may have affected the accuracy of the results.

### **3.6.1 The Mould**

The mould used to cast the specimens suffered from several problems. The mould was used several times by other students. The repeated use and cleaning of the mould created various cracks and bends in the mould. This had a minor effect on the geometrical configuration of the specimens, which could cause adverse effects on the accuracy of the results.

Moreover, the mould parts did not fit together perfectly. As a result, the composite started to leak out of the mould before the initial curing process was complete. However, this problem was solved by applying wax around the edges of the mould to prevent leaking, as illustrated in Figure 3.8.

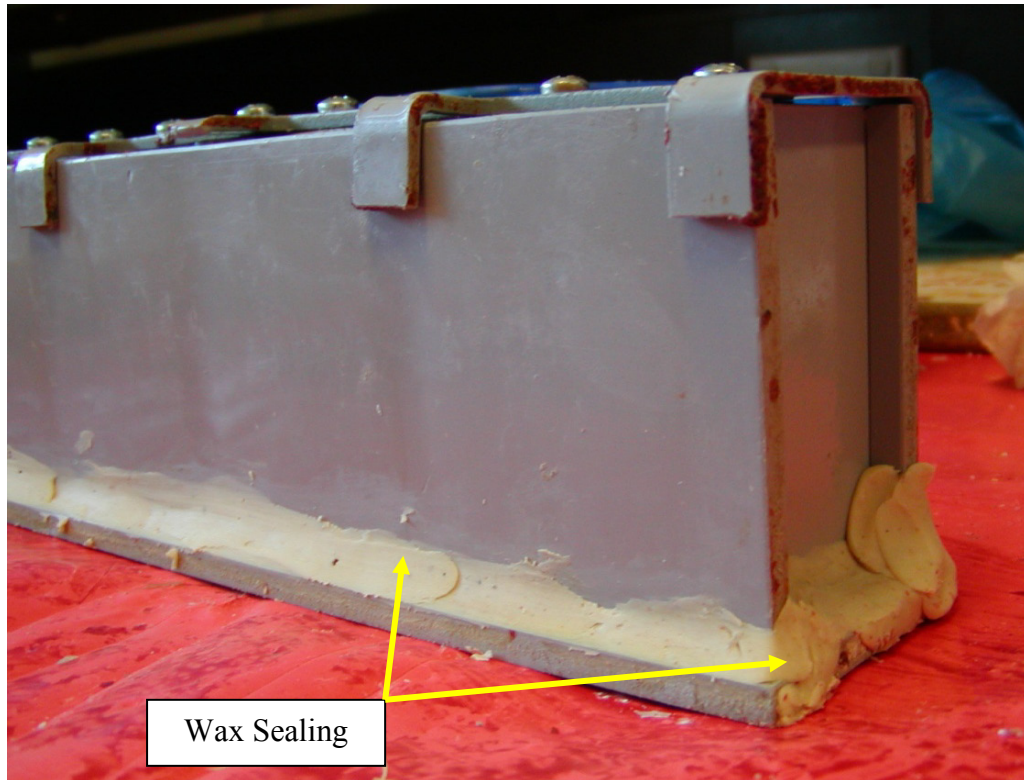


**Figure 3.8:** Wax sealing applied around the mould edges to prevent leaking

### 3.6.2 Chevron Slots

A number of the chevron slots did not fit perfectly in the mould. Some of them were excessively wide and had to be trimmed, whilst others were small and they did not reach the edge of the mould.

Another problem encountered was the chevron slots movement, when the composite was poured into the mould. The chevron slots were sometimes moving from the center of the mould, where they should be, to one side of the mould. However, this problem was easily solved by securing the chevron slots, using plastic tape at the middle of the mould, as shown in Figure 3.9.

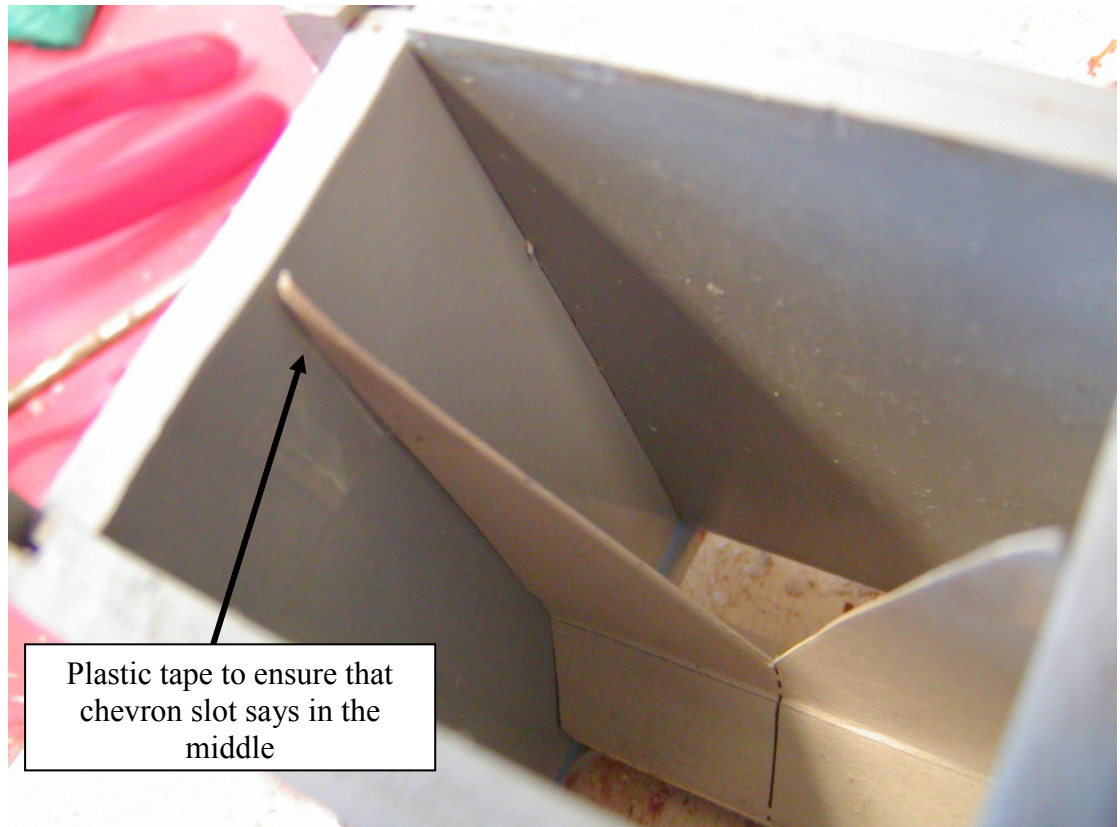


**Figure 3.9: Plastic tape is applied to the chevron slot to ensure that it will not move when the composite is poured in.**

## **Chapter 4 - Consequential Effects of Project**

### **4.1 Sustainability**

Since vinyl ester composites are already widely used in industry, it is unlikely that this project will cause any issues with sustainability apart from those that already exist. Furthermore, small amounts of specimens were produced in this project and they will cause no harm to the environment.

The biggest problem for sustainability with this composite is that it is a thermoset composite, thus, the curing process is not reversible and the composite cannot be recycled. Another factor to consider when discussing sustainability is that once the catalyst is added to the other materials, the polymer will begin to set, therefore any excess product instantly becomes waste, so it is important that only the required amount material is mixed.

### **4.2 Ethical Responsibility**

The findings from this study should encourage the use of vinyl ester composites as structural materials in certain applications, therefore it is important that results are accurately obtained and recorded. Any limitations in conducting the tests that may have any sort of effect on the accuracy of the results should be mentioned. Unexpected failure of structural components due to poor material properties would have disastrous consequences, possibly endangering human life and also resulting in a huge financial loss.

### **4.3 Risk Assessment**

Projects always involve different types of risks. In this project there are a number of risks associated with handling the composite materials, curing the specimens and the testing processes.

The handling of the composite material is done in a safely controlled environment with ventilation. Additionally, personal protective equipment (PPE) is required during both moulding and testing processes. The PPE includes fully covered shoes, face mask, gloves and goggles. In some situations, it is not necessary to wear all the PPEs. For example during the fracture test, it is not necessary to wear the face mask.

### **4.4 Risk Identification**

In any production of a material, there are potential hazards. Physical harm may occur if no proper action is taken to fix or address these hazards.

In this project there are three main types of hazards. The first type is associated with the handling of materials. For example, during the mixing of materials if the amount of the hardener added to the resin is excessively over the recommended amount, a violent reaction may occur. Additionally, the work space could be another potential hazard if the number of people using the equipment in an area is more than the value recommended by the health organisation. Testing machine is another possible risk present in this study. Harmful outcomes may occur when the machines are using high stresses for testing the specimens. All these risks will be discussed later in this chapter.

#### **4.4.1 Material Handling**

In this project the three components in making the vinyl ester composite are the filler, the vinyl ester resin and the hardener.

The following information represents the risks associated with each of the components and how to prevent the risks from occurring. Additionally, the recommended first aid procedures are also included. All the information below is extracted from the Material Safety Data Sheet (MSDS).

##### **Vinyl ester Resin (HETRON 922PAS)**

According to Nupol composites, vinyl ester resin is considered hazardous material. Vinyl ester resin can only be used in well ventilated areas. The health effects of acute vinyl ester overexposure can be very dangerous.

For example if vinyl ester resin is swallowed, it may cause irritation to gastrointestinal tract and ingestion causes nausea or vomiting. Vomiting may lead to aspiration of the material into the lungs and cause coughing, dyspnoea, and pulmonary oedema. Moreover, if it comes in to contact with the eye or the skin, it can cause damage to the affected areas. Additionally, if vinyl ester resin vapor is inhaled poisoning can occur.

To prevent these risks, one has to wear the proper PPEs. PPEs are very essential in reducing the risks. For example, eye contact can be avoided by wearing the safety goggles. Moreover, skin contact can be avoided by wearing neoprene or nitrile rubber gloves. Another way to prevent risk is no eating, drinking or smoking until washing hands thoroughly after handling the resin.

If any of the risks occurred, one has to seek immediate medical advice, and follow the recommended procedure according to the situation of the victim.

### **The Hardener (MEKP)**

MEKP is a colourless solution of Methyl Ethyl Ketone Peroxide in dimethyl phthalate, with 9% active oxygen (Sweet 1999). MEKP is classified as organic peroxides which are toxic and may be severe irritants and sensitizers to skin and eyes. The organic peroxides are also highly flammable and may decompose with explosive violence if not handled correctly. If MEKP is to be exposed to high temperatures or contamination with foreign materials, explosive decomposition may occur (Sweet 1999). MEKP is a strong irritant and can be fatal if ingested. If MEKP contacts with the eye, it may result in irreversible blindness.

If swallowed, large quantities of milk or water need to be taken and followed by consulting a physician immediately (Ku 2003). If contacted with the eyes, flush the eyes immediately with water for at least 30 minutes, and call a physician. While working with MEKP, protective equipment should always be worn, and these include goggles, gloves, protective clothing, and a respirator.

### **The Filler (Calcium carbonate)**

The filler is calcium carbonate produced by Biolab (Aust) Limited. Calcium carbonate is not classified as hazardous according to the criteria of NOHSC.

## 4.5 Testing

The universal tensile testing machine used for the testing is relatively safe. Nevertheless, this machine is capable to produce very large forces if used incorrectly thus, it can be very dangerous. For example if the user is not sure what each button on the machine does, he/she could accidentally activate the hydraulic actuator, possibly crushing his/her hand or arm.

Another hazard worth to be noted is that the machine is hydraulic. Being hydraulic, the pressure in connecting pipes can be extremely high. Thus, if any failure occurs to the pipes, the broken pipes may come off and whip the person. Furthermore, if the oil from the broken pipes is hot, the person may get burnt. In testing higher strength materials, the shroud must be down because fragments of failed materials may strike the user.

The possibilities of the risks mentioned above have an extremely low chance of happening. Nevertheless, the user should be aware of all possible hazards associated with the equipment being used.

## 4.6 Risk Control

Prior to performing any experiment, it is advisable go through the MSDS. Moreover, to reduce the risks associated with this project further, a flow chart Figure 4.1 is created. This chart will ensure complete understanding of the task, which will help to increase safety.

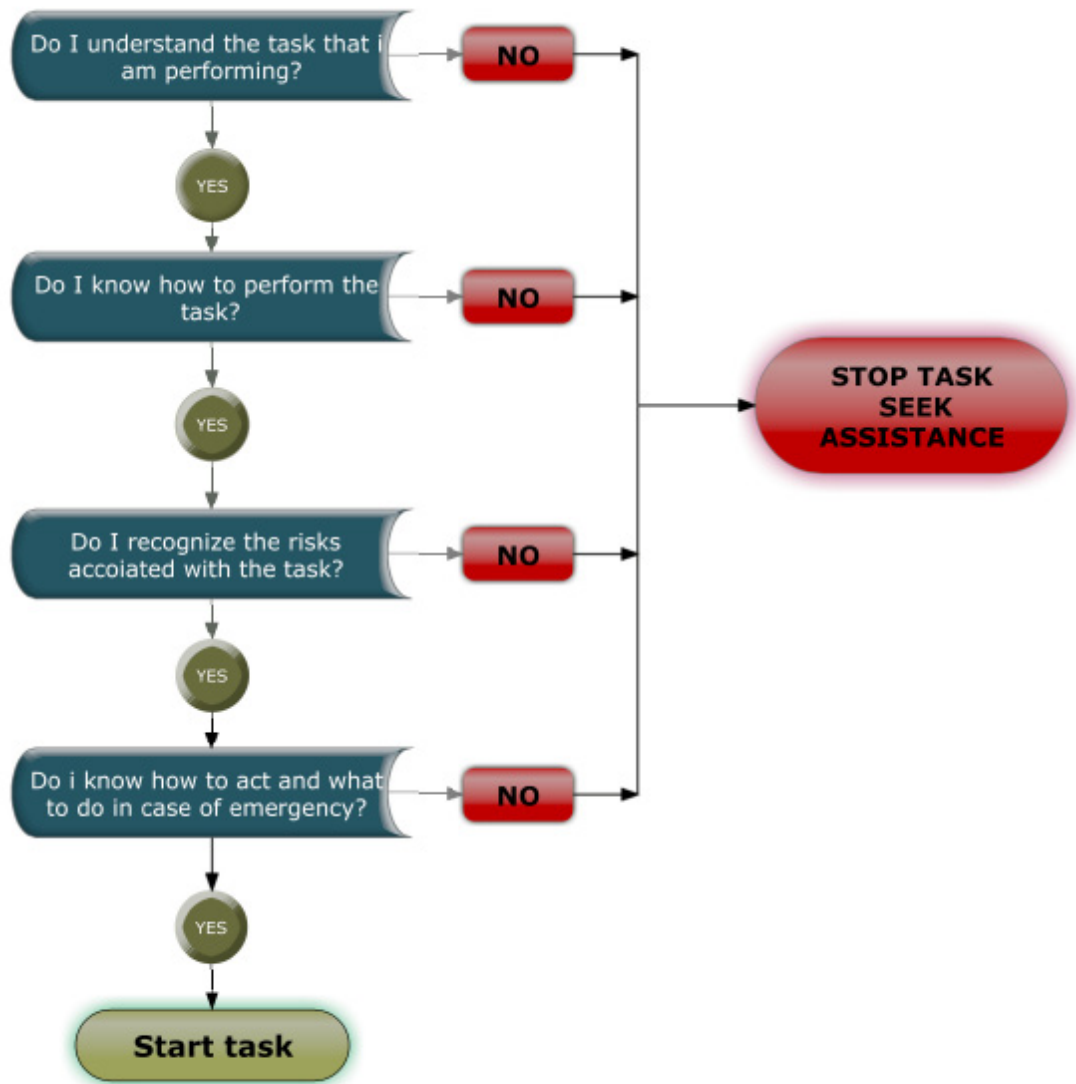


Figure 4.1: Risk Identification and control chart

## Chapter 5 - Fracture Mechanics

### 5.1 Introduction to Fracture Mechanics

The concept of fracture mechanics is to develop methods to predict and calculate the maximum load-carrying capacities of materials containing flaws or cracks of some size even if only sub-microscopic (Campbell 1982).

Since the early twenty century, engineers and metallurgists were trying to explain brittle fracture of materials that behaved in ductile manner in the laboratory strength tests. The fracture occurred at stress well below the net section with very little apparent plastic deformation and minimum absorption of energy, therefore theory was needed to reconcile these conflicting observations.

A famous example of a brittle fracture was the fracture of the World War Two tanker that occurred regardless of the steel grade that exhibited normal ductility as shown in Figure 5.1. George Rankine Irwin at the Naval Research Laboratory in Washington, DC led the research to investigate the problem. It was the research during his period that resulted in the development and definition of linear-elastic fracture mechanics (LEFM) (Shukla 2005).

Additionally, in the 1950's the aviation history experienced frequent fracture failures of the Comet, the first commercial jet aircraft produced in Britain, which strangely exploded while in level flight. Eventually, the cause was found to be a fault in the window design (Wells 1955). Small cracks were found at the windows of the aircraft and were caused by insufficient local reinforcement in combination with square

corners, which produced higher stress concentration and initiated the cracks into the airplane (Shukla 2005).

In addition to the examples mentioned, numerous bridges, train wheels and heavy equipment also suffer from the same problem (D. Antolovich & F. Antolovich 2002).

It is justifiable to point out that the scientific curiosity towards fracture mechanics became a significantly important engineering discipline after those unfortunate failures. Consequently, research and developments in the field of fracture mechanics was extensively initiated.

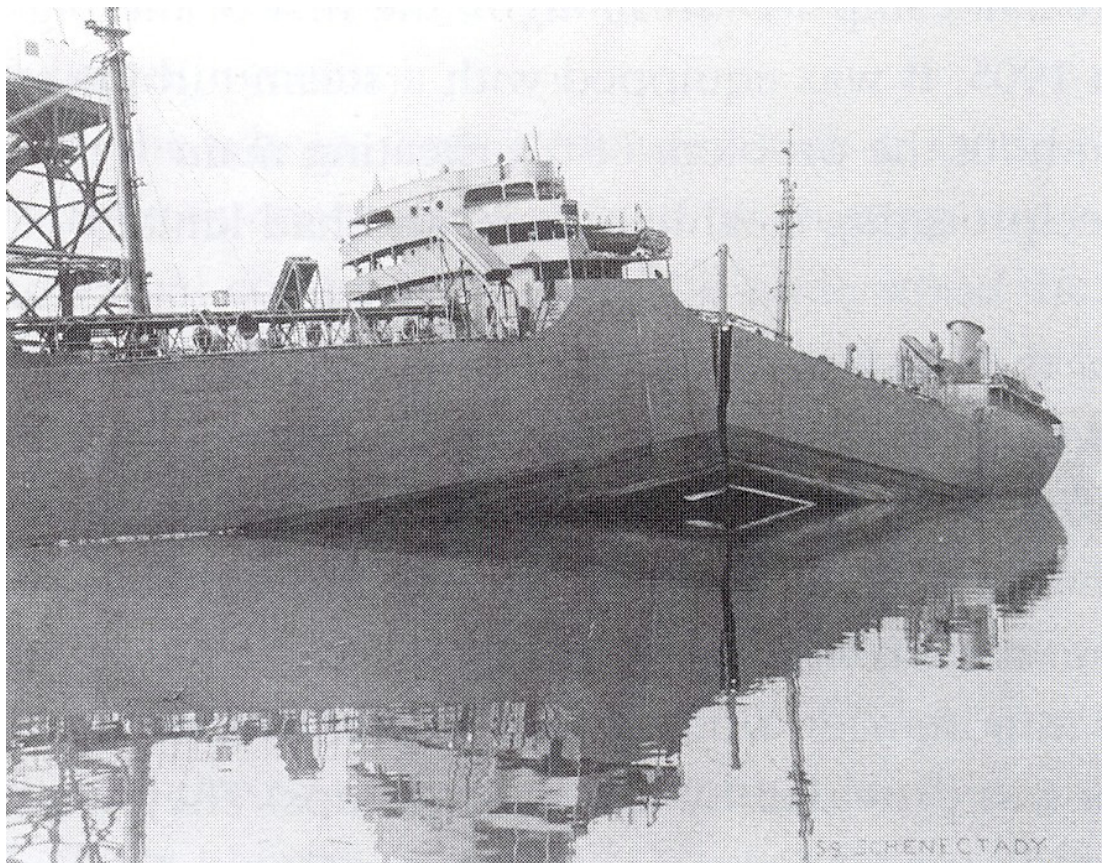


**Figure 5.1: S.S. Schenectady. T-2 tanker, broken in two in fitting-out dock, Portland, Oregon, January 16, 1943. (Source: Juvinal 1967, p. 71)**

## 5.2 Categories of Fracture Mechanics

Fracture mechanics is fundamentally divided into two categories, Linear Elastic Fracture Mechanics (LEFM) and Elastic-Plastic Fracture Mechanics (EPFM). LEFM, studies the behaviour of materials where cracking is assumed to take place under elastic conditions. Furthermore, LEFM assumes that the crack tip is sharp, with a limited amount of plasticity.

However, there are limitations to LEFM applications. Lower-strength steels can behave in a relatively plastic manner, so they are not easily characterized by LEFM. Consequently, EPFM evolved from LEFM for the study of more ductile materials. EPFM assumes that the crack tip is not sharp and that there is a degree of crack tip plasticity (Blinn & Williams 2002).

## 5.3 Fracture Toughness

Fracture toughness is a property that measures material resistance to the extension of a crack (Pollard & Fletcher 2005).

Essentially, the fracture occurrence can be stable or unstable. An unstable crack extension is often related with a brittle fracture event upon which the fracture occurs at a well-defined point and, fracture characterization can be given by a single value of the fracture parameter. On the other hand the stable fracture is often associated with a ductile fracture process where the fracture is an ongoing process that cannot be readily described by a point (Landes & Herrera 1989).

Fracture toughness is a material property that is determined experientially by one or more of a number of standard fracture toughness test methods. The standard fracture

toughness test methods are mostly for metal. Nevertheless, for many non-metals such as polymers, the equivalent standard for metals can be adapted.

Typically, a fracture toughness test can be accomplished by applying tensile stress to a specimen prepared with a flaw of known size and geometry (Figure 5.2).

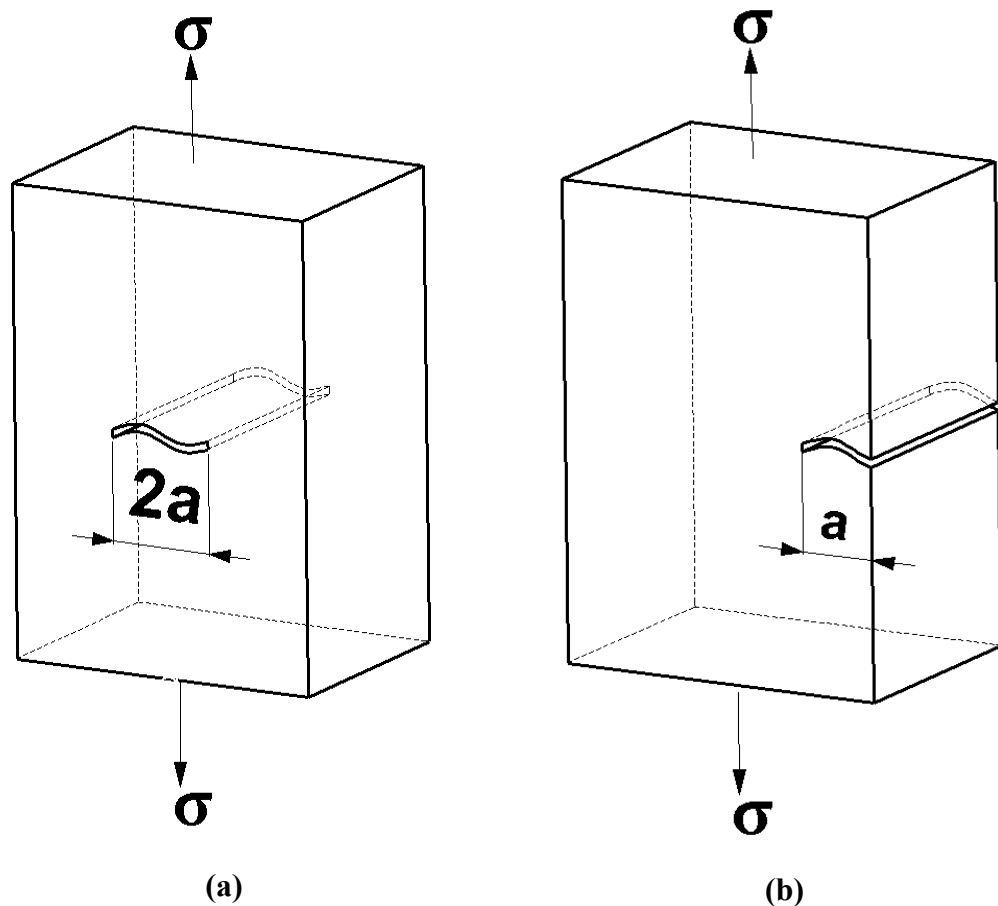


**Figure 5.2: Schematic drawing of fracture toughness specimens with (a) edge and (b) Internal flaws. (Source: Juvinal & Marshek 2006, p.232)**

As a result of the stress concentration at the flaw, the stress applied to the material is intensified at the flaw, as shown in Figure 5.3 (Askeland 1999).

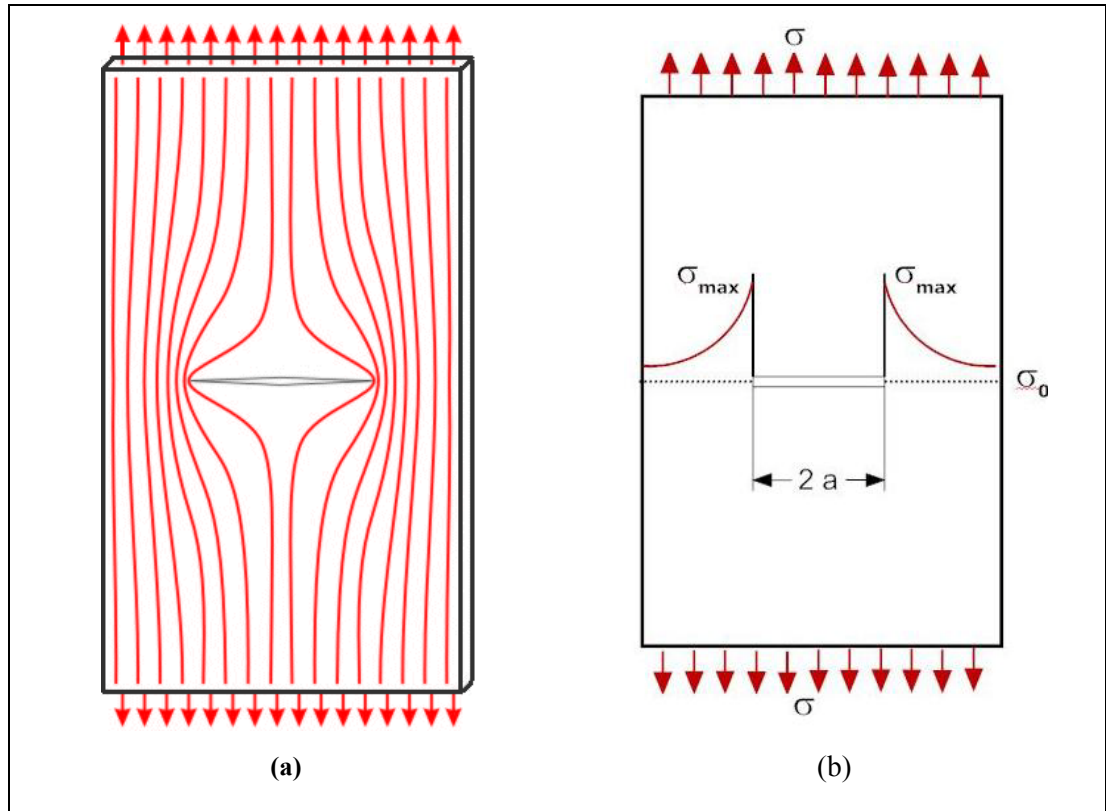


Figure 5.3: (a) crack force lines (b) demonstrating stress amplification at the flaw tips

For a simple stress loading case the stress intensity factor,  $K$ , is:

$$K = f\sigma\sqrt{\pi a} \quad (5.1)$$

where,  $f$  is the geometry factor for the specimen and flaw  
 $\sigma$  is the tensile stress applied to the specimen  
 $a$  is the flaw size

From equation 5.1 above, it can be seen that the stress intensity factors depend on the loading as well as the geometric configuration of the part and the flaw. The stress-intensity value for a given applied stress increases with increasing crack length, and for a given crack length increases with increasing applied stress. According to Asklund (1998), for a specimen that has infinite width with a through-thickness crack  $f \cong 1.0$  and for a specimen that has semi-infinite width  $f \cong 1.12$ .

The limiting value of  $K$  necessary for crack propagation in the material is called fracture toughness, or critical stress intensity factor,  $K_c$ , thus

$$K_c = f\sigma_c\sqrt{\pi a} \quad (5.2)$$

where,

$K_c = K$  needed to cause crack propagation

$\sigma_c$  is the stress to cause fracture

There are three methods of applying a force to cause a crack to propagate (Figure 5.4). The first method, called Mode I, is achieved by applying tensile loading perpendicular to the crack surfaces. The nomenclature for  $K_c$  is modified to include the loading mode. For example,  $K_{Ic}$  is the critical stress-intensity factor or fracture toughness under Mode I loading. The second and third methods pertain to shear loading and are called mode II and mode III. The fracture toughness in this case is denoted as  $K_{IIc}$  and  $K_{IIIc}$ , respectively (Wang 1996).

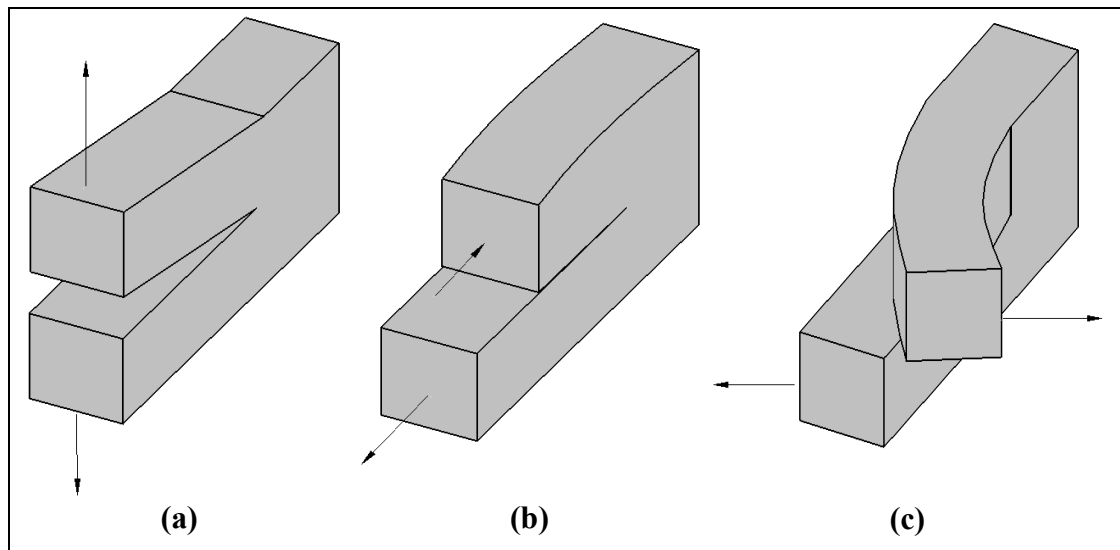


Figure 5.4: Three fracture modes, (a) opening mode (b) In-plane shear (c) out-of-plane shear

Fundamentally all three modes are similar; however most of the actual cracking and fracture cases belong to Mode I. A crack in the very early stage of development will turn into a direction in which it experiences only Mode I loading, unless it is prevented from doing so by geometrical confinement. For this reason, fracture mechanics is generally confined to Mode I (ASM International 2002, vo.18).

For relatively thin material,  $K_c$ , depends on the thickness of the material, However as the thickness increases,  $K_c$  decreases and become independent from the thickness.

In the case of thin plane, the crack root is in a state of plane stress. For plane stress, crack root material is free to contract in the thickness direction, making the stress in the thickness direction almost equal to zero, that is  $\sigma_3 \approx 0$ .

Furthermore, for the thick member, plane strain condition applies. For plane strain, material surrounding the crack is under stresses resisting contraction at the crack root thus, forcing the strain in the thickness direction to be almost equal to zero, that is  $\varepsilon_3 \approx 0$ . Plain strain tensile loading offer less opportunity to redistribute the high crack root' stress by shear yielding.

As a result of that, values of  $K_c$  for plain stress (thick members) are known as,  $K_{Ic}$ , and are significantly lower than those for plane stress (thin members). Therefore,  $K_{Ic}$  is known as the plain strain fracture toughness and its unit is  $MPa\sqrt{m}$  (ASTM 1999, p 422-452).

Figure 5.5 illustrates the relationship between the fracture toughness  $K_c$  and the thickness of the material. From Figure 5.5 it can be found that, as the thickness of the material increases the fracture toughness  $K_c$  decreases until it reaches a constant value where the condition of the plain strain exist " $K_{Ic}$ ".

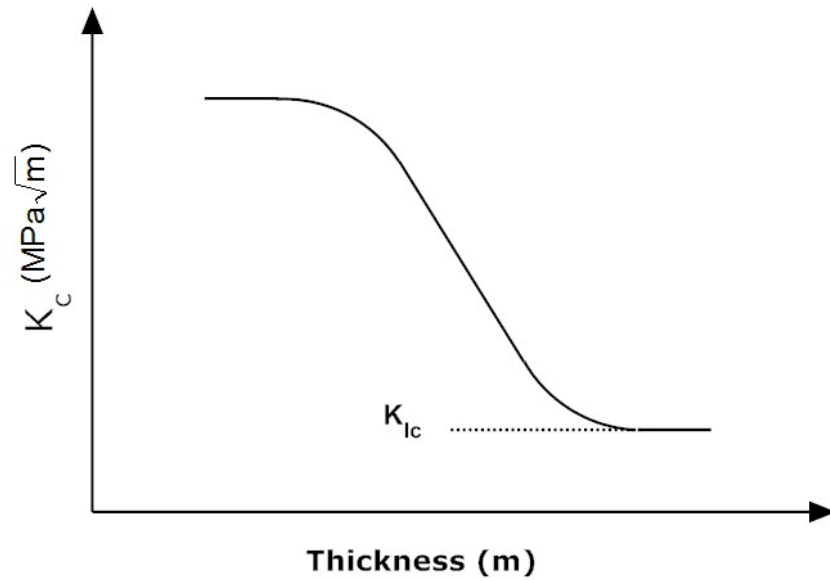


**Figure 5.5: The relationship between fracture toughness and material thickness**

Moreover, brittle materials have low  $K_{Ic}$  values and are vulnerable to catastrophic failure. On the other hand, ductile materials have high  $K_{Ic}$  values. Plane strain toughness fracture values for some polymeric materials are given in Table 5.1 (Callister 2003).

**Table 5.1: Room temperature plane strain fracture toughness and strength values for polymers**

Polymeric Materials	Fracture toughness, $K_{Ic}$ ( $MPa\sqrt{m}$ )
Epoxy	0.6
Nylon 6, 6	2.5-3.0
Polycarbonate	2.2
Polyethylene terephthalate (PET)	5
Polymethyl methacrylate (PMMA)	0.7-1.6
Polypropylene (PP)	3.0-4.5
Polystyrene (PS)	0.7-1.1
Polyvinyl chloride (PVC)	2.0-4.0
Polyester (thermoset)	0.6
Steel alloy 1040 (metal)	54

(Source: Callister 2003, p.787)

The ability of a material to resist the growth of a crack depends on a large number of factors. The ability of the material to deform and flaws size in the material are critical factors. Larger flaws reduce the permitted stress, therefore smaller flaw size help to improve fracture toughness. However, in ductile materials, the material near the tip of the flaw can deform, causing the tip of any crack to become blunt, reducing the stress intensity factor, and preventing growth of the crack. Increasing the strength of a given metal usually decreases the ductility and gives lower fracture toughness. Brittle materials such as ceramics and many polymers have much lower fracture toughness than metals (Askeland 2003).

Furthermore, thickness and rigidity of the material also affect the ability of it to resist the growth of a crack. Generally, thicker and more rigid pieces of a given material have lower fracture toughness than thin materials.

The rate of load application and the temperature of surrounding environment also affect the fracture toughness. Increasing the rate of application of the load, such as in an impact test, typically reduces the fracture toughness of the material. Similarly, increasing the temperature normally increases the fracture toughness (Askeland 2003).

Another factor is the grain size of the material. A small grain size normally improves fracture toughness, whereas more point defects and dislocations reduce fracture toughness. Thus, a fine-grained ceramic material may provide improved resistance to crack growth (Askeland 2003).

In certain ceramic materials, the advantage can be taken of stress-induced transformations that lead to compressive stresses in turn providing increased fracture toughness. (Askeland 2003)

### 5.3.1 Importance of Fracture Toughness

Fracture toughness is an important property that influences the material selection and design process, since the presence of flaws in the material is taken into consideration.

For example, if a crack is found in a structure, the magnitude of the maximum stress ( $\sigma_c$ ) that will cause the progression of the crack in the material can be calculated by equation 5.2 when maximum size of the flaw ( $a$ ) and the fracture toughness ( $K_c$ ) of the material are both known. Thus, the collision of the structure can be prevented by ensuring that the stress on the structure is much less than the critical calculated stress ( $\sigma_c$ ).

Similarly, if the flaw size and the applied stress are both known, the fracture toughness can be calculated using equation 5.2. This is helpful in the material selection process, for instance in this case a material that has fracture toughness large enough to prevent the crack from propagating will be selected.

## Chapter 6 - Scanning Electron Microscope

In this project, microscopic analysis is conducted on the fracture specimen to examine the failure modes of the composite and to study the effects of the filler percentage on the structural properties of the composite.

This chapter provides background information on electron microscopes and briefly explains how they work.

### 6.1 Background on Electron Microscopes

Electron microscopes are developed due to the limitations of optical microscopes, which are limited by the physics of light to 500x or 1000x magnification and a resolution of 0.2 micrometers. In the early 1930s, the optical microscope reached its limit and it was not sufficient for observing the fine details of the interior structures of organic cells, such as the nucleus and mitochondria, which required at least 10,000 times magnifications.

The Transmission Electron Microscope (TEM) was the first type of electron microscope developed according to the principle of the optical microscope except that a focused beam of electrons was used instead of light to "view" the specimen. The TEM was developed by Max Knoll and Ernst Ruska in Germany in 1931.

The Scanning Electron Microscope (SEM) was proposed in 1942 with its first commercial model available in 1965. Its late development was due to the electronics involved in "scanning" the beam of electrons across the sample (<http://www.unl.edu/CMRAcfem/em.htm>, September 2009).

## 6.2 Basic Systems of SEM

Scanning electron microscopes consist of a number of integrated systems:

- Illumination
- Vacuum
- Sample manipulation
- Signal detection and imaging

Scanning electron microscopes use a focussed beam of electrons (approximately 2-5-nm diameter) to scan the surface of the sample. Several types of detectors are used to obtain information from the sample and generate an image of the surface. The secondary electron detector provides high resolution topographical details. This is the most common method of viewing samples in the scanning electron microscope.

The backscattered electron detector can show areas in the sample with different average atomic numbers, indicating differences in composition. X-ray detectors may be used to determine the elemental composition of the sample. Photographic or digital cameras allow recording of the images (Chapman 1986). Figure 6.1 shows a diagram of the electron optical column of a typical scanning electron microscope.

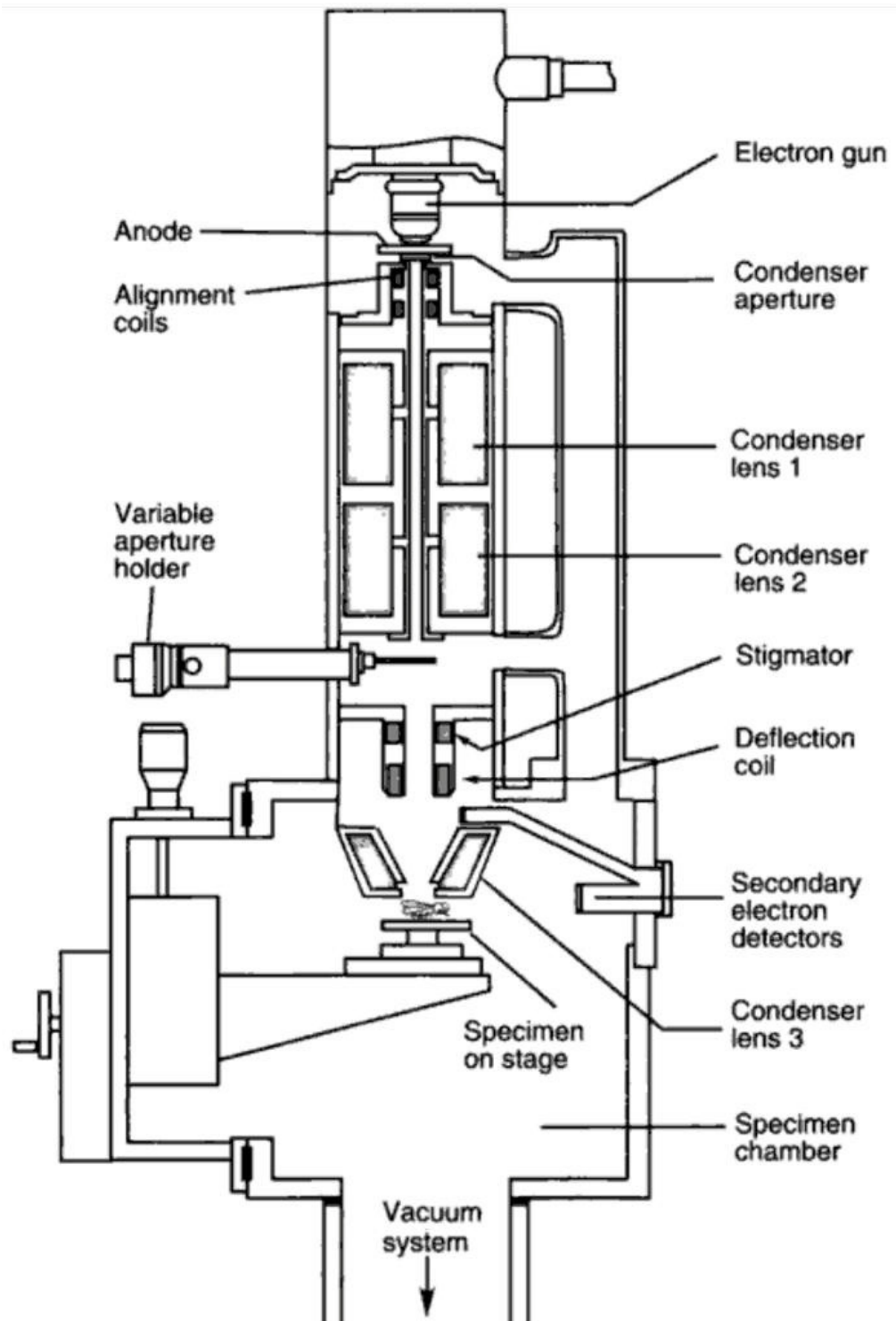


Figure 6.1: Diagram of the electron optical column of a typical scanning electron microscope.  
(Source: Bozzola & Russell 1992)

### **6.2.1 The Illumination system**

The illumination system in the SEM consists of the electron gun and the lens system.

#### **The Electron Gun**

The electron gun is made of three components: the filament, the Wehnelt cylinder, and the anode.

- The filament is the source of electrons in the SEM and it is usually made of tungsten wire. High voltage is applied to the filament to increase its temperature. Once the filament is heated, it starts to emit electrons.
- The Wehnelt cylinder is a cap-like structure with a small aperture used to guide the electrons into the imaging system. It is maintained at high negative potential to repel the electrons going through it.
- The anode is a positively charged aperture disc which is positioned directly under the Wehnelt assembly to attract the electrons.

Electron emission from the electron gun results in a bright and focussed spot of electrons, approximately 50 $\mu$ m diameter. This spot is the illumination source for the scanning microscope (Bozzola & Russell 1992).

#### **The Electromagnetic Lenses System**

The system of the electromagnetic lenses governs the control and refinement of the electron beam after it leaves the electron gun.

The lenses used in the scanning electron microscope are all electromagnetic lenses. The electromagnetic lenses consist of coils of copper wire, surrounding a soft iron

centrepiece or pole piece. Therefore, when a direct current is applied to a lens, a magnetic field is generated.

The condenser lenses in the scanning electron microscope focus emerging electrons from the electron gun onto the sample. These lenses also control the level of illumination or brightness and they can alter the size of the illumination (Chapman 1986).

Typically, a series of condenser lenses are used to demagnify the 50 $\mu$ m spot to approximately 2-50 nm diameter spot. There may be two or three lenses as follow: first condenser lens (C1), second condenser lens (C2), and final condenser lens (C3).

C1 is a high strength lens capable of demagnifying the size of the 50 $\mu$ m spot, from the electron gun, and produces approximately 80% of the total demagnification.

Furthermore, C2 is relatively weak lens that demagnifies the C1 around 15% of the total demagnification. The currents for C1 and C2 are usually controlled together as “spot size” control. The spot size regulates the number of electrons entering the rest of the lens system.

Finally, C3 lens demagnifies the C2 spot approximately 5% of the total demagnification and projects the spot onto the sample. C3 lens is the strongest lens in the scanning electron microscope and acts to focus the beam of electrons on sample. This final lens is used primarily to fine-tune the spot size without a loss of beam electrons (Bozzola & Russell 1992).

### 6.2.2 The Vacuum System

During the scanning process, the samples in the scanning electron microscope have to be in vacuum. The vacuum is needed for the following reasons:

- to increase the main free path of electrons;
- to prevent high voltage discharge in the gun region;
- to prevent oxidation of the filament; and
- to remove contaminating gases.

The vacuum system consists of several vacuum pumps, vacuum gauges, and switches and valves (Bozzola & Russell 1992). Figure 6.2 shows a diagram of the vacuum system of a scanning electron microscope (note: in Figure 6.2, A1-3, E1-2 are valves and IG is gauge).

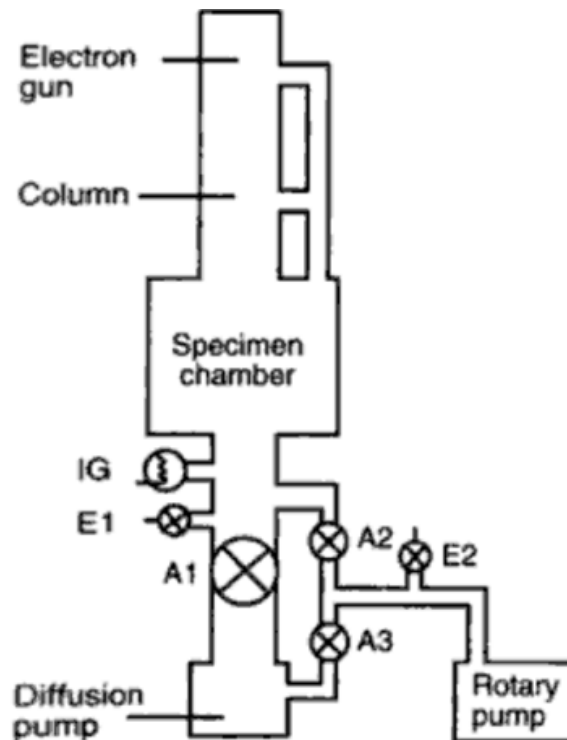


Figure 6.2: Diagram of the vacuum system of a scanning electron microscope  
(Source: Bozzola & Russell 1998)

### 6.2.3 Sample Manipulation System

Inside the scanning electron microscope, the samples are placed on support stubs. Stubs are usually made of aluminium; however there are other types available such as, carbon and steel stubs.

The sample stage, is part of the manipulation system, responsible for moving the sample in x and y directions. Additionally, the sample height may be adjusted, that is, the z direction. Moving the sample in the z direction affects resolution, strength of signal and size of sample that can be examined (Goldstein et al. 1992).

Furthermore, sample holders are also part of the manipulation system. Sample holders may allow tilt and rotation of the sample, in addition to heating and cooling. They may hold more than one stub and are usually inserted through an air lock which is evacuated via the vacuum system of the microscope (Bozzola & Russell 1992).

### 6.2.4 The Imaging System

To visualise the images obtained with a scanning electron microscope, display screen or cameras are used.

The display screen gives a visual image of electron signals collected by the secondary electron detector or the backscattered electron detector. On the other hand, a number of different formats can be used in cameras. One of the formats involves recording an image by time exposure of the face of a cathode ray tube as image, line by line, for one complete frame. Other formats may involve recording the image from a tube with high resolution and short persistence blue phosphor (Goldstein et al. 1992).

## Chapter 7 - Dynamic Mechanical Analysis

This chapter provides background information on Dynamic Mechanical Analysis (DMA). Additionally, the mechanical properties associated with the dynamic mechanical analysis, such as glass transition temperature, will also be discussed.

### 7.1 Theory of Dynamic Mechanical Analysis

DMA is a technique for measuring the mechanical properties of materials as a function of temperature, humidity, dissolution media or frequency. DMA can be also used for monitoring the change in the materials' mechanical properties (PerkinElmer Life 2007).

DMA differs from other mechanical testing in two essential ways. First of all, common tensile test devices focus only on the elastic component. However, in many applications the viscous component is important in determining properties such as impact resistance. Also, tensile test devices work mainly outside the linear viscoelastic range. DMA works primarily in the linear viscoelastic range, and is therefore more sensitive to structure (TA Instruments 2004).

Many materials, including polymers, behave both like elastic solid and viscous fluid, thus the term viscoelastic is given to such materials (Haddad 1995). DMA is the most useful method in studying the viscoelastic characteristics of polymers. It can measure the viscoelastic properties by using either transient or dynamic oscillatory tests. Transient or free oscillation techniques involve applying a force to a sample and allowing it to oscillate after the force is removed (Ku et al. 2008). For dynamic

oscillatory tests, the sample is subjected to continuous application of force. In this project, the dynamic oscillatory test was employed.

### 7.1.1 Dynamic Oscillatory Test

The dynamic oscillatory test involves the continuous application of a force to the sample. A sinusoidal stress is applied to the material and a resultant sinusoidal strain is measured as detailed in Figure 7.1.

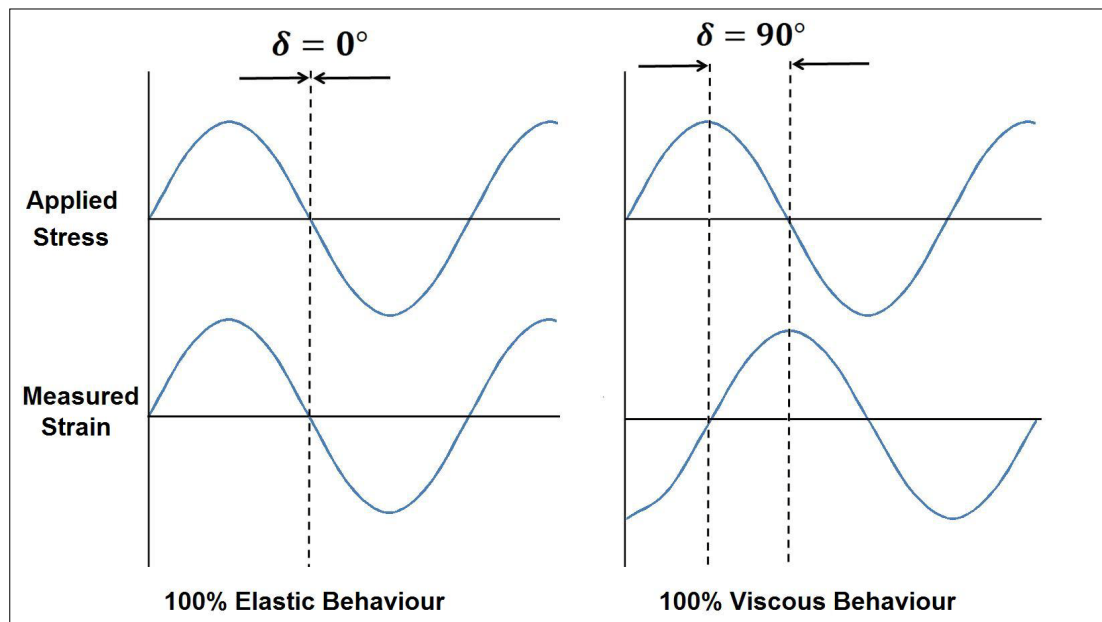


**Figure 7.1:** Phase lag of  $0^\circ$  and  $90^\circ$  indicating purely elastic behaviour and purely viscous behaviour respectively. (Source: TA Instruments 2004, p. 98)

The phase difference,  $\delta$ , between the two sine waves is measured. The phase lag will be zero degrees for purely elastic materials and 90 degrees for purely viscous materials. Viscoelastic materials, like polymers, will exhibit an intermediate phase difference (TA Instruments 2004). Figure 7.1 shows an example of purely elastic behaviour and purely viscous behaviour.

The sample deforms under the load. From this, the stiffness of the sample can be determined, and the sample modulus can be calculated. Since modulus is stress divided by strain, the complex modulus,  $E^*$ , can be calculated (Ku et al. 2008). From  $E^*$  and the measurement of  $\delta$ , the storage modulus,  $E'$ , and loss modulus,  $E''$ , can be calculated as illustrated in Figure 7.2.

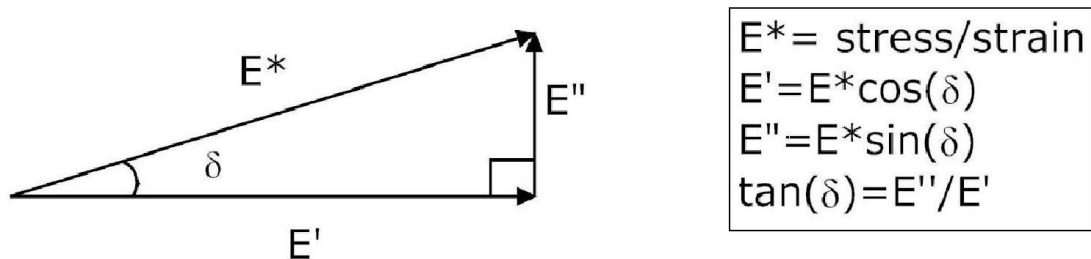


**Figure 7.2:** method of calculating the complex modulus,  $E^*$ , the storage modulus,  $E'$ , and the loss modulus,  $E''$ .

The storage modulus,  $E'$ , is the elastic component and is related to the sample's stiffness,  $E''$ . The loss modulus is the viscous component and is related to the sample's ability to dissipate mechanical energy through molecular motion. The tangent of phase lag, or  $\tan \delta$ , is another common parameter providing information on the relationship between the elastic and inelastic components. Moreover,  $\tan \delta$  is conventionally employed as a measure of internal friction. By measuring the time lag in the displacement compared to the applied force, it is possible to determine the damping properties of the material. All of these parameters can be calculated as a function of time, temperature, frequency, or amplitude (stress or strain) depending on the application (Behzad et al. 2004).

The main interest in this project is to analyse how the material preserves its properties under elevated temperatures. Therefore, all the parameters will be calculated as a

function of temperature. In this case, the DMA test is identified as Dynamic Mechanical Thermal Analysis or DMTA.

## 7.2 Glass Transition Temperature

The glass transition temperature ( $T_g$ ) is defined as the temperature at which materials change from hard and brittle to soft and pliable (Ping et al. 2008).  $T_g$  is often measured by DSC (Differential Scanning Calorimetry), but the DMA technique is more sensitive and generates much easier data for interpretation.

$T_g$  has a strong dependence on frequency but melting is frequency independent. DMA can resolve sub- $T_g$  transitions such as beta, gamma, and delta transitions whereas the DSC technique is not sensitive enough to pick them up in many materials. In addition, DMA provides modulus values (Ku et al. 2008).

Glass transition is characterised by a loss of material stiffness, which is exhibited by both the elastic modulus and shear modulus. Such degradation in properties may have serious implications on the overall performance of a structure (Davey 2004). Understanding the behaviour of this transition is essential in assessing the suitability of a polymer for certain applications.

Viscoelastic materials such as polymers typically exist in two distinct states. They exhibit the properties of glass (high modulus) at low temperatures and those of a rubber (low modulus) at higher temperatures. By scanning the temperature during a DMA experiment, the change of state, the glass transition or the alpha relaxation can be observed (Ku et al. 2008).

Cook et al. (1997) reported that the  $T_g$  strongly depended on the degree of cure of a vinyl ester resin, with a greater degree of cure leading to a higher  $T_g$ . One of the objectives of an elevated temperature post-cure is to control the rate of cure, so that a high cross-linking density is obtained and hence a high  $T_g$ .

Ziaee and Palmese (1999) studied the influence of curing cycles on the mechanical properties of vinyl ester resins. It was reported that post curing of materials performed below the “full-cure”  $T_g$ , resulted in glass transition temperatures below the ultimate full-cure  $T_g$ . However, post-curing performed above the ultimate  $T_g$  temperature, resulted in transition temperatures approaching the ultimate  $T_g$ , regardless of the initial isothermal cure temperature used.

Due to the relationship between the glass transition temperature and the degree of conversion of the mechanical structure network, the comparison of the  $T_g$  achieved after an ambient cure and after an elevated temperature post-cure, provide an indication of the initial degree of cure achieved in a network. The comparison also provides details regarding the development of properties of the network.

DMA provides three alternative values that are often interpreted as the glass transition temperature (TA Instruments 2004), namely:

- onset (extrapolated) of loss of storage modulus which occurs at the lowest temperature and relates to mechanical changes in the material;
- loss modulus peak which occurs at a middle temperature and is more closely related to the molecular changes attributed to the glass transition in plastics; and
- $\tan \delta$  peak which occurs at the highest temperature and is a good measure of the midpoint between the glassy and rubbery states.

The temperature at the peak of the  $\tan \delta$  curve appears to be the most widely applied measurement of glass transition temperature in polymer research (Li et al. 2000). Therefore, in this project the peak of the  $\tan \delta$  curve will be used to indicate the glass transition temperature.

## Chapter 8 - Dielectric Properties

Considerable effort has been invested to turn conducting polymers into useful product, because the polymers have interesting inherent electrical properties which can be used to develop novel microelectronics (Truong et al. 1994).

A dielectric material is a poor conductor of electricity, but an efficient supporter of electrostatic fields. An important property of a dielectric material is its ability to store an electrostatic field with minimal energy dissipation in the form of heat (Ku et al. 2008). The lower the dielectric loss (energy lost as heat), the more effective the dielectric material is.

Many potential applications for these materials have been proposed, such as Schottky junction, electrostatic charge protection and electromagnetic interference (EMI). All these complex applications require a need for thorough understanding of dielectric data because the nature of dielectric properties varies due to processes. That is, some materials become good conductors in some frequencies, and they turn into dielectric materials in other frequencies (Truong et al. 1994). It is also essential to increase our fundamental knowledge of dielectric properties of materials that will be processed in the microwave regime. This will play a significant role in the design of the microwave applicators (Metaxas & Meredith 1983).

### 8.1 Loss Tangent

The loss tangent ( $\tan \delta$ ) is a parameter of dielectric material. Loss tangent or dielectric loss is one of the most important properties in microwave processing because it indicates the amount of incoming electromagnetic energy loss, mostly in the form of

heat (Cardona et al. 2007). Moreover,  $\tan \delta$  is an essential material property that determines the effectiveness of the material as a capacitor.

In microwave processing, materials with high  $\tan \delta$  are favoured, because higher  $\tan \delta$  leads to higher energy loss as heat, resulting in a more effective heating process. This also helps in the curing process of polymers as it shortens the curing time. On the other hand, materials with low  $\tan \delta$  are favoured to be used in capacitors. This is because low loss tangent leads to low energy losses which result in a more efficient capacitor. Typical loss tangent values for common materials are shown in Table 8.1.

**Table 8.1: Typical dissipation factor. (Source: Bryce 1997, p.88)**

Material	Loss Tangent ( $\tan \delta$ )	
	from	to
Acetal	0.001	0.007
Acrylic	0.001	0.06
ABS	0.006	0.021
Liquid crystal polymer	0.01	0.06
Polyamide (nylon)	0.006	0.19
Polyarylate	0.001	0.022
Polycarbonate	0.0006	0.026
Polyester (TP)	0.0012	0.022
Polypropylene	0.003	0.014
Polysulfone	0.0008	0.009
PPO (modified)	0.0002	0.005
PPE	0.0002	0.005
Polyphenylene sulfide	0.001	0.002

A complex permittivity describes the behaviour of a dielectric under the influence of a high frequency field. The complex relative permittivity of a dielectric is defined by equation (8.1) (Metaxas & Meredith 1983):

$$\varepsilon = \varepsilon' - j\varepsilon'' \quad (8.1)$$

where  $\varepsilon$  is the complex permittivity;  
 $\varepsilon'$  is the dielectric constant; and  
 $\varepsilon''$  is the loss factor.

The real part of the permittivity,  $\varepsilon'$  sometimes called the dielectric constant, mostly determines how much of the incident energy is reflected at the air-sample interface, and how much it enters the sample. The imaginary part,  $\varepsilon''$ , is referred to as the loss factor and it includes the effects of conductivity. The ratio of these two values is the loss tangent:

$$\tan \delta = \varepsilon'' / \varepsilon' \quad (8.2)$$

The dielectric parameters such as the real part,  $\varepsilon'$ , and imaginary part,  $\varepsilon''$ , of the permittivity and loss tangent,  $\tan \delta$ , increase with increasing conductivity and concentration of the dispersant (Truong et al. 1994). For optimum conversion of microwave energy into thermal energy, a moderate value of  $\varepsilon'$  for adequate penetration should be combined with high values of  $\varepsilon''$  and  $\tan \delta$ . It is important to note that  $\varepsilon'$  and  $\varepsilon''$  can vary with both temperature and frequency, and the extent of variation depends on the material (Cardona et al. 2007).

In dielectric materials, the local charge moves in response to an applied electric field. Within materials, a bound charge and free charge exist, and motion of the bound

charge results in polarization. Alternating polarisation of the molecules consumes energy, causing polarisation loss. Polarization of an electric charge where the translational motion is restricted, or polarization of molecules where the rotational motion is restricted, results in a lag between the electric field and the polarization. This time lag, known as the relaxation time, is due to the dissipation of energy as heat within the material. Microwave heating is a result of this dielectric relaxation (Thostenson & Chou 1999).

## **8.2 Loss Tangent Measurements**

There are two main methods used to determine the loss tangent. In the first method, the loss tangent is obtained by measuring the capacitance and conductance with a meter and then calculating the loss tangent using standard formulas. This method is commonly used because most of the standard electrical meters have the ability to measure conductance and capacitance. The second method involves using a special meter which has the ability to measure the loss tangent directly. Both methods are discussed below, starting with the first method and ending with the second.

### 8.2.1 Calculating Loss Tangent

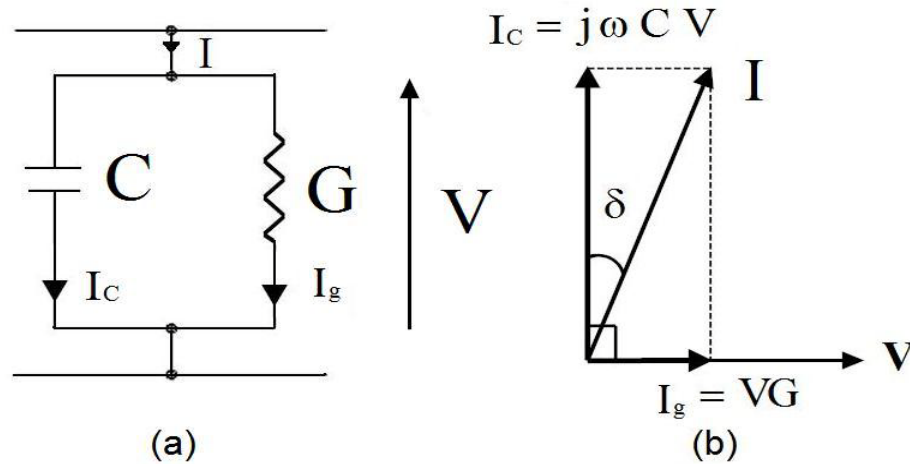


Figure 8.1: (a) parallel connection of C and G (b) Phasor diagram

Figure 8.1 (a) shows the schematic parallel connection of C and G. The distributed shunt capacitor, C and the conductance, G are both dependent on the properties of the dielectric material which separates the line conductors (Sharma 2006). The currents flow through the parallel combination of C and G as detailed in Figure 8.1 (a). The phasor relationship between C and G is shown in Figure 8.1 (b).

From the measurements, the real and imaginary parts of the dielectric loss can be calculated from the following relationships (Kraus 1992) and (Dalton & Van Genuchten 1986):

$$C = \frac{\epsilon_0 \epsilon_r A}{s} \quad (8.3)$$

where C is the capacitance in [Fm<sup>-1</sup>];

$\epsilon_0$  is the dielectric permittivity of free space =  $(1/36\pi) \times 10^{-9}$ ;

$\epsilon_r$  is the dielectric constant of the composite;

A is the surface area of the samples in [mm<sup>2</sup>]; and

s is the thickness of the composite sample in [mm<sup>2</sup>].

and

$$G = \frac{\sigma A}{s} \quad (8.4)$$

where  $G$  is the conductance of the composite in [ $\text{Sm}^{-1}$ ];

$\sigma$  is the dielectric bulk conductivity [ $\text{dS/m}$ ];and

$A$  and  $s$  are the same as above.

and

$$\sigma = \omega \varepsilon_0 \varepsilon'' \quad (8.5)$$

where  $\omega$  is the frequency in [Hz].

Rearrange equation (8.3) and solve for dielectric constant. From equation (8.6) the dielectric constant of the composite can be calculated since,  $s$ ,  $A$ , and  $\varepsilon_0$  are all known and  $C$  is measured.

$$\varepsilon_r = \varepsilon' = \frac{C s}{A \varepsilon_0} \quad (8.6)$$

To calculate the loss factor, equation (8.4) is substituted into equation (8.5). From equation (8.7) the loss factor can be calculated since,  $s$ ,  $A$ ,  $\omega$  and  $\varepsilon_0$  are all known and  $G$  is measured.

$$\varepsilon'' = \frac{G s}{A \omega \varepsilon_0} \quad (8.7)$$

Finally the loss tangent can be calculated using equation (8.2).

$$\tan \delta = \varepsilon'' / \varepsilon' \quad (8.2)$$

If the properties of the dielectric are constant over the frequency range of interest, then  $C$  will be constant and  $G$  will be proportional to frequency, and the loss tangent can be easily calculated by the equation (8.8) (Ball & Hancock 2007).

$$\tan \delta = \frac{G}{\omega C} \quad (8.8)$$

### 8.2.2 Measuring Loss Tangent

In this project, the loss tangent values were obtained directly from a meter. The meter used was the “Agilent 4263B LCR Meter” which is able to measure many electrical properties in the material, including the dissipation factor of the material. The Dissipation Factor (DF) and loss tangent are effectively the same. This is confirmed by Coombs (2001) in equation (8.9) below:

$$\tan \delta = DF \quad (8.9)$$

# **Chapter 9 – Fracture Toughness Tests and Measurements**

## **9.1 Fracture Toughness Tests**

The fracture toughness test is generally conducted on a pre-cracked test specimen. The pre-crack is a sharp crack introduced in to the test specimen by fatigue loading. The test is conducted on a machine that loads the specimen at a specific rate. Measurements of load and a displacement value are taken during the test. The data resulting from this are subjected to an analysis procedure to evaluate the desired toughness parameters (John 2002).

The American Society for Testing and Materials (ASTM) has standardised the testing procedures and specimen geometries for measuring the plan-strain fracture toughness of metallic materials.

## **9.2 Standard Fracture Toughness Tests**

In this section, most of the standard fracture toughness tests are mentioned and discussed. Additionally, the main advantages and disadvantages of each method are examined.

### 9.2.1 Plane-Strain Fracture Toughness Test (ASTM E: 399)

The “ASTM standard E 399” was the first fracture toughness test written as a standard. This test measures fracture toughness that mainly develops under linear-elastic loading with the crack-tip region subjected to near-plane-strain constraint conditions through the thickness. The test is developed for essentially ductile fracture conditions, but can also be used for brittle fracture (John 2002).

In this test, five different specimen geometrics are allowed. Additionally, all of the specimens for the  $K_{Ic}$  test must be pre-cracked in fatigue before testing.

The first two geometries are the single edge-notched bend specimen, SE (B), and the compact specimen, C (T) shown in Figure 9.1. These two geometries are traditional to fracture toughness specimen and are used in almost all fracture toughness test methods.

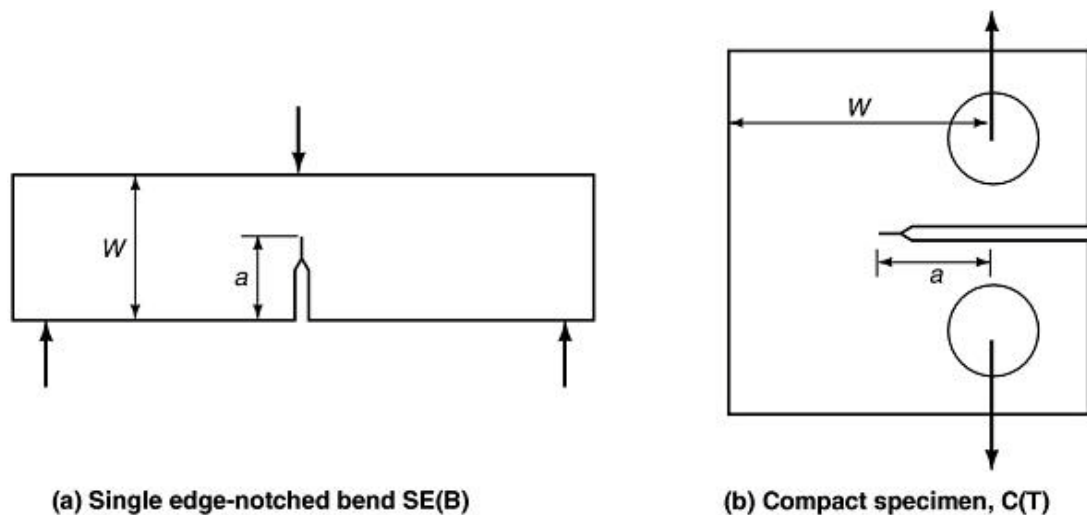


Figure 9.1: Specimens types used in the  $K_{Ic}$  test (ASTM E 399).

(a) Single edge-notched bend. (b) Compact specimen. (Source: ASM International 2002)

The other three geometries detailed in Figure 9.2 are the arc-shape tension specimen, A (T), disk-shape compact specimen, DC (T), and the arc-shape bend specimen, A (B). These geometries are less common and they represent special component structural forms.

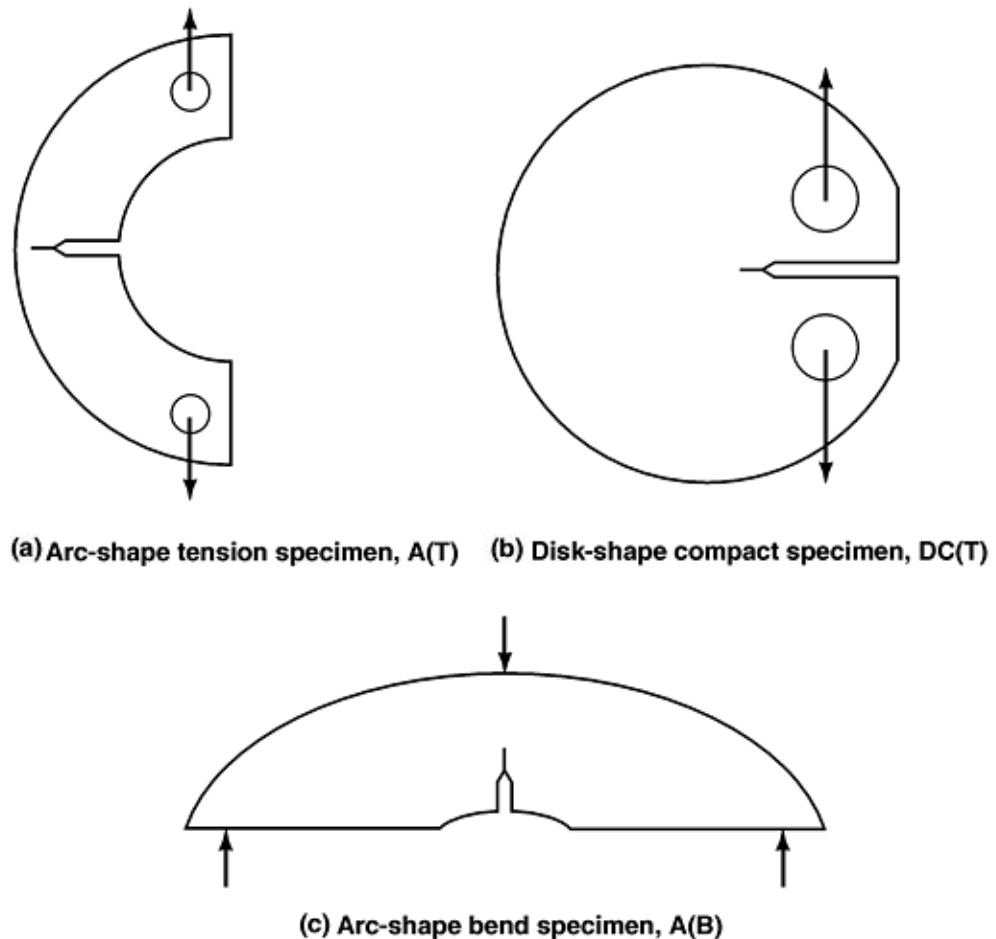


Figure 9.2: Specimens types used in the  $K_{Ic}$  test (ASTM E 399).

(a) Arc-shape tension specimen. (b) Disk-shape compact specimen.

(c) Arc-shaped bend specimen. (Source: ASM International 2002)

The  $K_{Ic}$ , ASTM E 399 testing method is the most reliable to get fracture toughness values at lower temperatures. The success of all other methods is based on their ability to give data comparable to this method.

However, one of main disadvantages of this method is the high cost of testing large number of specimens. Furthermore, this method does not provide valid  $K_{Ic}$  values at higher temperature since linear extrapolation from a valid  $K_{Ic}$  at lower temperatures to higher temperatures produces conservatism.

### **9.2.2 Other Fracture Toughness Tests**

Other standard fracture toughness testing methods are also available. These standard fracture toughness tests are briefly mentioned below, outlining the main advantages and disadvantages of each one.

#### **The $J$ -integral testing method (ASTM E 813)**

This method provides fracture toughness values that agree with  $K_{Ic}$ , ASTM E 399 testing method. Additionally, it yields realistic fracture toughness data at higher temperature and has the advantage of a sound theoretical basis, which permits evaluation of stable crack growth.

On the other hand, the “ASTM E 813” testing method suffers from several disadvantages. This method is not able to evaluate irregular crack propagation due to residual stress or at heat-affected zones near welds and it is not accurate enough at low temperatures. Moreover, measurements are inaccurate due to irregular crack fronts and it is not valid for thin materials (Venter & Hoepfner 1985).

#### **The crack-tip opening displacement method (BS 7448)**

The Crack-Tip Opening Displacement (CTOD) method provides fracture toughness values that agree with the ASTM  $K_{Ic}$  method and it yields realistic fracture toughness data at higher temperatures. CTOD results have shown good consistency and

comparability with toughness values using other methods. However, this method is restricted to temperature above  $-60^{\circ}\text{C}$  (Venter & Hoepfner 1985).

### **Simple equal energy testing method**

This testing method was developed by Griffith (1920). Griffith assumed that incipient fracture in ideally brittle materials takes place when the elastic energy supplied at the crack tip is equal to or greater than the energy required to create new crack surfaces (Irwin 1948).

The equal energy testing method is similar to the  $J$ -integral method and toughness data are identical or closely similar to  $J$ -integral data. This method also provides fracture toughness values that agree with ASTM  $K_{Ic}$  method and it yields realistic fracture toughness data at higher temperatures. Limitations in this method are similar to those of the  $J$ -integral method. This method is more empirical in nature, so  $J$ -integral testing is preferred (Venter & Hoepfner 1985).

### **The instrumented charpy testing method**

The charpy impact test is a standardised high strain-rate test which determines the amount of energy absorbed by a material during fracture. The absorbed energy is a measurement of a given material's toughness and acts as a tool in studying temperature-dependent brittle-ductile transition (Meyers & Chawla 1998).

This test requires small specimens compared to the other testing methods discussed above. It is practically suited for the determination of toughness with variations in small regions of complex parts, for example in heat-affected zones of welds, and in other locally embrittled zones. The error in fracture toughness values is small, in comparison to ASTM  $K_{Ic}$  method, for predominantly brittle failure.

Conversely, this test can provide very pessimistic values, particularly at higher temperatures. The fracture toughness values are slightly underestimated at low temperatures, but considerable scattering in measurements exists above the brittle-transition temperature within a factor of three due to small specimen size. Furthermore, it is difficult to separate the crack-initiation and crack propagation components in a fracture (Meyers & Chawla 1998).

### **9.3 Non-Standard Fracture Toughness Tests**

Standard fracture toughness tests are usually expensive and hard to fabricate. Therefore other methods were needed to determine fracture toughness, in a simple and inexpensive way. The non-standard tests meet this criterion as they are much cheaper and easier to fabricate compare to the standard testes.

Non-standard test results are related to the mechanical properties of the material. By means of mathematical models, these mechanical properties can be converted into fracture toughness value (Davey 2006).

#### **9.3.1 Charpy V-Notch Impact Test**

The Charpy V-notch impact test measures the ability of a material to resist an impact (Askeland 2003). This test involves the use of a specimen measuring 10x10x55 millimetres containing small notch to direct the crack propagation through it, as shown in Figure 9.3.

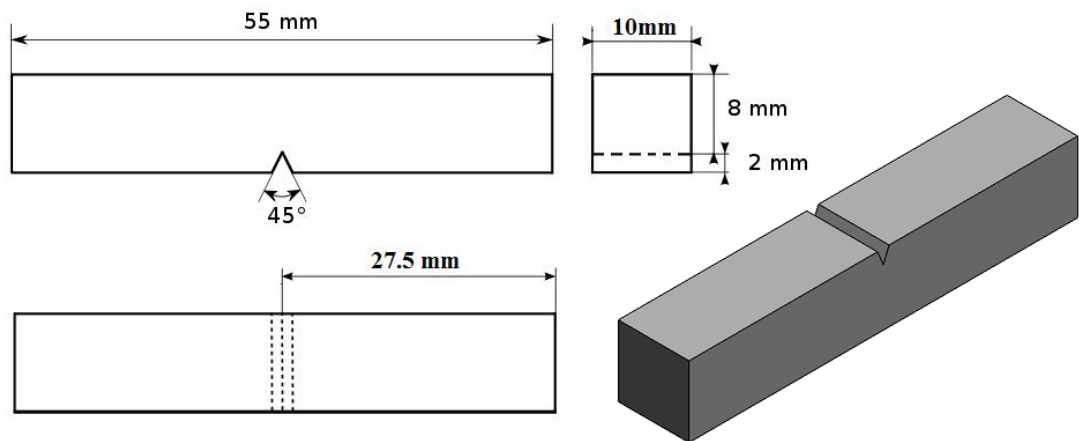


**Figure 9.3: Standard Charpy-V notch specimen.**

The specimen is subjected to a pendulum blow, as illustrated in Figure 9.4. The energy absorbed in fracturing the specimen is calculated by the height to which the pendulum rises after breaking the test piece (Askeland 2003).

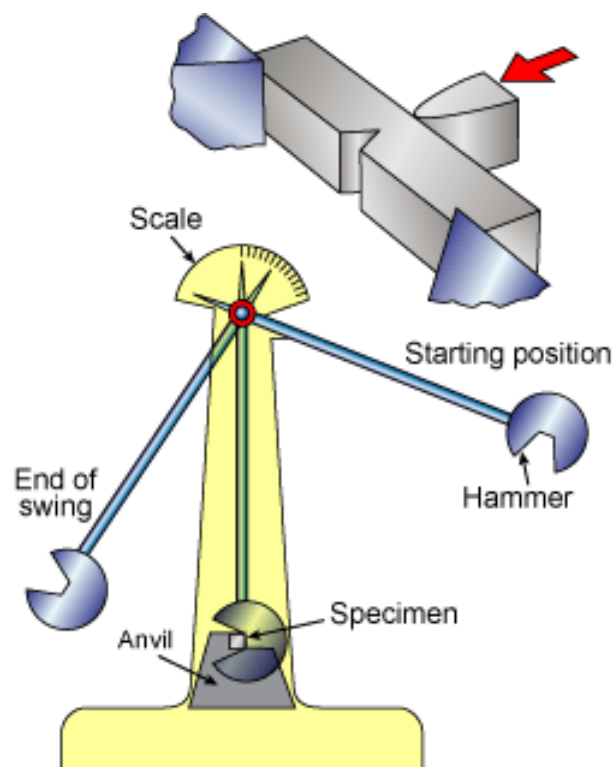


**Figure 9.4: Charpy V-notch impact test.**  
(Source: The Engineering Institution for Welding and Joining Professionals 2009).

The following equation is used to calculate the fracture toughness,  $K_{Ic}$ , via the Charpy V-notch impact test:

$$K_{Ic}^2 = 2 \times E \times \sqrt{CVN^3} \quad (9.1)$$

Where  $E$  is the modulus of elasticity of the material (Pa); and  
 $CVN$  is the Charpy V-notch test result (J).

### 9.3.2 Short Rod and Short Bar Test

The short rod/bar test method is a simple and inexpensive way to measure fracture toughness. Additionally, this method is applicable to a wide range of materials, such as metals, ceramics, polymers, and rocks. As a result, this method has gained a huge acceptance due to its simplicity and its economic advantages over other methods for determining fracture toughness (Barker 1981, pp.456-475).

The fracture toughness tests previously mentioned focus on the start of crack extension from a fatigue pre-crack. In contrast, fatigue pre-cracking is not required in this method, which is an additional major advantage over other fracture toughness tests as it simplifies the testing procedure (John 2002).

The geometries of the specimens used in this test are divided into two categories, as shown in Figure 9.5. The first category is the specimens with rectangular cross section, usually called “short bar” specimens. The second category is the specimens with round cross section or “short rod” specimens.

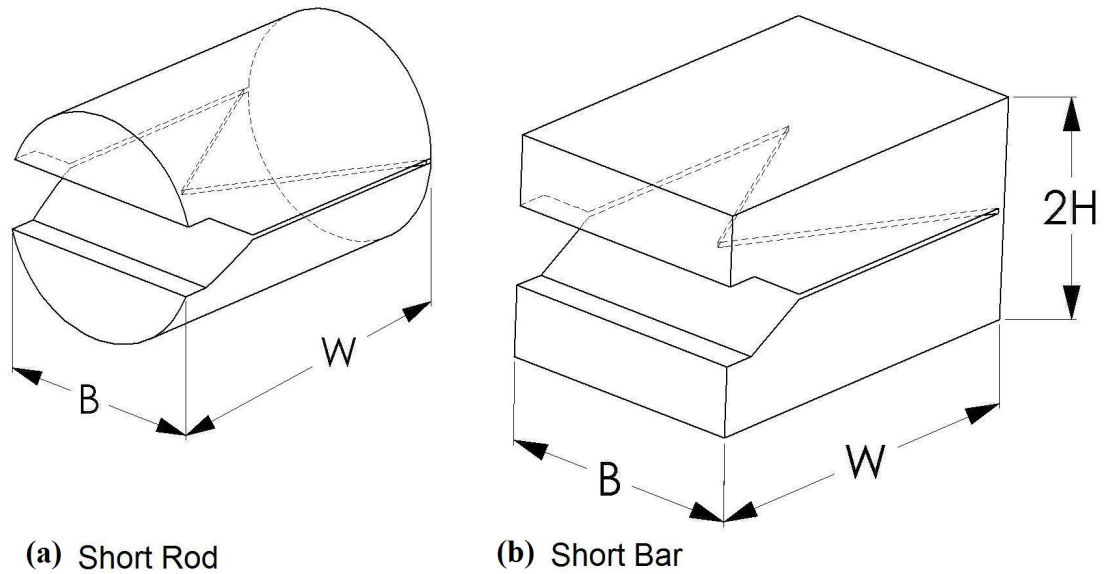


**Figure 9.5: Short rod (a) and short bar (b) and testing specimen.**

An opening load is applied to the specimen, in an attempt to fracture it. The fracture is initiated at a point called the chevron slot tip. Afterward, when the crack has developed and is in the central region of the specimen, the toughness measurement is made. Methods have been derived to calculate the plane strain fracture toughness using the peak load that the specimen can withstand and the extension in the specimen.

The short rod and the short bar test is reviewed fully in the next section.

## 9.4 Detailed Information on Short Rod and Short Bar Test

### 9.4.1 Introduction

Barker (1977) acknowledged the need to create simple and less expensive method of measuring the fracture toughness of metallic materials. Therefore, he developed a new testing method called “Short rod and short bar test”.

Short rod and short bar specimens have been shown to be applicable to a wide variety of materials, like metals, polymers, ceramics, and rocks (Barker 1981). The short rod and short bar specimens are capable to produce valid measurements using smaller specimens than other standard tests for plain-strain fracture toughness, such as the ASTM standard E399-78a. The short bar and short rod method is being used often nowadays to evaluate the impact properties of a range of materials (Barker 1981).

The geometries of the specimens used in this test are divided into two categories, specimens with rectangular cross-sections and specimens with round cross-sections. Both geometries have test characteristics that are experimentally identical. Thus, statements about one of these geometries are equally valid to the other one (Barker 1981). Therefore, only one of these two geometries is discussed in the next section, this is the **short bar** geometry.

### 9.4.2 Development of Short Bar Geometry

To select the dimensional relationships of the specimens, large numbers of tests are conducted on specimens with different length-to-diameter ratios and various chevron slot geometries. From these tests, the short bar specimen geometries are selected as a

reasonable compromise in an attempt for an optimal geometry (Barker 1981). These geometries are detailed in Figure 9.6 and Figure 9.7. The load line shown in the figures is the line along which the opening load is applied in the mouth of the specimen.

Figure 9.6 and Figure 9.7 detail two different chevron slot geometries, straight and curved chevron slots, respectively. Therefore, different methods of machining or creating the chevron slot are required.

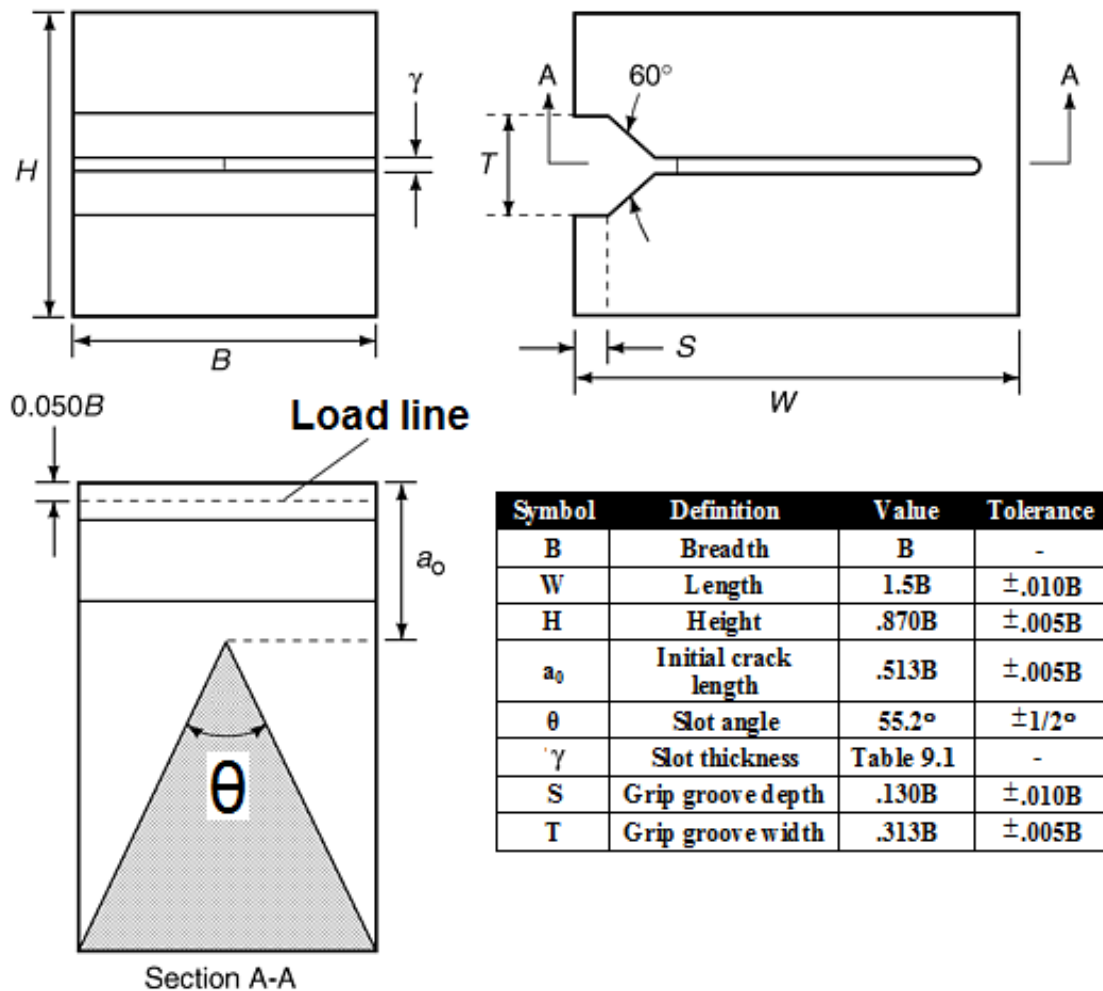


Figure 9.6: Short Bar Specimen with Straight Chevron Slots. (Source: Barker 1981, p. 457)

Straight chevron slots Figure 9.6 are created by feeding a saw or cutter through the specimen or by placing a thin piece of material cut to size into the mould before pouring.

The curved chevron slots Figure 9.7 are created from a plunge-type feed of a saw blade into the specimen. The modern way to produce the slot is to use electro discharge wire cutting (EDWC) (Baddeley & Ballard 1991).

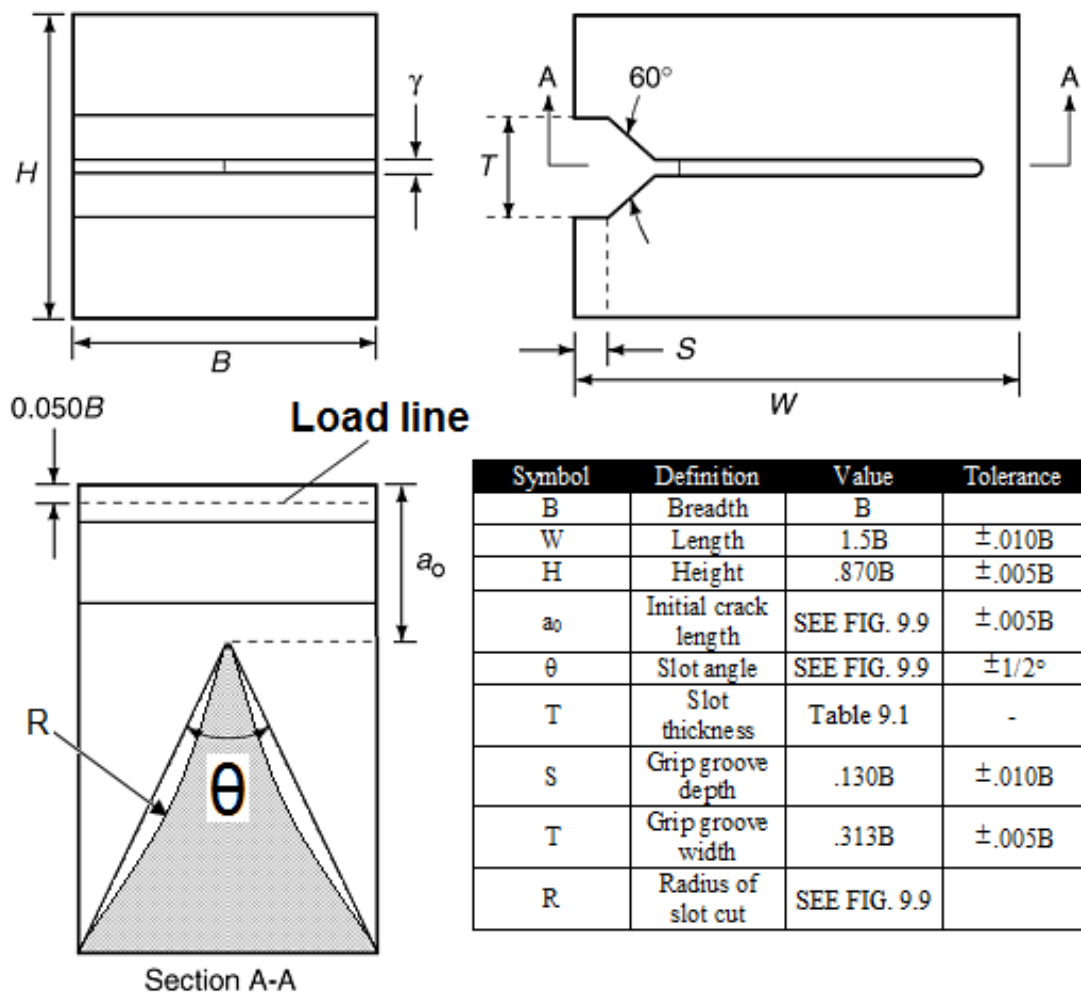
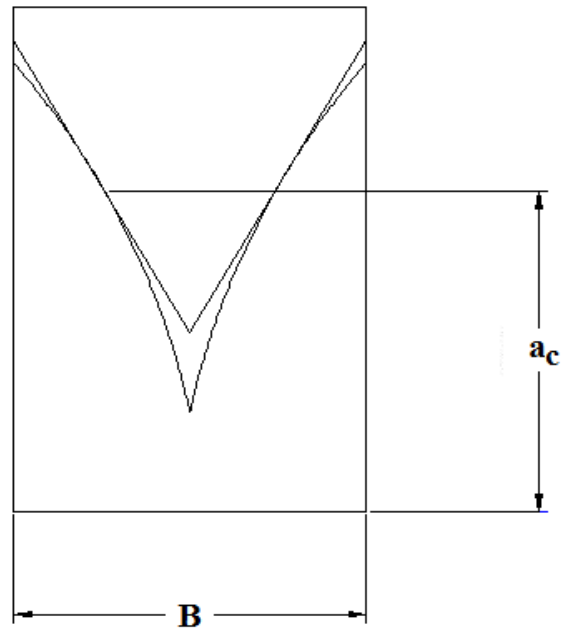


Figure 9.7: Short Bar Specimen with Curved Chevron Slots. (Source: Barker 1981, p. 460)

The section A-A of the rectangular short bars are identical with those of the round short rods. The height of the short bar is selected to be  $0.87 B$  in order to comply with the derivative with respect to crack length equal to that of the short rod. Thus the short bar and short rod calibrations should be equivalent, and Barker (1979) showed them to be equivalent by an experiment.

The calibration of the straight-slotted specimens of Figure 9.6 was also shown to be equivalent to that of the curved-slotted specimens of Figure 9.7. The plan views of the two geometries are superimposed and the slot configurations are adjusted until the straight and curved slot bottoms are tangent to each other at the critical crack length,  $a_c$ , where the peak load occurs in a linear elastic fracture mechanics test and the fracture toughness is measured (Figure 9.8). Thus, when the crack is near to the position where the toughness measurement is taken, both geometries have essentially the same crack-front width, rate of change of crack-front width with crack length, and compliance derivative, which causes their calibration to be essentially equivalent.

The four specimen geometries short rod, short bar, straight chevron slots and curved chevron slots are therefore equivalent and the user has the flexibility to choose the most convenient short rod or short bar specimen geometry (Barker 1981).



**Figure 9.8: Curved and Straight Slots Tangent at  $a_c$ . (Source: Barker 1981, p. 461)**

Furthermore, Barker (1981) has discovered that when machining the chevron slots in a curved-slotted specimen, it is easier to measure the distance to the point of the chevron slot,  $a_0$ , and the slot chord angle,  $\theta$ , than to measure the slots passing through the desired tangency point at the required angle.

The values of  $a_0$ , and  $\theta$  which produce the desired tangency have been calculated as a function of saw blade diameter and are shown in Figure 9.9. Thus, an effectively constant specimen calibration can be obtained using  $a_0$  and  $\theta$  derived from Figure 9.9, regardless of the specimen size, when the crack is in the vicinity of the critical length,  $a_c$  (Barker 1981, p. 461)

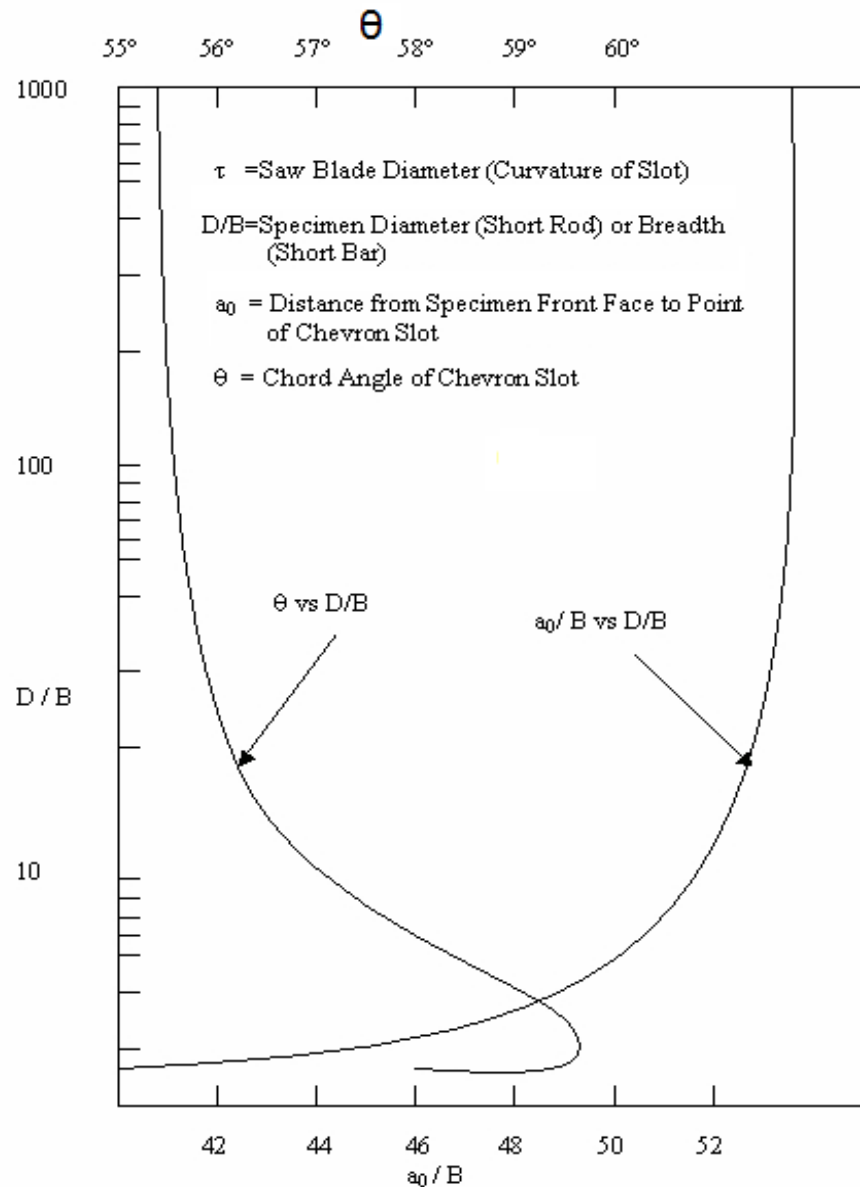


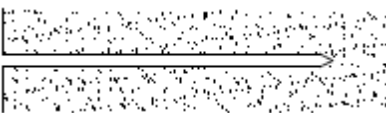
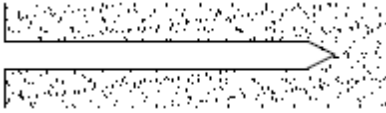
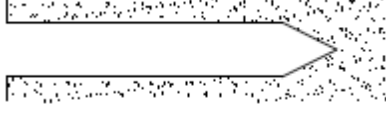
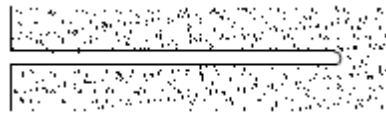
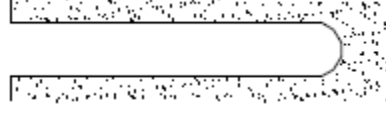
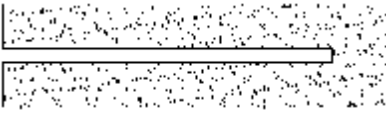
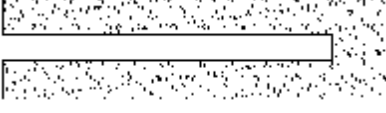
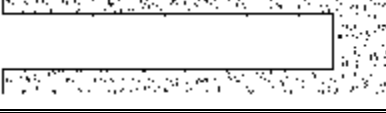
Figure 9.9: Chevron slot angle,  $\theta$ , and initial crack length,  $a_0$ , for curved chevron slots. (Source: Barker 1981, p. 462)

### 9.4.3 Thickness and Sharpness of the Chevron Slot

The fracture toughness results are greatly affected by the thickness and sharpness of the bottom of the chevron slot. Designing the slots properly can significantly enhance the degree of plain-strain along the crack front. Better slot geometries lead to a smaller plain-stress or plastic zone in comparison to the size of the specimen hence an enhanced plain-strain region (Barker 1981).

By controlling the plain-strain constraint with the slot geometries, a range of materials can be tested precisely from very tough, brittle low yield materials, to high yield ductile materials. Table 9.1 lists the result of a study on the chevron slot geometries and depicts the best slot configurations.

**Table 9.1: Effect of chevron slot geometry** (*Source: Barker 1981, p. 466*)

Slot Configuration	Slot Thickness (mm)	Effects On Specimen Calibration	Plan-Strain Constraint	Effect On The Measurements
	0.38	0	Excellent	< +2%
	0.8	-1%	Excellent	< +2%
	1.6	-3%	Excellent	< +2%
	0.38	0	Excellent	< +2%
	0.8	-1%	Good	< +5%
	1.6	-3%	Poor	> +5%
	0.38	0	Good	< +5%
	0.8	-1%	Poor	> +5%
	1.6	-3%	Poor	> +5%

#### 9.4.4 Short Bar Method Test and Sample Size

According to Barker (1981) the testing procedures are as important as the specimen geometry and preparation. Therefore, to obtain accurate testing data the testing procedure must also be controlled.

To measure the fracture toughness using the short bar testing method, an opening load is applied near the mouth of the specimen, causing a crack to initiate at the point of the chevron slot. Ideally, the opening load should be less than the load that will be required to further advance the crack. A continually increasing load must be supplied until the crack length reaches the critical crack length,  $a_c$ . Beyond  $a_c$ , the load should decrease, as shown in Figure 9.10.

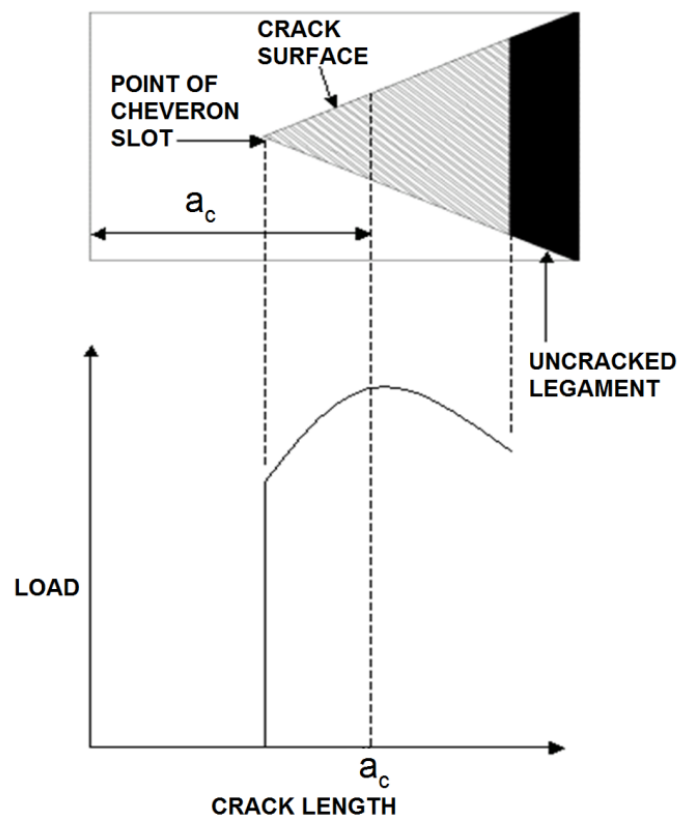


Figure 9.10: Variation of load versus crack length. (Source: Barker 1981, p. 468)

The equation for fracture toughness in a short bar test can be derived from basic fracture mechanics using the assumptions of linear elastic fracture mechanics (LEFM). The equation for the material plane strain critical stress intensity factor,  $K_{ICSR}$ , is given by the following equation (Munz 1981):

$$K_{ICSB} = \frac{(F_{max} Y_m^*)}{B\sqrt{W}} \quad (9.2)$$

where  $K_{ICSB}$  is the fracture toughness of the short bar specimen ( $MPa\sqrt{m}$ )

$F_{max}$  is the peak load (N);

$Y_m^*$  is the compliance calibration according to ASTM E-399-08;

$B$  is the breadth of the specimen (mm); and

$W$  is the width of the specimen (mm).

The compliance calibration,  $Y_m^*$ , is used as a correction factor to accommodate the dimensional change in the specimen from the standard dimensions.  $Y_m^*$  for the short bar test method from ASTM standard E-399-78 is given by:

$$Y_m^* = \{-0.36 + 5.48\omega + 0.08\omega^2 + (30.56 - 27.49\omega + 7.46\omega)\alpha_0 + (65.90 + 18.44\omega - 9.76\omega)\alpha_0^2\} \left\{ \frac{\alpha_1 - \alpha_0}{1 - \alpha_0} \right\}^{1/2} \quad (9.3)$$

$$\text{where } \omega = \frac{W}{H} \quad (9.4)$$

$$\alpha_0 = \frac{a_0}{W} \quad (9.5)$$

$$\alpha_1 = \frac{a_1}{W} \quad (9.6)$$

$W$ ,  $H$ ,  $a_0$  and  $a_1$  given in the equations above, are the measured specimen dimensions in millimetres. Where, ( $W$ ) is the width of the specimen, ( $H$ ) is the height of the specimen, ( $a_1$ ) is the distance from the edge of sample to the end of the slot, ( $a_0$ ) is the

distance from the edge of sample to the top point of the slot.  $a_1$ ,  $a_0$  and  $W$  are detailed in Figure 9.11 below.

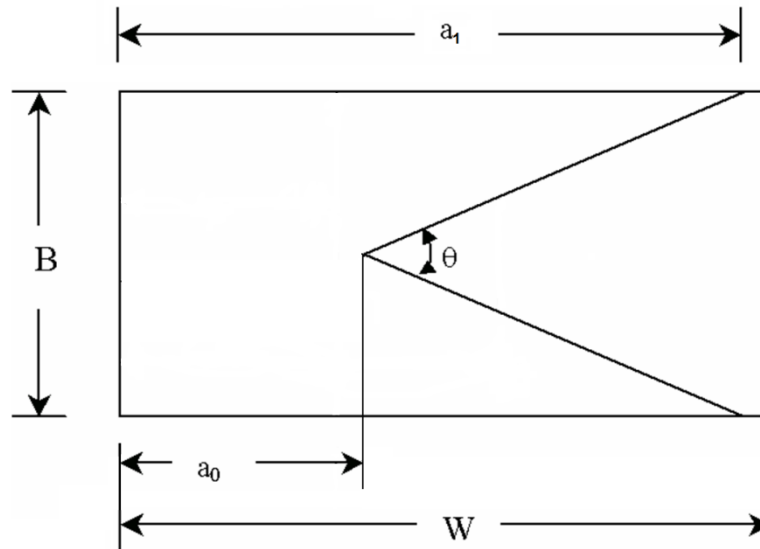


**Figure 9.11: Cross-section dimension of short bar specimen showing  $a_1$ ,  $a_0$  and  $W$ .**

After taking all the measurements, they need to be recorded so that they can be used in equations (9.4), (9.5) and (9.6). The measurements for the specimens are tabulated in Appendix D.

## Chapter 10– Fracture Toughness Apparatus

### 10.1 Test Configuration Requirements

The short bar and short rod test can be conducted using several methods. However, to be able to obtain valid fracture toughness results the selected method must fulfil specific criteria.

Barker (1981) specified four main testing criteria for short bar and short rod testing. These criteria are the test machine stiffness, load-line deviation, friction and plastic deformation. These testing criteria are explained in the next sub-sections.

#### 10.1.1 Test Machine Stiffness

Several materials can exhibit a behaviour called “pop in” crack initiation behaviour. This occurs when the load to initiate the crack at the point of the chevron slot is higher than the load during the test. When this occurs, the mouth of the specimen must continue to open at a constant rate, as the load decreases due to crack propagation. Only a stiff testing machine is able to ensure a constant rate of extension. However, if the testing machine is not stiff enough, the mouth opening of the specimen will increase in response to a load drop by means of additional elastic energy. This will invalidate the test results since the crack may propagate through the entire specimen catastrophically (Barker 1981).

Figure 10.1 shows the characteristics of a stiff testing machine and a soft testing machine.

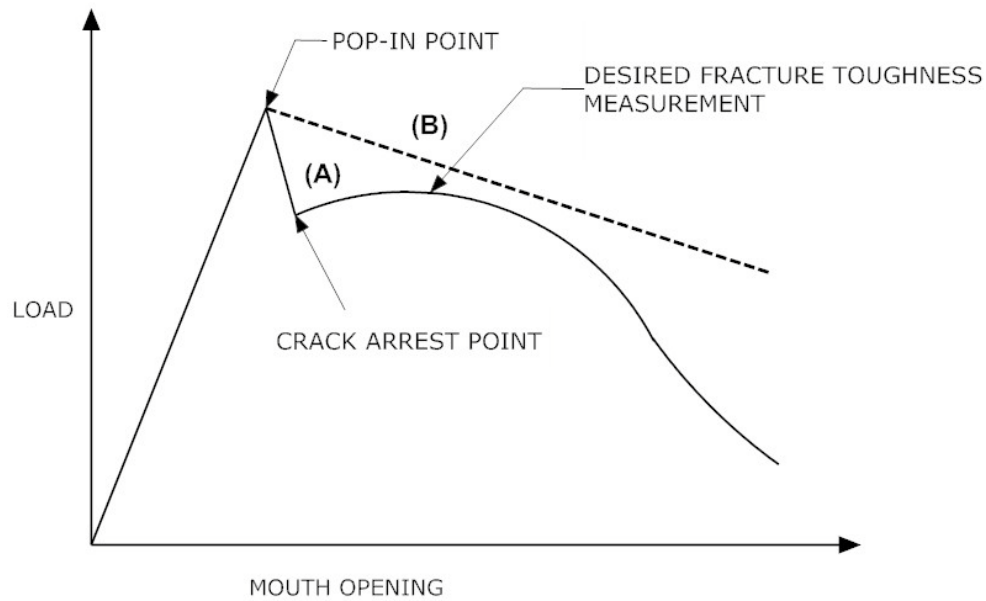


**Figure 10.1:** Stiff and soft machine characteristics. (Source: Barker 1981, pp. 469)

In Figure 10.1, A is the curve for a sufficiently stiff testing machine. The stiff testing machine allows crack arrest, after pop in occurs, and therefore leads to an accurate fracture toughness measurement. However, a soft or un-stiff machine (curve B) maintains more load, thus causing the crack to run through the entire specimen catastrophically, leading to inaccurate fracture toughness results.

### 10.1.2 Load-Line Variation

The opening load must be applied along the intended load-line on the specimen (refer to Figure 9.6 ). Variation in the load line position can cause invalid results since the specimen calibration is a function of the load-line location. Flexing of the specimen can also change the position of load application; nevertheless with brittle materials this is not a severe problem as elongation is minimal before crack propagation (Barker 1981).

### **10.1.3 Friction**

Another factor that affects the accuracy of the results is friction. According to Barker (1981) friction between the load transducer and the specimen, in addition to friction resulting from flexure of the specimen during the test, influences the accuracy of the results. Therefore, to increase the test accuracy, any adverse friction effects must be minimised.

### **10.1.4 Plastic Deformation**

Plastic deformation occurs where the loading mechanism makes contact with the specimen. Plastic deformation must be minimised, because it can result in friction due to specimen flexing and it can also change the location of the load-line (Barker 1981, pp. 469)

## **10.2 Short Rod and Bar Testing Methods**

There are a few test methods available for testing fracture toughness of short rod and short bar test specimens. The Fracjack testing mechanism, Flatjack testing mechanism and the MTS 810 material testing system are available methods for testing. All of these methods meet the testing system requirements discussed in section 10.1. Nevertheless, only the MTS 810 was available for use, and therefore the MTS 810 material testing system was selected to conduct the short bar fracture toughness tests in this project.

### 10.3 The MTS 810 Material Testing System

The MTS 810 Material Testing System, sourced from the University of Southern Queensland (USQ), was used in this project to conduct the short bar fracture toughness test. The MTS 810 Material Testing System meets all the requirements discussed in section 10.1.

The main components of the MTS 810 Material Testing System are shown in Figure 10.2. Additionally, Figure 10.3 shows the operation system layout of the MTS 810 Material Testing System.

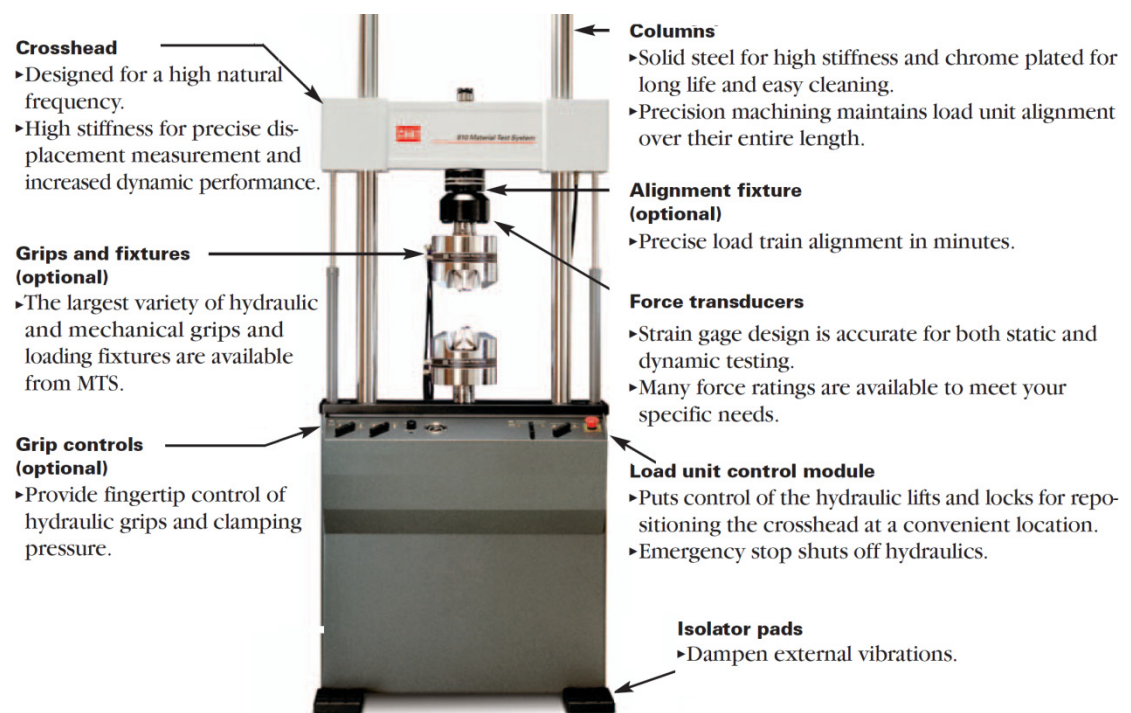
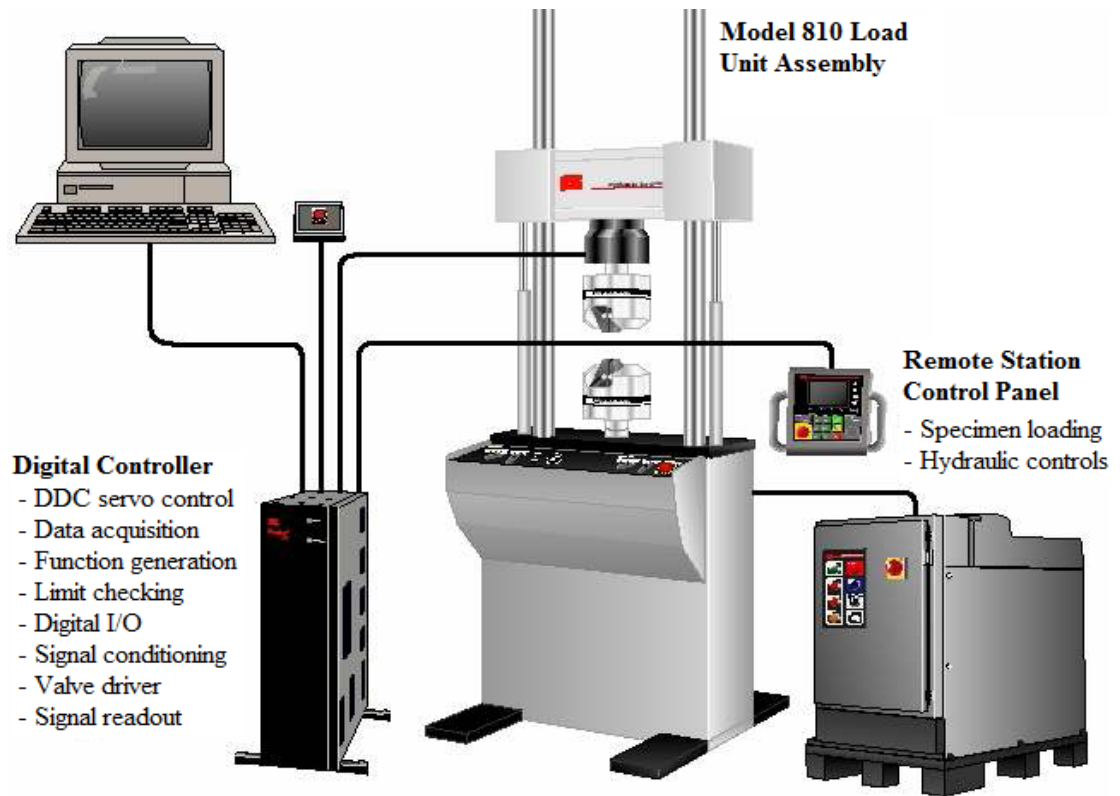


Figure 10.2: The MTS 810 Load Unit

(Source: MTS 810 FlexTest™ Material Testing Systems 2006).



**Figure 10.3: The operating system layout of the MTS 810 Material Testing Systems**  
 (Source: MTS 810 Material Testing Systems 2003).

The major advantages of the MTS 810 testing machine are as follow:

- **Flexibility:** It can be used to conduct different tests, such as tensile tests, fatigue tests and soil test, by simply changing or adjusting the grips and the fixtures.
- **User-friendly:** Conducting tests is easy and efficient, since the load unit is integrated with the digital controller and the remote station control panel, as shown in Figure 10.3. The system is able to generate the results in the form of a graph or table for individual specimens and also for an array of samples. The important statistical variables, such as mean and standard deviations, are also included in the result.
- **Accuracy:** Excellent axial and lateral stiffness are achieved through a low weight crosshead and an integrated force transducer design.

## 10.4 The MTS 810 Short Bar Testing

The MTS 810 Material Testing System is used to determine the fracture toughness of a short bar specimen. A force is applied to the load line of the specimen using grippers to fracture the specimen, as detailed in Figure 10.4.

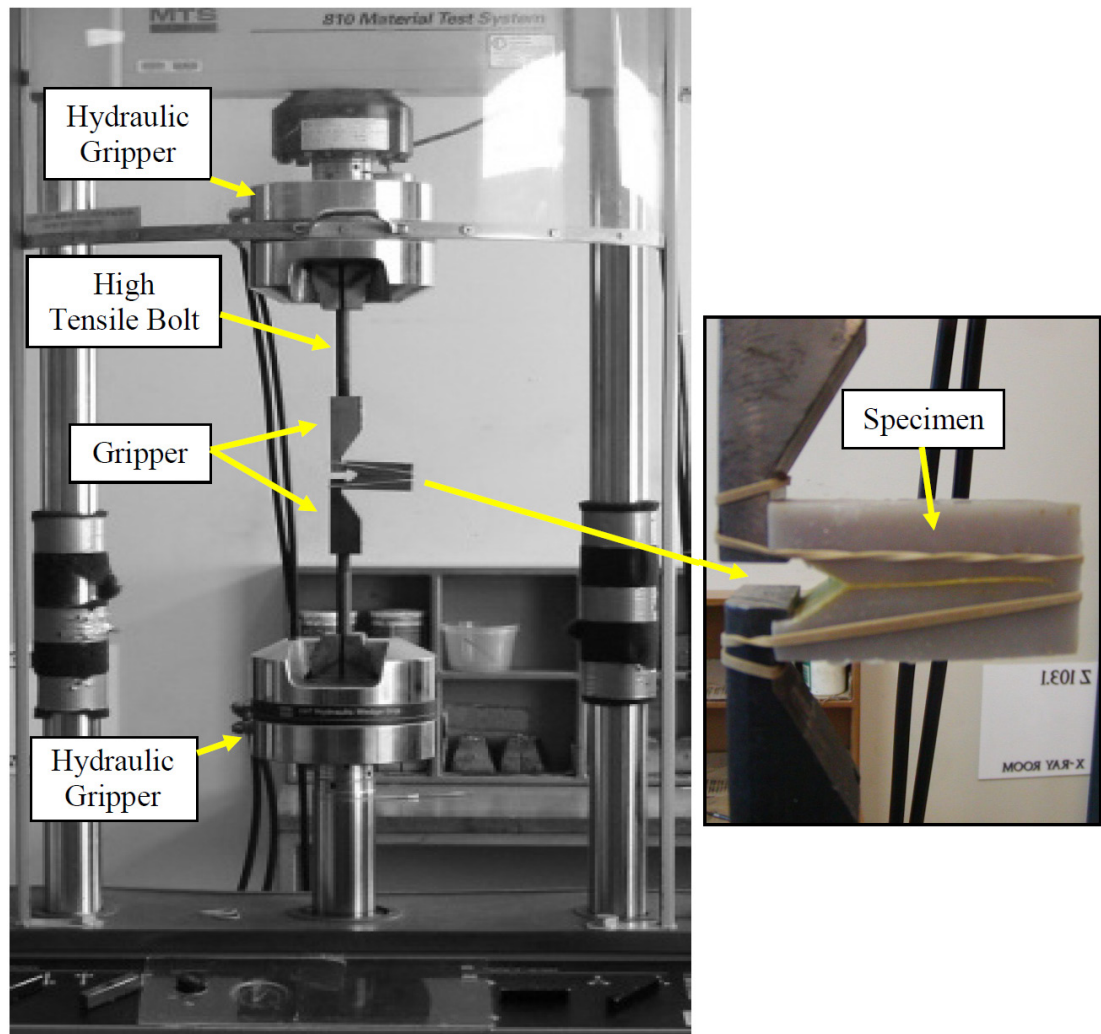


**Figure 10.4:** A short bar specimen attached to the MTS 810 Material Testing System.

### 10.4.1 Gripper Design

The design of the short bar testing grippers for the Instron Universal Testing Machine was used. These grippers, as seen in Figure 10.5, were design by Phelon (1990) to be used with the Instron Universal Testing Machine. The Instron Universal Testing Machine and the MTS 810 Material Testing System are very similar. Consequently, slight modifications were needed to enable the grippers to be used in the MTS 810 Material Testing System.



**Figure 10.5: Gripper used in MTS 810 Material Testing System**

The grippers are held by high tensile bolts, which in turn are held by the MTS 810 Load Units hydraulic grippers as illustrated in Figure 10.4. These grippers are able to withstand a force of up to 50 kN before failure.

As can be seen in Figure 10.4, the specimen was mounted to the grippers using two rubber bands. That was done to ensure that the load line did not deviate during the test.

### 10.4.2 Obtaining the Test Results

All the results from the tests can be accessed easily once the testing is done. The system is able to generate the results in the form of a graph or table for individual specimens and also for an array of samples. The important statistical variables, such as mean and standard deviations, are also included in result.

Figure 10.6 shows the results obtained for an individual vinyl ester composite specimen, reinforced with 15% by weight with calcium carbonate. The results for all the specimens are in Appendix F.

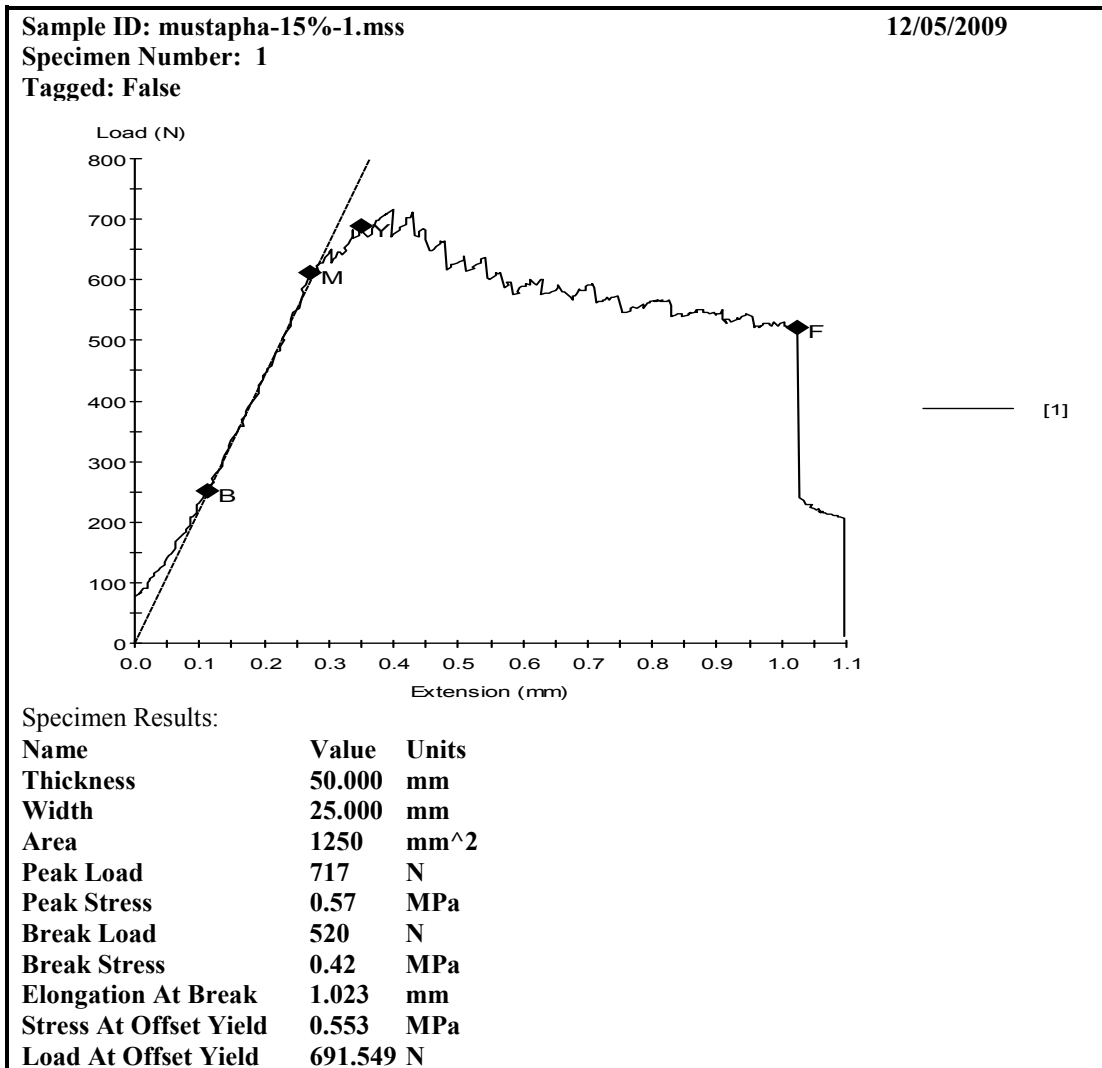


Figure 10.6: Results printout from the MTS 810 Material Testing System for an individual 15% by weight of filler specimen.

It is worth noting that the curve in Figure 10.6 matches curve (A) shown in Figure 10.1, which is the desired fracture toughness measurement curve.

The dimensions of the test specimens were measured after the test using digital vernier callipers, as seen in Figure 10.7, to calculate the compliance calibration,  $Y_m^*$ , used in equation (9.2), from which the fracture toughness is calculated. All the measurements are tabled in Appendix D.



**Figure 10.7: Taking measurement of the test specimen using digital vernier callipers.**

# Chapter 11 - DMA, SEM and Loss Tangent

## Specimens Preparation and Apparatus

### 11.1 Specimens Preparation

#### 11.1.1 SEM Specimens Preparation

Due to the construction and functional requirements of the scanning electron microscope, samples must be dry, clean and conductive (electrically and thermally) before they can be successfully imaged or analysed (Michael et al. 2003). Heat build-up from the electron beam may damage the sample. Likewise, charge build-up will repel the incident electron beam, since electrons from the beam have a negative charge, resulting in loss of signal from the sample.

The surface of the chevron edge cut specimen is non-conductive and has a corroded surface. Therefore, to improve conductivity, the sample is coated with a thin layer of metal. The metal used in this case was gold. Gold coating is performed by using a sputter coater as shown in Figure 11.1 .



**Figure 11.1: A sputter coater**

The sputter coater operates at relatively low vacuum ( $10^{-1}$ Pa), where an inert gas (argon) is introduced into a high voltage (1-3 kV) field. The gas molecules are ionised ( $\text{Ar}^+$ ) and are accelerated into metal targets. For gold coating, the target is a gold foil. Metal atoms are dislodged from the target, and the dislodged atoms continue to interact with argon, producing a cloud. Gold atoms preferentially deposit on the sample, due to the configuration of the sample, and build up a metallic coating on the sample (Goldstein et al. 1992). Figure 11.2 illustrates a diagrammatic representation of a sputter coater.

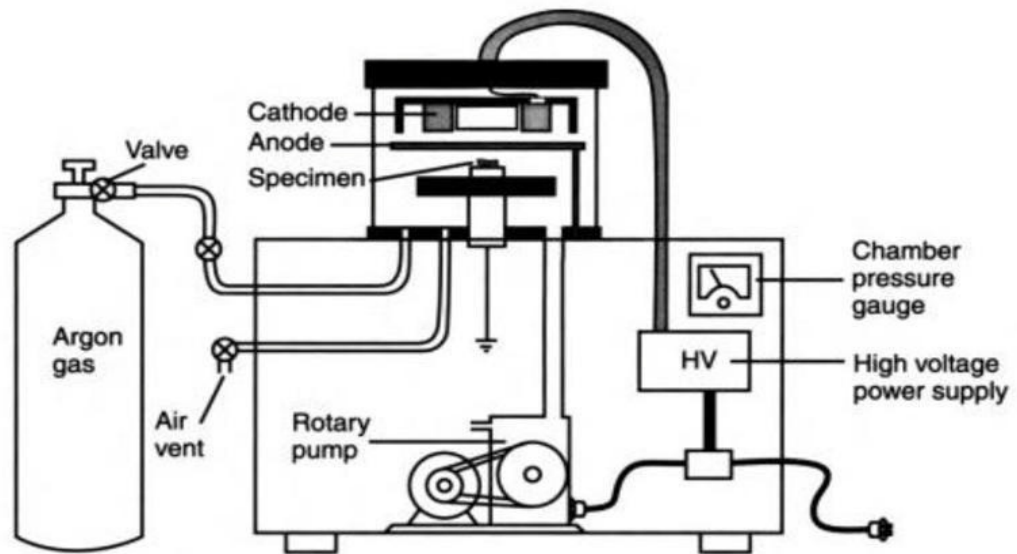


Figure 11.2: Diagrammatic representation of a sputter coater (Source: Bozzola & Russell 1992)

Furthermore, the samples need to be in suitable size because they must be fitted into the sample chamber of the scanning electron microscopy. Correct sample size also gives an even gold coating. The original dimensions of specimens are too big to fit into the gold-coating test rig; the specimen could therefore not be coated evenly. Hence, part of the fractured specimen must be cut away as shown in Figure 11.3. Reducing the size of the samples will also reduce the time needed for coating.

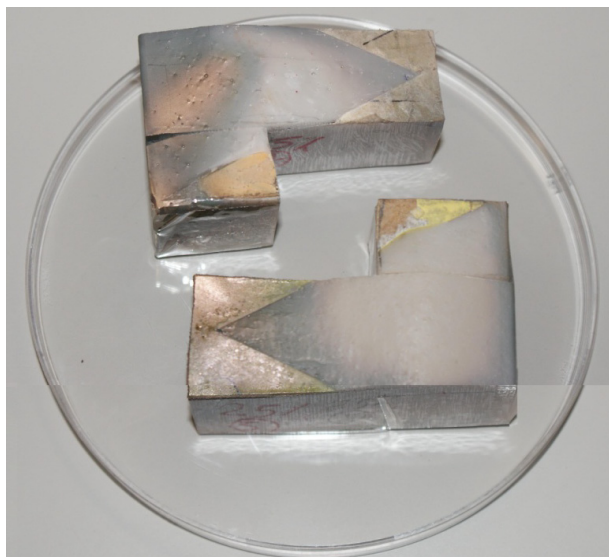
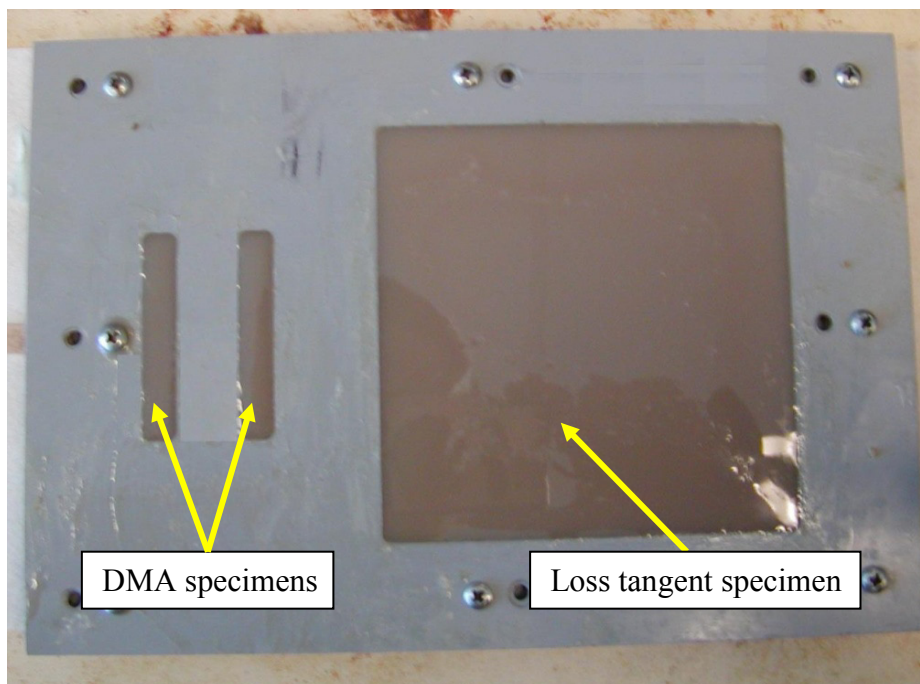


Figure 11.3: Two gold coated samples with the extra parts removed

### 11.1.2 DMA and Loss Tangent Specimens Preparation

Figure 11.4 shows the mould used to cast both DMA and the loss tangent specimens. DMA samples used in the test were cast to the size of 60 mm long, 10 mm wide and 4 mm thick which is an appropriate size so that the specimen can fit in the dynamic mechanical analyser. Similarly, the loss tangent specimens were cast to the size of 120 mm long, 120 mm wide and 4 mm thick.



**Figure 11.4:** The mould used to cast both DMA and the loss tangent specimens.

The preparation procedure of the composite is identical to the one outlined in section 3.4. However, for the DMA and for the loss tangent test, the samples selected were vinylester reinforced with 5, 10 and 15 percent by weight of calcium carbonate powder. For each percentage, two different specimens were tested. One of the specimens was prepared and cured in ambient conditions, while the other was first cured in ambient conditions for 24 hours, and then post cured at an elevated temperature.

## 11.2 Apparatus

### 11.2.1 Scanning Electron Microscope Apparatus

A Scanning Electron Microscope (SEM), supplied by Queensland University of Technology (QUT) is used in this project for conducting the microscopic analysis on the fractured specimens.



**Figure 11.5: Scanning Electron Microscope at QUT**

The scanning electron microscope used is a FEI Quanta 200 Environmental SEM, shown in Figure 11.5. The SEM can operate at high vacuum as a conventional SEM, or in environmental mode using a low vacuum in the specimen chamber.

### 11.2.2 Dynamic Mechanical Analysis Apparatus

A dynamic mechanical analysis of the composite was performed on a TA Instruments Q800 DMA in dual cantilever mode as detailed in Figure 11.6.



(A)

(B)

**Figure 11.6: (A) The Dynamic Mechanical Analyser “DMA Q800” (B) Test specimen positioned in the DMA dual cantilever clamp arrangement**

In the test, an oscillating displacement of  $\pm 10\mu\text{m}$  is applied to a sample and the resulting displacement of the sample is measured. The frequency of oscillation was at 1 Hz. The analysis was conducted from  $20^\circ\text{C}$  to  $180^\circ\text{C}$  with a heating ramp of  $3^\circ\text{C}/\text{min}$ . UNIVERSAL ANALYSIS 2000 software was used to carry out the calculations. From these experiments, graphs of tangent delta loss and storage modulus were produced.

### 11.2.3 Loss Tangent Apparatus

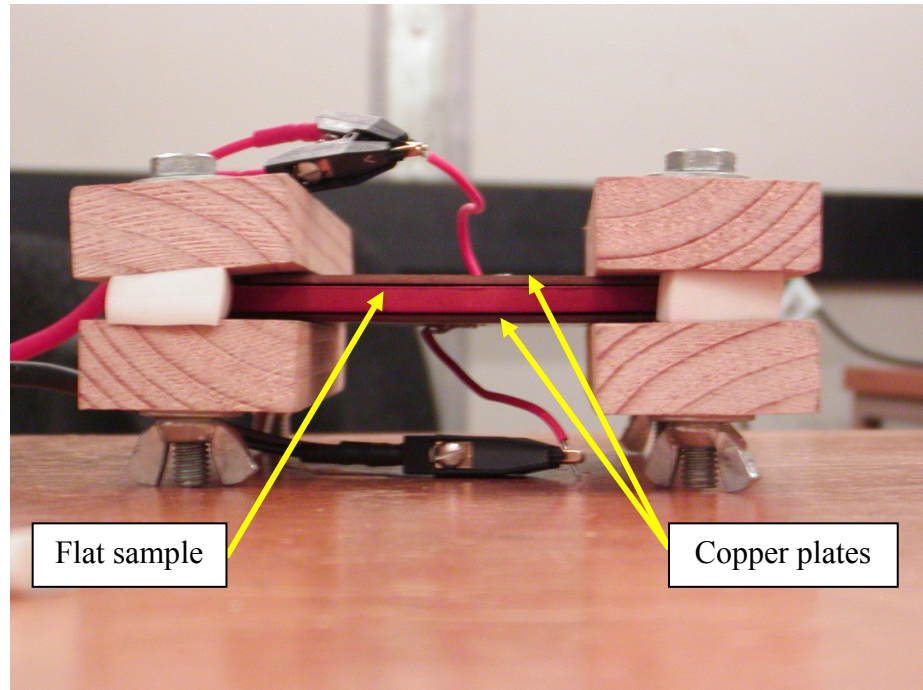
In this project, the loss tangent values were obtained directly from a meter. The meter used was the “Agilent 4263B LCR Meter”, shown in Figure 11.7.



Figure 11.7: Agilent 4263B LCR Meter.

This meter is able to measure many electrical properties in the material which include the dissipation factor or the loss tangent of the material.

Two copper plates were used to form the parallel plate capacitor with a flat sample sandwiched in between as the dielectric, as detailed in Figure 11.8. Moreover, the sample size should be at least 120 mm x 120 mm to ensure that it is an efficient supporter of electro static fields. One should be aware of the air gap and hence the plate should not be too large either.



**Figure 11.8: Two copper plates forming the parallel plate capacitor with a sample sandwiched between two copper plates**

The set-up was then connected to the “Agilent 4263B LCR Meter” to complete the circuit for measurements. The loss tangent is frequency dependant. This experiment will be made at 100 Hz, 120Hz, 1 kHz, 10 kHz, 20 kHz 100 kHz. This is within the range of the measuring device (Ball & Hancock 2007).

The loss tangents of all the selected specimens were measured. The values were read from the display and were recorded in Appendix G for analysis. Additional electrical properties were also measured and listed in Appendix G. These properties include impedance “Z”, admittance “Y”, phase angle “ $\theta$ ”, resistance “R”, equivalent series inductance “Ls”, equivalent parallel inductance “Lp”, equivalent series capacitance “Cs”, equivalent parallel capacitance “Cp”, conductance “G”, reactance “X” and susceptance “B”.

## Chapter 12 - Results and Discussions

### 12.1 Fracture Toughness

The fracture toughness was determined using equations (9.2) to (9.6) , from Chapter 9. To demonstrate the calculations procedures, specimen 1 for the 10% by weight of the filler was selected and its fracture toughness was calculated by the following procedure:

The geometry measurements of the specimen are required in the calculations. Table 12.1 shows the actual geometry measurements of specimen 1 required in the calculations. All the values listed in Table 12.1 are extracted from Table D.3 in Appendix D.

**Table 12.1: The measured geometry of the 10% by weight filler specimen 1.**

Filler (% by weight)	Specimen Number	W	H	a <sub>0</sub>	a <sub>1</sub>
10%	1	73.4mm	38.3mm	23.7mm	70.6mm

The measured values from Table 12.1 for specimen number 1 are substituted into equations (9.4), (9.5) and (9.6) from Chapter 9, respectively, thus:

$$\omega = \frac{W}{H} = \frac{73.4}{38.3} = 1.916 \quad (9.4)$$

$$\alpha_0 = \frac{a_0}{W} = \frac{23.7}{73.4} = 0.323 \quad (9.5)$$

$$\alpha_1 = \frac{a_1}{W} = \frac{70.6}{73.4} = 0.962 \quad (9.6)$$

Then, the compliance calibration,  $Y_m^*$ , for the short bar test method for this specimen can be calculated using equation (9.3):

$$Y_m^* = \{-0.36 + 5.48\omega + 0.08\omega^2 + (30.56 - 27.49\omega + 7.46\omega)\alpha_0 + (65.90 + 18.44\omega - 9.76\omega)\alpha_0^2\} \left\{ \frac{\alpha_1 - \alpha_0}{1 - \alpha_0} \right\}^{1/2} \quad (9.3)$$

$$\begin{aligned} \therefore Y_m^* &= \{-0.36 + 5.48 \times 1.916 + 0.08 \times 1.916^2 + \\ &(30.56 - 27.49 \times 1.916 + 7.46 \times 1.916)0.323 \\ &+ (65.90 + 18.44 \times 1.916 - 9.76 \times 1.916)0.323^2\} \left\{ \frac{0.962 - 0.323}{1 - 0.323} \right\}^{1/2} = 16.0534 \end{aligned}$$

$$\therefore Y_m^* = 16.0534$$

The fracture toughness can now be calculated using equation (9.2), where

$B = 50mm$  (by design),  $F_{max} = 504N$  (extracted from Appendix F) and  $H = 73.4mm$  from Table 12.1, thus:

$$K_{ICSB} = \frac{(F_{max} Y_m^*)}{B\sqrt{W}} \quad (9.2)$$

$$\therefore K_{ICSB} = \frac{(504 \times 16.0534)}{50\sqrt{73.4}} = 18.89 \text{ MPa}\sqrt{m}$$

$$\therefore K_{ICSB} = 18.89 \text{ MPa}\sqrt{m}$$

Similarly, all the other fracture toughness values have been calculated by following the same process outlined above.

Table 12.2 shows the fracture toughness values and the standard deviation values of all the specimens.

**Table 12.2: fracture toughness of VE with varying percentage by weight of CaCO<sub>3</sub> post-cured in oven with the standard deviation given.**

% by weight of filler (CaCO <sub>3</sub> )	0%	5%	10%	15%	20%	25%	30%	35%	40%
Fracture Toughness* (MPa√m)	30.32	23.17	20.32	22.00	21.75	18.07	16.02	21.97	21.15
Standard deviation	4.195	3.623	1.555	2.672	1.833	0.657	2.875	3.693	1.220

\*The Average fracture toughness of six specimens is used for each filler percentage (all the values listed in the table are extracted from Appendix E).

The fracture toughness values listed in Table 12.2 are plotted in Figure 12.1. Figure 12.1 illustrates the fracture toughness of VE/CaCO<sub>3</sub> at varying percentage by weight of CaCO<sub>3</sub>.

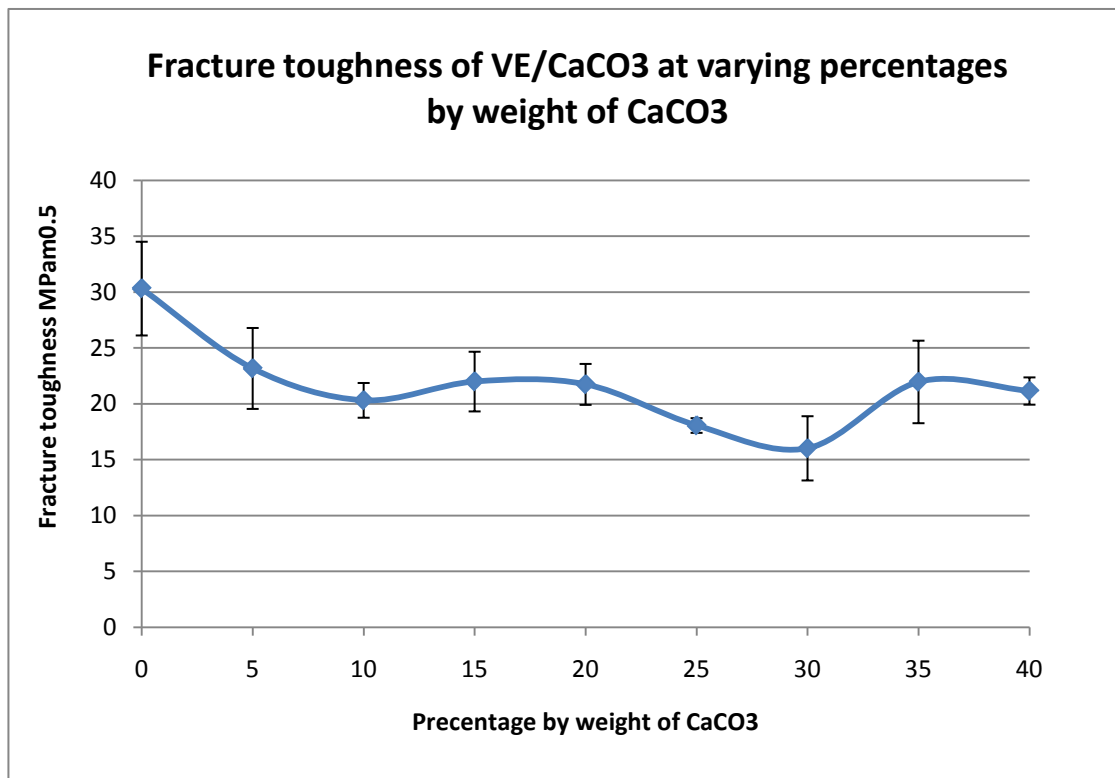


**Figure 12.1: Fracture toughness of vinyl ester reinforced with varying percentages of calcium carbonate.**

It was found that the fracture toughness of the neat resin (0 % by weight of CaCO<sub>3</sub>) produced the highest value (30.32  $MPa\sqrt{m}$ ). The value dropped rapidly to 23.17  $MPa\sqrt{m}$  when the CaCO<sub>3</sub> by weight was 5%; afterwards the values varied from 20.32 to 21.75  $MPa\sqrt{m}$  as the percentage by weight of CaCO<sub>3</sub> increases from 10 to 20%. All the values were within the five percent markers of 23.17  $MPa\sqrt{m}$  (5 % CaCO<sub>3</sub>) as depicted in Figure 12.1. The fracture toughness was observed to remain steady when the percentages by weight of CaCO<sub>3</sub> varied from 5% to 20%. The fracture toughness dropped gradually to 16.02  $MPa\sqrt{m}$  when the percentage by weight of CaCO<sub>3</sub> was 30%. It then increased to 21.97  $MPa\sqrt{m}$  at 35 % by weight of CaCO<sub>3</sub>. After this, it decreased slowly to 21.15  $MPa\sqrt{m}$  at 40% by weight of CaCO<sub>3</sub>.

In general, the standard deviations of the fracture toughness were small (see Table 12.2). The toughness values were reliable even though the behaviour was slightly strange due to the unexpectedly increase at 35% by weight of CaCO<sub>3</sub>.

However, such a case was not isolated; similar behaviour was observed by Cardona et al. (2007) when the fracture toughness of phenol formaldehyde composites reinforced with ceramic hollow spheres (SLG) was measured (refer to Figure 2.7 in section 2.8). In both cases, there were unpredictable increases in the fracture toughness from the low point, 30 % by weight of filler in Figure 12.1, and 25 % by weight of filler in Figure 2.7. The trends of the curves were the same.

Such eccentric behaviour in fracture toughness was due to the weak matrix/filler interaction, in which the participation of filler particles in accommodating the deformation force was much less in these composites. When the small filler particles could occupy the interstitial volume, the available surface area of contact increased, which in turn increased the fracture toughness. The minimum fracture toughness was

at 30 % by weight of filler and increased gradually with the increment in filler loading. At 40 % by weight of filler, the fracture toughness decreased again. With such large filler loading, the resins was not enough to encapsulate the calcium carbonate particles completely, leading to the generation of a large number of voids, therefore the fracture toughness was reduced.

Furthermore, this kind of loading not only reduced the stress bearing areas but also acted as stress raisers. As a result, cracks started to form (Ray et al. 2006). The behaviour of the fracture toughness in this study was similar to that in Ray et al.'s (2006) case; hence both cases could be explained in the same manner.

The abnormal increase in the fracture toughness of the composites at 35% by weight of the filler could also be explained by the change in morphology. The morphology remained the same from 35% to 40% by weight of CaCO<sub>3</sub> so the values of fracture toughness remained stable in this range of percentages by weight of filler. Referring to section 2.8.4, this argument was confirmed by Auad et al. (2001) who observed similar behaviours.

Moreover, an Izod impact strength test was conducted on polypropylene (PP) composites reinforced with calcium carbonate powder. The results showed that the toughness of the material increased steadily from 2.6 KJ/m<sup>2</sup> (for neat PP) to 4.3 KJ/m<sup>2</sup> (for 15% particulate loading); it then dropped back to approximately the neat resin value when the percentage by weight of the reinforcer was 40% (Guo et al. 2005).

Yang et al. (2006) did similar experiments and found relatively identical results. The trend of the curve was different in this study because thermoset resin was used instead of thermoplastic resin. It was useful to make a comparison between fracture toughness and Izod impact toughness because both measured the toughness of materials.

In general, interfacial adhesion between particles and matrix has very significant effect on composite fracture toughness. Strong adhesion leads to high toughness in thermoplastic matrices but not necessarily true in thermosetting matrices due to different failure mechanism (Fu et al. 2008)

## 12.2 Dynamic Mechanical Analysis

The DMA results are discussed in detail for each filler percentage in the following subsections.

### 12.2.1 For 5% by Weight Filler

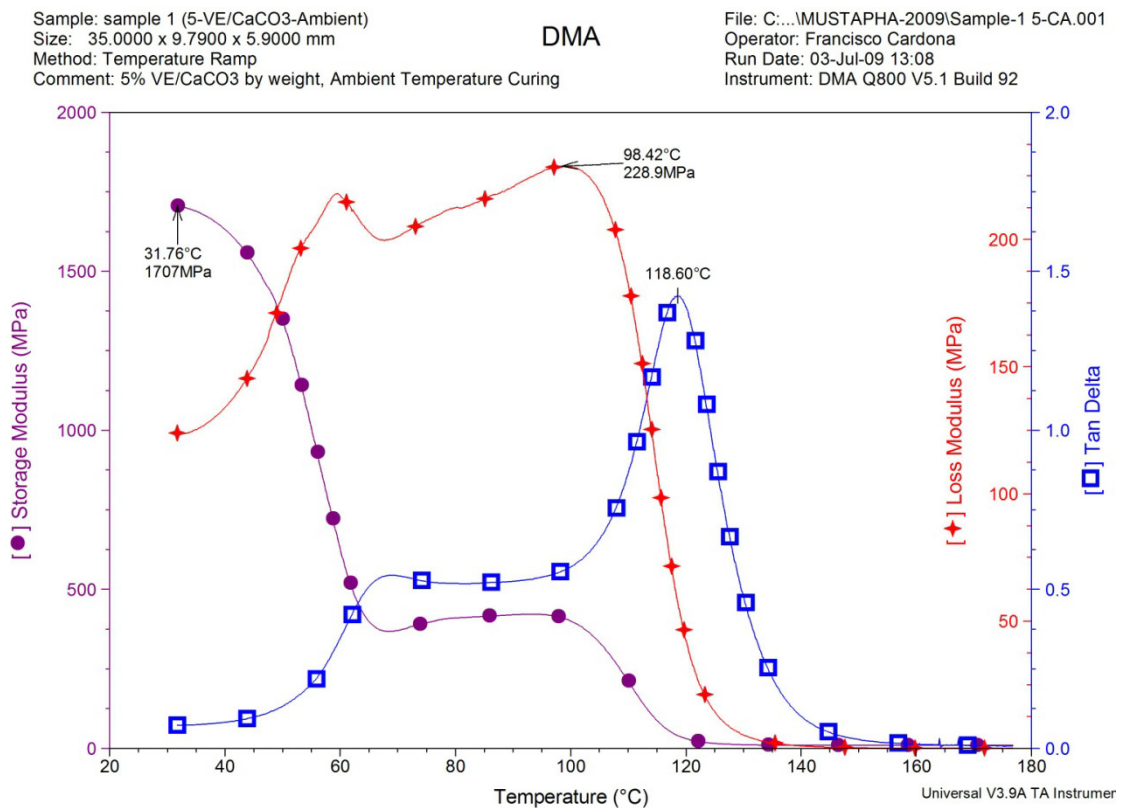
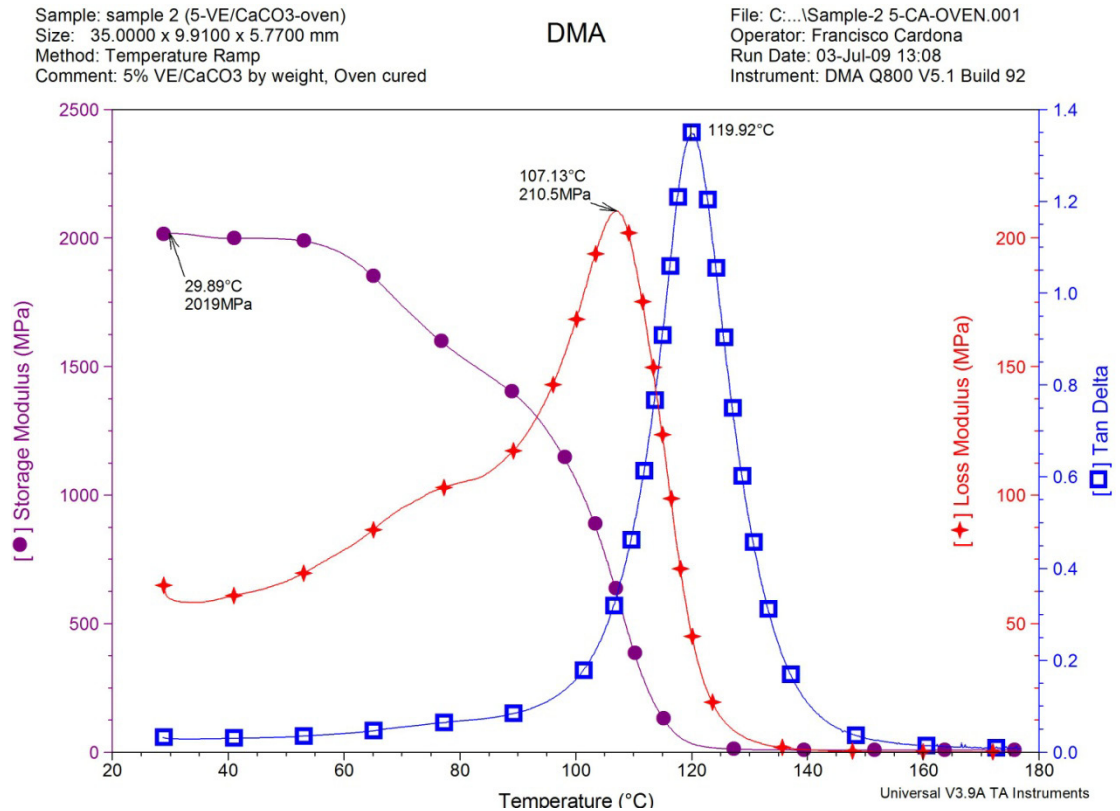


Figure 12.2: DMA results of vinyl ester reinforced with 5% by weight of calcium carbonate powder cured in ambient conditions for 24 hours



**Figure 12.3: DMA results of vinyl ester reinforced with 5% by weight of calcium carbonate powder cured in ambient conditions for 24 hours plus post-cured in an oven.**

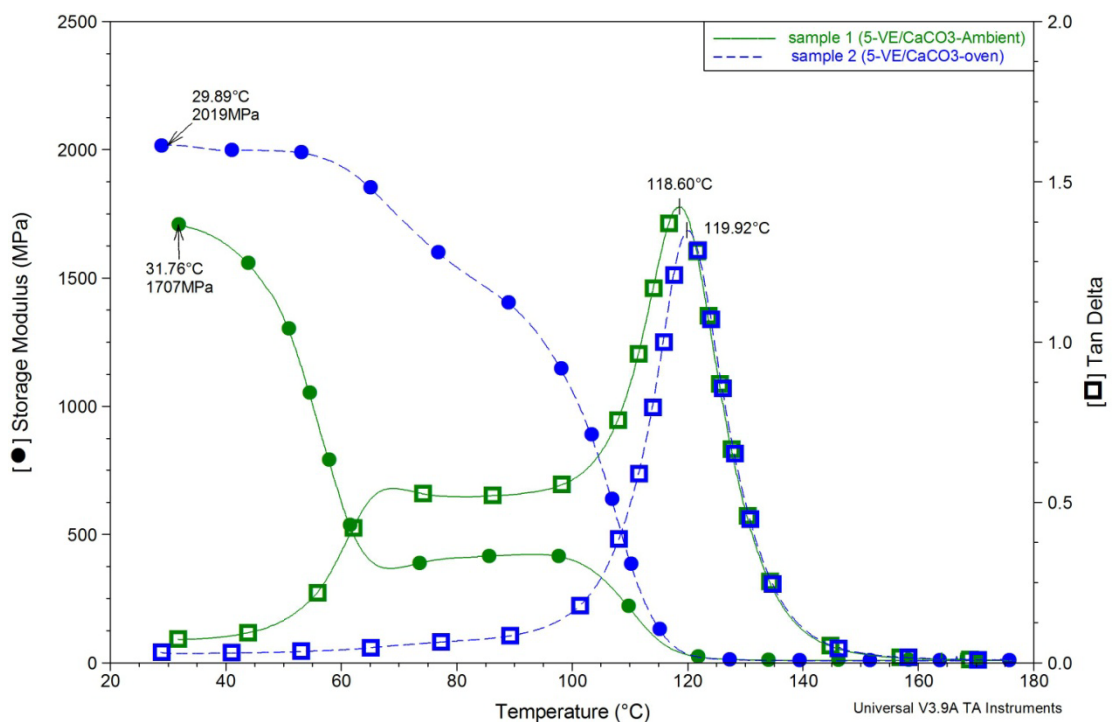
Figure 12.2 and Figure 12.3 illustrate the DMA results of vinyl ester samples reinforced with 5% by weight of calcium carbonate powder cured in ambient conditions, and in ambient conditions plus post-cured in an oven, respectively.

These figures show that the glass transition temperatures for samples cured in ambient conditions and in ambient conditions plus post-cured in an oven are 118.60 °C and 119.92 °C, respectively. From the figures, the maximum storage and loss moduli of them are 1,707 MPa and 228.9 MPa, respectively for the ambient cured specimen and 2,019 MPa and 210 MPa, respectively for the ambient plus post-cured specimen.

The glass transition temperature for the ambient plus oven post-cured specimen is slightly higher than that of its counterpart. This means that, the ambient plus oven post-cured specimen will change from hard and brittle to soft and pliable at a

temperature higher than that of the ambient cured specimen. In term of storage modulus, the ambient plus oven post-cured specimen is 312 MPa higher than the ambient cured specimen. Such indication shows that the post-cured sample is able to store more energy than its counterpart.

Furthermore, the loss modulus of the post-cured sample is lower than that of its counterpart. Low loss moduli yields stiff material therefore post-cured sample is stiffer than ambient cured sample. In conclusion, the glass transition temperature, storage modulus and loss modulus support the fact that post-cured sample is stiffer than its counterpart due to higher degree of curing.



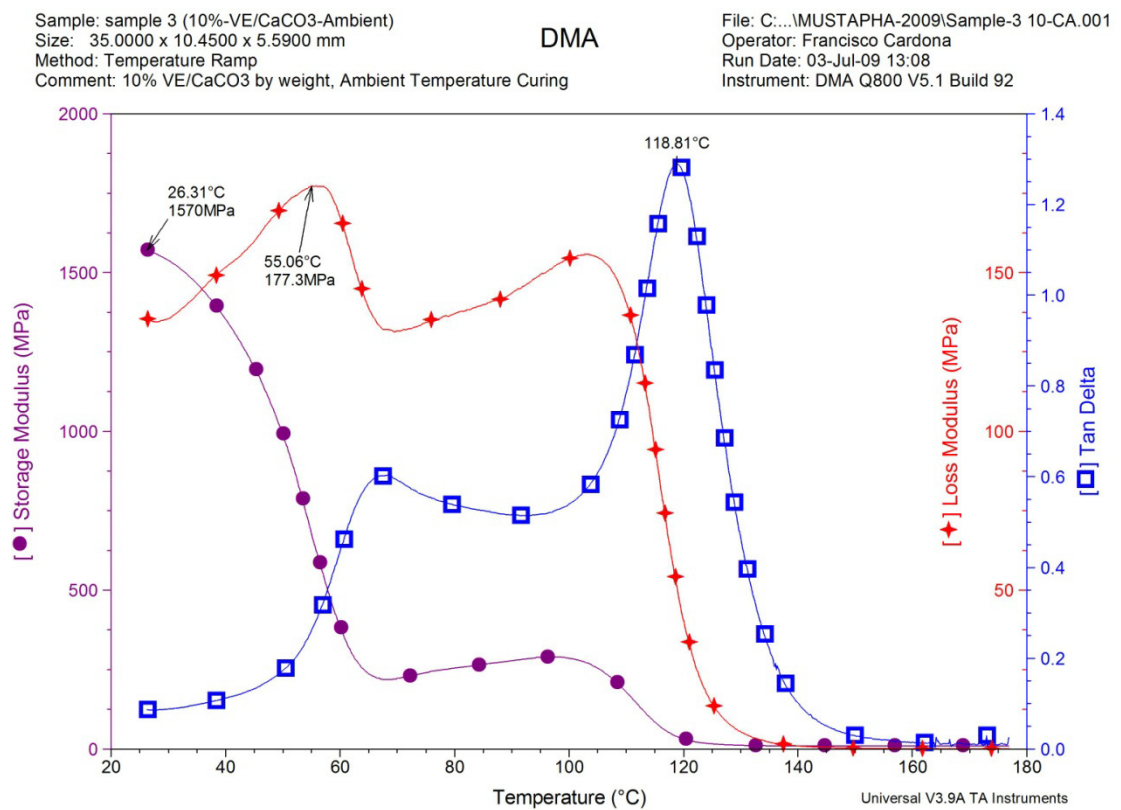
**Figure 12.4: DMA results of two vinyl ester samples reinforced with 5% by weight of calcium carbonate powder cured in ambient conditions for 24hours, and cured in ambient conditions for 24hours plus post-cured in an oven.**

Figure 12.4 compares the result obtained for the 5% by weight of calcium carbonate for both ambient cured and ambient plus oven post-cured specimens. It is worthwhile to note that the results for both specimens have similar trends in both storage modulus

and glass transition curves. This indicates that post curing do not change the viscoelastic properties of the composite significantly.

### 12.2.2 For 10% by Weight Filler

Figure 12.5 and Figure 12.6 illustrate the DMA results of vinylester samples reinforced with 10% by weight of calcium carbonate powder cured in ambient conditions, and in ambient conditions plus post-cured in an oven respectively.



**Figure 12.5: DMA results of vinylester reinforced with 10% by weight of calcium carbonate powder cured in ambient conditions for 24hours.**

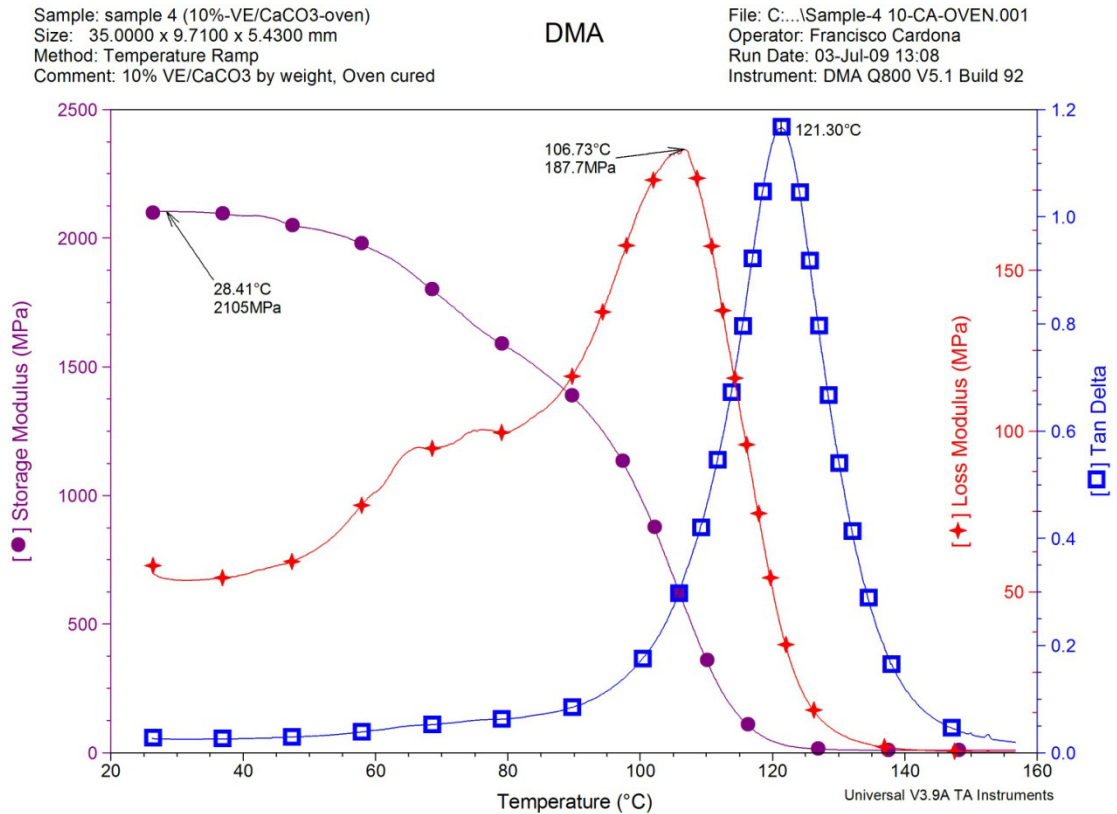


**Figure 12.6: DMA results of vinyl ester reinforced with 10% by weight of calcium carbonate powder cured in ambient conditions for 24 hours plus post-cured in an oven.**

The glass transition temperature for sample cured in ambient conditions plus post-cured conventionally is higher than the ambient cured sample. This implies that the post-cured sample will change from hard and brittle to soft and pliable at a higher temperature. The storage modulus is also higher for post-cured sample, which shows that post-cured sample is able to store more energy than its counterpart.

The loss modulus of the post-cured sample is lower than that of its counterpart. As a result, oven cured sample is softer than the ambient cured sample since higher loss moduli produces softer material. Hence, the glass transition temperature, storage modulus and loss modulus support the fact that post-cured sample is stiffer than its counterpart due to higher degree of curing.

It is worth noting that the DMA results for both 5% and 10% by weight calcium carbonate powder reinforced samples are fairly similar. This can be observed clearly by comparing Figure 12.4 with Figure 12.7. In both figures, the curves are almost identical and have the same trends. This useful observation leads to the fact that adding 5% more of the filler, calcium carbonate powder, do not have significant effects on the viscoelastic properties of the composite.

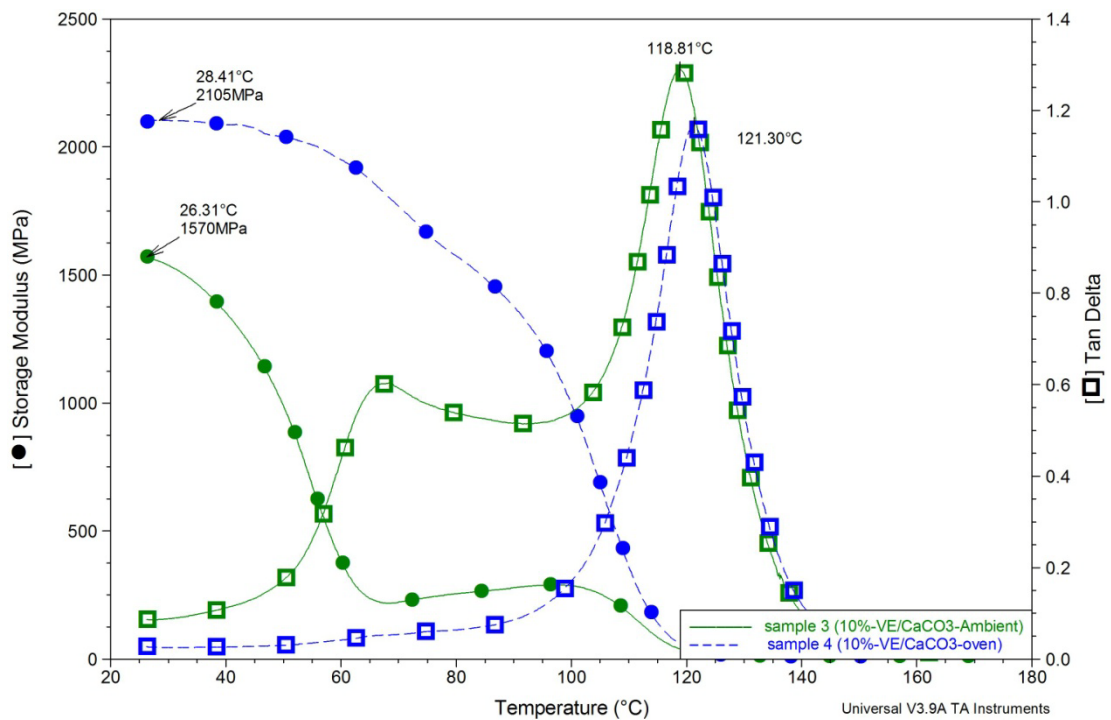


**Figure 12.7:** DMA results of two vinyl ester samples reinforced with 10% by weight of calcium carbonate powder cured in ambient conditions for 24hours, and cured in ambient conditions for 24hours plus post-cured in an oven.

### 12.2.3 For 15% by Weight Filler

Figure 12.8 and Figure 12.9 show the DMA results of vinyl ester samples reinforced with 15% by weight of calcium carbonate powder cured in ambient conditions, and in ambient conditions plus post-cured in an oven respectively.

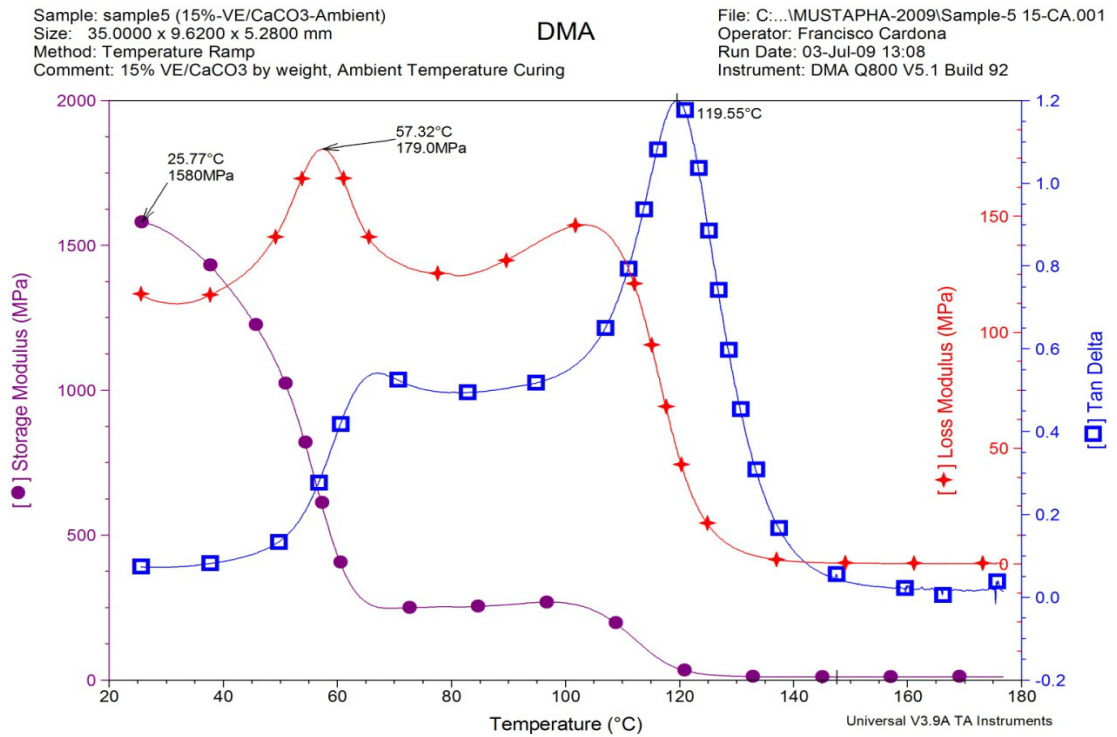


**Figure 12.8:** DMA results of vinylester reinforced with 15% by weight of calcium carbonate powder cured in ambient conditions for 24hours

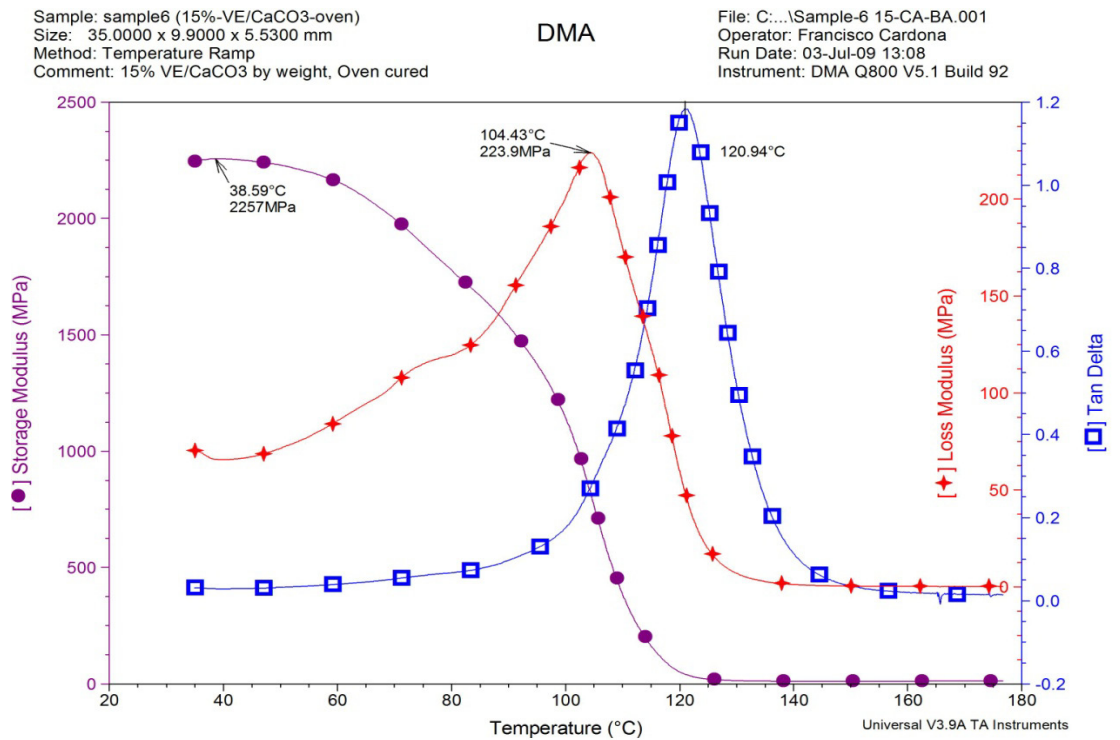


**Figure 12.9:** DMA results of vinylester reinforced with 15% by weight of calcium carbonate powder cured in ambient conditions for 24hours plus post-cured in an oven.

Similar to the 10% by weight of calcium carbonate powder, the glass transition temperature for sample cured in ambient conditions plus post-cured conventionally is also higher than the ambient cured sample. Likewise, the storage modulus is also higher since the post-cured sample is able to store more energy than its counterpart. The loss modulus of the post-cured sample is higher than its counterpart. As a result, post-cured sample is softer since high loss modulus gives soft material.

The DMA results for 15% by weight of calcium carbonate powder are similar to the two cases above, by comparing Figure 12.4, Figure 12.7 and Figure 12.10. From the figures, the curves are almost identical and have the same trends. This means that until this stage, adding the filler, calcium carbonate powder, do not have significant effects on the viscoelastic properties of the composite.

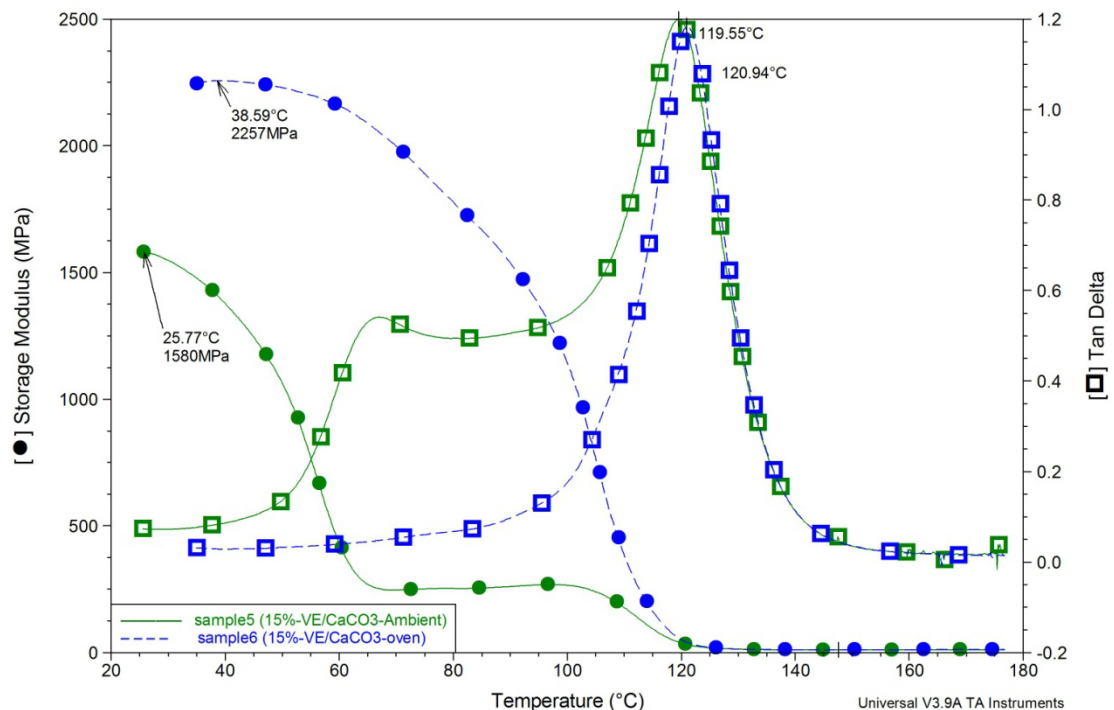


**Figure 12.10:** DMA results of two vinyl ester samples reinforced with 15% by weight of calcium carbonate powder cured in ambient conditions for 24hours, and cured in ambient conditions for 24hours plus post-cured in an oven.

### 12.2.4 DMA Measurement Summary

Table 12.3 summaries all the results obtained from the DMA measurements. The values for the glass transition temperature for all the samples are found to be around 119 °C. Moreover, the values for the storage modulus for the ambient cured samples are always lower than the storage modulus for the oven post cured sample. Similarly, the loss modulus for ambient cured samples is lower with only one exception at 5% by weight of the filler. Further work will be required to explore this phenomenon in more detail.

**Table 12.3: DMA results for all the samples with different curing method and filler percentages.**

<b>Curing method</b>	<b>CaCO<sub>3</sub> % by weight</b>	<b>Glass transition temperature (°C)</b>	<b>Maximum storage modulus (MPa)</b>	<b>Maximum loss modulus (MPa)</b>
Ambient	5%	118.6	1707	228.9
Ambient	10%	118.81	1570	177.3
Ambient	15%	119.55	1580	179
Ambient plus oven	5%	119.92	2019	210.5
Ambient plus oven	10%	121.3	2105	187.7
Ambient plus oven	15%	120.94	2257	223.9

### 12.3 Microscopic Analysis

The fractured surfaces of the samples are analysed by using a scanning electron microscope. Six fractured samples are illustrated in Figure 12.11.



**Figure 12.11: Six samples of fractured specimens**

It is expected that samples with different filler percentages by weight would have slight changes in their microstructures, which in turn would affect the material properties like its fracture toughness. Four critical points of the chevron fracture were analysed and illustrated in Figure 12.12.

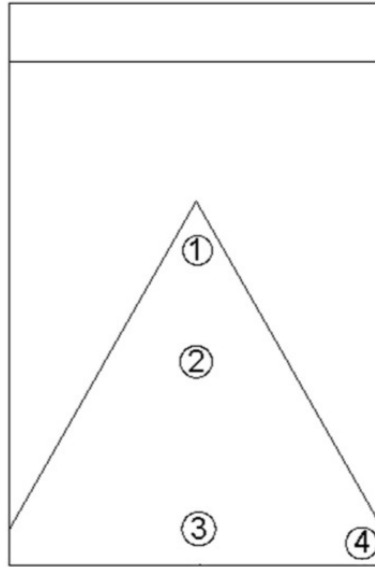


**Figure 12.12: Four critical points for the fractured surface to be analysed**

The values of fracture toughness and other important parameters for the selected vinyl ester composites with different percentage by weight of  $\text{CaCO}_3$  powder are shown in Table 12.4

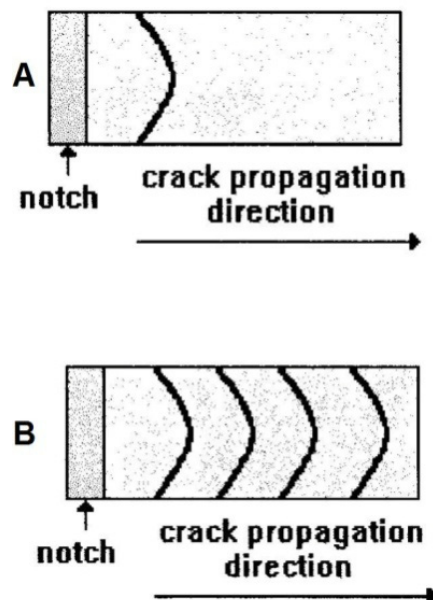
**Table 12.4: Result of the fracture toughness and other parameters for VE with different filler percentage**

$\text{CaCO}_3$ % by weight	0%	25%	35%
Specimen Number	1	5	6
Elongation at Peak (mm)	0.854	0.652	0.76
Peak Load (N)	953	475	891
Elongation at Break (mm)	0.907	0.978	1.054
Break Load (N)	937	336	747
Fracture toughness ( $\text{MPa}\sqrt{m}$ )	34.34	18.05	36.96

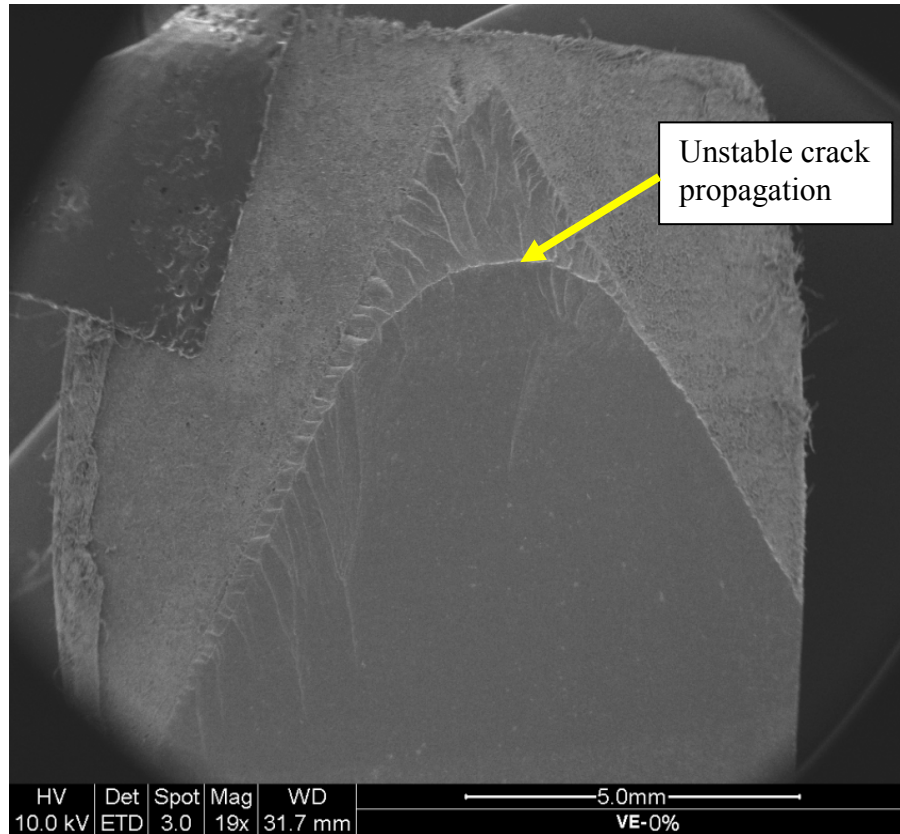
Specimens of neat resin and those with the highest and lowest fracture toughness values are chosen for investigation. The first specimen is chosen from the six samples

of the neat resin which have the highest average fracture toughness values; the second specimen is VE/CaCO<sub>3</sub> (35%) which has the highest fracture toughness value between the filled specimens, and the third specimen is VE/CaCO<sub>3</sub> (25%) which is the composite with the lowest fracture toughness values among all the samples. It is expected that the fracture surface with highest value of fracture toughness,  $K_{Ic}$  would have lesser flaws than the specimen with lowest value (Chew et al. 2005). Also, it can be foreseen that some area of the chevron edge cut will show ductile failure and some will display brittle cleavage.

The first specimen chosen is from the neat resin specimen. Neat resins generally are characterized by unstable crack propagation (Figure 12.13); that is when the load reaches a critical value required for crack propagation, the initial crack propagates at an extremely high rate and specimen failure occurs almost abruptly (Dreerman et al. 1998).



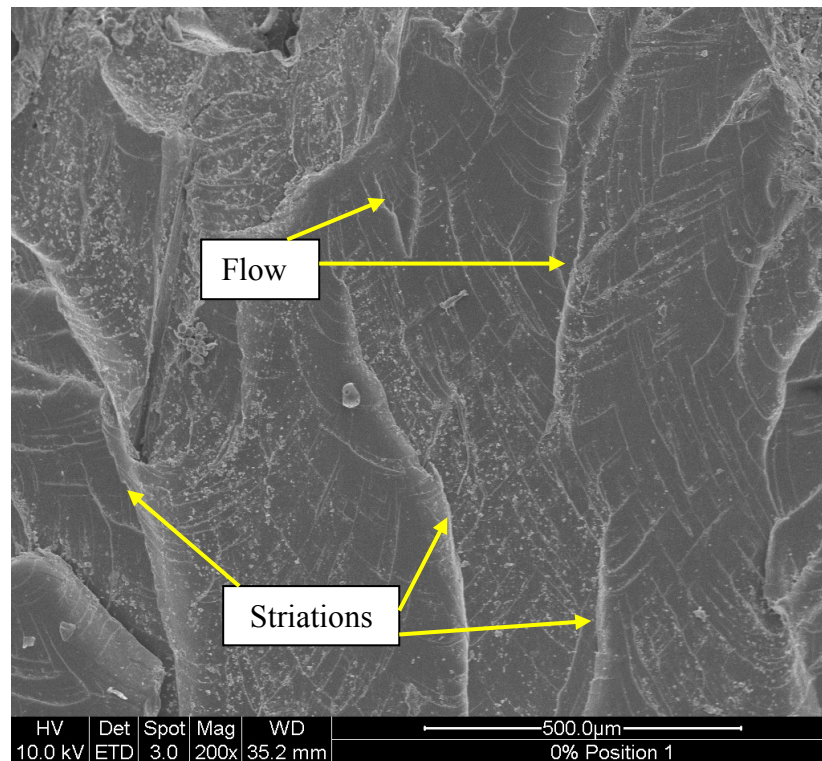
**Figure 12.13:** Schematic illustration of a fracture surface: (a) unstable crack propagation and (b) stick-slip crack propagation. (Source: Dreerman et al. 1998, p. 651)



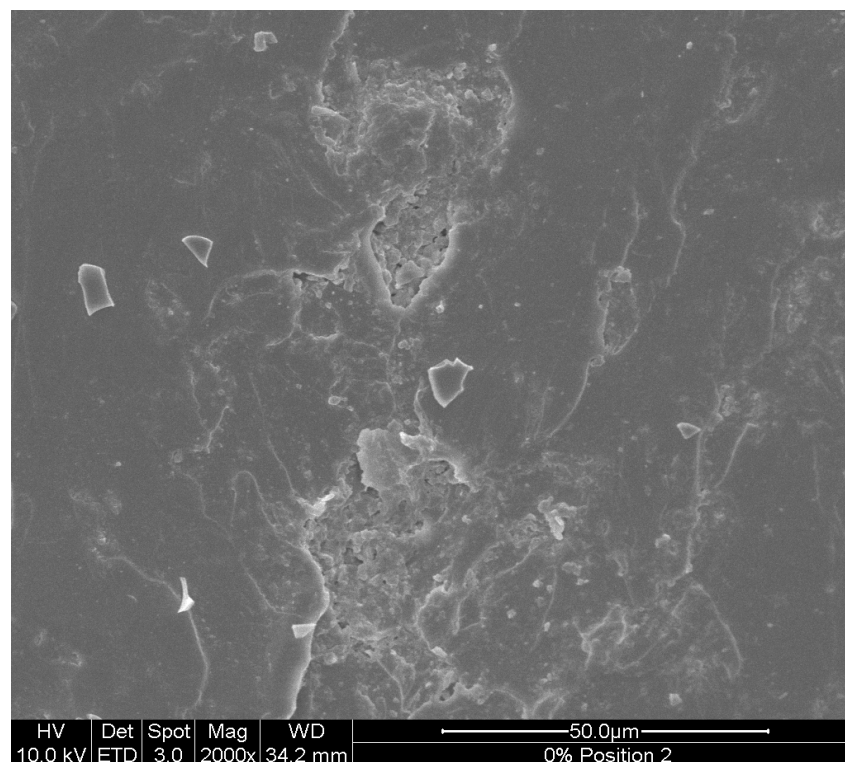
**Figure 12.14:** The fractured surface of neat vinyl ester resin showing typical unstable crack propagation.

Figure 12.14 shows a clear unstable crack propagation of neat resin sample. Furthermore, the fractured surface of the neat vinyl ester is relatively smooth, which is typical for brittle materials. For ease of analysis, the four critical points (Figure 12.12) are magnified up to 2000 times as depicted in Figure 12.15 through Figure 12.18.

Figure 12.15, magnified at 200 times, is the micrograph of area 1, which illustrates the fractured surface of neat vinyl ester resin. Striations are followed by a turbulent flow pattern of the fractured zone.

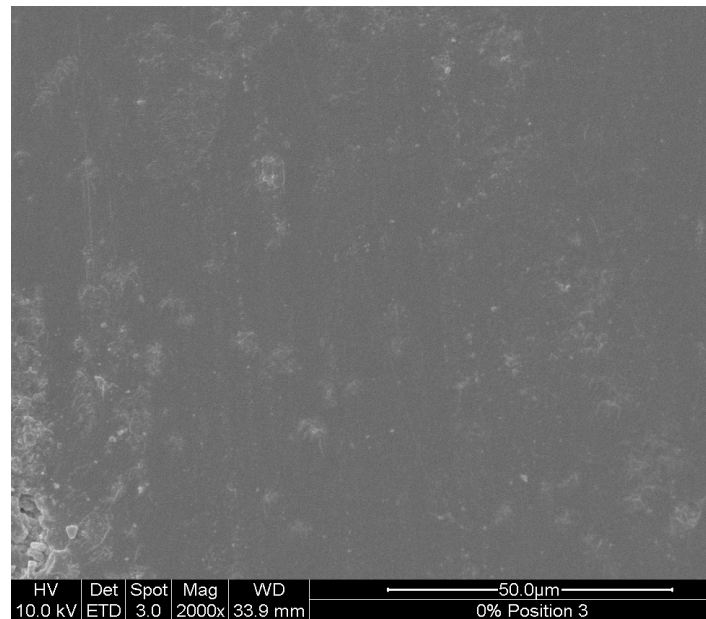


**Figure 12.15: The fractured surface of neat vinyl ester resin, illustrating striations followed by a turbulent flow pattern of the fracture zone, 200X.**

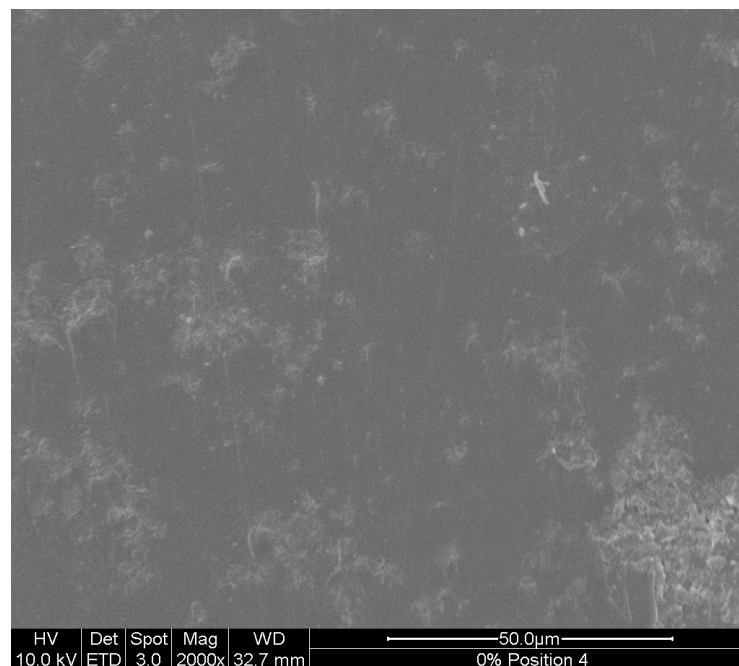


**Figure 12.16: Micrograph of area 2 is the stretched-zone, shows some micro voids and some scratches on the fractured surface 2000X.**

Figure 12.16 shows the micrograph of area 2, the stretched-zone; illustrating some micro voids and some scratches on the fractured surface. Figure 12.17 is the micrograph of area 3; showing some elongated matrix. Figure 12.18 is the micrograph of area 4, which exhibits that the matrix failed in brittle manner.

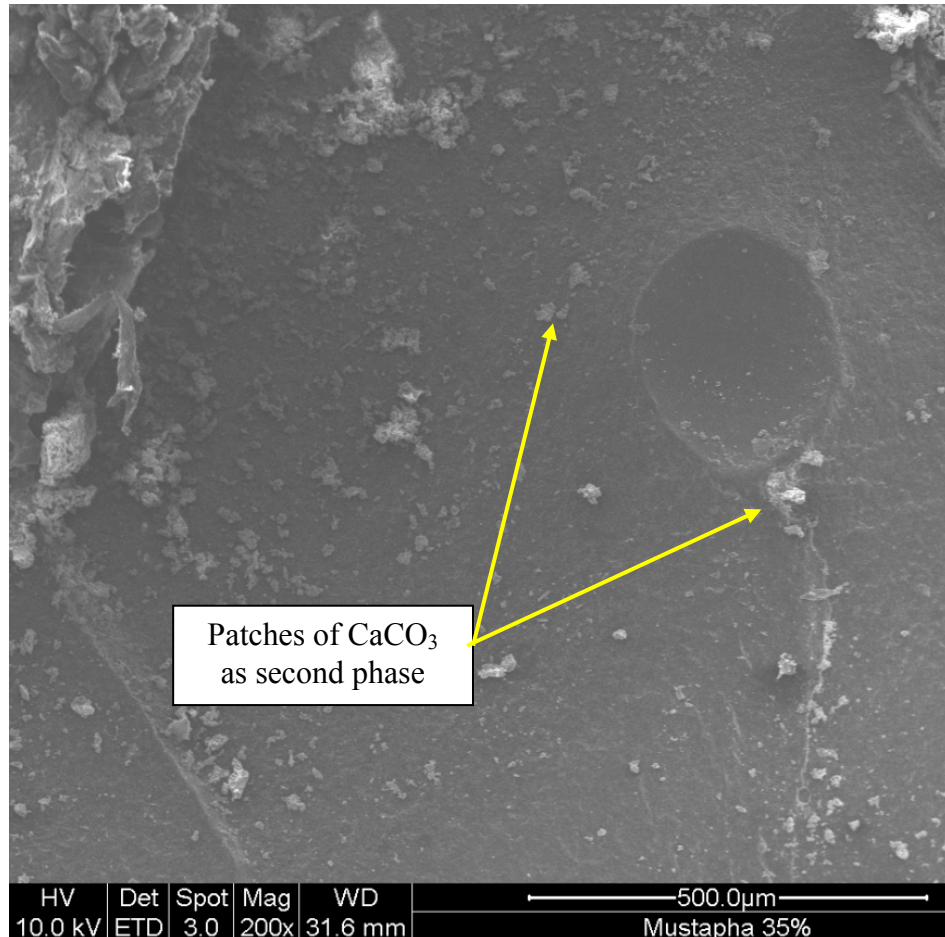


**Figure 12.17: Micrograph of area 3, 2000X**



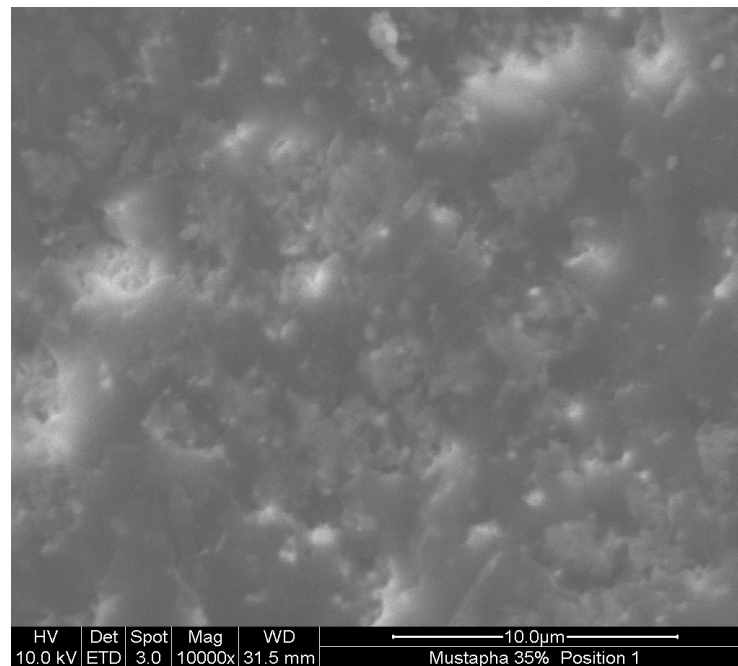
**Figure 12.18: Micrograph of area 4, 2000X**

The second specimen is VE/CaCO<sub>3</sub> (35%) which has the highest fracture toughness value. The filler mixes with the resin very well and there is only one phase in the system. As a result, it can be argued that the CaCO<sub>3</sub> powder actually dissolved into the resin.



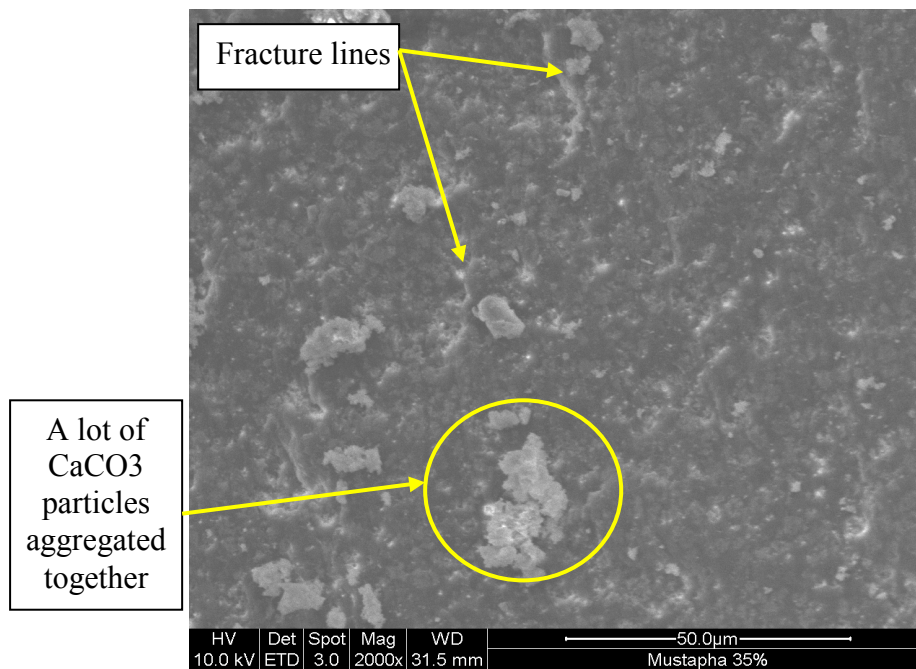
**Figure 12.19:** The fractured surface of 35% calcium carbonate powder by weight filled vinyl ester composites, where patches of calcium carbonate appear as second phase and strengthen the structure, 200 X.

Appearing as second phase in Figure 12.19; patches of calcium carbonates help to strengthen the structure. For further investigation, the chosen four critical points are magnified up to 10000 times and are depicted in Figure 12.20 through Figure 12.23.

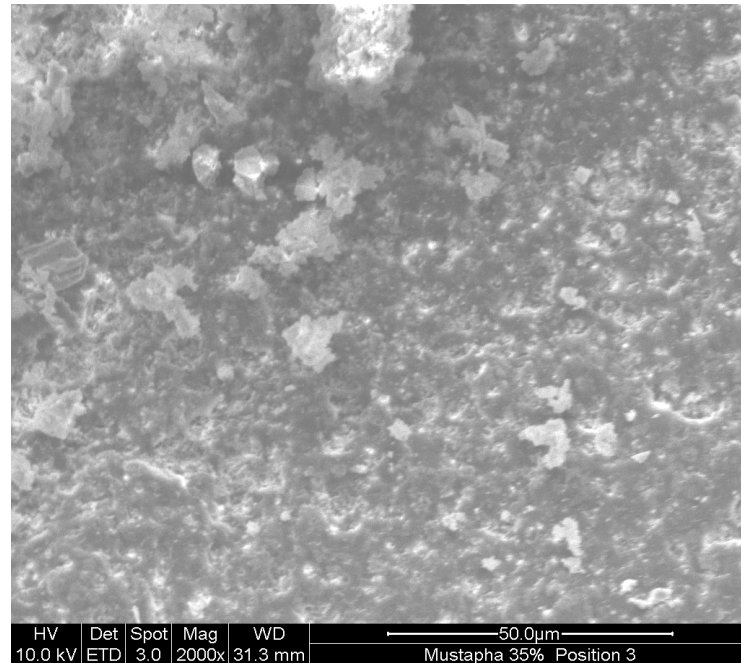


**Figure 12.20: The micrograph of area 1, the  $\text{CaCO}_3$  powder partially dissolves in the resin, 10000X**

Figure 12.20 is the micrograph of area 1 and it shows that the  $\text{CaCO}_3$  particles actually dissolve into the resin as no sharp edges of  $\text{CaCO}_3$  particles can be observed.

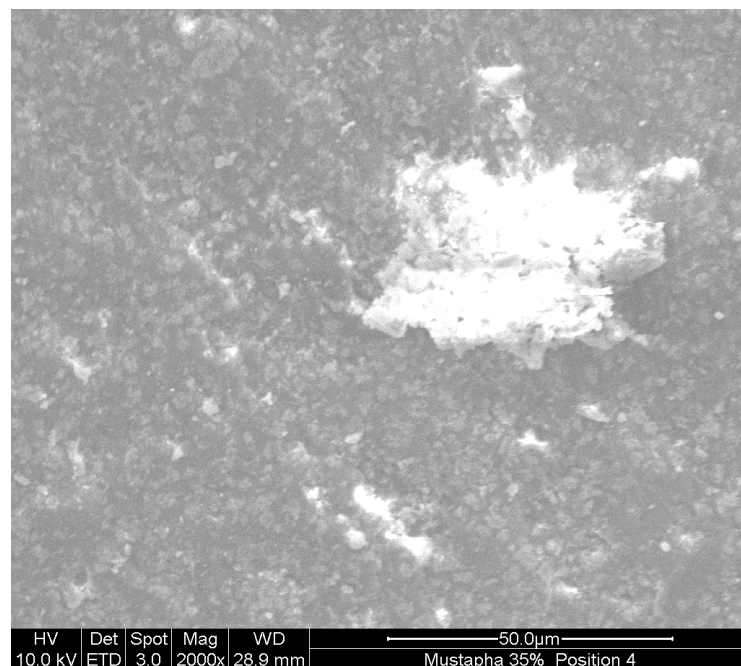


**Figure 12.21: The micrograph of area 2 shows brittle fracture lines and aggregated particles of  $\text{CaCO}_3$ , 2000X**



**Figure 12.22:** The micrograph of area 3 shows different sizes of CaCO<sub>3</sub> aggregated particles.

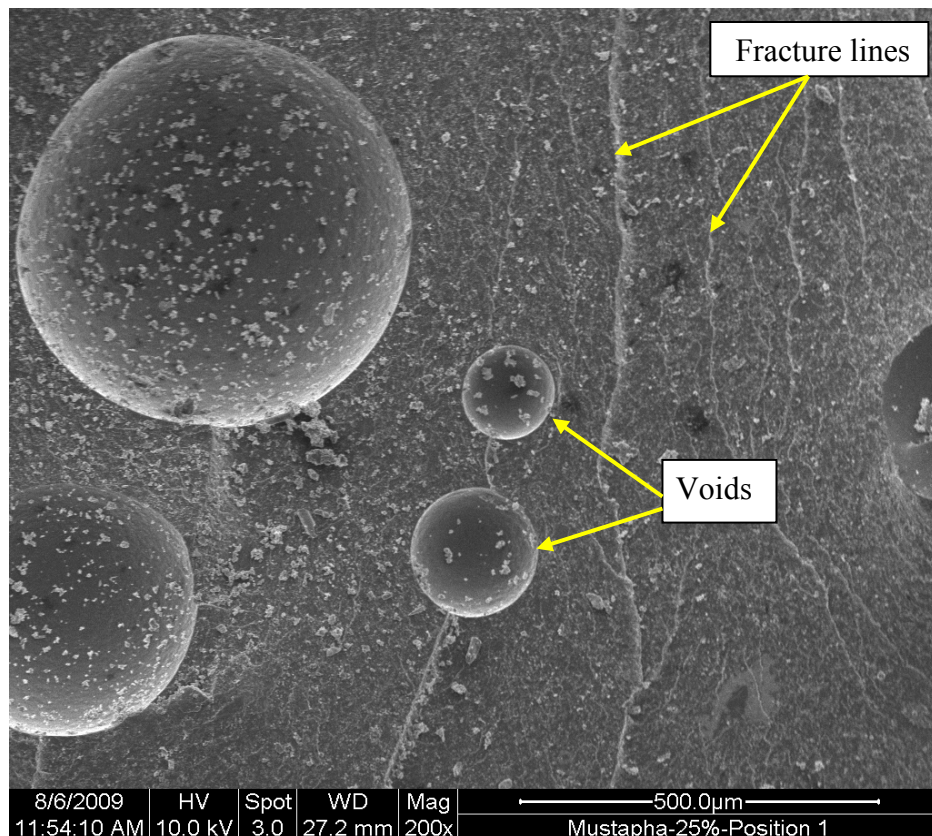
Figure 12.21 is the micrograph of area 2; which depicts brittle fracture lines and a mixture of aggregated CaCO<sub>3</sub> particles of different sizes. Figure 12.22 is the micrograph of area 3; in which most of the fractured surfaces have been damaged.



**Figure 12.23:** The micrograph of area 4, 2000X

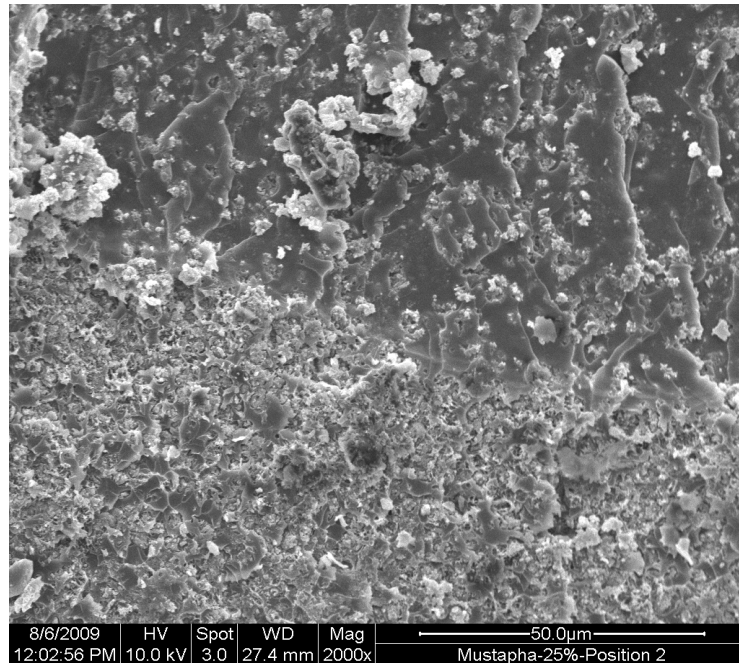
Figure 12.23 is the micrograph of area 4; it shows that the material has failed in brittle manner and some big chunk of aggregated particles of  $\text{CaCO}_3$  can be observed.

The third specimen is VE/ $\text{CaCO}_3$  (25%) which has the lowest fracture toughness value. Similarly, four critical points are analysed with magnification up to 2000 times as depicted in Figure 12.24 through Figure 12.27.



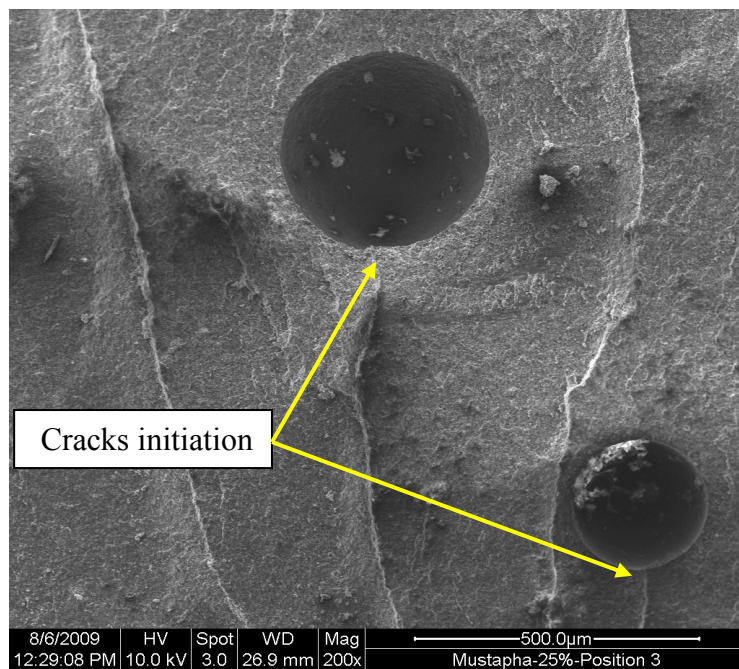
**Figure 12.24:** The micrograph of area 1 shows large voids

Figure 12.24 is the micrograph of area 1; showing large air bubbles and brittle fracture lines.



**Figure 12.25:** The micrograph of area 2 shows that most of the fracture surface has been damaged

Figure 12.25 is the micrograph of area 2 in which most of the fracture surface has been damaged.



**Figure 12.26:** The micrograph of area 3 shows that some of the fracture lines initiated at the air voids

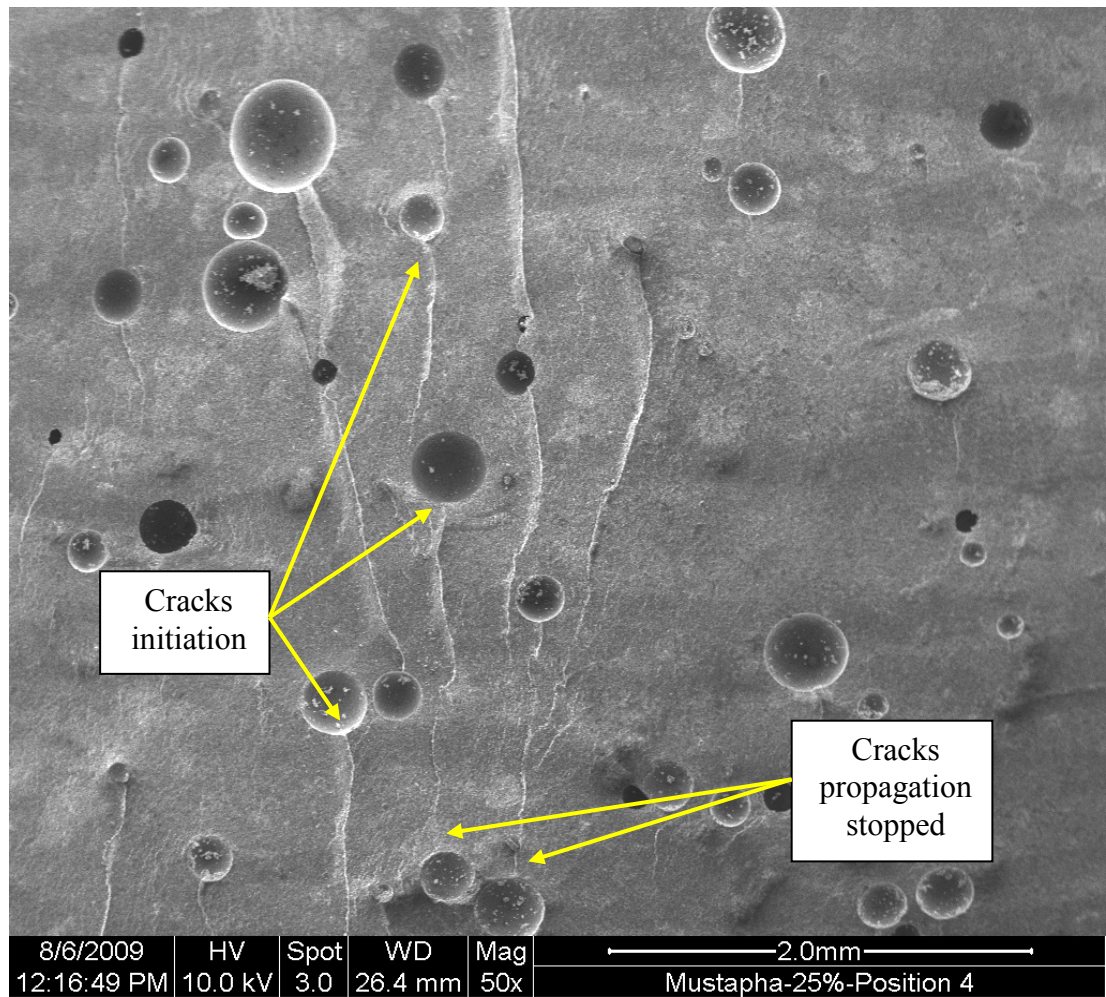


**Figure 12.27:** The micrograph of area 4 shows that air voids are shown to serve both as crack initiators and crack arrestors.

Figure 12.26 is the micrograph of area 3 in which some of the fracture lines are initiated at the air voids. This explains the low values of fracture toughness obtained. Finally, Figure 12.27 is the micrograph of area 4 and it illustrates that the air voids can serve as either crack initiators or crack arrestors.

## 12.4 Loss Tangent Test

In this test, it is necessary to divide the results into two groups according to the frequency used to measure the properties of the composites. The first group is the low frequency group which can go up to 1 kHz. The second group is the high frequency group which can reach 10 kHz or more (Ku et al. 2008).

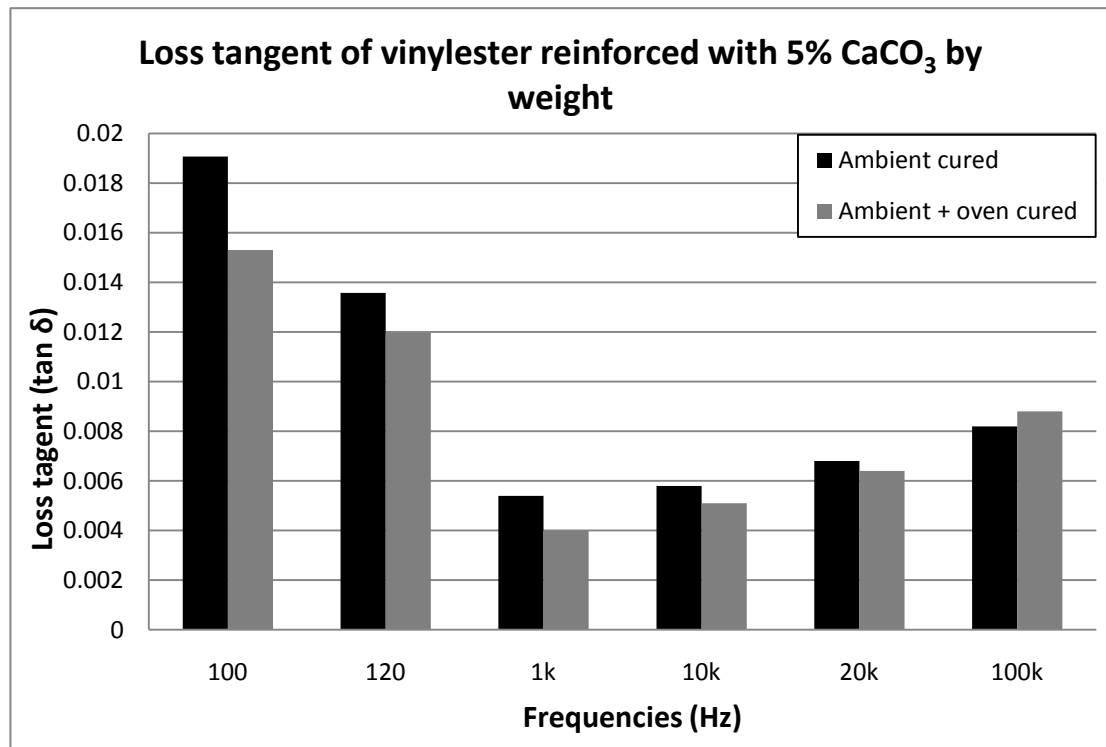


Figure 12.28: Loss tangent of vinylester reinforced with 5% CaCO<sub>3</sub> by weight.

Figure 12.28 shows the loss tangent results of vinylester samples reinforced with 5% by weight of calcium carbonate powder at different frequencies. The results shown are for two specimens. One of them is cured in ambient conditions, whilst the other is cured in ambient conditions and later post-cured in an oven. The values for loss tangent vary from a maximum of 0.019 at 100Hz to a minimum of 0.0054 at 100 kHz, as shown in Figure 12.28. In low frequency group, the microwave ambient cured specimens have higher loss tangent values than their counterparts. The same is true

for the higher frequency group except at 100-kHz. Generally, the ambient cured samples have higher loss tangent than the ambient and post-cured samples.

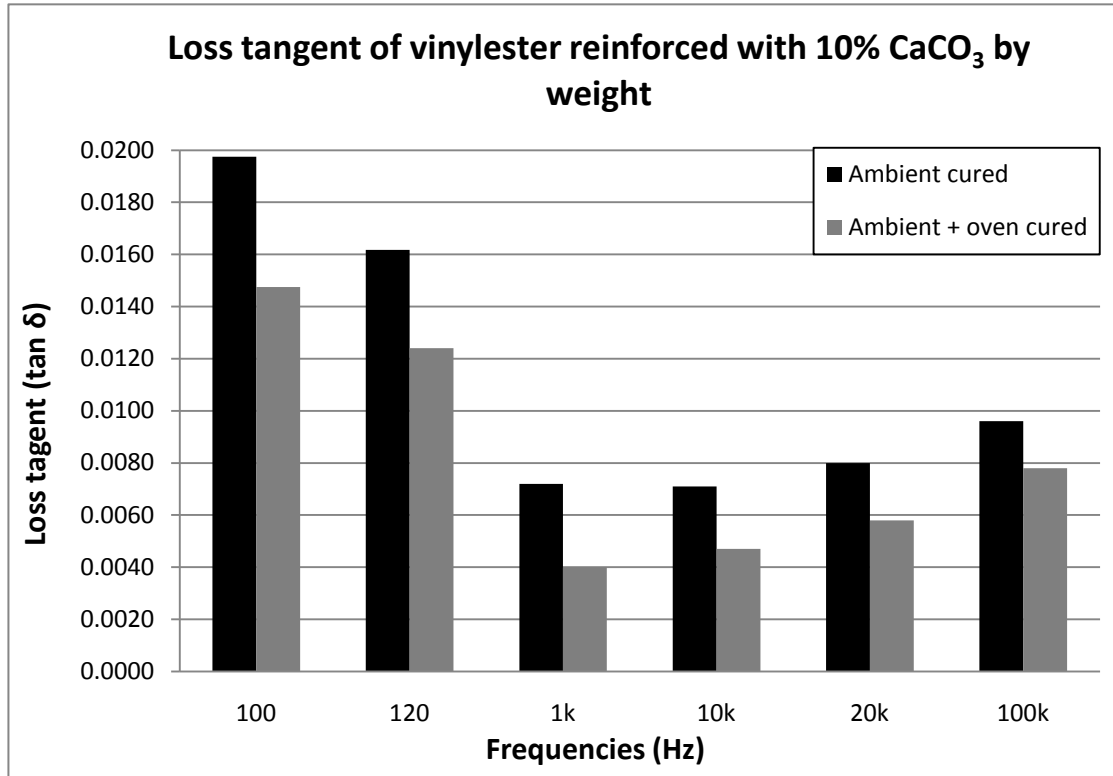


Figure 12.29: Loss tangent of vinyl ester reinforced with 10% CaCO<sub>3</sub> by weight.

Figure 12.29 shows the loss tangent results of vinyl ester samples reinforced with 10% by weight of calcium carbonate powder at different frequencies. These results have similar trend to the results obtained at 5% calcium carbonate filler. In this case, the values for loss tangent vary from a maximum of 0.02 at 100Hz to a minimum of 0.004 at 100 kHz, as shown in Figure 12.29. In general, the ambient cured samples have higher loss tangent than the ambient and post-cured samples, in both high and low frequency groups.

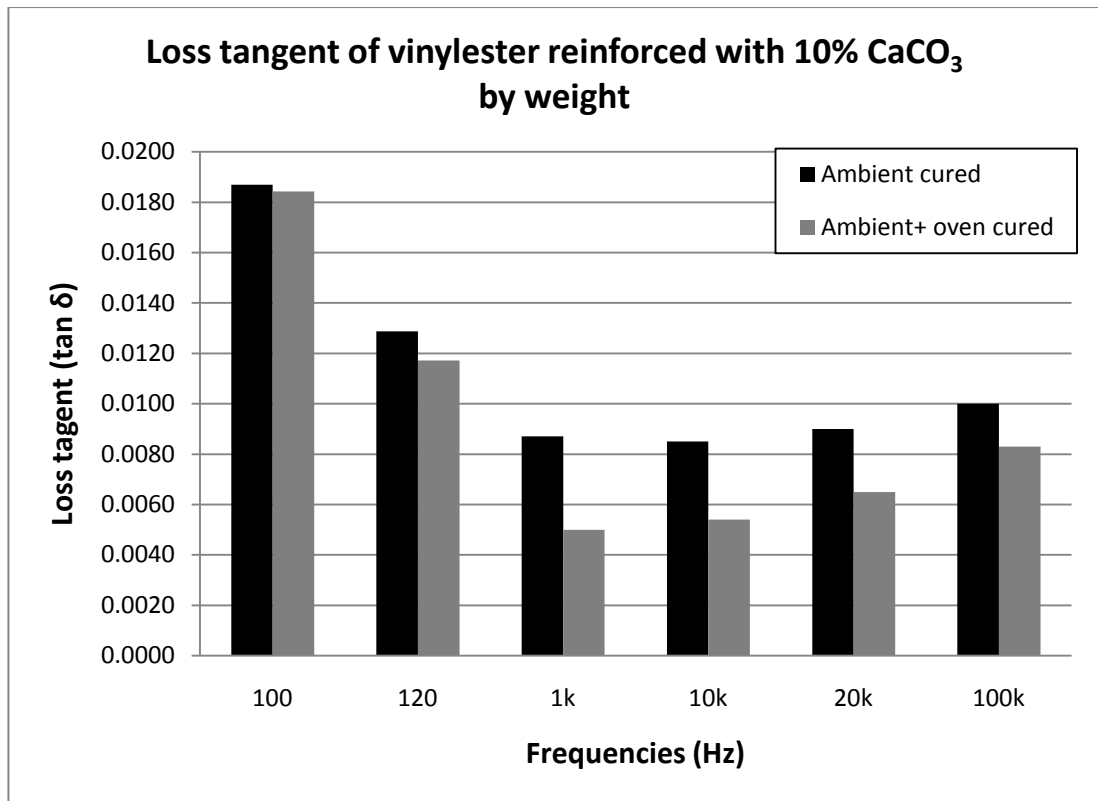


Figure 12.30: Loss tangent of vinylester reinforced with 15% CaCO<sub>3</sub> by weight.

Figure 12.30 shows the loss tangent results of vinylester samples reinforced with 15% by weight of calcium carbonate powder at different frequencies. These results have similar trend to the results obtained at 5% and 10% of calcium carbonate filler. In this case, the values for loss tangent vary from a maximum of 0.019 at 100Hz to a minimum of 0.005 at 100 kHz, as shown in Figure 12.30. Overall, the ambient cured samples have higher loss tangent than the ambient and post-cured samples, in both high and low frequency groups.

In conclusion, the specimens cured at ambient temperature and later post cured in a conventional oven have lower loss tangent than their counterparts. It can be argued that the dielectric behaviour of these specimens is due to the water content. Since the ambient cured samples have higher loss tangent values, it implies that they have more

water content and because post-curing in an oven will remove the water content of the samples; hence loss tangent values will be lower.

The loss tangent values tangent values for different frequencies, curing methods and filler percentages are listed in Table 12.5.

**Table 12.5: Loss tangent values for different frequencies, curing methods and filler percentages.**

CaCO <sub>3</sub> percentage by weight	Curing method	Frequencies (Hz)					
		100	120	1k	10k	20k	100k
5%	Ambient	0.0191	0.0136	0.0054	0.0058	0.0068	0.0082
	Ambient plus oven	0.0153	0.0120	0.004	0.0051	0.0064	0.0088
10%	Ambient	0.0198	0.0162	0.0072	0.0071	0.0080	0.0096
	Ambient plus oven	0.0148	0.0124	0.0040	0.0047	0.0058	0.0078
15%	Ambient	0.0187	0.0129	0.0087	0.0085	0.0090	0.0100
	Ambient plus oven	0.0184	0.0117	0.0050	0.0054	0.0065	0.0083

## **12.5 Concluding Remarks**

### **12.5.1 Fracture Toughness**

The values of fracture toughness of calcium carbonate powder reinforced vinyl ester resin with varying percentage of filler by weight were measured by short bar tests. It was found that fracture toughness became lower in all the filled composites. This agreed with the generalization made by Fu et al. (2008) that strong adhesion led to high toughness in thermoplastic matrices but not necessarily true in thermosetting matrices due to different failure mechanism. The fractured surfaces were examined under a SEM and were correlated with the mechanical properties. Even  $\text{CaCO}_3$  powder is a good construction material; it was not a suitable filler for vinyl ester resin if fracture toughness was the required property in those specific applications.

### **12.5.2 Dynamic Mechanical Analysis**

The DMA measurement showed that the glass transition temperature for all the samples, ambient cured and ambient cured plus post-cured in an oven for different percentages were similar. Moreover, the values for the storage modulus for the ambient cured samples were always lower than their counterparts. Similarly, the loss modulus for ambient cured samples was lower than their counterparts except at 5% by weight of the filler.

Furthermore, adding the filler, calcium carbonate powder, did not have significant effects on the viscoelastic properties of the composites. Mostly, the glass transition temperature, storage modulus and loss modulus support the fact that post-cured sample is stiffer than its counterpart due to higher degree of curing.

### **12.5.3 Microscopic Analysis**

The results obtained from the SEM analysis showed some important features such as brittle or ductile behaviour and elongation of the fractured surface of the composite. Samples with lower fracture toughness were found to have more bubbles in the microstructures than those with higher fracture toughness. It concluded that the micrographs gave reasonable explanations to the mechanical behaviour of the samples. Additionally, it was observed that the calcium carbonate powder could partially dissolve into the vinylester resin.

Magnification should be increased to 10, 000 times or more for obtaining more information from the images. A few of the micrographs acquired shows that the surface of the chevron cut deteriorates by being scratched or compressed by other materials. This may damage the important features of the crack. Therefore, the specimens have to be kept in a solid container, and should be taken for viewing under SEM as soon as possible after tensile tests.

More information can be obtained if computer software is used to analyse and simulate the experimental results, such as the area of maximum fracture toughness. The COSMOS software package is suggested because it is user-friendly and can be incorporated with other software such as SolidsWorks.

### **12.5.4 Loss Tangent**

The specimens cured at ambient temperature and later post-cured in a conventional oven have lower loss tangent than their counterpart. The main contributor to this phenomenon is due to the water content in the specimens. The oven post-cured

specimens have less water content than the ambient cured specimens, since the post curing in oven removes the water content in the specimens. Therefore, the loss tangent values for the oven post-cured specimens will be lower than those in the ambient cured specimens.

## **12.6 Further Research**

This project can be expanded to include improvement on the existing techniques used in measuring the fracture, or even introduce new methods in predicting fracture toughness.

Moreover, different methods in improving the fracture toughness can also be devised. Two methods for fracture toughness investigation are proposed in this project. The first method uses a different filler concentration across the thickness or at specific locations in the material. Therefore the final material can be, for example, brittle in the middle but ductile near the surface which may have a positive effect on fracture toughness. The second method is associated with the filler particles arrangements. For example, this can be using ferromagnetic filler materials such as iron or nickel, instead of calcium carbonate, and ensuring specific arrangements of the filler particles by applying a magnetic field to the specimen. In this case, the investigation will focus on comparing dissimilar filler arrangements in determining the best arrangement that gives the highest fracture toughness.

### 12.6.1 Predicting Fracture Toughness using FEA

Fracture toughness can be modelled by means of finite element analysis (FEA) which will help in predicting fracture toughness. In this project, an attempt is made to model the fracture toughness. However, the modelling is difficult since most of the calcium carbonate particles dissolve in the resin and their shape cannot be easily defined for modelling.

The following presents an idea on how to conduct the FEA analysis:

The objective of conducting the FEA elastic-plastic analysis provides help in understanding the effects of the filler particles on the plastic zone, on which the crack starts to progress through the material (Huang & Kinloch 1992).

In addition to the mechanical properties of the composite that is needed to run the FEA test, the prediction will also be based on the shape factor of the filler particles, the percentage by weight of the filler material in the composite, and the strength of the chemical bond between the vinyl ester composite and the filler material (Huang & Kinloch 1992).

Figure 12.31 illustrates a model which replicates a small region in the composite material. The white circular spheres in the model represent the calcium carbonate particles. This model can be used to calculate the fracture toughness by obtaining the strain energy density at the edge of the calcium carbonate particles.

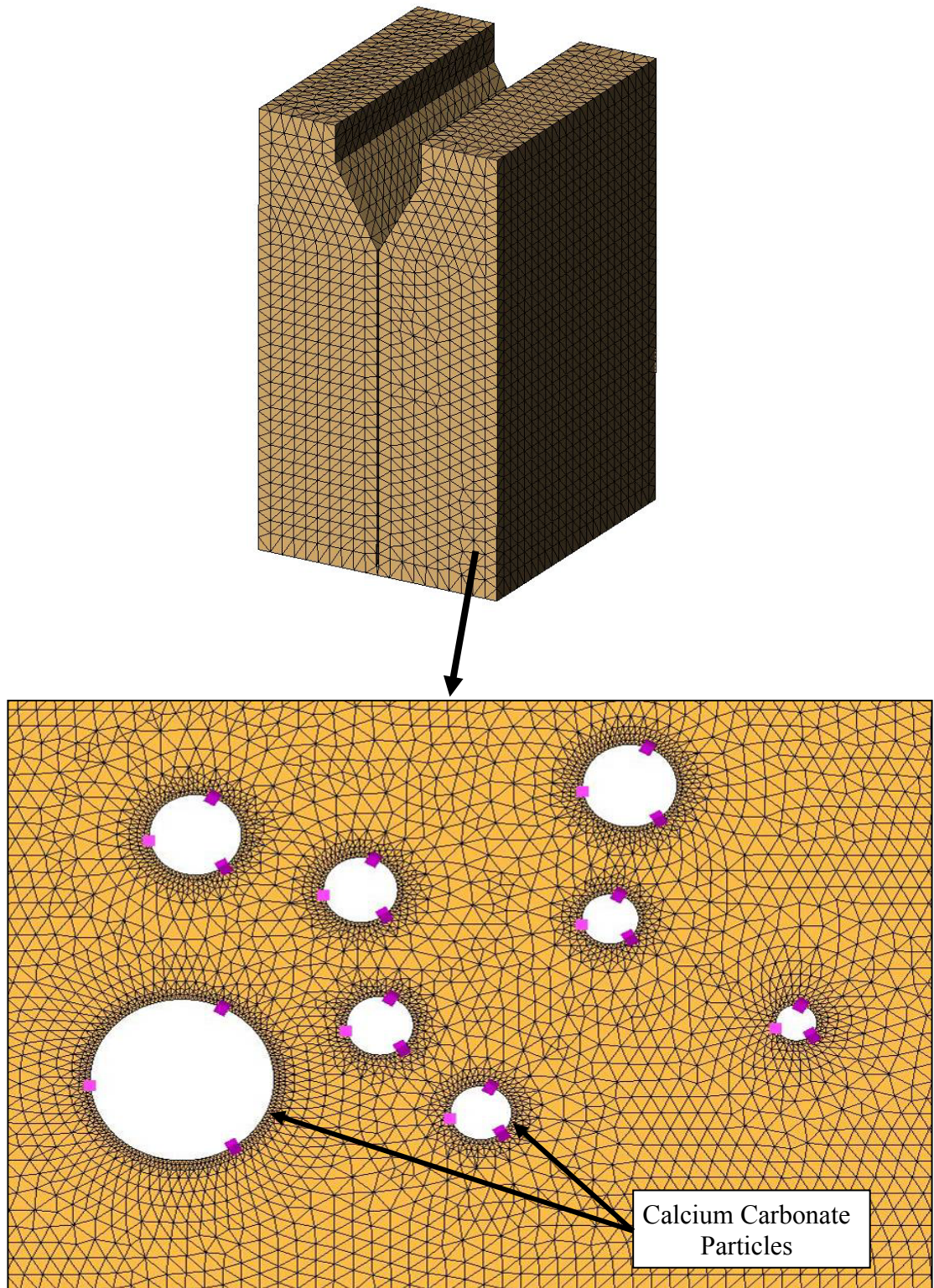


**Figure 12.31: The mesh of the model (random distribution of the particles) – mesh density is increased at the matrix/particle border.**

### 12.6.2 Different Filler Concentrations

The majority of the previous studies had investigated the best percentage of particular filler in a resin, but most of them were not thorough enough. Those cases did not study the effects of different particles arrangements nor did they use different percentages of the filler across the thickness of the material.

New moulds will be used to achieve different concentrations of the filler across the material thickness; these moulds will have the same shape but in a different scale of the original mould. The preparation procedures of the specimen will be similar to those mentioned before, and the number of these procedures will depend on the required number of different percentages in a sample.

For example, to prepare a specimen with three different filler percentages (zero, five and ten percent), three moulds will be required. As mentioned before these three moulds will have the same shape but in different scales. First of all, the zero percent composite is poured into the smallest mould, in which the specimen is then cured. It will then be removed and placed in the bigger mould, where the composite that contains five percent is then poured. Finally after this composite is cured, it will be removed from the mould and placed in the last mould to which the vinyl ester composite containing ten percent of the filler will be added. The final mould will be kept until the specimen is cured, then the sample will be removed to start the post curing process. It can be noticed that the scale of the mould will vary depending on the required thickness of each composition.

Figure 12.32 shows a sample of a rectangular block, made up of three different percentages of the filler.

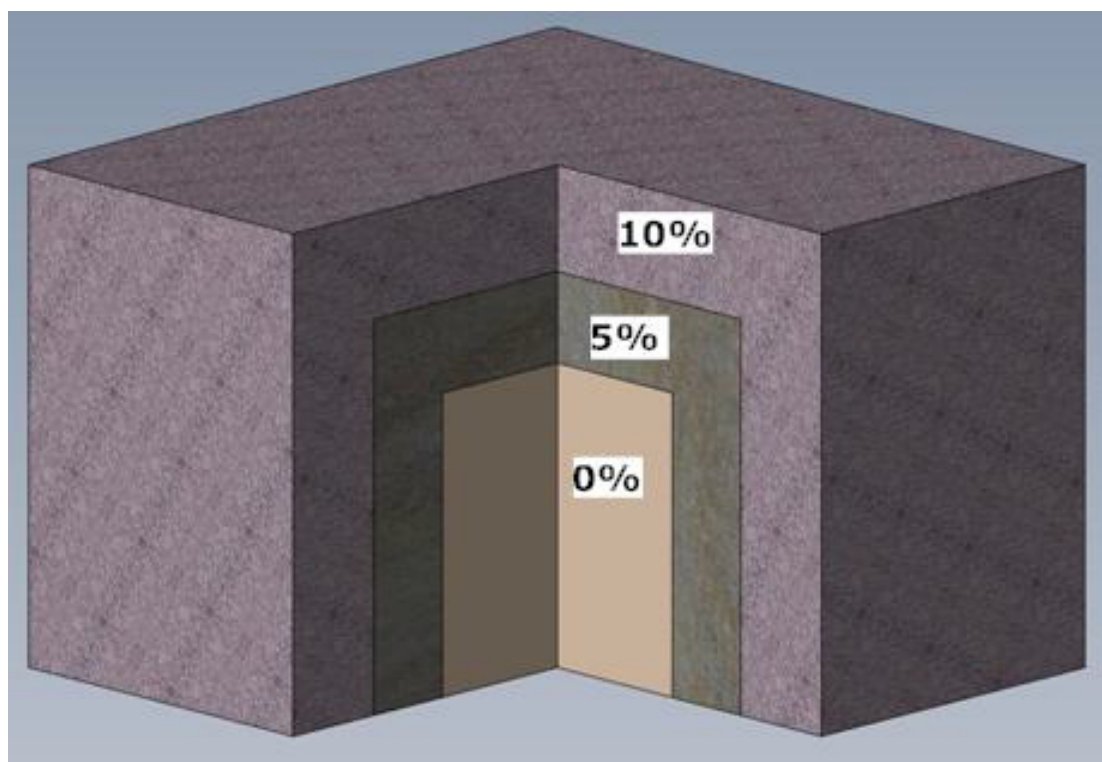


**Figure 12.32: Simple geometry with three different percentages of the filler**

## References

Agarwal, BD, Broutman, LJ & Chandrashekhara, K 2006, *Analysis and performance of fiber composites*, John Wiley & Sons Inc., 3<sup>rd</sup> edn, NJ.

American Society for Testing and Materials 1999, *Standard Test Method for Plane-Strain Fracture Toughness of Metallic Materials*, E 399-90, Annual Book of ASTM Standards, vol. 03.01, p 422–452.

Antolovich, SD & Antolovich, BF 2002, *An introduction to fracture mechanics*, Fatigue and Fracture, vol. 19, ASM Handbook, ASM International, USA.

Arist Craft 2009, *Calcium carbonate*, Aristocrat Holdings, viewed 4 June 2009, <<http://www.aristocratholding.com/calris-5.html>> .

Askeland, DR 1999, *The science and engineering of materials*, 4<sup>th</sup> edn, Stanley Thornes, USA.

ASM International 2003, *Fracture toughness and fracture mechanics*, Mechanical testing and evaluation, vol. 8, ASM Handbook, ASM International, USA.

ASM Metals Reference Book 1981, American Society for Metals, USA.

Astrom, BT 1997, *Manufacturing of polymer composites*, Chapman and Hall, UK, pp.74-83, 432-4.

Auad, ML, Frontini, PM, Borrajo, J & Aranguren, MI 2001, 'Liquid rubber modified vinyl ester resins: fracture and mechanical behaviour', *Polymer*, vol. 42, pp. 3723-3730.

Baddeley, DT & Ballard J 1991, 'Evaluate the short rod/bar fracture mechanics test', BEng thesis, School of mechanical and manufacturing engineering, Queensland University of Technology, Australia.

Baker, LM 1980, 'Development of the short rod method of fracture toughness measurement', *Proceedings of wear and fracture prevention conference*, 21-22 May, ASM, Metals Park, Ohio, pp. 163-180.

Baker, LM 1981, 'Short Rod and Short Bar Fracture Toughness Specimen Geometries and Test Methods for Metallic Materials', *Proceedings of the thirteenth conference, Fracture Mechanics*, ASMT STP 743, pp. 456-475.

Baker, LM 1981, 'Short Rod and Short Bar Fracture Toughness Specimen Geometries and Test Methods for Metallic Materials', in *Fracture mechanics: proceedings of the thirteenth conference*, ASMT STP 743, pp. 456-475.

Ball, J & Hancock, N 2007, *ELE 4605 Fields and waves: study book*, University of Southern Queensland, Toowoomba.

Barbero, EJ 1998, *Introduction to composite materials design*, Taylor & Francis, Philadelphia, PA.

Barker, L M 1977, *Engineering fracture mechanics*, vol. 9, pp. 361-369.

Barker, LM 1979, *Fracture mechanics applied to brittle materials*, ASTM, STP 678, American Society for Testing and Materials, Philadelphia, pp.73-82.

Barker, LM 1981, 'Short Rod and Short Bar Fracture Toughness Specimen Geometries and Test Methods for Metallic Materials', *Fracture Mechanics:*

*Thirteenth Conference, ASTM STP 743*, Richard Roberts, Ed., American Society for Testing and Materials, Philadelphia, pp. 456-475.

Behzad, M, Tajvidi, M, Ehrahimi, G & Falk, RH 2004, 'Dynamic mechanical analysis of compatibilizer effect on the mechanical properties of wood flour-high density polyethylene composites', *International Journal of Engineering*, vol. 17, no.1, pp. 95-104.

Blankenship, LT, White, MN & Puckett, PM 1989, *Vinyl ester resins: versatile resins for composites*, 34<sup>th</sup> International SAMPE Symposium, Dow Chemical U.S.A., Freeport, TX.

Blinn, MP & Williams, RA 2002, *Categories of Fracture Mechanics*, Materials Characterization Laboratory, vol. 20, ASM Materials information, USA.

Bozzola, JJ & Russell, LD 1992, *Electron microscopy-principles and techniques for biologists*, Jones and Bartlett Publishers, New York.

Bryce, DM 1997, *Plastic injection molding: material selection and product design fundamentals*, vol. 2, SME, Dearborn, Michigan, p.88.

Callister, WD 2003, *Materials science and engineering: an introduction*, 6<sup>th</sup> edn, John Wiley and Sons, Inc., New York, pp. 201-203, p. 787.

Campbell, JE, Gerberich, WW & Underwood, JH 1982, *Application of Fracture Mechanics for Selection of Metallic Structural Materials*, ASM.

Cardona, F, Ku, H, Pattarachaiyakoop, N, Rogers, D & Trada, M 2007, 'Fracture Toughness of Phenol Formaldehyde Composites post-cured in Microwaves', *Journal of Electromagnetic Waves and Applications*, vol. 21, no. 14, pp. 2137-2146.

- Cardona, F, Ku, H, Pattarachaiyakooop, N, Trada, M & Rogers, D 2009, 'Fracture toughness of phenol formaldehyde composites reinforced with E-spheres', *Journal of composite materials*, vol. 43, no. 7, pp. 741-754.
- Cardona, F, Rogers, D, Gurney, R, Trada, M and Ku, H 2009, 'Flexural Tests of Phenol Formaldehyde and SLG Composites: Preliminary Results', *Journal of Reinforced Plastic and Composites*, (accepted for publication).
- Chapman, SK 1986, *Working with a scanning electron microscope*, Lodgemark press.
- Chew, CS, Ku, H, Snook, C and Baddeley, D 2005, 'Micrographs of the Fracture of Vinyl Ester Composites Cured by Microwaves: Pilot Study', *Journal of Electromagnetic Waves and Applications*, vol. 19, no. 1, pp. 67-82.
- Cook, WD, Simon, GP, Burchill, PJ, Lau, M & Fitch, TJ 1997, 'Curing Kinetics and Thermal Properties of Vinyl Ester Resins', *Journal of Applied Polymer Science*, vol. 64, pp. 769-781.
- Coombs, CF 2001, *Printed circuits handbook*, 5<sup>th</sup> edn, McGraw-Hill Professional, New York.
- Dalton, FN & Van Genuchten, MT 1986, *The time-domain reflectometry method for measuring soil water content and salinity*, *Geoderma*, vol. 38, pp. 237-250.
- Davey, R 2006, 'Best percentage by weight of micro-spheres as fillers in phenolic resins, with fracture toughness as a benchmark', BEng thesis, University of Southern Queensland, Australia.

- Davey, SW 2004, 'A foundational investigation of vinyl ester / cenosphere composite materials for civil and structural engineering', PhD thesis, University of Southern Queensland, Australia.
- Divecha, AP, Fishman, SG & Karmarkar, SD 1981, *Silicon carbide reinforced aluminum—a formable composite*, *JOM*, vol. 33, no. 9, pp. 12–17.
- Dreerman, E, Narkis, M, Siegmann, A, Joseph, R, Dodiuk, H & Dibenedetto, AT 1998, 'Mechanical behaviour and structure of rubber modified vinyl ester resins', *Journal of Applied Polymer Science*, vol. 72, no. 5, pp. 647-657.
- Dykstra, MJ & Reuss, LE 2003, *Biological electron microscopy: theory, techniques, and troubleshooting*, 2nd edn, pp. 389-393.
- Fu, S, Feng, X, Lauke, B & Mai, Y 2008, 'Effects of particle size, particle/matrix interface adhesion and particle loading on mechanical properties of particulate-polymer composites', *Composites Part B engineering*, Elsevier, vol. 39, no. 6, pp. 933-961.
- Goldstein, JI, Newbury, DE, Echlin, P, Joy, DC, Romig, AD, Lyman, CE, Fiori, C & Lifshin, E 1992, *Scanning electron microscopy and x-ray microanalysis a text for biologists, materials scientists, and geologists*, Plenum Press, New York.
- Griffith, AA 1921, "The phenomena of rupture and flow in solids", *Philosophical Transactions of the Royal Society of London*, vol. 221, pp. 163-198.
- Guo, T, Wang, L, Zhang, A & Cai, T 2005, 'Effects of nano calcium carbonate modified by lanthanum compound on the properties of polypropylene', *Journal of Applied Polymer Science*, no. 97, pp. 1154 – 1160.

Haddad, YM 1995, *Viscoelasticity of engineering materials*, London: Chapman and Hall, Hanser Publishers, New York.

Huang Y & Kinloch AJ 1992, 'Modelling of the toughening mechanisms in rubber modified epoxy polymers', *Journal of Materials Science*, vol. 27, pp. 2753–2769.

Irwin, GR 1948, *Fracture dynamic in fracturing metals*, American Society of Metals, Cleveland.

ISRM 1981a, *Rock characterization testing and monitoring: ISRM suggested methods*, International Society for Rock Mechanics, Pergamon Press, United kingdom.

ISRM 1981b, *Suggested methods for determining hardness and abrasiveness of rocks, Part 3*, Commission on Standardisation of Laboratory and Field Tests, Pergamon Press, United kingdom, pp. 101–102.

John, D 2002, *Linear-elastic fracture toughness testing*, ASM Handbook online, vol.19, University Of Tennessee, Knoxville.

Juinall, RC & Marshek, KM 2006, *Fundamentals of machine component design*, 4th edn, Wiley & Sons, USA.

Juinall, RC 1967, *Engineering considerations of stress, strain, and strength*, illustrated edn, McGraw-Hill, the University of Michigan, USA.

Katz, HS & Milewski, JV 1987, *Handbook of Fillers for Plastics*, Van Nostrand Reinhold, New York.

- Kenneth, G, Michael, K 2005, *Engineering Materials, Properties and Selection*. New Jersey: The GTS Companies/York, PA Campus.
- Kraus, J D 1992, *Electromagnetics*, 4<sup>th</sup> edition, McGraw-Hill, pp. 95-98, 186-189.
- Ku, H, Cardona, F, Ball, J, Jacobsen, W & Trada, M 2008, 'Relationship between electrical and mechanical loss tangents of SLG reinforced phenolic composites: pilot study', *Journal of Composite Materials*, vol. 42, no. 19, pp. 2083-2095.
- Ku, HS, Fok, SC & Siores, E 2009, 'Contrasts on fracture toughness and flexural strength of varying percentages of SLG-reinforced phenolic composites', *Journal of Composite Materials*, vol. 43, no. 8, pp. 885-895.
- Ku, SH 2003, 'Curing vinyl ester particle reinforced composites using microwaves', *Journal of Composite Materials*, vol. 37, no. 22, pp. 2027 - 2042.
- Kulshreshtha, AK & Vasile, C 2002, *Handbook of polymer blends and composites*, illustrated edn, iSmithers Rapra Publishing, UK.
- Landes, JD & Herrera, R 1989, *Micromechanisms of elastic/plastic fracture toughness  $J_{Ic}$* , ASM Materials Science Seminar, ASM International, pp. 111-130.
- Li, H, Burts, E, Bears, K, Ji, Q, Lesko, JJ, Dillard, DA, Riffle, JS & Puckett, PM 2000, 'Network structure and properties of dimethacrylate-styrene matrix materials', *Journal of Composite Materials*, vol. 34, no. 18, pp. 1512-1528.
- Li, L 200, *Dynamic mechanical analysis (DMA), basics and beyond*, Perkin Elmer Inc., pp. 3, 15, 17.
- Mallick, PK 1997, *Composites Engineering Handbook*, Marcel Dekker, USA.

- Matsuki, K, Matsune, S and Takahashi, H 1991, 'Boundary element analysis for standard specimen configurations in the ISRM suggested methods for determining fracture toughness of rock', *International journal of rock mechanics and mining sciences & geomechanics abstracts*, vol. 28, no. 5, Pergamon, pp. 355–363.
- Metaxas, AC & Meredith, RJ 1983, *Industrial microwave heating*, illustrated edn, vol. 4, IET, Peter Peregrinus Ltd, United Kingdom.
- Meyers, MA & Chawla, KK 1998, *Mechanical Behaviours of Materials*, Prentice-Hall, New Jersey.
- Microscopy Society of America 2009, Microscopy Society of America, Virginia, USA, viewed on 25 August 2009, < <http://www.microscopy.org>>.
- Miracle, DB & Donaldson, SL 2003, 'Introduction to composites', *Composites*, ASM handbook, vol. 21, ASM International, Materials Park.
- Munz, D 1981, 'Determination of fracture toughness of high strength aluminum alloys with chevron notched short rod and short bar specimens', *Engineering Fracture Mechanics*, vol. 15, no. 1-2, pp. 231-236.
- Osswald, TA & Menges, G 1995, 'Materials science of polymers for engineers', *Mechanical properties of films and coating*, Thermal analysis, PerkinElmer Life, USA, pp. 1-12.
- Osswald, TA 1998, *Polymer processing fundamentals*, Hanser Verlag, pp. 15-17.
- Pérez, JDE, Wiesenborn, DP, Ulven, CA, Haagenson, DM & Brudvik, RL 2009, 'Epoxy resins from high-oleic oils applied to composites', *ASABE Annual*

*International Meeting*, The American Society of Agricultural and Biological Engineers, Nevada.

Ping, D, Yanbing, W & Zhixiong, H 2008, 'Effect of thermal crosslink conditions on dynamic mechanical behaviors of flexible epoxy', *Journal of Wuhan University of Technology-Mater*, Wuhan University of Technology, vol. 23, no. 6, pp. 825-829.

Pollard, D & Fletcher, R 2005, *Fundamentals of structural geology*, Cambridge University Press, p.357.

Pritchard, G (Editor) 1999, 'Reinforced plastics durability', *SAMPE Journal*, Woodhead publishing Ltd., pp. 282-93.

Rai, US & Singh, RK 2004, 'Synthesis and mechanical characterization of polymer-matrix composites containing calcium carbonate/white cement filler', *Materials Letters*, vol. 58, no. 1-2, pp. 235-240.

Ramo, S, Whinnery, JR & Van Duzer, T 1994, *Fields and waves in communication electronics*, 3rd edn, John Wiley and Sons, New York.

Ray, D, Bhattacharya, D, Mohanty, AK, Drzal, LT & Misra, M 2006, 'Static and dynamic mechanical properties of vinyl ester resin matrix composites filled with fly ash', *Macromolecular Materials and Engineering*, vol. 291, pp. 784 – 792.

Reade Advanced Materials 2006, Reade Advanced Materials, Rhode Island, USA, viewed on 4 June 2009,

<[http://www.reade.com/Products/Minerals\\_and\\_Ores/calcium\\_carbonate.html](http://www.reade.com/Products/Minerals_and_Ores/calcium_carbonate.html)>.

Rittner, MN 2000, 'Metal matrix composites in the 21st century: markets and opportunities', *Report GB-108R*, Business Communications Co., Norwalk, CT.

- Robinette, EJ, Ziaee, S & Palmese, GR 2004, 'Toughening of vinyl ester resin using butadiene-acrylonitrile rubber modifier', *Polymer*, vol. 45, pp. 6143-6154.
- Scott, TF, Cook, WD & Forsythe, JS 2002, 'Kinetics and network structure of thermally cured vinyl ester resins', *European Polymer Journal*, no. 38, pp. 705-716.
- Sharma, R 2006, *ELE 1801 Electrical Technology: study book*, University of Southern Queensland, Toowoomba.
- Shukla, A 2005, *Practical fracture mechanics in design*, illustrated edn, vol. 183, CRC Press, New York, USA.
- Solvay Precipitated Calcium Carbonate 2007, Solvay S.A, rheinberg, Germany, viewed on 4 June 2009,  
<[http://www.solvaypcc.com/safety\\_environment/0,0,1000044-\\_EN,00.html](http://www.solvaypcc.com/safety_environment/0,0,1000044-_EN,00.html)>.
- Stuart, ML 1989, *Dictionary of composite materials technology*, CRC Press, California, USA.
- Sumerak, JE & Martin, JD 2001, 'Pultrusion', *composites*, ASM Handbook, vol. 21.
- TA Instruments 2004, Dynamic Mechanical Analysis (DMA) Training Course Manual, pp.10-13
- The British Standards Institution 1991, 'Fracture Mechanics Tests, Part 1: Method for Determination of  $K_{Ic}$ , Critical CTOD and Critical J Values of Metallic Materials', BS 7448: Part 1.

Thostenson, ET & Chou, TW 1999, 'Microwave processing: fundamental and applications', *Composites Part A: Applied Science and Manufacturing*, vol. 30, no.9, pp. 1055–1071.

Truong, VT, Codd, AR & Forsyth, M 1994, 'Dielectric properties of conducting polymer composites at microwave frequencies', *Journal of Materials Science*, vol. 29, pp. 4331-4338.

University of Nebraska, Lincoln, viewed on 26 August 2009,

<[www.unl.edu/CMRACfem/em.htm](http://www.unl.edu/CMRACfem/em.htm)>

Venter, RD & Hoepfner, DW 1985, 'Crack and Fracture Behavior in Tough Ductile Materials', *Report submitted to the Atomic Energy Control Board of Canada*, Canada.

Wang, CH 1996, *Introduction to Fracture Mechanics*, Airframes and Engines Division Aeronautical and Maritime Research Laboratory, Australia.

Wells, AA 1955, 'The condition of fast fracture in aluminium alloys with particular reference to comet failures', *British Welding Research Association Report*, UK.

Yang, K, Yang, Q, Li, Q, Sun, Y & Feng, D 2006, 'Morphology and mechanical properties of polypropylene/calcium carbonate nano composites', *Materials Letter*, vol. 60, no. 6, pp. 805-809.

Ziaee, S & Palmese, GR 1999, 'Effects of temperature on cure kinetics and mechanical properties of vinyl-ester resins', *Journal of Polymer Science: Part B: Polymer Physics*, vol. 37, pp. 725-744.

Zweben, C 1998, 'Composite Materials And Mechanical Design', *Mechanical Engineers' Handbook*, 2nd edn, Myer Kutz, Ed, John Wiley & Sons, New York.

## Appendix A - Project Specification

University of Southern Queensland  
Faculty of Engineering and Surveying

### ENG 4111/4112 Research Project

#### PROJECT SPECIFICATION

TOPIC: **Measurement of fracture toughness of calcium carbonate reinforced vinyl ester composites.**

STUDENT: Mustapha Jamal Eddine - 0050060811

SUPERVISOR: Dr. Harry Ku

ENROLMENT: ENG4111 – S1, 2009;  
ENG4112 – S2, 2009

#### PROJECT AIM:

To evaluate the fracture toughness of vinyl ester specimens that contains different percentage to weight of fillers. Findings will be analysed in detail in order to establish behavioural trends and, if time permits, formulas that can be used for theoretical prediction of filled polymer behaviour.

#### PROGRAMME: (Issue A, 24<sup>th</sup> March 2009)

1. Research for information on vinyl ester and Calcium carbonate.

Begin : 6<sup>th</sup> March 2009

Completion : 20<sup>th</sup> March 2009

Approx. Hours : 20 hours

2. Research for basic information on fracture mechanics.

Begin : 20<sup>th</sup> March 2009

Completion : 30<sup>th</sup> March 2009

Approx. Hours : 8 hours

3. Check and analysis the existing Design of the cast mould for short bar tests.

Begin : 30<sup>th</sup> March 2009

Completion : 10<sup>th</sup> April 2009

Approx. Hours : 10 hours

4. Perform the fracture toughness test and collect and examine the results.

Begin : 10<sup>th</sup> April 2009

Completion : 8<sup>th</sup> May 2009

Approx. Hours : 35 hours

5. Literature review

Begin : 8<sup>th</sup> May 2009

Completion : 30<sup>th</sup> May 2009

Approx. Hours : 60 hours

6. Analyse the results.

Begin : 30<sup>th</sup> May 2009

Completion : 29<sup>th</sup> June 2009

Approx. Hours : 40 hours

7. Draw up conclusion based on the obtained results.

Begin : 29<sup>th</sup> June 2009

Completion : 30<sup>th</sup> July 2009

Approx. Hours : 40 hours

8. Discussion for the thesis outline with supervisor.

Begin : 30<sup>th</sup> July 2009

Completion : 17<sup>th</sup> August 2009

Approx. Hours : 10 hours

9. Thesis initial drafting. Each chapter in draft form to be shown to supervisor.

Begin : 17<sup>th</sup> August 2009

Completion : 9<sup>th</sup> October 2009

Approx. Hours : 60 hours

10. Finalise the thesis and incorporate modification suggested by supervisor.

Begin : 9<sup>th</sup> October 2009

Completion : 20<sup>th</sup> October 2009

Approx. Hours : 10 hours

9. Complete the thesis in requested format.

Begin : 20<sup>th</sup> October 2009

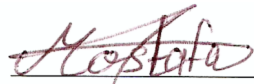
Completion : 29<sup>th</sup> October 2009

Approx. Hours : 25 hours

*As time permits:*

1. Perform a Dynamic Mechanical Analysis (DMA) on the specimens.
2. Conduct a scanning electron microscope analysis (SEM) on the fractured specimens.
3. Examine the electrical properties of the composite.

AGREED:

 (student)

Student: Mustapha Jamal Eddine

Date: 24/03/2009

 (Supervisor)

Supervisor: Dr. Harry Ku

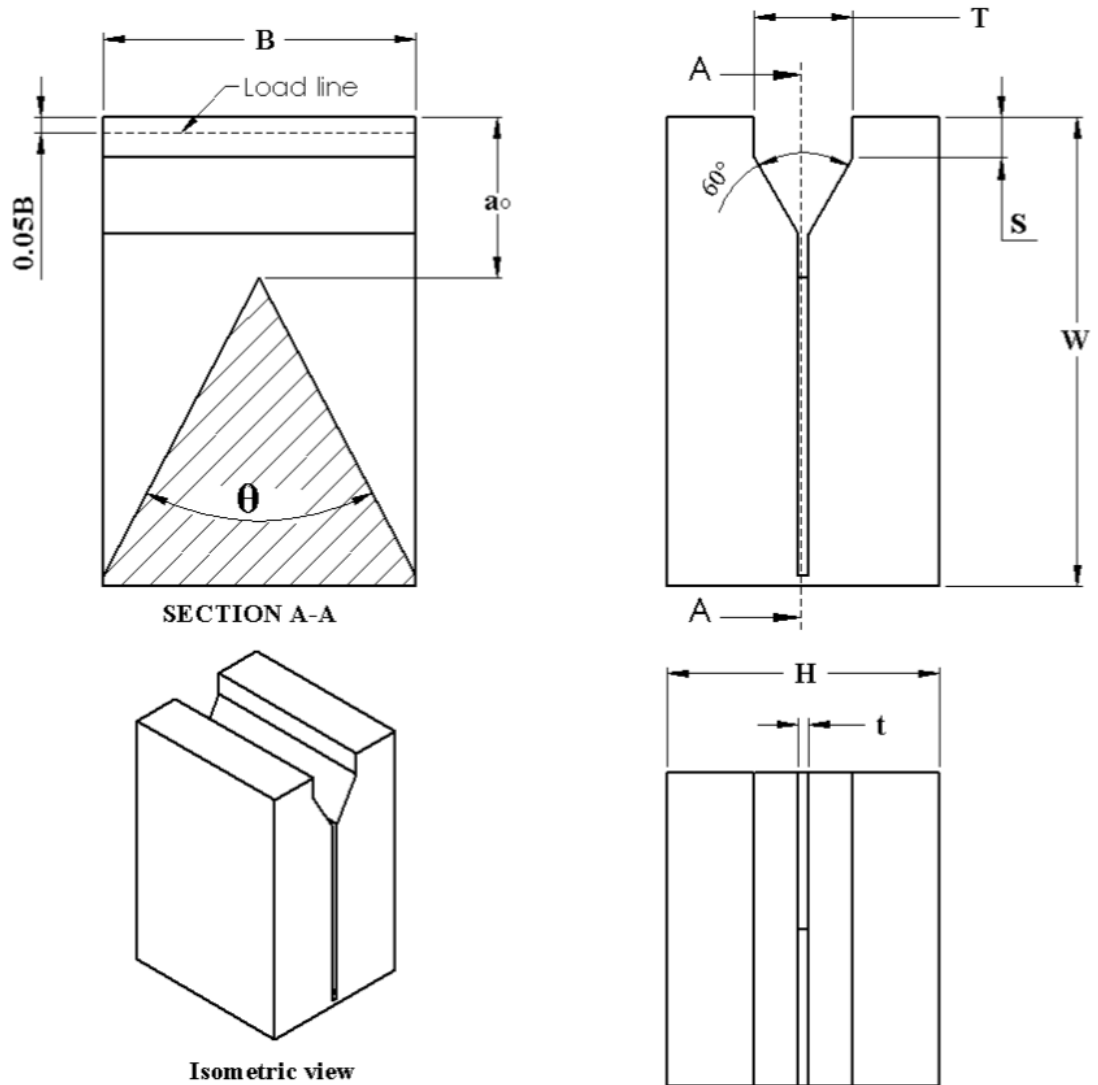
Date: 24/03/2009

## Appendix B - Specimen Dimensions

The geometries of the short bar and short rod were selected based on seven specific criteria (Barker 1981, p. 459).

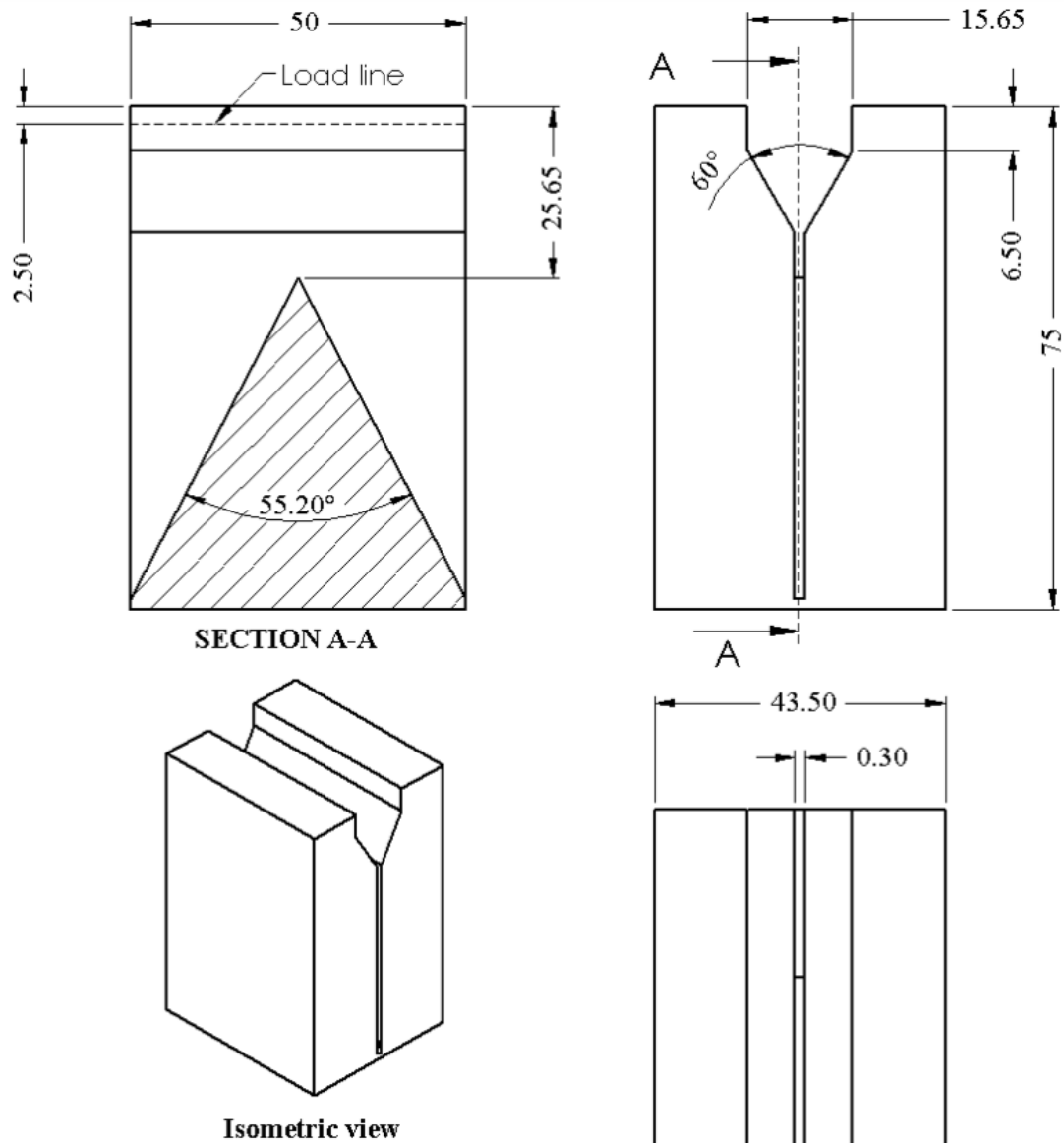
- 1. The tendency for the crack to “pop in” at initiation should be reduced; the crack initiation should be as smooth as possible.*
- 2. The crack should be well guided by the chevron slot.*
- 3. The width of the crack front should be an appreciable proportion of the specimen diameter at the time of the fracture toughness measurement.*
- 4. The crack should be near the centre of the specimen at the time of the fracture toughness measurement.*
- 5. The load should be at or near its peak value at the time of the toughness measurement.*
- 6. The specimen geometry should be as simple as possible for ease of specimen fabrication.*
- 7. The specimen should be economical in its use of sample material.*

The selected short bar geometry is shown in. shows the dimensions of the specimen when the breadth is selected as 50mm (i.e. B=50mm).



Symbol	Definition	Value	Tolerance
B	Breadth	B	-
W	Length	1.5B	$\pm .010B$
H	Height	0.870B	$\pm .005B$
$a_0$	Initial crack length	0.513B	$\pm .005B$
$\theta$	Slot angle	55.2°	$\pm 1/2^\circ$
t	Slot thickness	See Table 9.1	-
S	Grip groove depth	0.130B	$\pm .010B$
T	Grip groove width	0.313B	$\pm .005B$

Figure B.1: The selected geometry of the specimens. (Source: Barker 1981, p. 457)



Symbol	Definition	Value (mm)	Tolerance (mm)
B	Breadth	B=50	-
W	Length	75	$\pm 0.5$
H	Height	43.5	$\pm 0.25$
$a_0$	Initial crack length	25.65	$\pm 0.25$
$\theta$	Slot angle	$55.2^\circ$	$\pm 1/2^\circ$
T	Slot thickness	0.3	-
S	Grip groove depth	6.5	$\pm 0.5$
T	Grip groove width	15.65	$\pm 0.25$

Figure B.2: The standard dimensions of the short bar specimen for (B=50).

## Appendix C - Mixture Tables

Table C.1: Weight of materials required to make 1000 g of VE/CaCO<sub>3</sub> (0%).

Materials Parameters	Resin (R)	Catalyst (C)	R+C	CaCO <sub>3</sub>	VE/CaCO <sub>3</sub>
Percentage by weight of the resin and catalyst mixture	98%	2%	100%	--	--
Net percentage by weight	98%	2%	100%	0%	100%
Weight of material in 1000g of VE/CaCO <sub>3</sub> (0%)	980 (g)	20 (g)	1000 (g)	0 (g)	1000 (g)

Table C.2: Weight of materials required to make 1000 g of VE/CaCO<sub>3</sub> (5%).

Materials Parameters	Resin (R)	Catalyst (C)	R+C	CaCO <sub>3</sub>	VE/CaCO <sub>3</sub>
Percentage by weight of the resin and catalyst mixture	98%	2%	100%	--	--
Net percentage by weight in 1000g of VE/CaCO <sub>3</sub>	93.1%	1.9%	95%	5%	100%
Weight of material in 1000g of VE/CaCO <sub>3</sub> (5%)	931 (g)	19 (g)	950(g)	50 (g)	1000 (g)

Table C.3: Weight of materials required to make 1000 g of VE/CaCO<sub>3</sub> (10%).

Materials Parameters	Resin (R)	Catalyst (C)	R+C	CaCO <sub>3</sub>	VE/CaCO <sub>3</sub>
Percentage by weight of the resin and catalyst mixture	98%	2%	100%	--	--
Net percentage by weight in 1000g of VE/CaCO <sub>3</sub>	88.2%	1.8%	90%	10%	100%
Weight of material in 1000g of VE/CaCO <sub>3</sub> (10%)	882 (g)	18 (g)	900(g)	100 (g)	1000 (g)

Table C.4: Weight of materials required to make 1020 g of VE/CaCO<sub>3</sub> (15%).

Materials Parameters	Resin (R)	Catalyst (C)	R+C	CaCO <sub>3</sub>	VE/CaCO <sub>3</sub>
Percentage by weight of the resin and catalyst mixture	98%	2%	100%	--	--
Net percentage by weight in 1020g of VE/CaCO <sub>3</sub>	83.3%	1.7%	85%	15%	100%
Weight of material in 1020g of VE/CaCO <sub>3</sub> (15%)	849.7 (g)	17.3 (g)	867(g)	153 (g)	1020 (g)

Table C.5: Weight of materials required to make 1050 g of VE/CaCO<sub>3</sub> (20%).

<b>Parameters</b> \ <b>Materials</b>	<b>Resin (R)</b>	<b>Catalyst (C)</b>	<b>R+C</b>	<b>CaCO<sub>3</sub></b>	<b>VE/CaCO<sub>3</sub></b>
<b>Percentage by weight of the resin and catalyst mixture</b>	98%	2%	100%	--	--
<b>Net percentage by weight in 1050g of VE/CaCO<sub>3</sub></b>	78.4%	1.6%	80%	20%	100%
<b>Weight of material in 1050g of VE/CaCO<sub>3</sub> (20%)</b>	823.2 (g)	16.8 (g)	840 (g)	210 (g)	1050 (g)

Table C.6: Weight of materials required to make 1120 g of VE/CaCO<sub>3</sub> (25%).

<b>Parameters</b> \ <b>Materials</b>	<b>Resin (R)</b>	<b>Catalyst (C)</b>	<b>R+C</b>	<b>CaCO<sub>3</sub></b>	<b>VE/CaCO<sub>3</sub></b>
<b>Percentage by weight of the resin and catalyst mixture</b>	98%	2%	100%	--	--
<b>Net percentage by weight in 1120g of VE/CaCO<sub>3</sub></b>	73.5%	1.5%	75%	25%	100%
<b>Weight of material in 1120g of VE/CaCO<sub>3</sub> (25%)</b>	823.2 (g)	16.8 (g)	840 (g)	280 (g)	1120 (g)

Table C.7: Weight of materials required to make 1200 g of VE/CaCO<sub>3</sub> (30%).

<b>Parameters</b> \ <b>Materials</b>	<b>Resin (R)</b>	<b>Catalyst (C)</b>	<b>R+C</b>	<b>CaCO<sub>3</sub></b>	<b>VE/CaCO<sub>3</sub></b>
<b>Percentage by weight of the resin and catalyst mixture</b>	98%	2%	100%	--	--
<b>Net percentage by weight in 1200g of VE/CaCO<sub>3</sub></b>	68.6%	1.4%	70%	30%	100%
<b>Weight of material in 1200g of VE/CaCO<sub>3</sub> (30%)</b>	823.2 (g)	16.8 (g)	840 (g)	360 (g)	1200 (g)

Table C.8: Weight of materials required to make 1300 g of VE/CaCO<sub>3</sub> (35%).

<b>Parameters</b> \ <b>Materials</b>	<b>Resin (R)</b>	<b>Catalyst (C)</b>	<b>R+C</b>	<b>CaCO<sub>3</sub></b>	<b>VE/CaCO<sub>3</sub></b>
<b>Percentage by weight of the resin and catalyst mixture</b>	98%	2%	100%	--	--
<b>Net percentage by weight in 1300g of VE/CaCO<sub>3</sub></b>	63.7%	1.3%	65%	35%	100%
<b>Weight of material in 1300g of VE/CaCO<sub>3</sub> (35%)</b>	828.1 (g)	16.9 (g)	845 (g)	455 (g)	1300 (g)

Table C.9: Weight of materials required to make 1400 g of VE/CaCO<sub>3</sub> (40%).

<b>Parameters</b>	<b>Resin (R)</b>	<b>Catalyst (C)</b>	<b>R+C</b>	<b>CaCO<sub>3</sub></b>	<b>VE/CaCO<sub>3</sub></b>
<b>Percentage by weight of the resin and catalyst mixture</b>	98%	2%	100%	--	--
<b>Net percentage by weight in 1400g of VE/CaCO<sub>3</sub></b>	58.8%	1.2%	60%	40%	100%
<b>Weight of material in 1400g of VE/CaCO<sub>3</sub> (40%)</b>	823.2 (g)	16.8 (g)	840 (g)	560 (g)	1400 (g)

## Appendix D – Actual Specimen Measurements

Certain geometrical measurements of the specimens are required in the fracture toughness calculations. These measurements are taken after the **oven post-curing process**. These measurements are tabulated in this appendix for each specimen and for every filler percentage. (Refer to Figure 9.11 for the definition of  $a_o$  and  $a_1$ ).

**Note: All the measurements are in millimetres (mm).**

**Table D.1: specimens' geometrical measurements for 0 wt% of VE/CaCO<sub>3</sub>.**

Percentage by weight of filler	Specimen Number	Specimen width (W)	Specimen height (H)	$a_o$	
0	1	72.6	37.5	23.2	66.6
	2	71.5	38	23.1	71.4
	3	71.3	37.4	22.8	69.3
	4	72.4	38.5	23.9	68.8
	5	70.3	38.3	22.9	67.9
	6	72.8	38.2	23.5	70.6

**Table D.2: specimens' geometrical measurements for 10 wt% of VE/CaCO<sub>3</sub>.**

Percentage by weight of filler	Specimen Number	Specimen width (W)	Specimen height (H)	$a_o$	
10	1	73.4	38.3	23.7	70.6
	2	74.5	37.3	23.9	71.2
	3	73.6	38.6	23.3	71.2
	4	72.9	37.8	20.9	67.6
	5	72.8	39.7	24.7	69.2
	6	72.5	37.6	23.5	68.3

**Table D.3: specimens' geometrical measurements for 10 wt% of VE/CaCO<sub>3</sub>.**

Percentage by weight of filler	Specimen Number	Specimen width (W)	Specimen height (H)	$a_o$	
10	1	73.4	38.3	23.7	70.6
	2	74.5	37.3	23.9	71.2
	3	73.6	38.6	23.3	71.2
	4	72.9	37.8	20.9	67.6
	5	72.8	39.7	24.7	69.2
	6	72.5	37.6	23.5	68.3

Table D.4: specimens' geometrical measurements for 15 wt% of VE/CaCO<sub>3</sub>.

Percentage by weight of filler	Specimen Number	Specimen width (W)	Specimen height (H)	$a_o$	
15	1	69.8	38.1	18.5	64.3
	2	71.1	38.3	19.6	65.6
	3	70.1	38.1	22.5	65.1
	4	71.8	37.9	21.5	67.2
	5	71	38.3	21.7	67
	6	69.8	38.5	15.2	64.8

Table D.5: specimens' geometrical measurements for 20 wt% of VE/CaCO<sub>3</sub>.

Percentage by weight of filler	Specimen Number	Specimen width (W)	Specimen height (H)	$a_o$	
20	1	73.5	38.7	20.1	70.4
	2	73.6	37.8	23.3	70.8
	3	73	37.4	22.2	71.4
	4	74.1	37.9	20.8	72.8
	5	73.3	38	23.4	71.3
	6	73.6	37.8	23.3	70.8

Table D.6: specimens' geometrical measurements for 25 wt% of VE/CaCO<sub>3</sub>.

Percentage by weight of filler	Specimen Number	Specimen width (W)	Specimen height (H)	$a_o$	
25	1	74.1	38.5	21.8	72.3
	2	73.4	39.3	22	72.9
	3	74.4	37.2	23.6	72.1
	4	73.8	37.7	23.6	71.5
	5	74	37.7	24.3	71.4
	6	74	38.1	24.5	71.8

Table D.7: specimens' geometrical measurements for 30 wt% of VE/CaCO<sub>3</sub>.

Percentage by weight of filler	Specimen Number	Specimen width (W)	Specimen height (H)	$a_o$	
30	1	74.1	38.1	24.9	72.5
	2	75	36.9	22.4	71.8
	3	75.1	37	26.4	73
	4	75.5	38.4	24.4	72.8
	5	74.6	36.3	26.2	73.6
	6	75.2	37	26.4	73

Table D.8: specimens' geometrical measurements for 35 wt% of VE/CaCO<sub>3</sub>.

Percentage by weight of filler	Specimen Number	Specimen width (W)	Specimen height (H)	$a_o$	
35	1	73.4	37.8	24.4	71.4
	2	73.8	36.7	25.8	72.2
	3	73.7	37.5	26.2	71.1
	4	74.1	37.6	25.1	73.3
	5	74	37.7	26.1	73
	6	73.3	35.8	25.9	72.2

Table D.9: specimens' geometrical measurements for 40 wt% of VE/CaCO<sub>3</sub>.

Percentage by weight of filler	Specimen Number	Specimen width (W)	Specimen height (H)	$a_o$	
40	1	75.7	37.3	29.3	74.5
	2	73.6	38.2	28.8	73.5
	3	73.9	37.2	28.8	74.2
	4	74.7	38.5	28.9	73.3
	5	75.5	40	28.6	73.3
	6	74.8	38.7	28.9	73.3

## Appendix E – Fracture Toughness Results

The fracture toughness for all the tested specimens was calculated using equation (9.2) following the same procedure outlined in section 12.1 of Chapter 12. All the numerical calculations were done using excel. The results are listed in the tables below.

**NOTE:** The compliance calibration,  $Y_m^*$ , was calculated using equation (9.3) and the geometrical values given in Appendix D. The peak force,  $F_{max}$ , for the specimen was obtained from the MTS 810 testing system data shown in Appendix F.

**Table E.1: Fracture toughness calculation for 0 wt% of CaCO<sub>3</sub>.**

wt% filler	Specimen Number	$F_{max}$ (N)	$Y_m^*$	W (mm)	$K_{ICSB}$ (MPa $\sqrt{m}$ )	Average $K_{ICSB}$ (Std. Dev.)
0	1	953	15.35	72.6	34.34	30.32 (4.195)
	2	674	16.51	71.5	26.32	
	3	967	16.04	71.3	36.74	
	4	722	16.22	72.4	27.52	
	5	731	16.21	70.3	28.27	
	6	759	16.15	72.8	28.73	

**Table E.2: Fracture toughness calculation for 5 wt% of CaCO<sub>3</sub>.**

wt% filler	Specimen Number	$F_{max}$ (N)	$Y_m^*$	W (mm)	$K_{ICSB}$ (MPa $\sqrt{m}$ )	Average $K_{ICSB}$ (Std. Dev.)
5	1	628	15.55	73.2	22.82	23.17 (3.623)
	2	685	15.00	71.7	24.27	
	3	728	15.30	60	28.75	
	4	598	14.25	72.4	20.02	
	5	577	14.63	71.3	20.00	
	6	-	-	-	-	

**Table E.3: Fracture toughness calculation for 10 wt% of CaCO<sub>3</sub>.**

wt% filler	Specimen Number	$F_{max}$ (N)	$Y_m^*$	W (mm)	$K_{ICSB}$ (MPa $\sqrt{m}$ )	Average $K_{ICSB}$ (Std. Dev.)
10	1	504	16.05	73.4	18.89	20.32 (1.555)
	2	576	15.91	74.5	21.23	
	3	510	15.85	73.6	18.84	
	4	598	14.21	72.9	19.90	
	5	588	16.64	72.8	22.93	
	6	540	15.86	72.5	20.11	

**Table E.4: Fracture toughness calculation for 15 wt% of CaCO<sub>3</sub>.**

wt% filler	Specimen Number	$F_{max}$ (N)	$Y_m^*$	W (mm)	$K_{ICSB}$ (MPa $\sqrt{m}$ )	Average $K_{ICSB}$ (Std. Dev.)
15	1	717	13.30	69.8	22.83	22.00 (2.672)
	2	585	13.71	71.1	19.02	
	3	641	15.53	70.1	23.78	
	4	566	14.77	71.8	19.73	
	5	726	15.08	71	25.99	
	6	726	11.88	69.8	20.64	

**Table E.5: Fracture toughness calculation for 20 wt% of CaCO<sub>3</sub>.**

wt% filler	Specimen Number	$F_{max}$ (N)	$Y_m^*$	W (mm)	$K_{ICSB}$ (MPa $\sqrt{m}$ )	Average $K_{ICSB}$ (Std. Dev.)
20	1	712	14.03	73.5	23.31	21.75 (1.833)
	2	648	15.79	73.6	23.86	
	3	587	15.47	73	21.25	
	4	571	14.60	74.1	19.37	
	5	559	16.03	73.3	20.94	

**Table E.6: Fracture toughness calculation for 25 wt% of CaCO<sub>3</sub>.**

wt% filler	Specimen Number	$F_{max}$ (N)	$Y_m^*$	W (mm)	$K_{ICSB}$ (MPa $\sqrt{m}$ )	Average $K_{ICSB}$ (Std. Dev.)
25	1	500	15.03	74.1	17.46	18.07 (0.657)
	2	493	15.41	73.4	17.74	
	3	500	15.92	74.4	18.46	
	4	470	16.02	73.8	17.53	
	5	475	16.34	74	18.05	
	6	499	16.53	74	19.17	

**Table E.7: Fracture toughness calculation for 30 wt% of CaCO<sub>3</sub>.**

wt% filler	Specimen Number	$F_{max}$ (N)	$Y_m^*$	W (mm)	$K_{ICSB}$ (MPa $\sqrt{m}$ )	Average $K_{ICSB}$ (Std. Dev.)
30	1	340	16.86	74.1	13.32	16.02 (2.875)
	2	276	15.06	75	9.60	
	3	483	17.49	75.1	19.50	
	4	465	16.11	75.5	17.24	
	5	343	17.67	74.6	14.04	

**Table E.8: Fracture toughness calculation for 35 wt% of CaCO<sub>3</sub>.**

wt% filler	Specimen Number	$F_{max}$ (N)	$Y_m^*$	W (mm)	$K_{ICSB}$ (MPa $\sqrt{m}$ )	Average $K_{ICSB}$ (Std. Dev.)
35	1	540	16.62	73.4	20.95	21.97 (3.693)
	2	675	17.49	73.8	27.48	
	3	579	17.59	73.7	23.72	
	4	485	17.13	74.1	19.30	
	5	445	17.76	74	18.37	
	6	891	17.75	73.3	36.96*	

\*was not included in the calculations

**Table E.9: Fracture toughness calculation for 40 wt% of CaCO<sub>3</sub>.**

wt% filler	Specimen Number	$F_{max}$ (N)	$Y_m^*$	W (mm)	$K_{ICSB}$ (MPa $\sqrt{m}$ )	Average $K_{ICSB}$ (Std. Dev.)
40	1	494	19.46	75.7	22.10	21.15 (1.220)
	2	480	20.00	73.6	22.38	
	3	422	19.92	73.9	19.56	
	4	449	19.46	74.7	20.22	
	5	495	18.88	75.5	21.51	

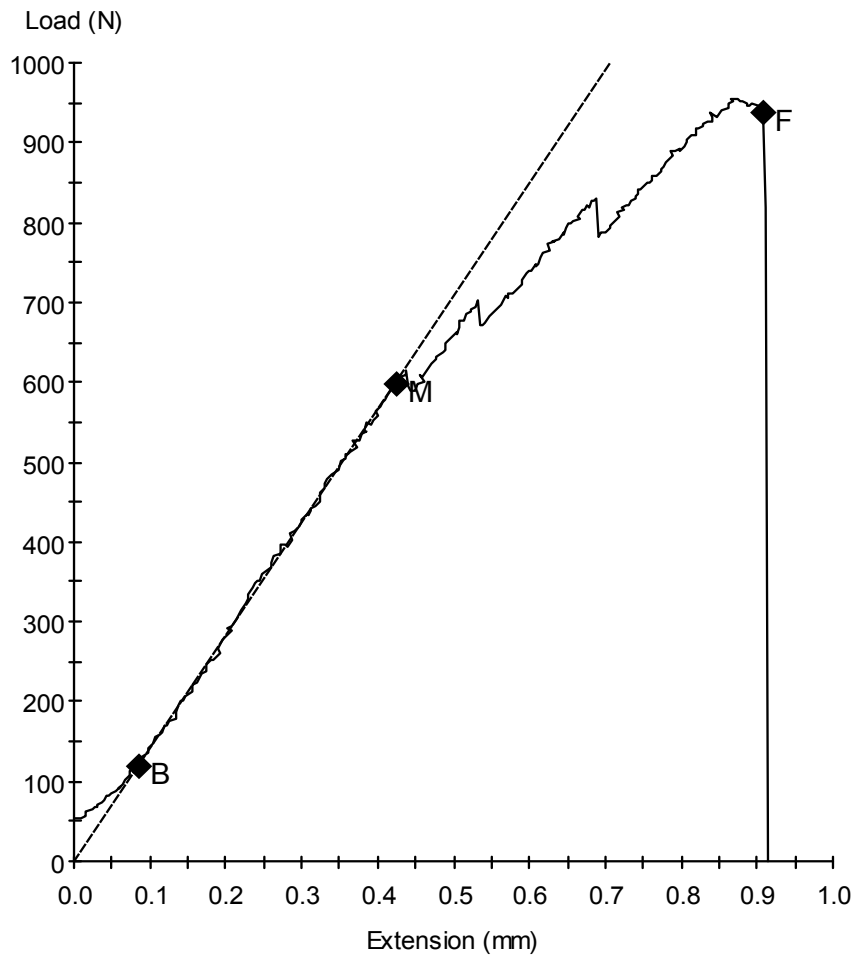
## **Appendix F – MTS 810 Testing System Data**

### MTS 810 Testing System Data

#### **0% by Weight of Filler**

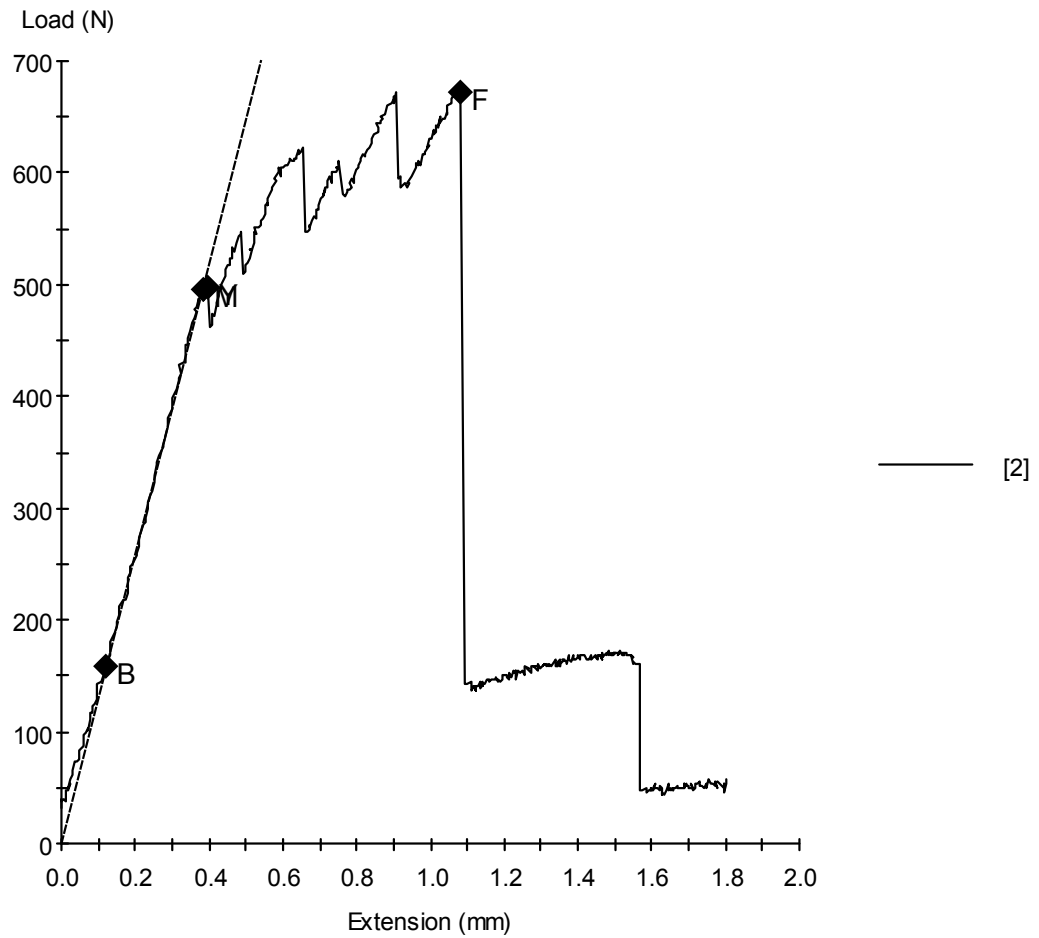
11/05/2009

Sample ID: mustapha-0%-1.mss  
Specimen Number: 1  
Tagged: False

**Specimen Results:**

Name	Value	Units
Thickness	50.000	mm
Width	30.000	mm
Area	1500	mm <sup>2</sup>
Peak Load	953	N
Peak Stress	0.64	MPa
Break Load	937	N
Break Stress	0.62	MPa
Elongation At Break	0.907	mm
Stress At Offset Yield	0.546	MPa
Load At Offset Yield	819.117	N

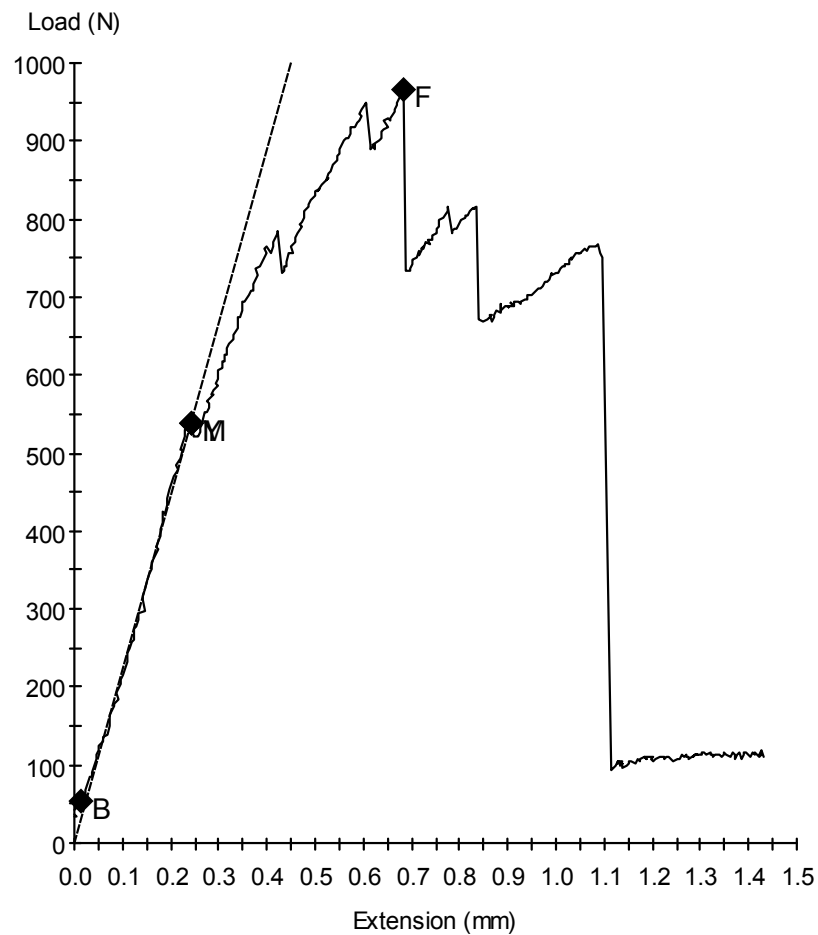
Sample ID: mustapha-0%-2.mss  
Specimen Number: 2  
Tagged: False

**Specimen Results:**

Name	Value	Units
Thickness	50.000	mm
Width	25.000	mm
Area	1250	mm <sup>2</sup>
Peak Load	674	N
Peak Stress	0.54	MPa
Break Load	673	N
Break Stress	0.54	MPa
Elongation At Break	1.081	mm
Stress At Offset Yield	0.408	MPa
Load At Offset Yield	510.269	N

11/05/2009

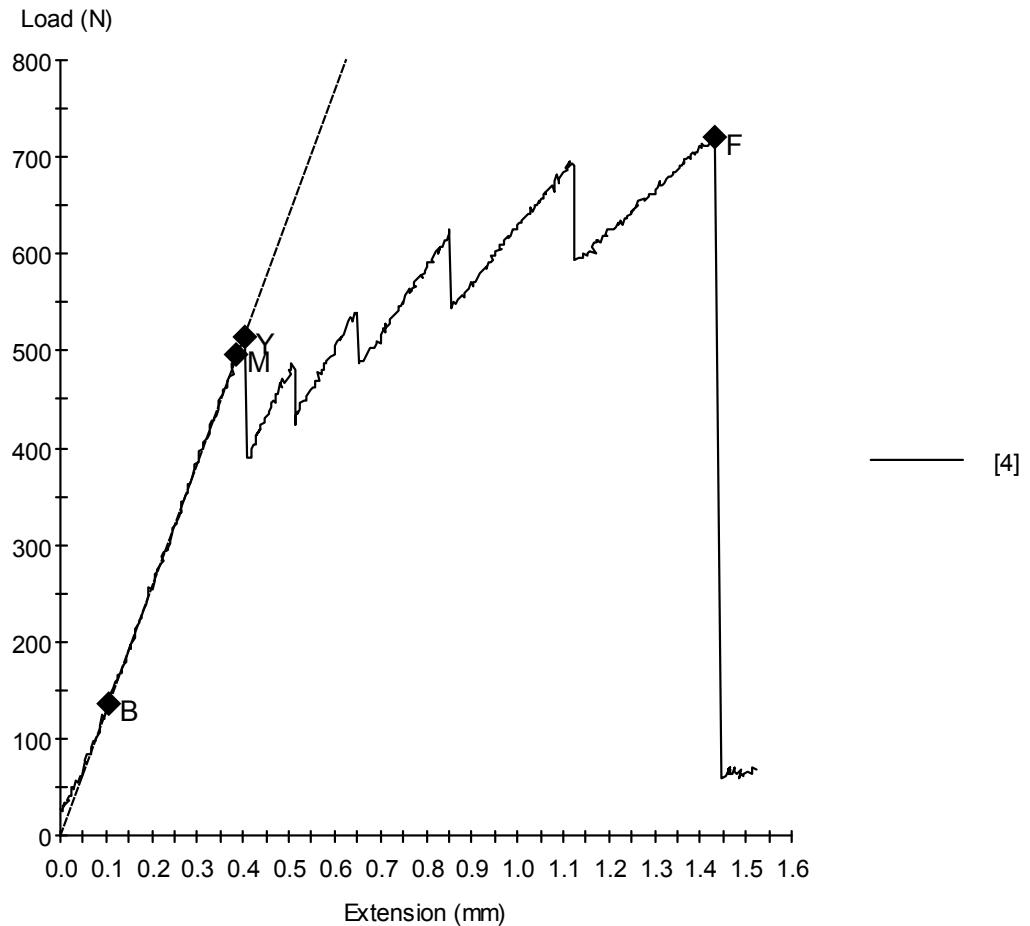
Sample ID: mustapha-0%-3.mss  
Specimen Number: 3  
Tagged: False

**Specimen Results:**

Name	Value	Units
Thickness	50.000	mm
Width	25.000	mm
Area	1250	mm <sup>2</sup>
Peak Load	967	N
Peak Stress	0.77	MPa
Break Load	967	N
Break Stress	0.77	MPa
Elongation At Break	0.683	mm
Stress At Offset Yield	0.585	MPa
Load At Offset Yield	731.834	N

11/05/2009

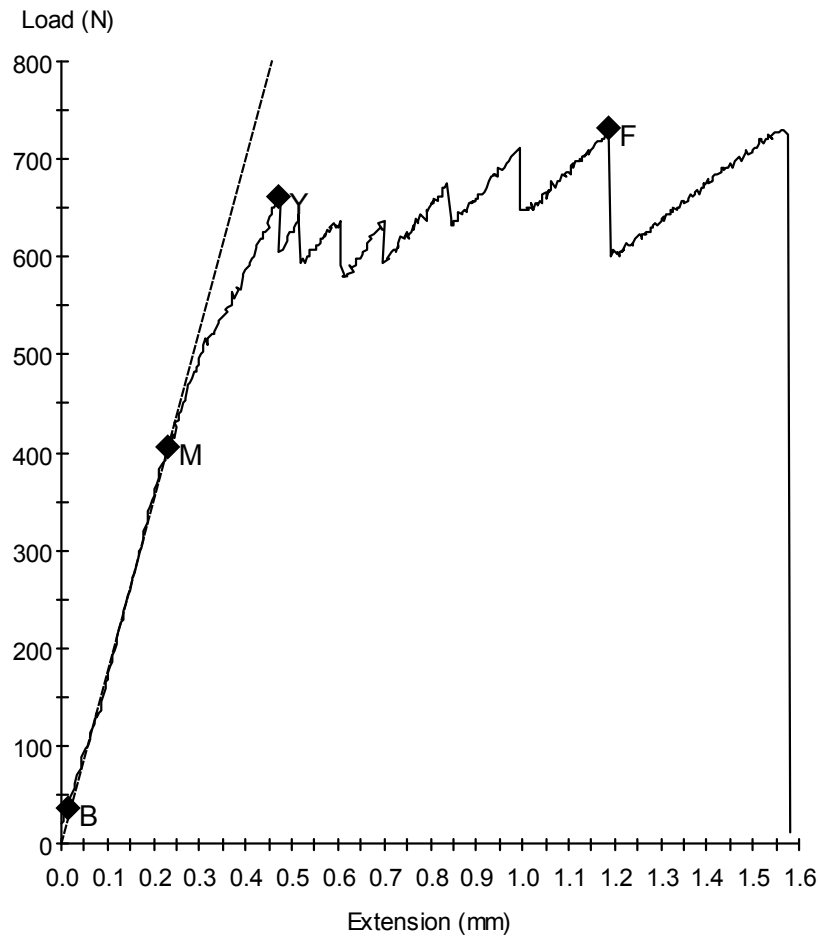
Sample ID: mustapha-0%-4.mss  
Specimen Number: 4  
Tagged: False

**Specimen Results:**

Name	Value	Units
Thickness	50.000	mm
Width	25.000	mm
Area	1250	mm <sup>2</sup>
Peak Load	722	N
Peak Stress	0.58	MPa
Break Load	722	N
Break Stress	0.58	MPa
Elongation At Break	1.432	mm
Stress At Offset Yield	0.312	MPa
Load At Offset Yield	390.088	N

11/05/2009

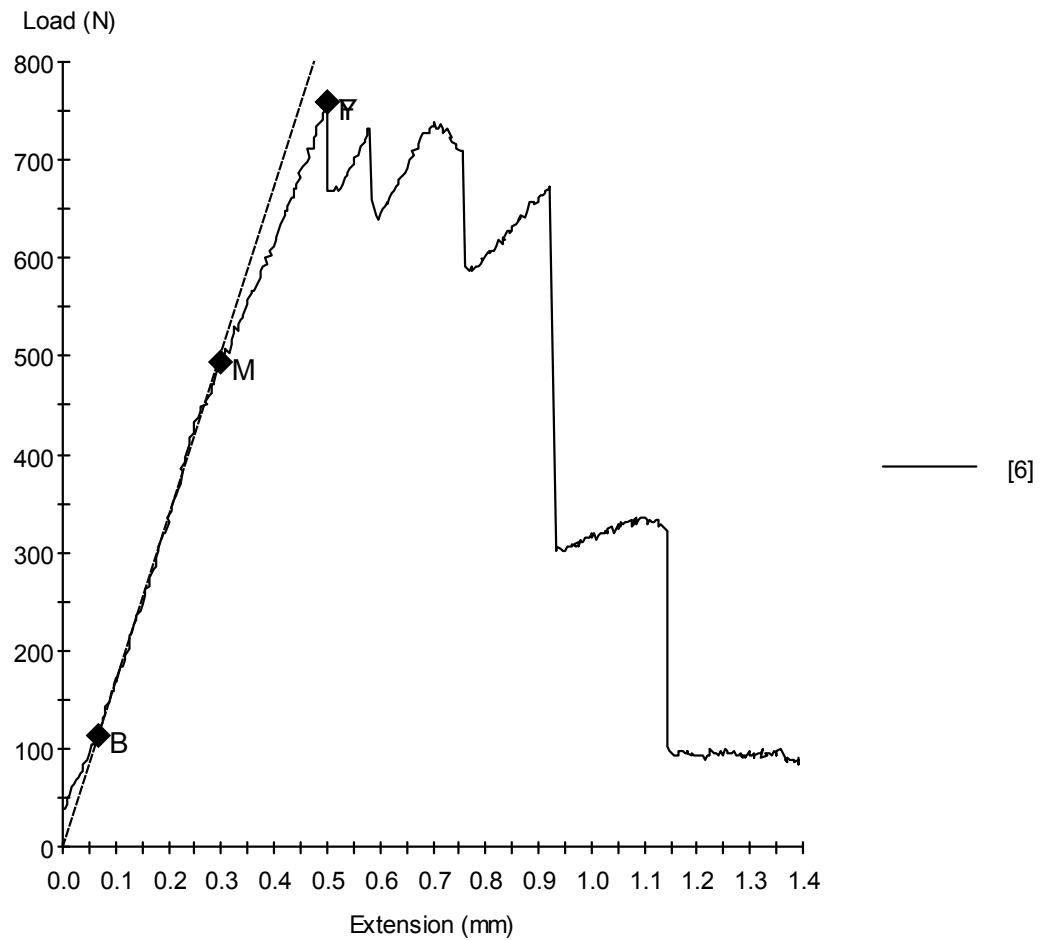
Sample ID: mustapha-0%-5.mss  
Specimen Number: 5  
Tagged: False

**Specimen Results:**

Name	Value	Units
Thickness	50.000	mm
Width	25.000	mm
Area	1250	mm <sup>2</sup>
Peak Load	731	N
Peak Stress	0.58	MPa
Break Load	731	N
Break Stress	0.58	MPa
Elongation At Break	1.187	mm
Stress At Offset Yield	0.526	MPa
Load At Offset Yield	657.979	N

11/05/2009

Sample ID: mustapha-0%-6.mss  
Specimen Number: 6  
Tagged: False

**Specimen Results:**

Name	Value	Units
Thickness	50.000	mm
Width	25.000	mm
Area	1250	mm <sup>2</sup>
Peak Load	759	N
Peak Stress	0.61	MPa
Break Load	759	N
Break Stress	0.61	MPa
Elongation At Break	0.500	mm
Stress At Offset Yield	0.535	MPa
Load At Offset Yield	668.722	N

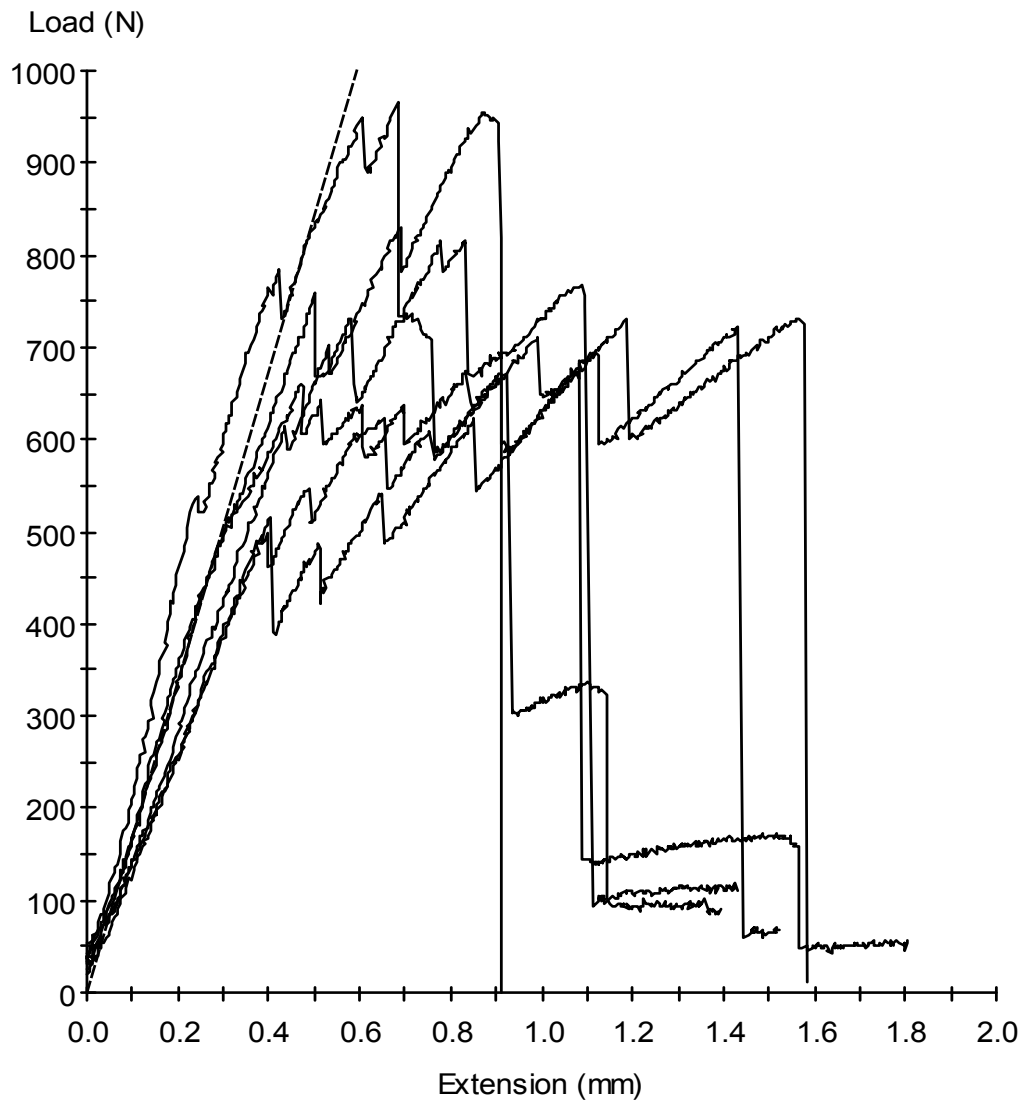
Test Date : 11/05/2009

Method : MMT fracture toughness Test .msm

**Specimen Results:**

Specimen #	Thickness mm	Width mm	Area mm <sup>2</sup>	Peak Load N	Peak Stress MPa	Break Load N	Break Stress MPa
1	50.000	30.000	1500	953	0.64	937	0.62
2	50.000	25.000	1250	674	0.54	673	0.54
3	50.000	25.000	1250	967	0.77	967	0.77
4	50.000	25.000	1250	722	0.58	722	0.58
5	50.000	25.000	1250	731	0.58	731	0.58
6	50.000	25.000	1250	759	0.61	759	0.61
<b>Mean</b>	<b>50.000</b>	<b>25.833</b>	<b>1292</b>	<b>801</b>	<b>0.62</b>	<b>798</b>	<b>0.62</b>
<b>Std Dev</b>	<b>0.000</b>	<b>2.041</b>	<b>102</b>	<b>126</b>	<b>0.08</b>	<b>123</b>	<b>0.08</b>

Specimen #	Elongation At Break mm	Stress At Offset Yield MPa	Load At Offset Yield N				
1	0.907	0.546	819.117				
2	1.081	0.408	510.269				
3	0.683	0.585	731.834				
4	1.432	0.312	390.088				
5	1.187	0.526	657.979				
6	0.500	0.535	668.722				
<b>Mean</b>	<b>0.965</b>	<b>0.486</b>	<b>629.668</b>				
<b>Std Dev</b>	<b>0.341</b>	<b>0.104</b>	<b>155.119</b>				

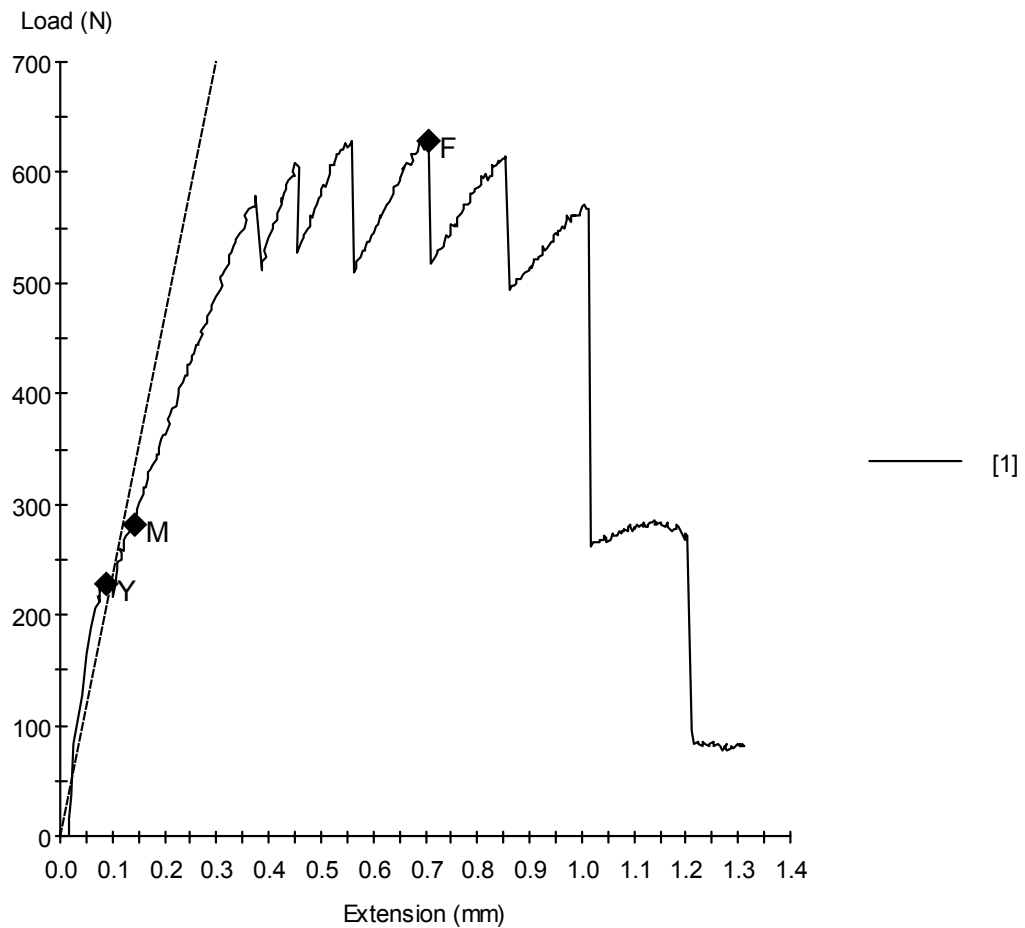


# MTS 810 Testing System Data

## **5% by Weight of Filler**

11/05/2009

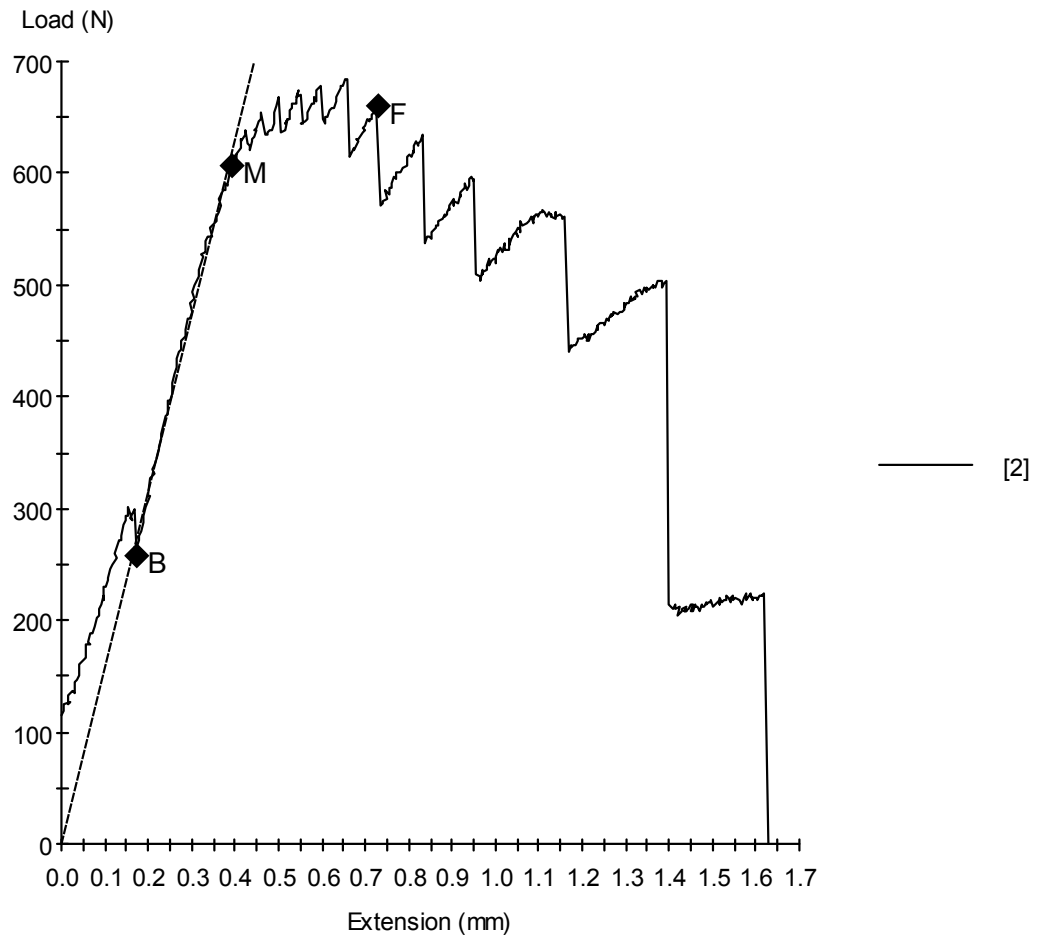
Sample ID: mustapha-5%-1.mss  
Specimen Number: 1  
Tagged: False

**Specimen Results:**

Name	Value	Units
Thickness	50.000	mm
Width	25.000	mm
Area	1250	mm <sup>2</sup>
Peak Load	628	N
Peak Stress	0.50	MPa
Break Load	628	N
Break Stress	0.50	MPa
Elongation At Break	0.708	mm
Stress At Offset Yield	0.397	MPa
Load At Offset Yield	496.841	N

11/05/2009

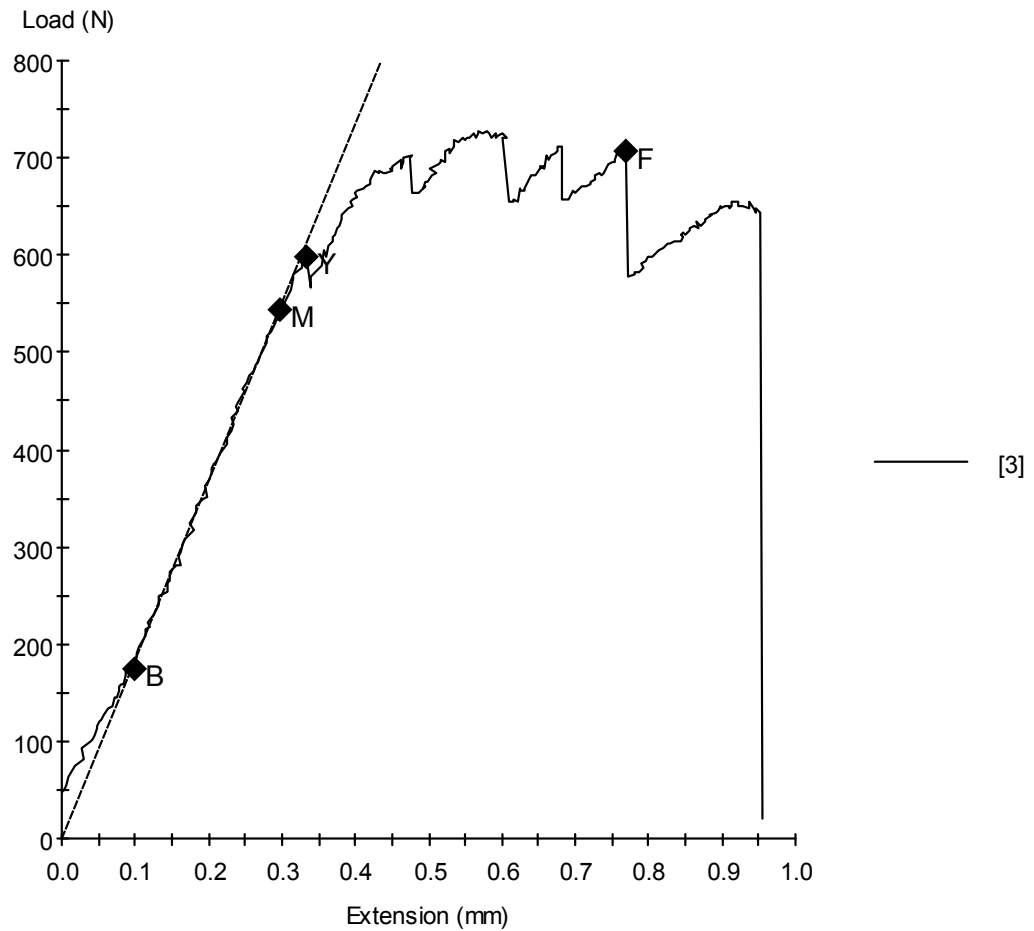
Sample ID: mustapha-5%-2.mss  
Specimen Number: 2  
Tagged: False

**Specimen Results:**

Name	Value	Units
Thickness	50.000	mm
Width	25.000	mm
Area	1250	mm <sup>2</sup>
Peak Load	685	N
Peak Stress	0.55	MPa
Break Load	661	N
Break Stress	0.53	MPa
Elongation At Break	0.728	mm
Stress At Offset Yield	0.509	MPa
Load At Offset Yield	636.494	N

11/05/2009

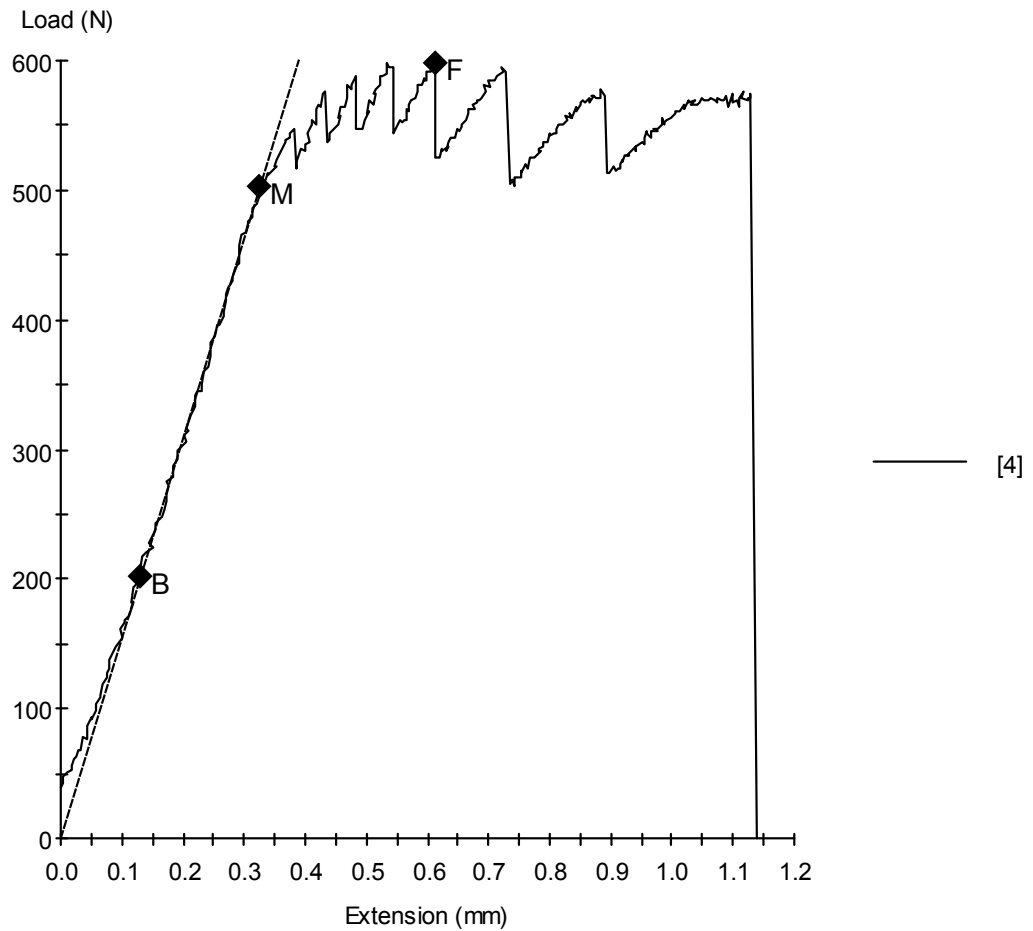
Sample ID: mustapha-5%-3.mss  
Specimen Number: 3  
Tagged: False

**Specimen Results:**

Name	Value	Units
Thickness	50.000	mm
Width	25.000	mm
Area	1250	mm <sup>2</sup>
Peak Load	728	N
Peak Stress	0.58	MPa
Break Load	707	N
Break Stress	0.57	MPa
Elongation At Break	0.769	mm
Stress At Offset Yield	0.532	MPa
Load At Offset Yield	664.693	N

11/05/2009

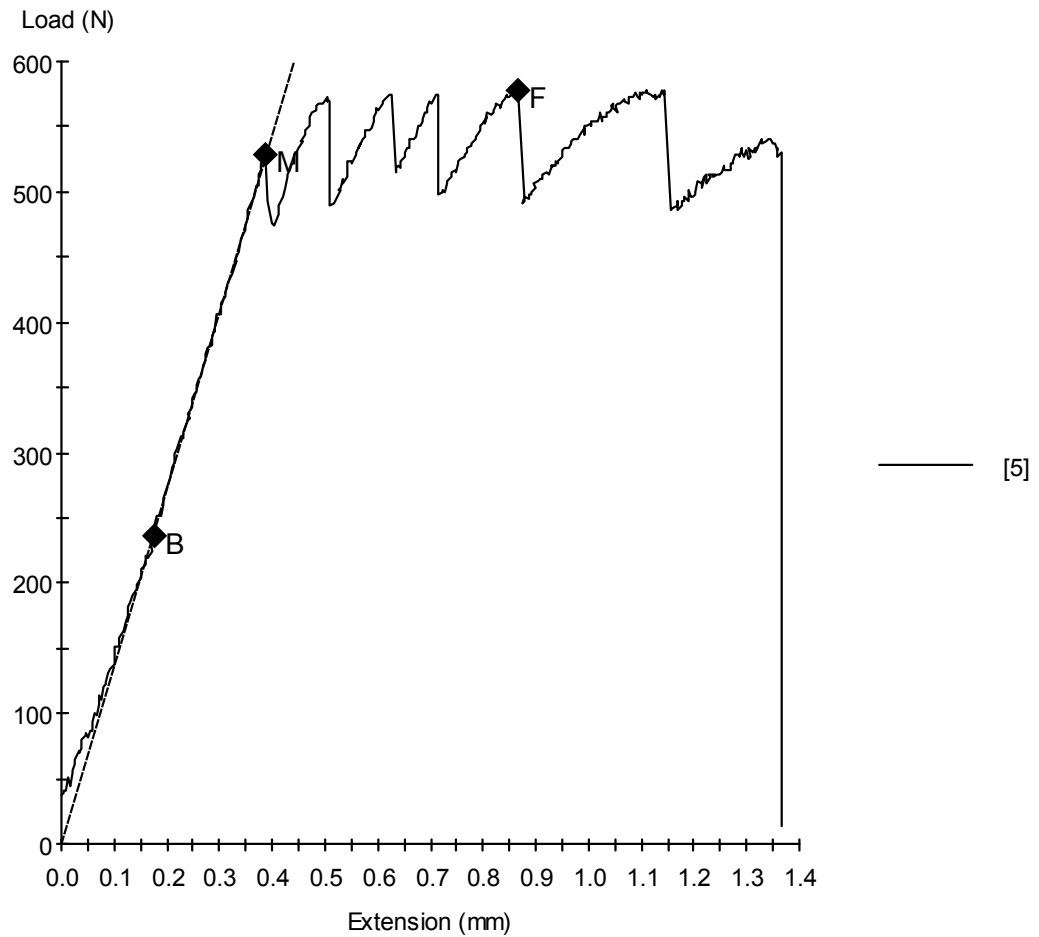
Sample ID: mustapha-5%-4.mss  
Specimen Number: 4  
Tagged: False

**Specimen Results:**

Name	Value	Units
Thickness	50.000	mm
Width	25.000	mm
Area	1250	mm <sup>2</sup>
Peak Load	598	N
Peak Stress	0.48	MPa
Break Load	598	N
Break Stress	0.48	MPa
Elongation At Break	0.611	mm
Stress At Offset Yield	0.471	MPa
Load At Offset Yield	588.153	N

11/05/2009

Sample ID: mustapha-5%-5.mss  
Specimen Number: 5  
Tagged: False

**Specimen Results:**

Name	Value	Units
Thickness	50.000	mm
Width	25.000	mm
Area	1250	mm <sup>2</sup>
Peak Load	577	N
Peak Stress	0.46	MPa
Break Load	577	N
Break Stress	0.46	MPa
Elongation At Break	0.868	mm
Stress At Offset Yield	0.392	MPa
Load At Offset Yield	490.127	N

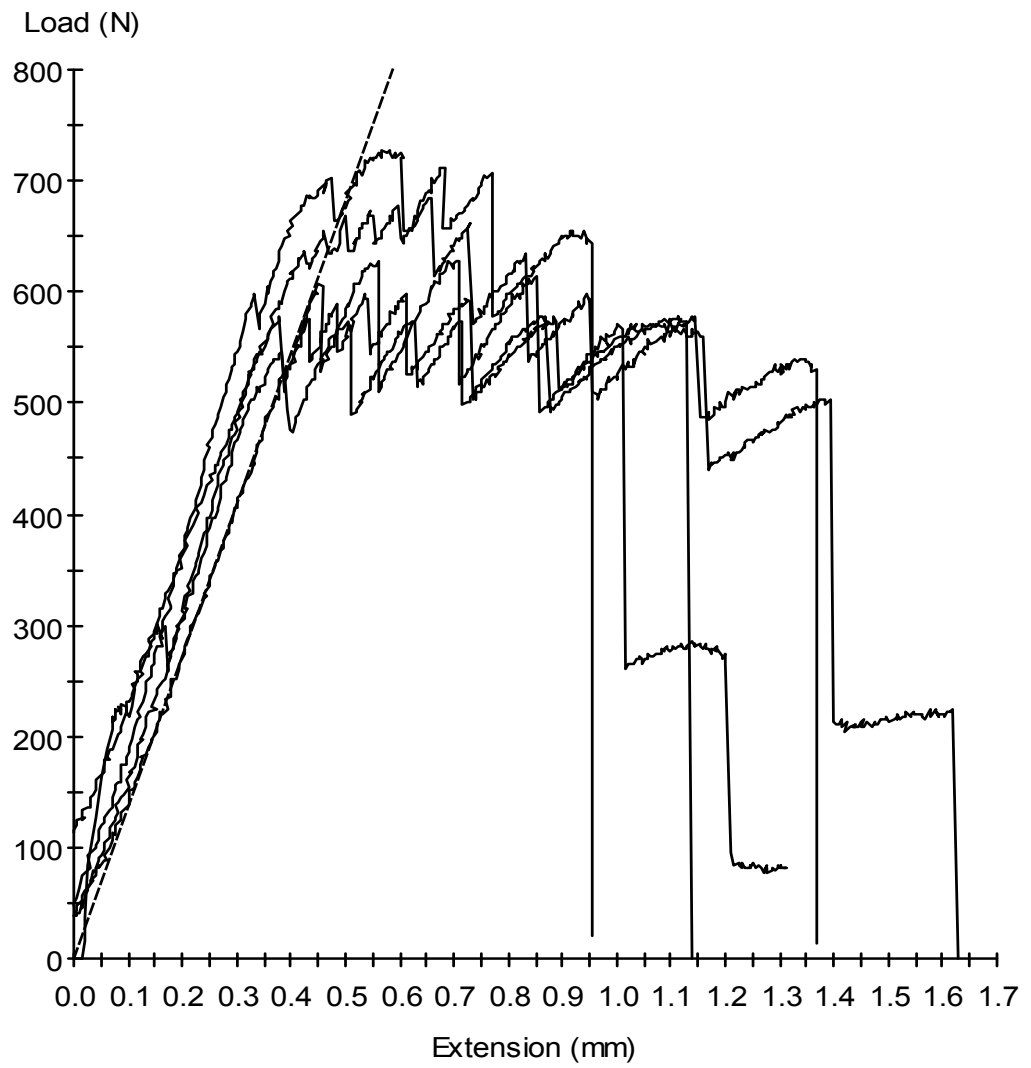
Test Date : 11/05/2009

Method : MMT fracture toughness Test .msm

**Specimen Results:**

Specimen #	Thickness mm	Width mm	Area mm <sup>2</sup>	Peak Load N	Peak Stress MPa	Break Load N	Break Stress MPa
1	50.000	25.000	1250	628	0.50	628	0.50
2	50.000	25.000	1250	685	0.55	661	0.53
3	50.000	25.000	1250	728	0.58	707	0.57
4	50.000	25.000	1250	598	0.48	598	0.48
5	50.000	25.000	1250	577	0.46	577	0.46
<b>Mean</b>	<b>50.000</b>	<b>25.000</b>	<b>1250</b>	<b>643</b>	<b>0.51</b>	<b>634</b>	<b>0.51</b>
<b>Std Dev</b>	<b>0.000</b>	<b>0.000</b>	<b>0</b>	<b>63</b>	<b>0.05</b>	<b>51</b>	<b>0.04</b>

Specimen #	Elongation At Break mm	Stress At Offset Yield MPa	Load At Offset Yield N				
1	0.708	0.397	496.841				
2	0.728	0.509	636.494				
3	0.769	0.532	664.693				
4	0.611	0.471	588.153				
5	0.868	0.392	490.127				
<b>Mean</b>	<b>0.737</b>	<b>0.460</b>	<b>575.262</b>				
<b>Std Dev</b>	<b>0.094</b>	<b>0.064</b>	<b>79.547</b>				

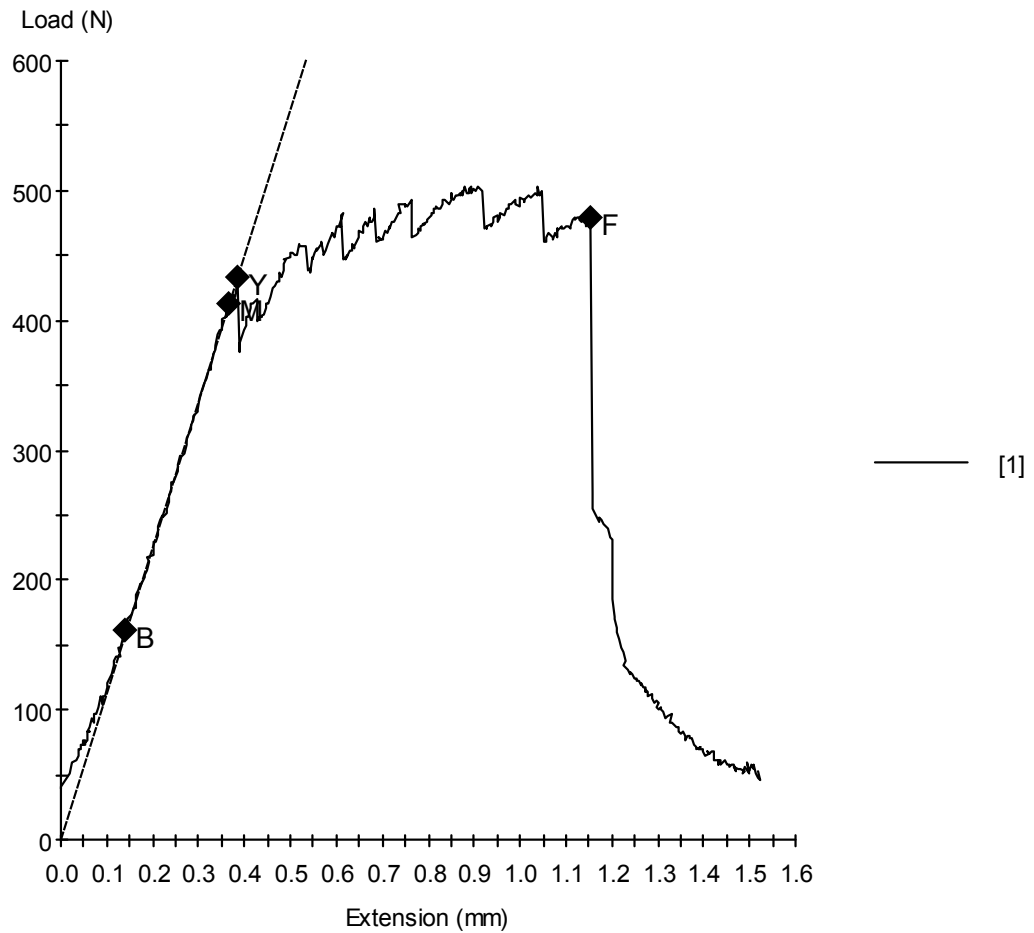


# MTS 810 Testing System Data

## **10% by Weight of Filler**

11/05/2009

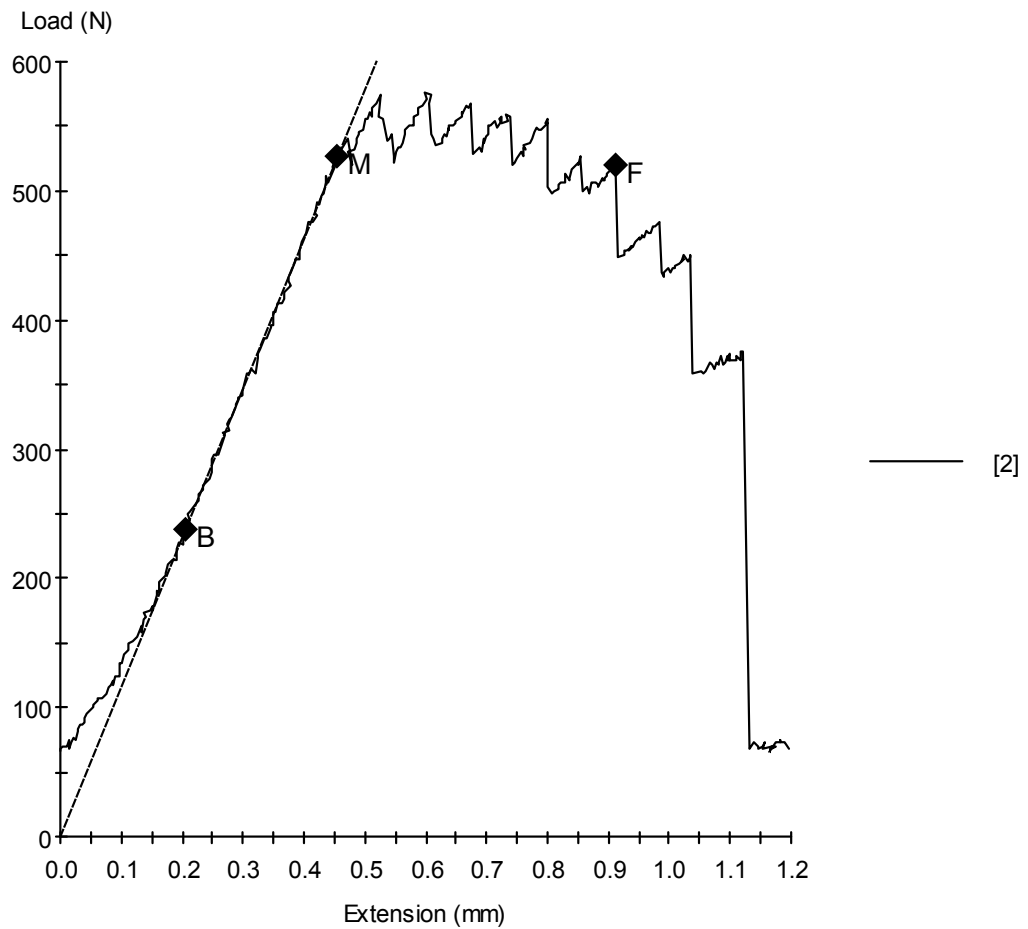
Sample ID: mustapha-10%-1.mss  
Specimen Number: 1  
Tagged: False

**Specimen Results:**

Name	Value	Units
Thickness	50.000	mm
Width	25.000	mm
Area	1250	mm <sup>2</sup>
Peak Load	504	N
Peak Stress	0.40	MPa
Break Load	480	N
Break Stress	0.38	MPa
Elongation At Break	1.152	mm
Stress At Offset Yield	0.359	MPa
Load At Offset Yield	449.171	N

11/05/2009

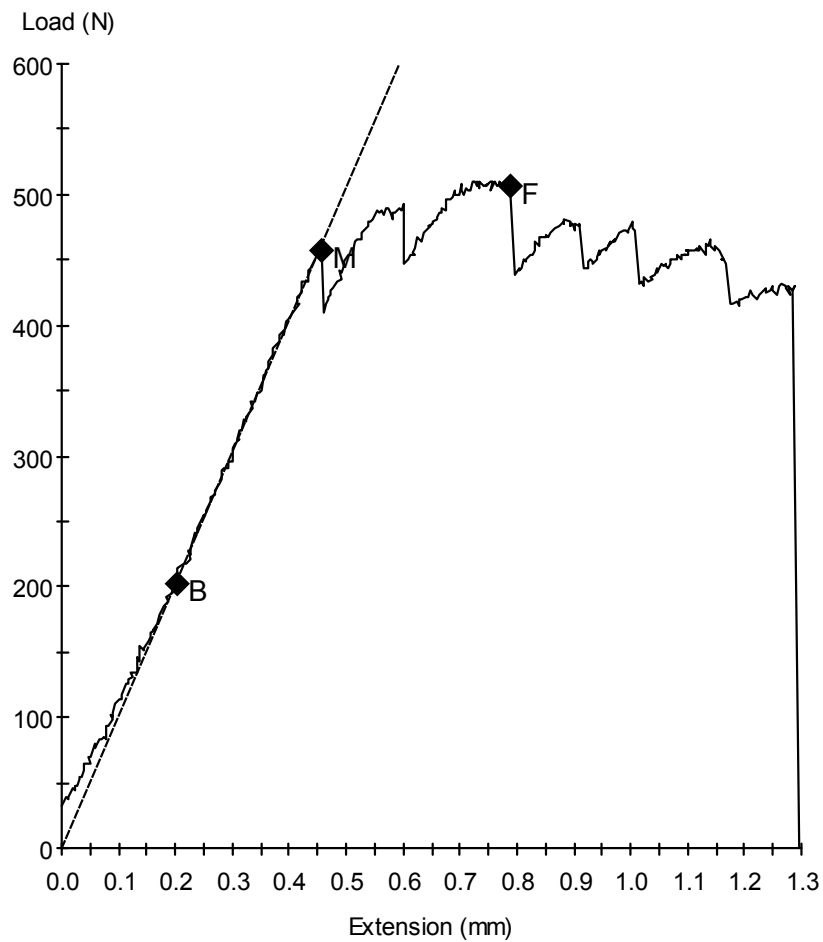
Sample ID: mustapha-10%-2.mss  
Specimen Number: 2  
Tagged: False

**Specimen Results:**

Name	Value	Units
Thickness	50.000	mm
Width	25.000	mm
Area	1250	mm <sup>2</sup>
Peak Load	576	N
Peak Stress	0.46	MPa
Break Load	520	N
Break Stress	0.42	MPa
Elongation At Break	0.911	mm
Stress At Offset Yield	0.440	MPa
Load At Offset Yield	550.554	N

11/05/2009

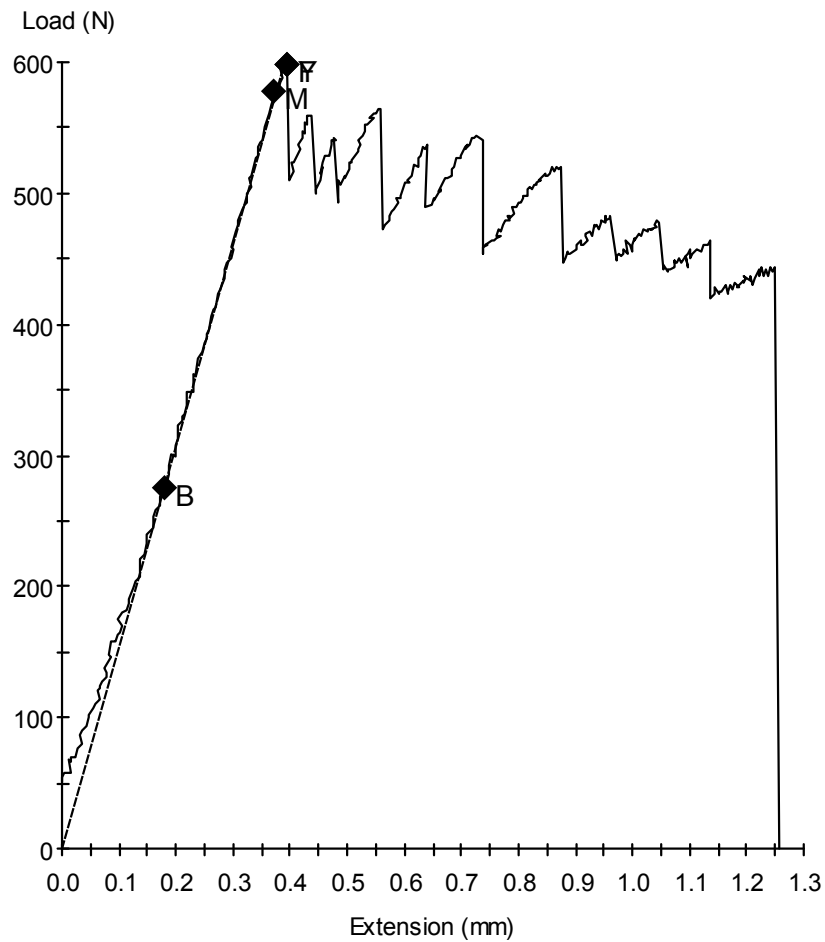
Sample ID: mustapha-10%-3.mss  
Specimen Number: 3  
Tagged: False

**Specimen Results:**

Name	Value	Units
Thickness	50.000	mm
Width	25.000	mm
Area	1250	mm <sup>2</sup>
Peak Load	510	N
Peak Stress	0.41	MPa
Break Load	506	N
Break Stress	0.40	MPa
Elongation At Break	0.788	mm
Stress At Offset Yield	0.385	MPa
Load At Offset Yield	480.728	N

11/05/2009

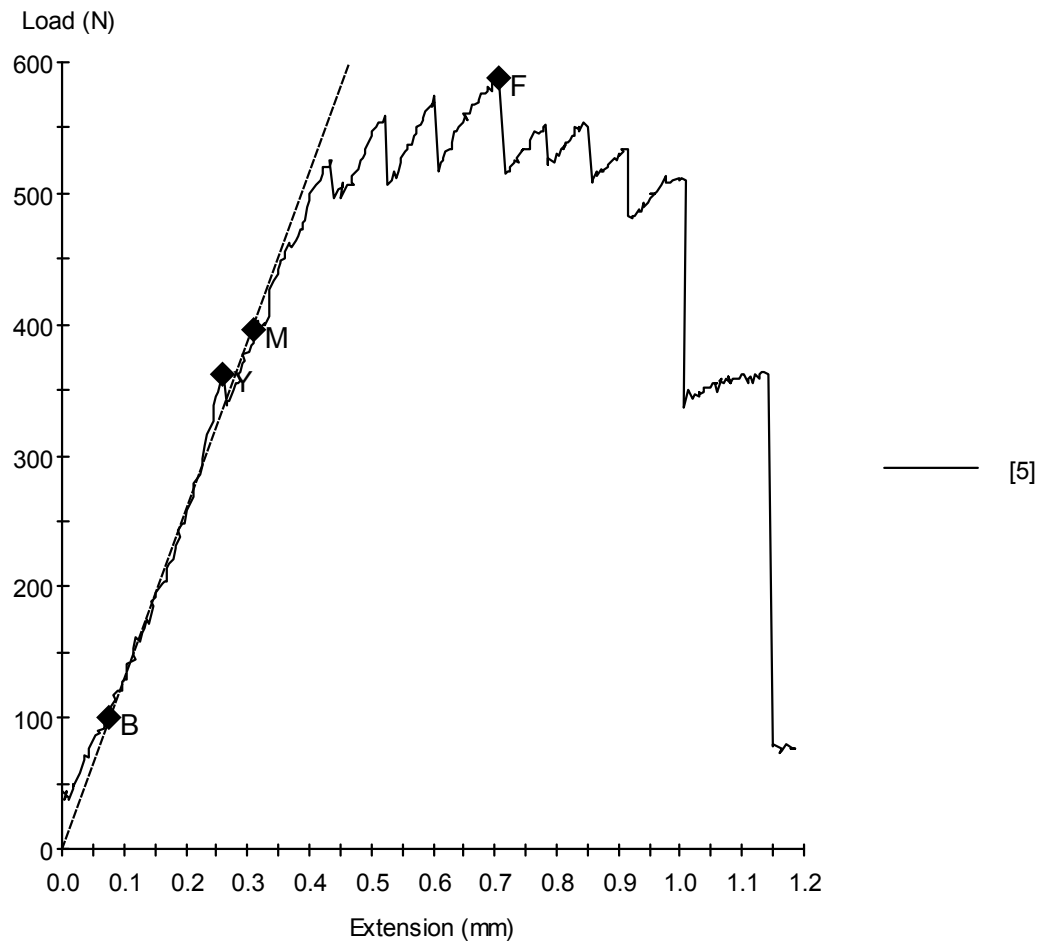
Sample ID: mustapha-10%-4.mss  
Specimen Number: 4  
Tagged: False

**Specimen Results:**

Name	Value	Units
Thickness	50.000	mm
Width	25.000	mm
Area	1250	mm <sup>2</sup>
Peak Load	598	N
Peak Stress	0.48	MPa
Break Load	598	N
Break Stress	0.48	MPa
Elongation At Break	0.394	mm
Stress At Offset Yield	0.400	MPa
Load At Offset Yield	500.198	N

11/05/2009

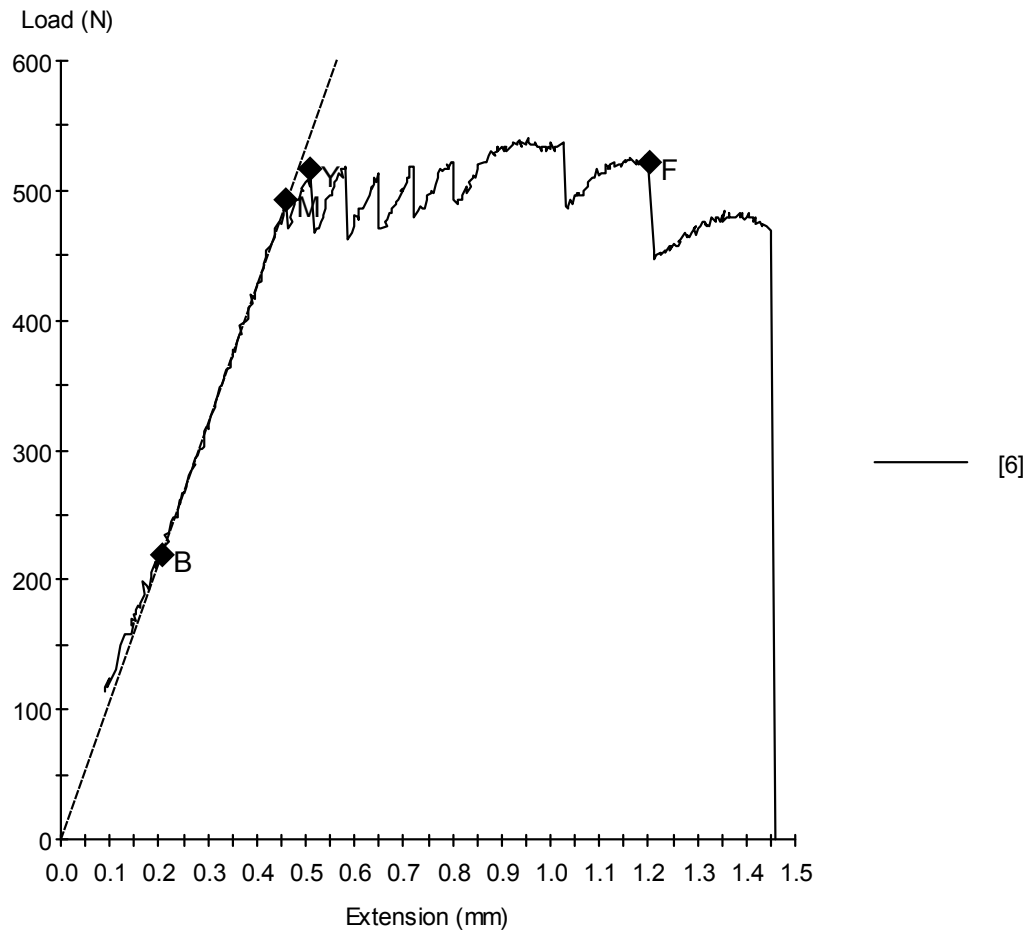
Sample ID: mustapha-10%-5.mss  
Specimen Number: 5  
Tagged: False

**Specimen Results:**

Name	Value	Units
Thickness	50.000	mm
Width	25.000	mm
Area	1250	mm <sup>2</sup>
Peak Load	588	N
Peak Stress	0.47	MPa
Break Load	588	N
Break Stress	0.47	MPa
Elongation At Break	0.707	mm
Stress At Offset Yield	0.406	MPa
Load At Offset Yield	506.912	N

11/05/2009

Sample ID: mustapha-10%-6.mss  
Specimen Number: 6  
Tagged: False

**Specimen Results:**

Name	Value	Units
Thickness	50.000	mm
Width	25.000	mm
Area	1250	mm <sup>2</sup>
Peak Load	540	N
Peak Stress	0.43	MPa
Break Load	522	N
Break Stress	0.42	MPa
Elongation At Break	1.201	mm
Stress At Offset Yield	0.370	MPa
Load At Offset Yield	462.600	N

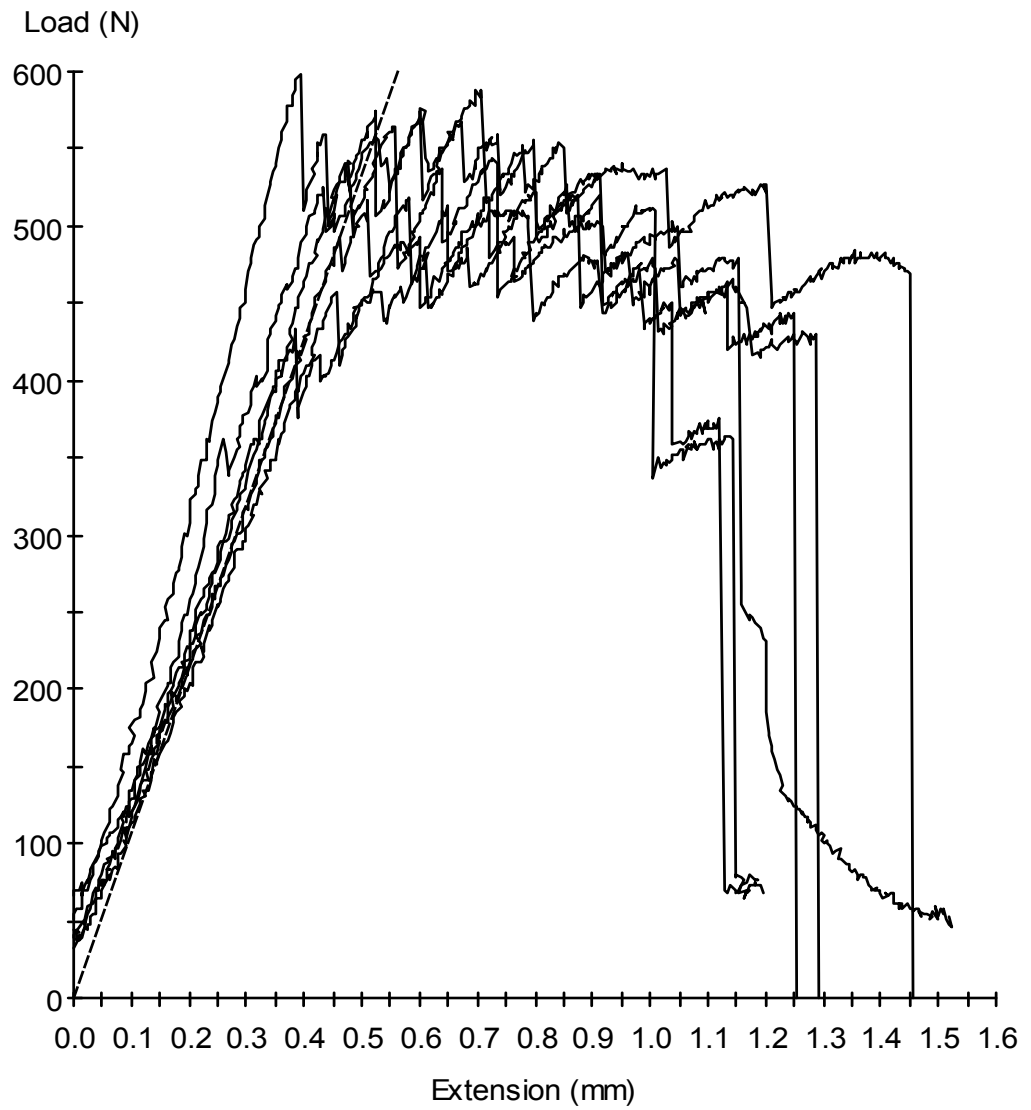
Test Date : 11/05/2009

Method : MMT fracture toughness Test .msm

**Specimen Results:**

Specimen #	Thickness mm	Width mm	Area mm <sup>2</sup>	Peak Load N	Peak Stress MPa	Break Load N	Break Stress MPa
1	50.000	25.000	1250	504	0.40	480	0.38
2	50.000	25.000	1250	576	0.46	520	0.42
3	50.000	25.000	1250	510	0.41	506	0.40
4	50.000	25.000	1250	598	0.48	598	0.48
5	50.000	25.000	1250	588	0.47	588	0.47
6	50.000	25.000	1250	540	0.43	522	0.42
<b>Mean</b>	<b>50.000</b>	<b>25.000</b>	<b>1250</b>	<b>553</b>	<b>0.44</b>	<b>536</b>	<b>0.43</b>
<b>Std Dev</b>	<b>0.000</b>	<b>0.000</b>	<b>0</b>	<b>40</b>	<b>0.03</b>	<b>47</b>	<b>0.04</b>

Specimen #	Elongation At Break mm	Stress At Offset Yield MPa	Load At Offset Yield N				
1	1.152	0.359	449.171				
2	0.911	0.440	550.554				
3	0.788	0.385	480.728				
4	0.394	0.400	500.198				
5	0.707	0.406	506.912				
6	1.201	0.370	462.600				
<b>Mean</b>	<b>0.859</b>	<b>0.393</b>	<b>491.694</b>				
<b>Std Dev</b>	<b>0.300</b>	<b>0.029</b>	<b>36.175</b>				

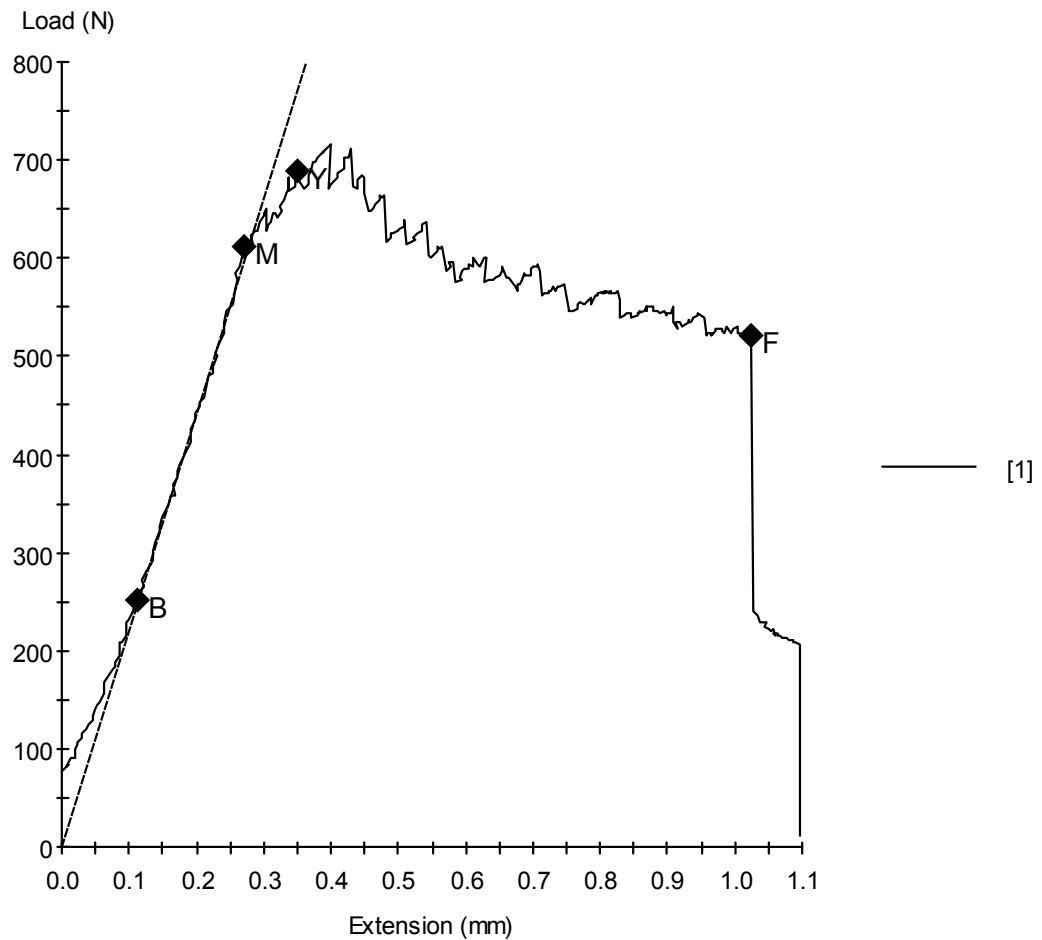


# MTS 810 Testing System Data

## **15% by Weight of Filler**

12/05/2009

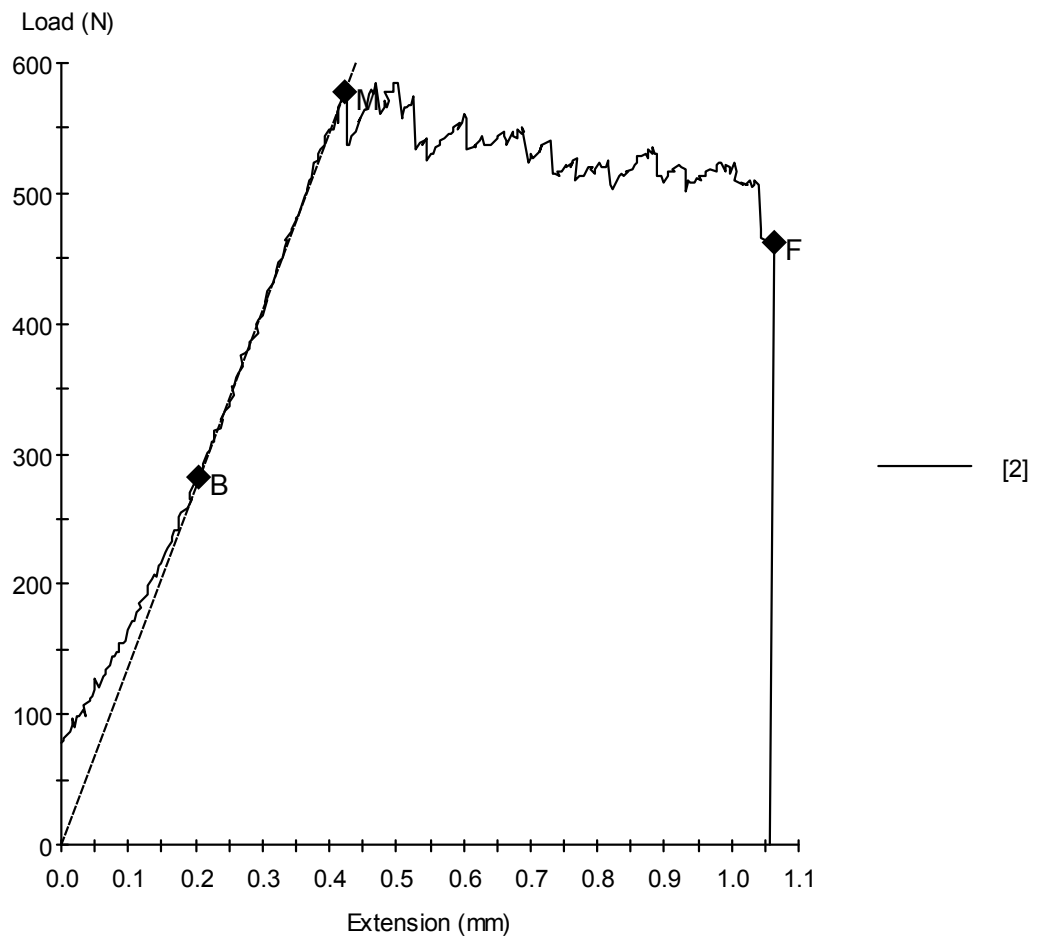
Sample ID: mustapha-15%-1.mss  
Specimen Number: 1  
Tagged: False

**Specimen Results:**

Name	Value	Units
Thickness	50.000	mm
Width	25.000	mm
Area	1250	mm <sup>2</sup>
Peak Load	717	N
Peak Stress	0.57	MPa
Break Load	520	N
Break Stress	0.42	MPa
Elongation At Break	1.023	mm
Stress At Offset Yield	0.553	MPa
Load At Offset Yield	691.549	N

12/05/2009

Sample ID: mustapha-15%-2.mss  
Specimen Number: 2  
Tagged: False

**Specimen Results:**

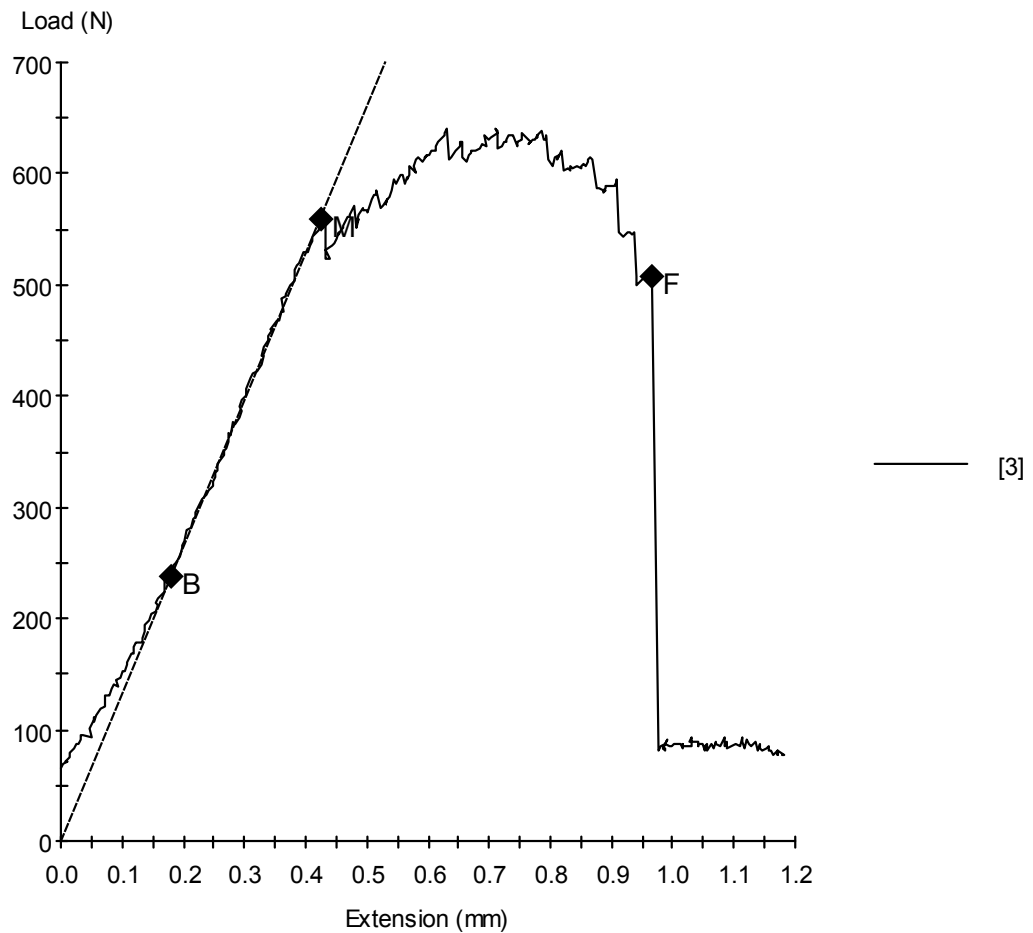
Name	Value	Units
Thickness	50.000	mm
Width	25.000	mm
Area	1250	mm <sup>2</sup>
Peak Load	585	N
Peak Stress	0.47	MPa
Break Load	462	N
Break Stress	0.37	MPa
Elongation At Break	1.063	mm
Stress At Offset Yield	0.446	MPa
Load At Offset Yield	557.268	N

12/05/2009

Sample ID: mustapha-15%-3.mss

Specimen Number: 3

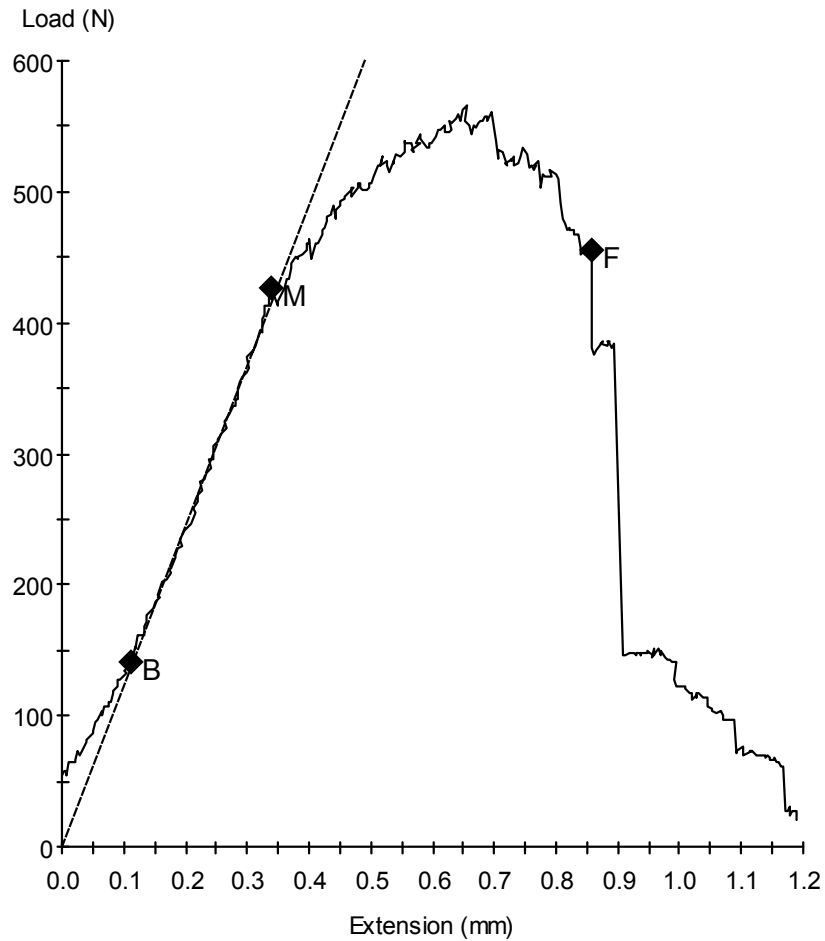
Tagged: False

**Specimen Results:**

Name	Value	Units
Thickness	50.000	mm
Width	25.000	mm
Area	1250	mm <sup>2</sup>
Peak Load	641	N
Peak Stress	0.51	MPa
Break Load	507	N
Break Stress	0.41	MPa
Elongation At Break	0.966	mm
Stress At Offset Yield	0.464	MPa
Load At Offset Yield	579.424	N

12/05/2009

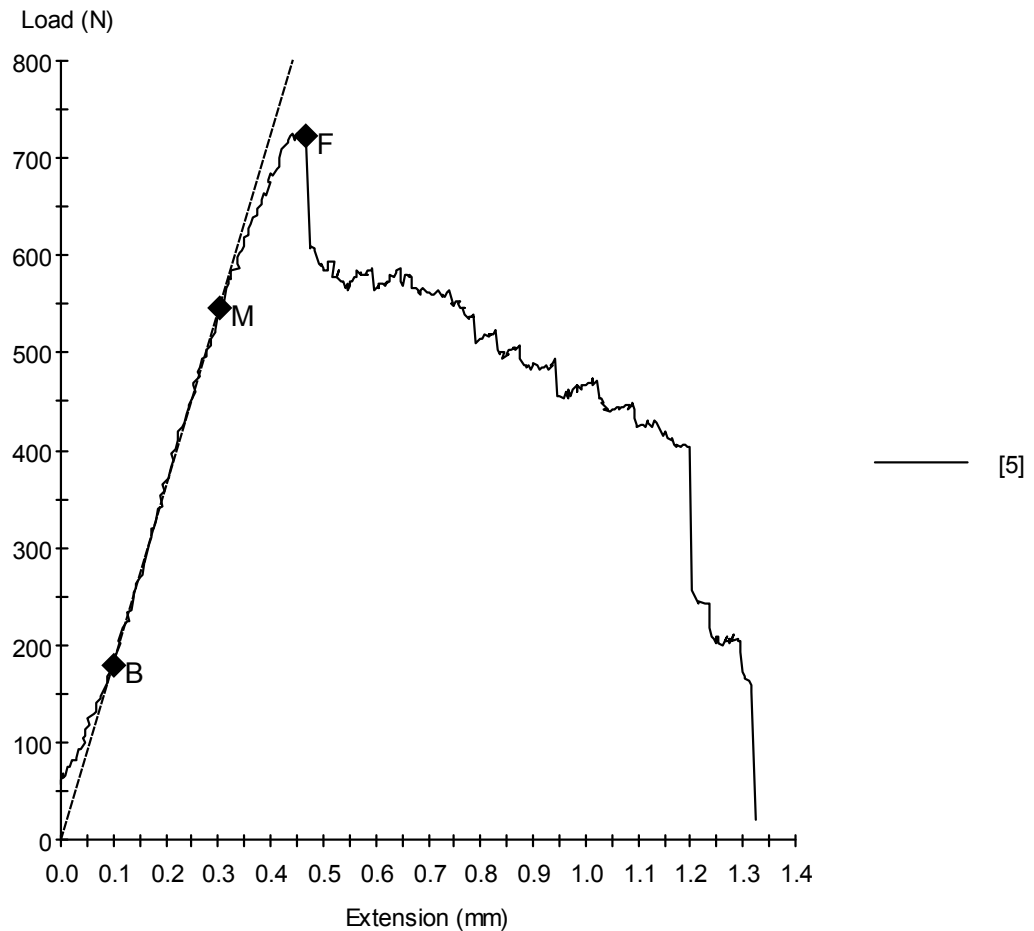
Sample ID: mustapha-15%-4.mss  
Specimen Number: 4  
Tagged: False

**Specimen Results:**

Name	Value	Units
Thickness	50.000	mm
Width	25.000	mm
Area	1250	mm <sup>2</sup>
Peak Load	566	N
Peak Stress	0.45	MPa
Break Load	455	N
Break Stress	0.36	MPa
Elongation At Break	0.857	mm
Stress At Offset Yield	0.415	MPa
Load At Offset Yield	519.333	N

12/05/2009

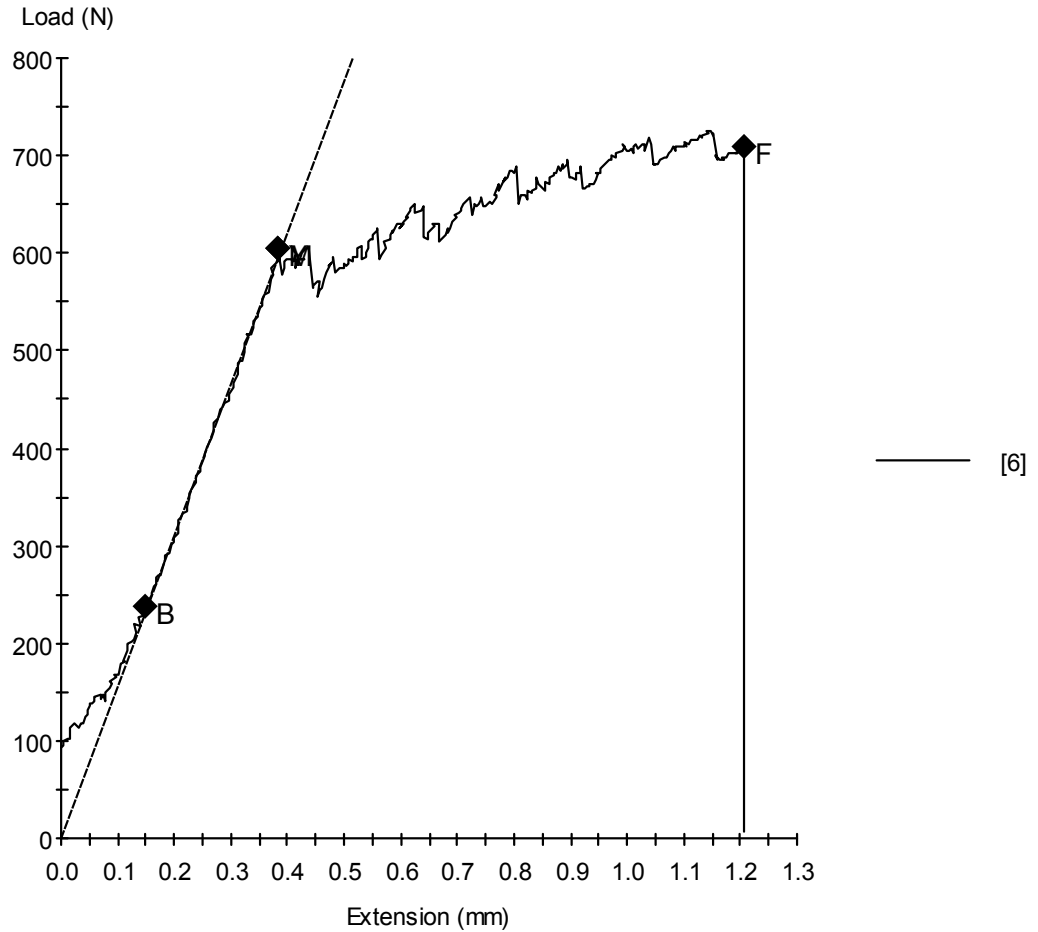
Sample ID: mustapha-15%-5.mss  
Specimen Number: 5  
Tagged: False

**Specimen Results:**

Name	Value	Units
Thickness	50.000	mm
Width	25.000	mm
Area	1250	mm <sup>2</sup>
Peak Load	726	N
Peak Stress	0.58	MPa
Break Load	724	N
Break Stress	0.58	MPa
Elongation At Break	0.465	mm
Stress At Offset Yield	0.486	MPa
Load At Offset Yield	607.624	N

12/05/2009

Sample ID: mustapha-15%-6.mss  
Specimen Number: 6  
Tagged: False

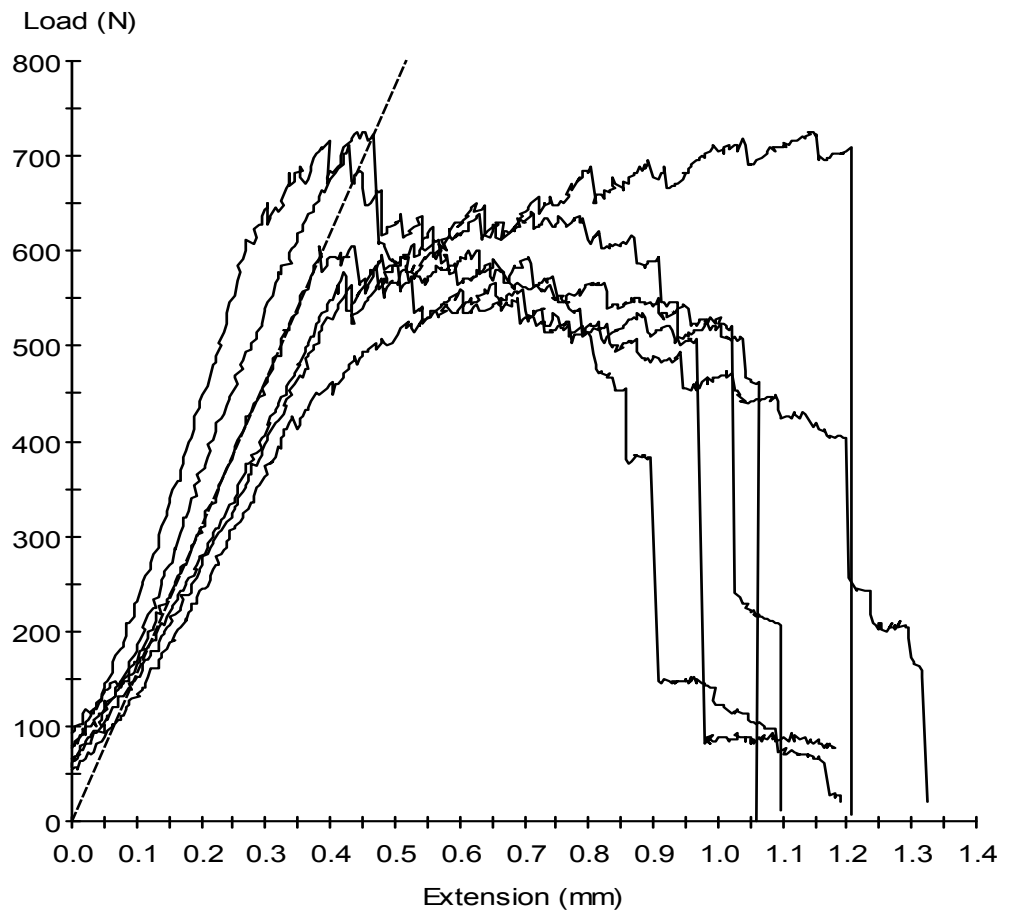
**Specimen Results:**

Name	Value	Units
Thickness	50.000	mm
Width	25.000	mm
Area	1250	mm <sup>2</sup>
Peak Load	726	N
Peak Stress	0.58	MPa
Break Load	708	N
Break Stress	0.57	MPa
Elongation At Break	1.205	mm
Stress At Offset Yield	0.464	MPa
Load At Offset Yield	579.424	N

**Specimen Results:**

Specimen #	Thickness mm	Width mm	Area mm <sup>2</sup>	Peak Load N	Peak Stress MPa	Break Load N	Break Stress MPa
1	50.000	25.000	1250	717	0.57	520	0.42
2	50.000	25.000	1250	585	0.47	462	0.37
3	50.000	25.000	1250	641	0.51	507	0.41
4	50.000	25.000	1250	566	0.45	455	0.36
5	50.000	25.000	1250	726	0.58	724	0.58
6	50.000	25.000	1250	726	0.58	708	0.57
<b>Mean</b>	<b>50.000</b>	<b>25.000</b>	<b>1250</b>	<b>660</b>	<b>0.53</b>	<b>563</b>	<b>0.45</b>
<b>Std Dev</b>	<b>0.000</b>	<b>0.000</b>	<b>0</b>	<b>73</b>	<b>0.06</b>	<b>122</b>	<b>0.10</b>

Specimen #	Elongation At Break mm	Stress At Offset Yield MPa	Load At Offset Yield N				
1	1.023	0.553	691.549				
2	1.063	0.446	557.268				
3	0.966	0.464	579.424				
4	0.857	0.415	519.333				
5	0.465	0.486	607.624				
6	1.205	0.464	579.424				
<b>Mean</b>	<b>0.930</b>	<b>0.471</b>	<b>589.104</b>				
<b>Std Dev</b>	<b>0.255</b>	<b>0.047</b>	<b>58.150</b>				

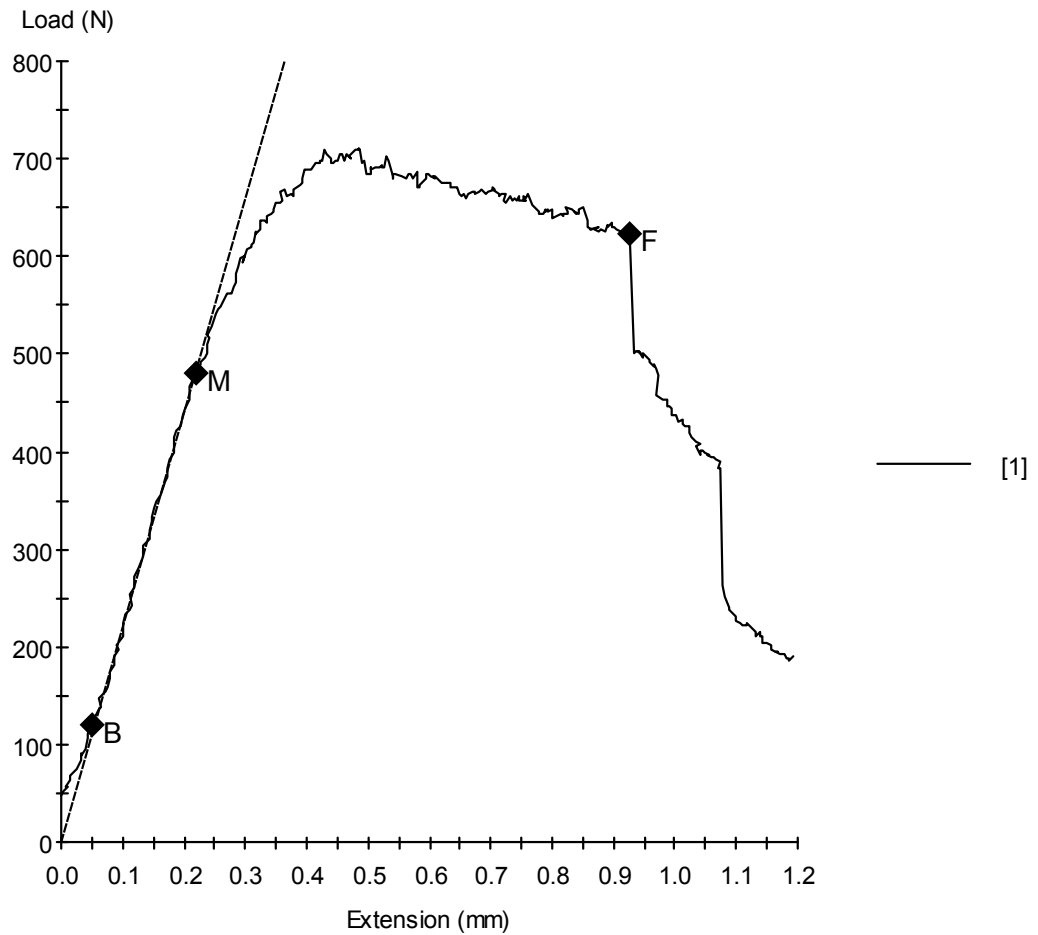


# MTS 810 Testing System Data

## **20% by Weight of Filler**

12/05/2009

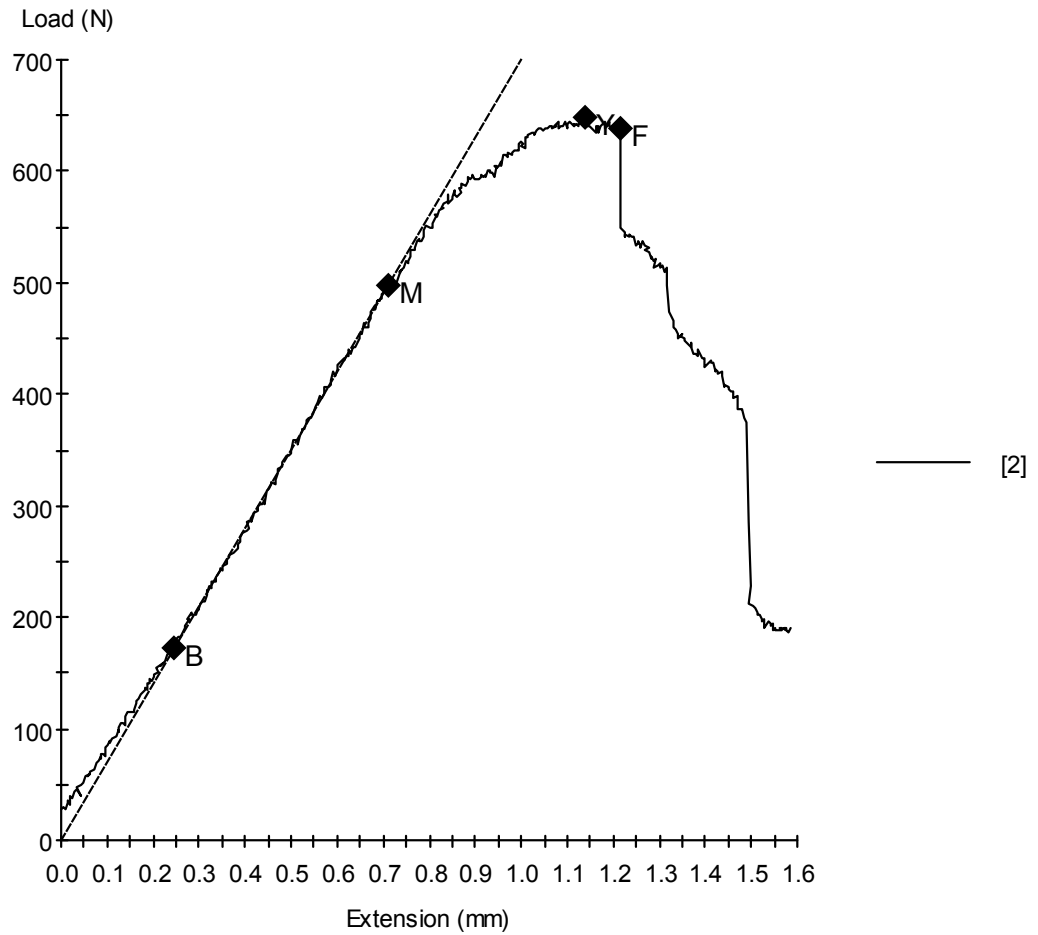
Sample ID: mustapha-20%-1.mss  
Specimen Number: 1  
Tagged: False

**Specimen Results:**

Name	Value	Units
Thickness	50.000	mm
Width	25.000	mm
Area	1250	mm <sup>2</sup>
Peak Load	712	N
Peak Stress	0.57	MPa
Break Load	624	N
Break Stress	0.50	MPa
Elongation At Break	0.926	mm
Stress At Offset Yield	0.556	MPa
Load At Offset Yield	694.906	N

12/05/2009

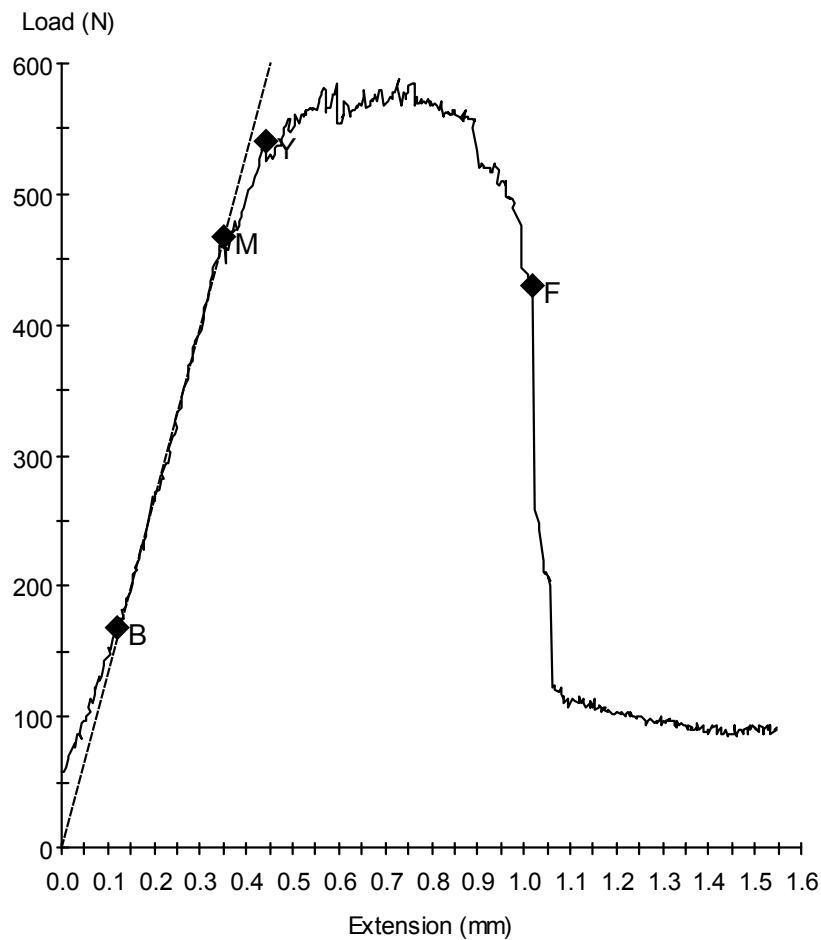
Sample ID: mustapha-20%-2.mss  
Specimen Number: 2  
Tagged: False

**Specimen Results:**

Name	Value	Units
Thickness	50.000	mm
Width	25.000	mm
Area	1250	mm <sup>2</sup>
Peak Load	648	N
Peak Stress	0.52	MPa
Break Load	638	N
Break Stress	0.51	MPa
Elongation At Break	1.214	mm
Stress At Offset Yield	0.492	MPa
Load At Offset Yield	614.673	N

12/05/2009

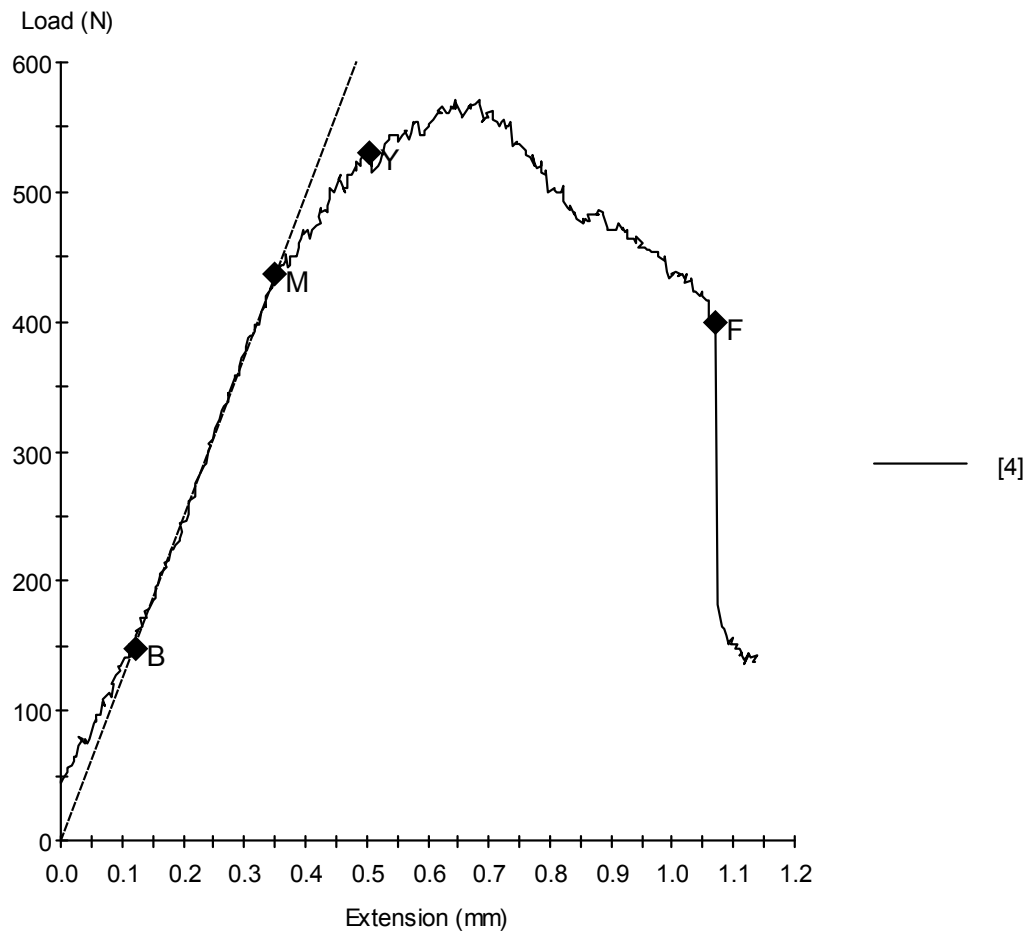
Sample ID: mustapha-20%-3.mss  
Specimen Number: 3  
Tagged: False

**Specimen Results:**

Name	Value	Units
Thickness	50.000	mm
Width	25.000	mm
Area	1250	mm <sup>2</sup>
Peak Load	587	N
Peak Stress	0.47	MPa
Break Load	430	N
Break Stress	0.34	MPa
Elongation At Break	1.020	mm
Stress At Offset Yield	0.451	MPa
Load At Offset Yield	563.982	N

12/05/2009

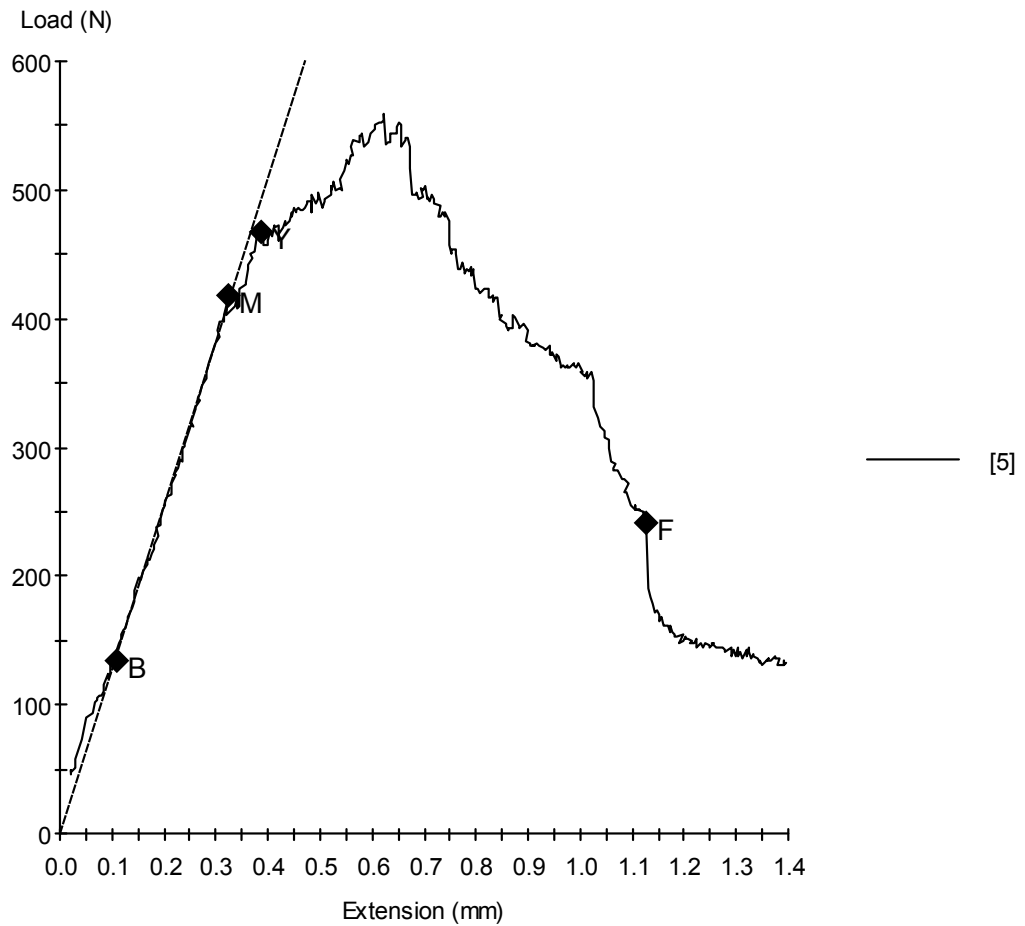
Sample ID: mustapha-20%-4.mss  
Specimen Number: 4  
Tagged: False

**Specimen Results:**

Name	Value	Units
Thickness	50.000	mm
Width	25.000	mm
Area	1250	mm <sup>2</sup>
Peak Load	571	N
Peak Stress	0.46	MPa
Break Load	399	N
Break Stress	0.32	MPa
Elongation At Break	1.072	mm
Stress At Offset Yield	0.432	MPa
Load At Offset Yield	540.483	N

12/05/2009

Sample ID: mustapha-20%-5.mss  
Specimen Number: 5  
Tagged: False

**Specimen Results:**

Name	Value	Units
Thickness	50.000	mm
Width	25.000	mm
Area	1250	mm <sup>2</sup>
Peak Load	559	N
Peak Stress	0.45	MPa
Break Load	242	N
Break Stress	0.19	MPa
Elongation At Break	1.127	mm
Stress At Offset Yield	0.387	MPa
Load At Offset Yield	483.413	N

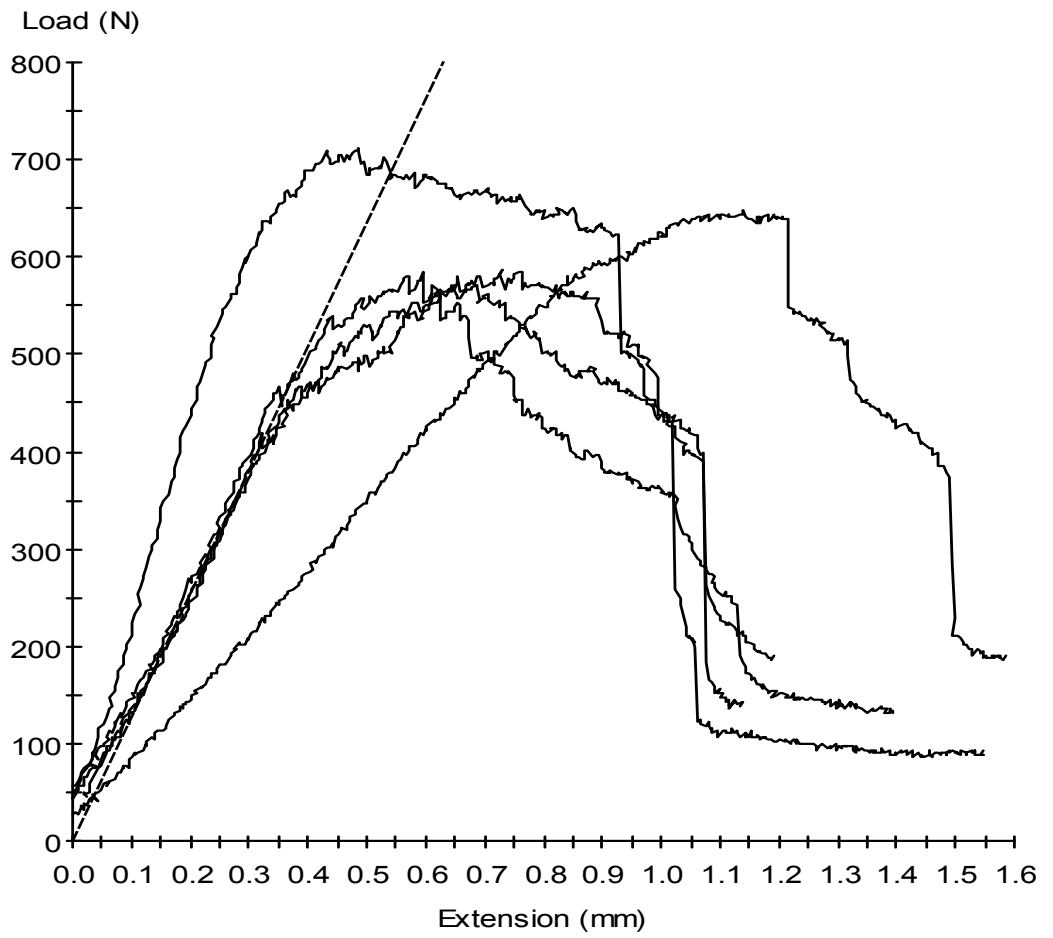
Test Date : 12/05/2009

Method : MMT fracture toughness Test .msm

**Specimen Results:**

Specimen #	Thickness mm	Width mm	Area mm <sup>2</sup>	Peak Load N	Peak Stress MPa	Break Load N	Break Stress MPa
1	50.000	25.000	1250	712	0.57	624	0.50
2	50.000	25.000	1250	648	0.52	638	0.51
3	50.000	25.000	1250	587	0.47	430	0.34
4	50.000	25.000	1250	571	0.46	399	0.32
5	50.000	25.000	1250	559	0.45	242	0.19
<b>Mean</b>	<b>50.000</b>	<b>25.000</b>	<b>1250</b>	<b>615</b>	<b>0.49</b>	<b>467</b>	<b>0.37</b>
<b>Std Dev</b>	<b>0.000</b>	<b>0.000</b>	<b>0</b>	<b>64</b>	<b>0.05</b>	<b>166</b>	<b>0.13</b>

Specimen #	Elongation At Break mm	Stress At Offset Yield MPa	Load At Offset Yield N				
1	0.926	0.556	694.906				
2	1.214	0.492	614.673				
3	1.020	0.451	563.982				
4	1.072	0.432	540.483				
5	1.127	0.387	483.413				
<b>Mean</b>	<b>1.072</b>	<b>0.464</b>	<b>579.492</b>				
<b>Std Dev</b>	<b>0.108</b>	<b>0.064</b>	<b>79.924</b>				

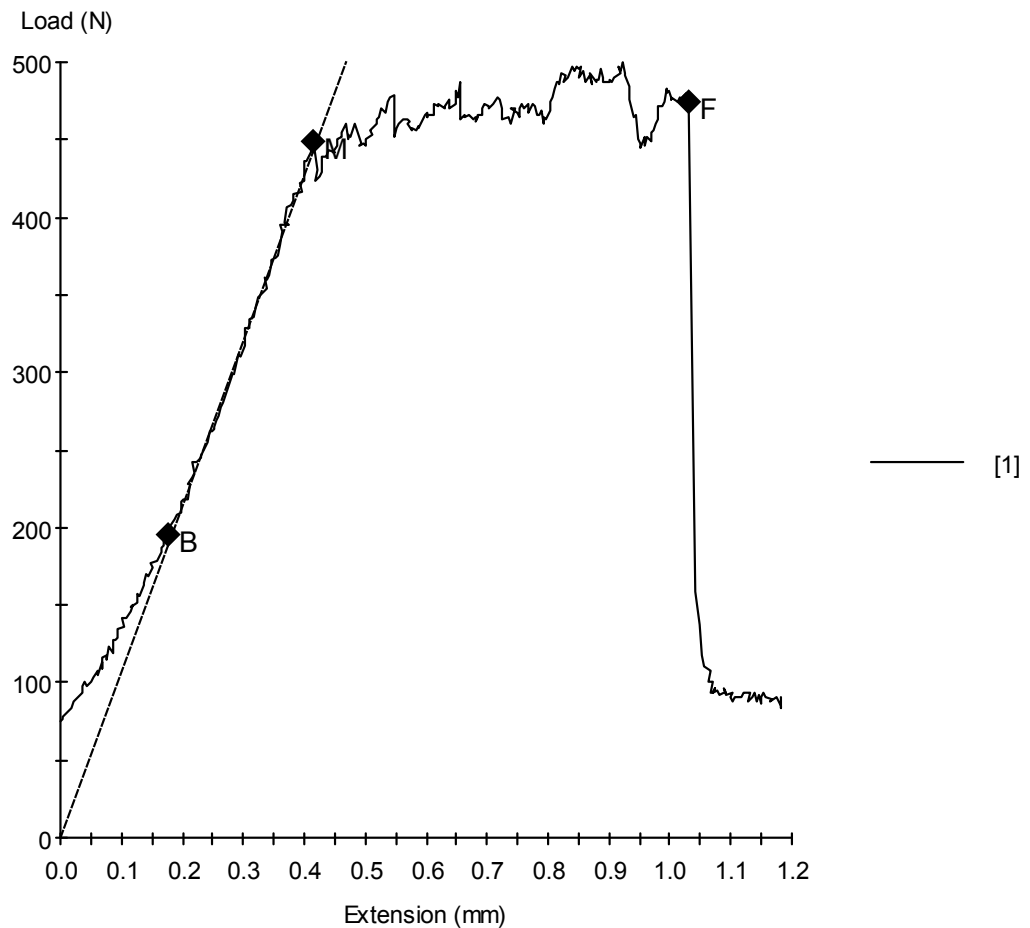


# MTS 810 Testing System Data

## **25% by Weight of Filler**

12/05/2009

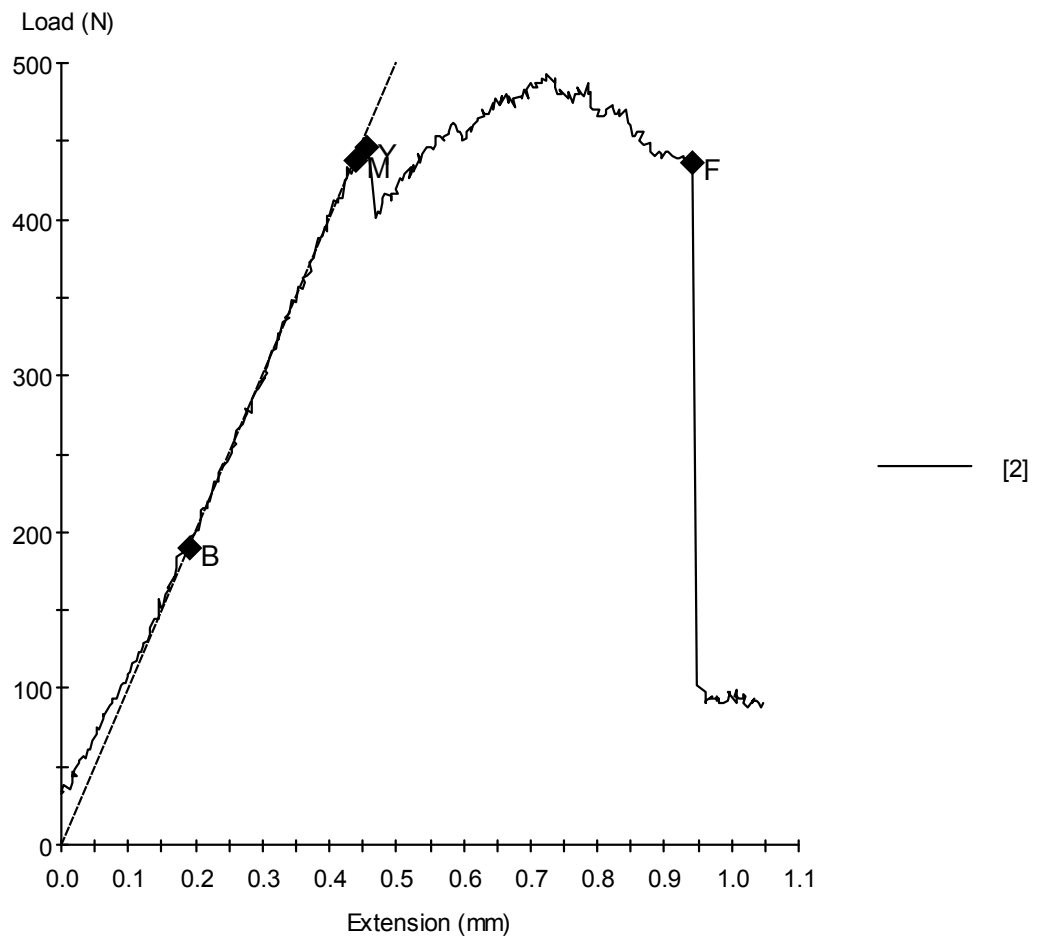
Sample ID: mustapha-25%-1.mss  
Specimen Number: 1  
Tagged: False

**Specimen Results:**

Name	Value	Units
Thickness	50.000	mm
Width	25.000	mm
Area	1250	mm <sup>2</sup>
Peak Load	500	N
Peak Stress	0.40	MPa
Break Load	474	N
Break Stress	0.38	MPa
Elongation At Break	1.032	mm
Stress At Offset Yield	0.361	MPa
Load At Offset Yield	451.857	N

12/05/2009

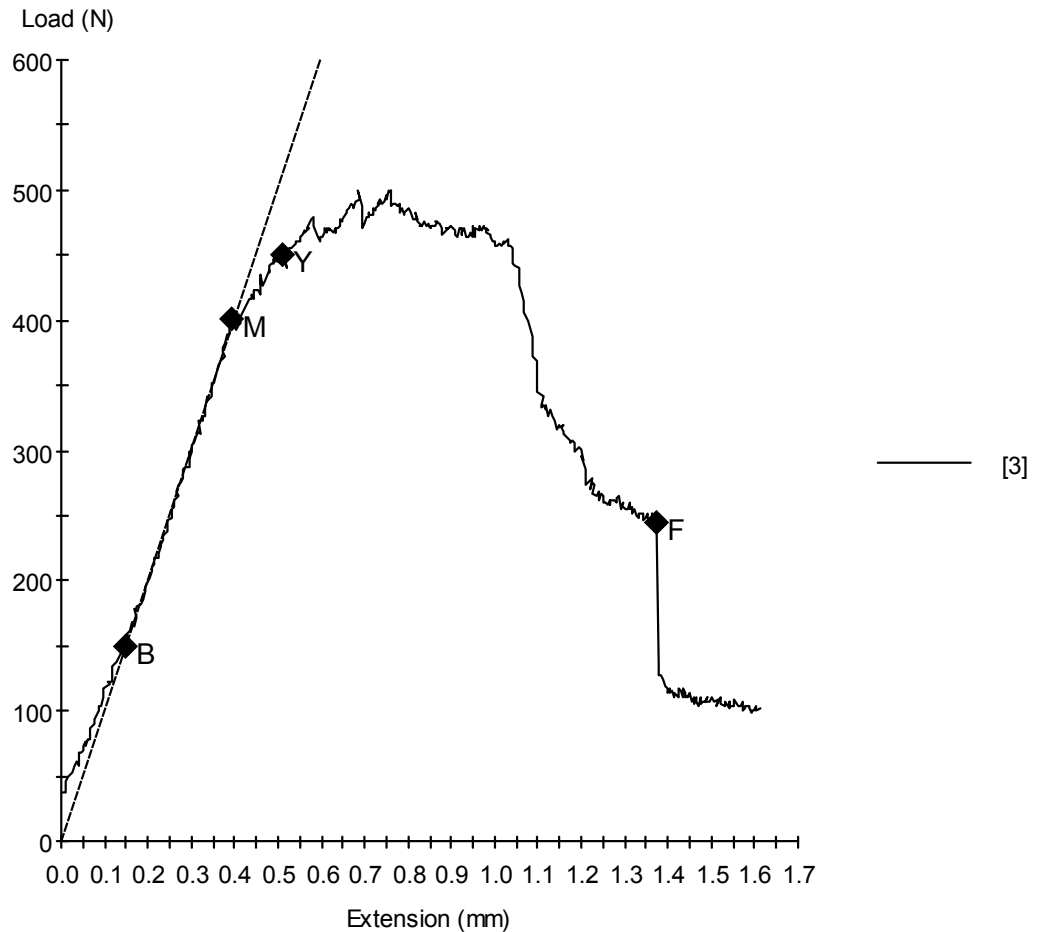
Sample ID: mustapha-25%-2.mss  
Specimen Number: 2  
Tagged: False

**Specimen Results:**

Name	Value	Units
Thickness	50.000	mm
Width	25.000	mm
Area	1250	mm <sup>2</sup>
Peak Load	493	N
Peak Stress	0.39	MPa
Break Load	436	N
Break Stress	0.35	MPa
Elongation At Break	0.942	mm
Stress At Offset Yield	0.357	MPa
Load At Offset Yield	446.486	N

12/05/2009

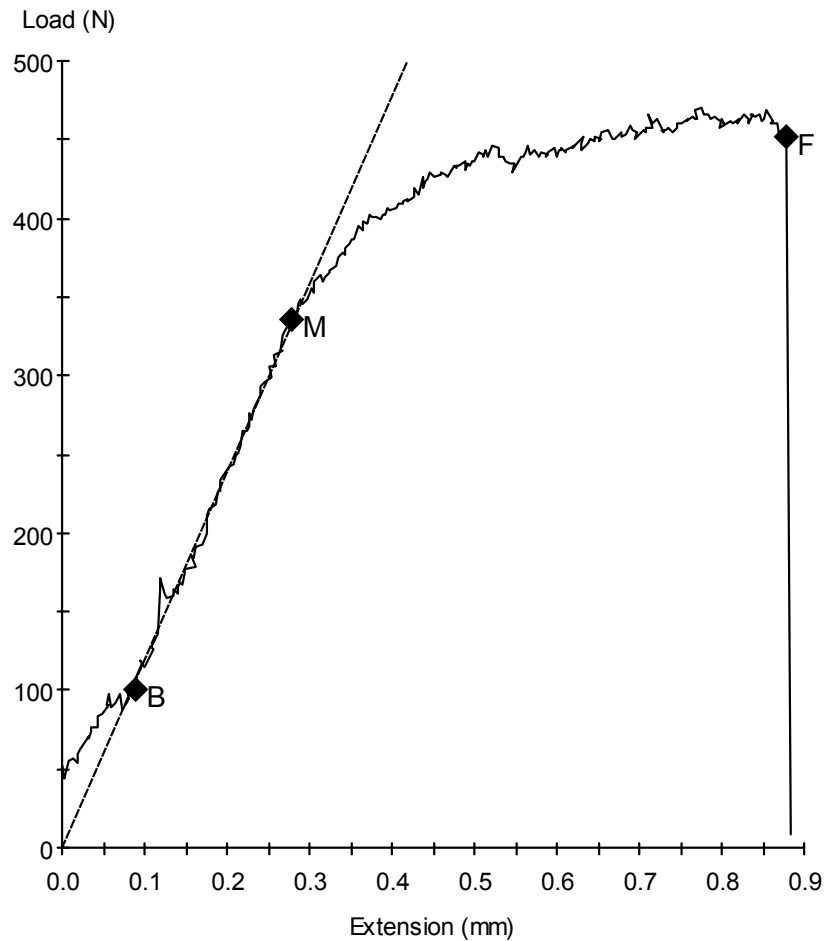
Sample ID: mustapha-25%-3.mss  
Specimen Number: 3  
Tagged: False

**Specimen Results:**

Name	Value	Units
Thickness	50.000	mm
Width	25.000	mm
Area	1250	mm <sup>2</sup>
Peak Load	500	N
Peak Stress	0.40	MPa
Break Load	245	N
Break Stress	0.20	MPa
Elongation At Break	1.371	mm
Stress At Offset Yield	0.376	MPa
Load At Offset Yield	469.985	N

12/05/2009

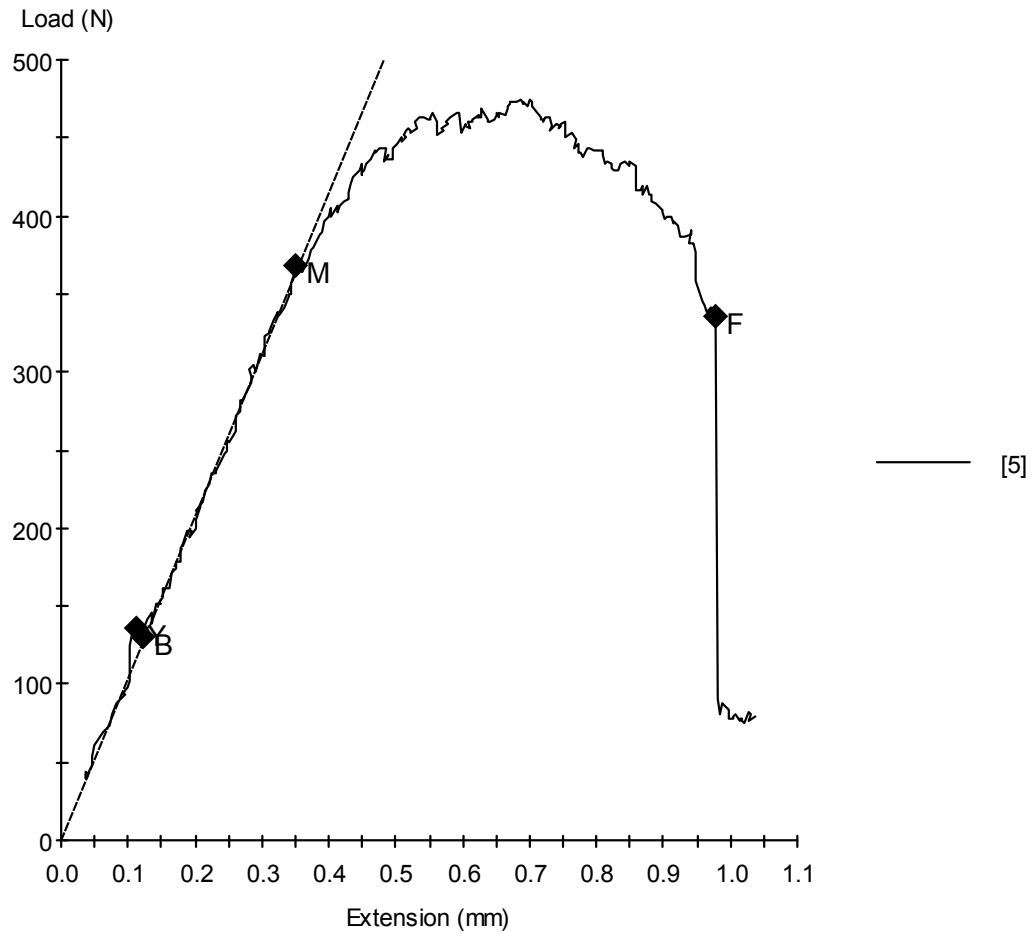
Sample ID: mustapha-25%-4.mss  
Specimen Number: 4  
Tagged: False

**Specimen Results:**

Name	Value	Units
Thickness	50.000	mm
Width	25.000	mm
Area	1250	mm <sup>2</sup>
Peak Load	470	N
Peak Stress	0.38	MPa
Break Load	452	N
Break Stress	0.36	MPa
Elongation At Break	0.878	mm
Stress At Offset Yield	0.342	MPa
Load At Offset Yield	427.519	N

12/05/2009

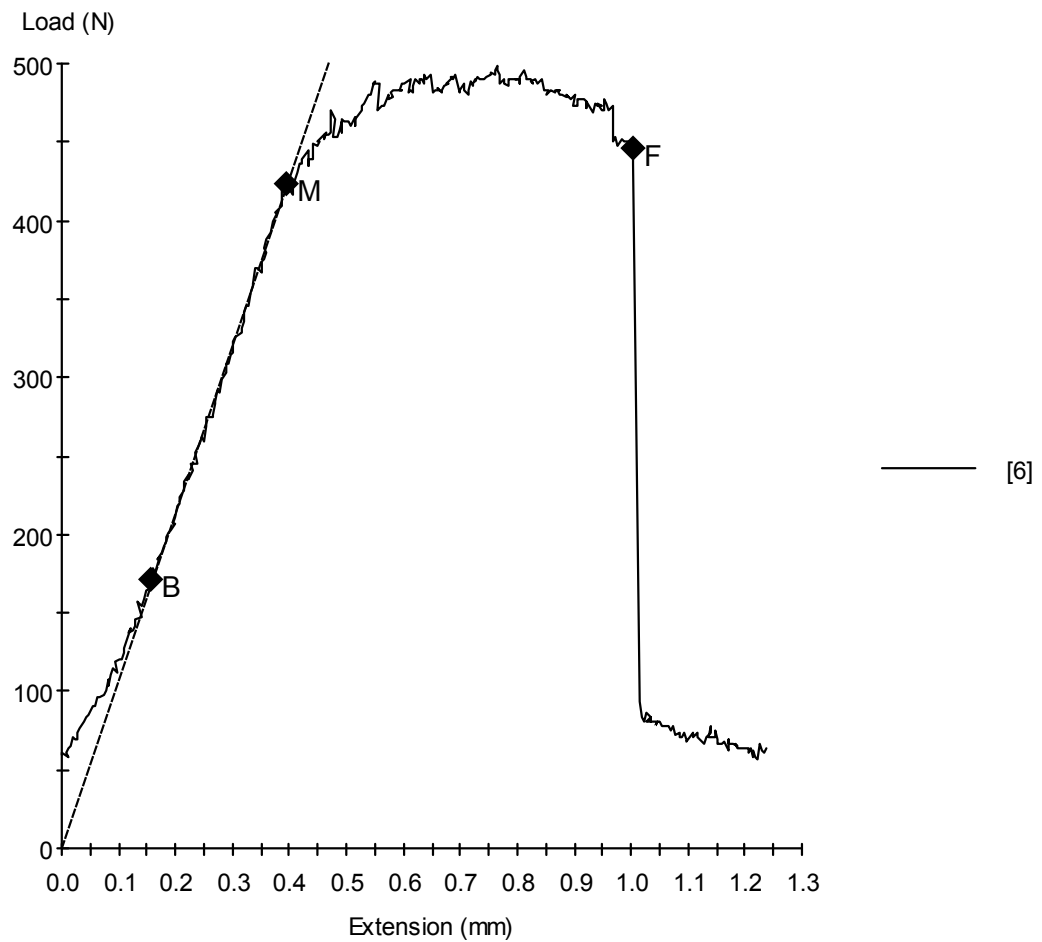
Sample ID: mustapha-25%-5.mss  
Specimen Number: 5  
Tagged: False

**Specimen Results:**

Name	Value	Units
Thickness	50.000	mm
Width	25.000	mm
Area	1250	mm <sup>2</sup>
Peak Load	475	N
Peak Stress	0.38	MPa
Break Load	336	N
Break Stress	0.27	MPa
Elongation At Break	0.978	mm
Stress At Offset Yield	0.370	MPa
Load At Offset Yield	462.432	N

12/05/2009

Sample ID: mustapha-25%-6.mss  
Specimen Number: 6  
Tagged: False

**Specimen Results:**

Name	Value	Units
Thickness	50.000	mm
Width	25.000	mm
Area	1250	mm <sup>2</sup>
Peak Load	499	N
Peak Stress	0.40	MPa
Break Load	446	N
Break Stress	0.36	MPa
Elongation At Break	1.003	mm
Stress At Offset Yield	0.389	MPa
Load At Offset Yield	486.770	N

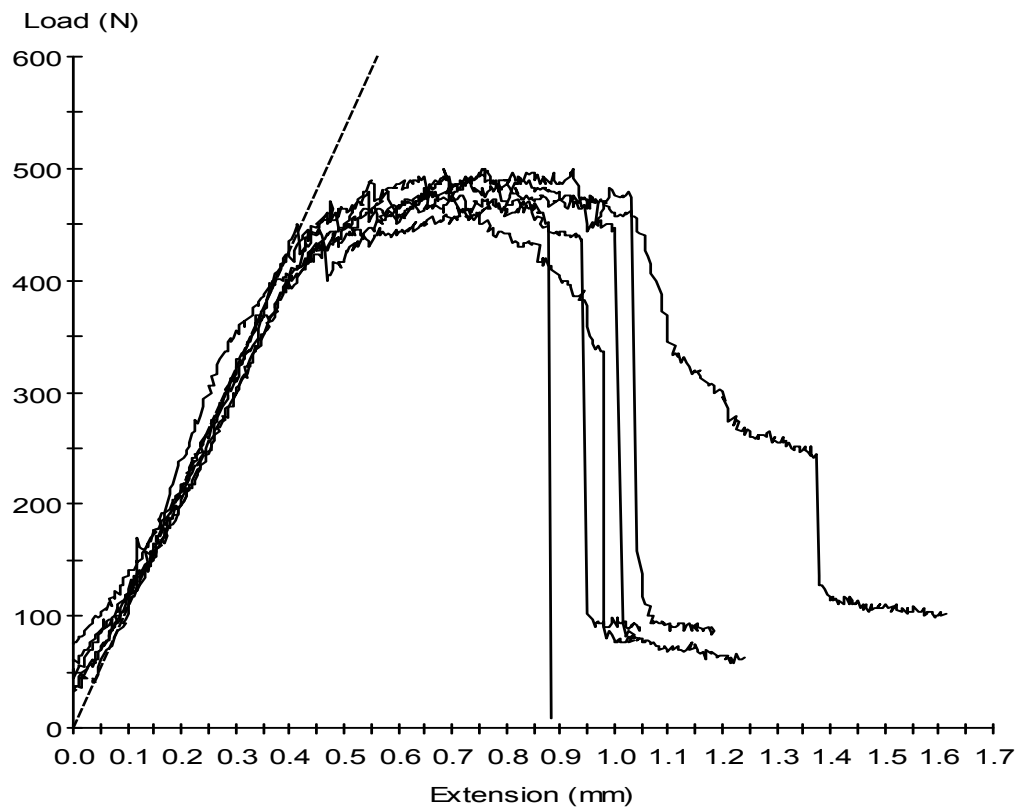
Test Date : 12/05/2009

Method : MMT fracture toughness Test .msm

**Specimen Results:**

Specimen #	Thickness mm	Width mm	Area mm <sup>2</sup>	Peak Load N	Peak Stress MPa	Break Load N	Break Stress MPa
1	50.000	25.000	1250	500	0.40	474	0.38
2	50.000	25.000	1250	493	0.39	436	0.35
3	50.000	25.000	1250	500	0.40	245	0.20
4	50.000	25.000	1250	470	0.38	452	0.36
5	50.000	25.000	1250	475	0.38	336	0.27
6	50.000	25.000	1250	499	0.40	446	0.36
<b>Mean</b>	<b>50.000</b>	<b>25.000</b>	<b>1250</b>	<b>490</b>	<b>0.39</b>	<b>398</b>	<b>0.32</b>
<b>Std Dev</b>	<b>0.000</b>	<b>0.000</b>	<b>0</b>	<b>13</b>	<b>0.01</b>	<b>89</b>	<b>0.07</b>

Specimen #	Elongation At Break mm	Stress At Offset Yield MPa	Load At Offset Yield N				
1	1.032	0.361	451.857				
2	0.942	0.357	446.486				
3	1.371	0.376	469.985				
4	0.878	0.342	427.519				
5	0.978	0.370	462.432				
6	1.003	0.389	486.770				
<b>Mean</b>	<b>1.034</b>	<b>0.366</b>	<b>457.508</b>				
<b>Std Dev</b>	<b>0.174</b>	<b>0.016</b>	<b>20.440</b>				

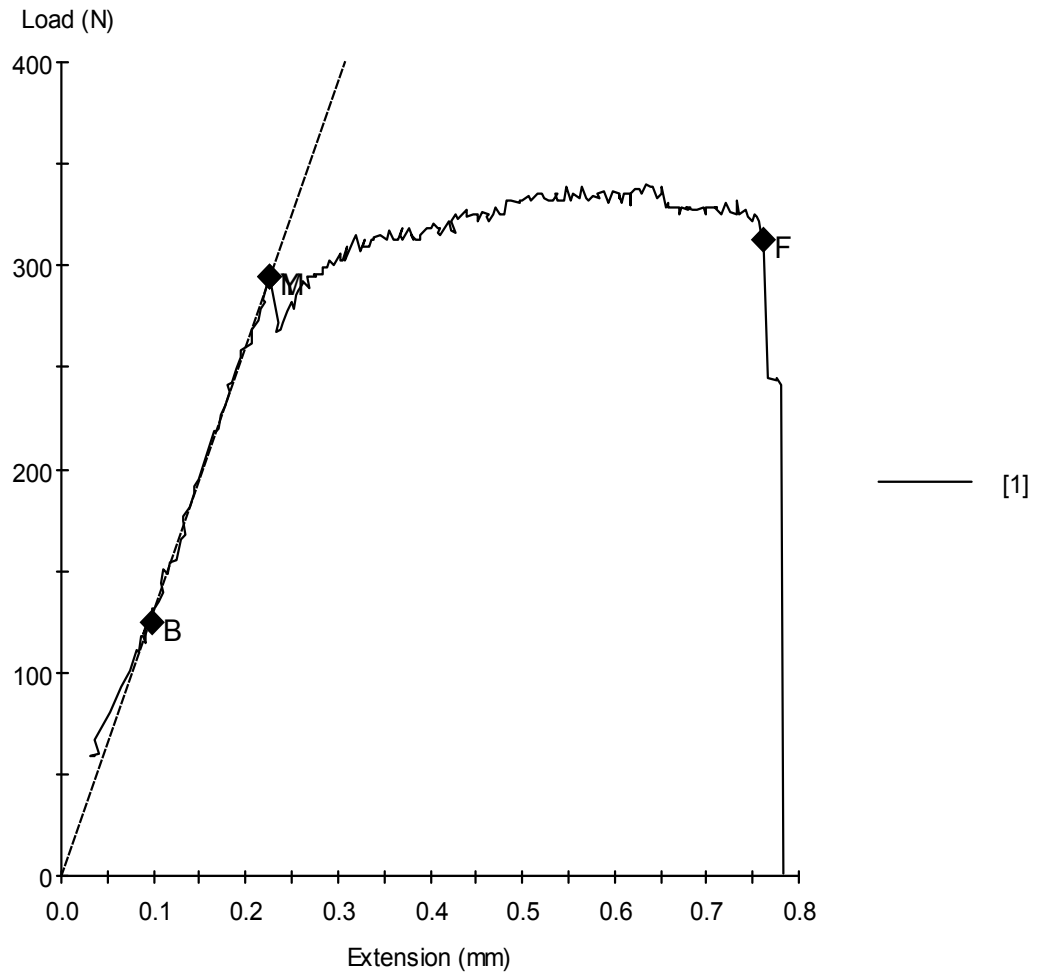


# MTS 810 Testing System Data

## **30% by Weight of Filler**

12/05/2009

Sample ID: mustapha-30%-1.mss  
Specimen Number: 1  
Tagged: False

**Specimen Results:**

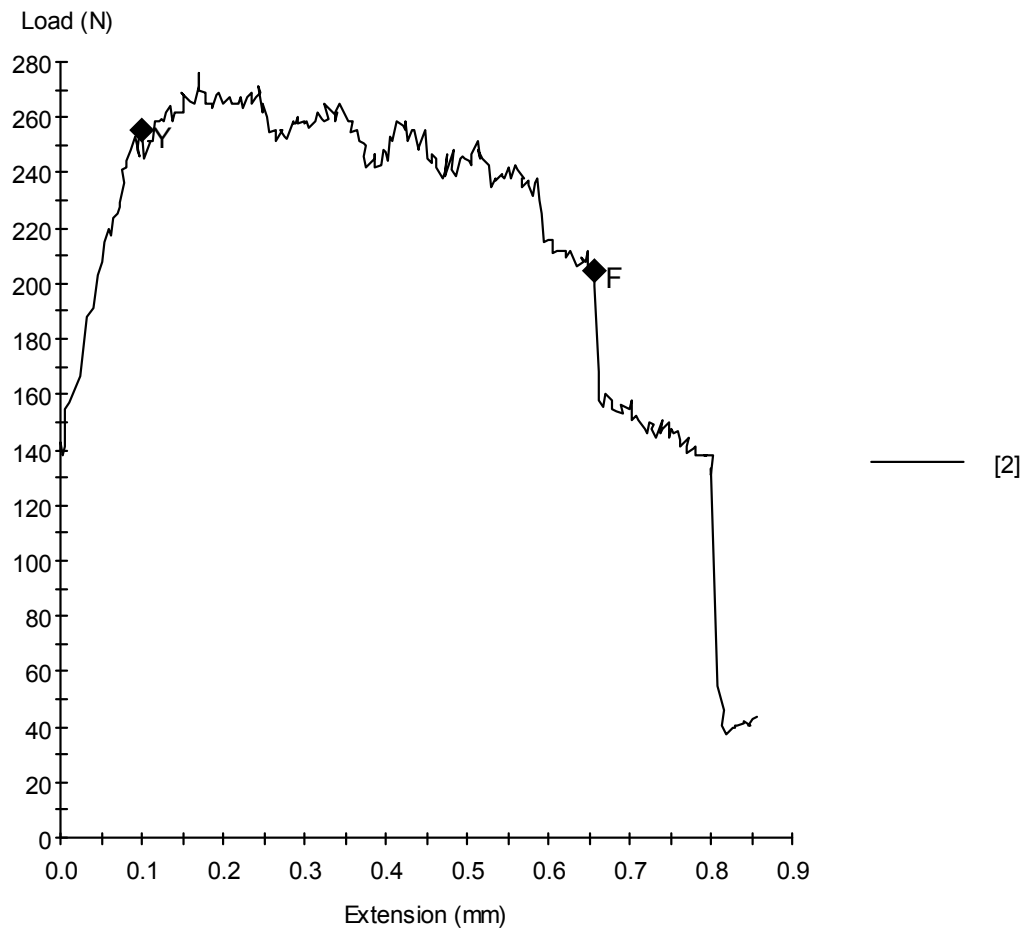
Name	Value	Units
Thickness	50.000	mm
Width	25.000	mm
Area	1250	mm <sup>2</sup>
Peak Load	340	N
Peak Stress	0.27	MPa
Break Load	312	N
Break Stress	0.25	MPa
Elongation At Break	0.763	mm
Stress At Offset Yield	0.252	MPa
Load At Offset Yield	315.561	N

12/05/2009

Sample ID: mustapha-30%-2.mss

Specimen Number: 2

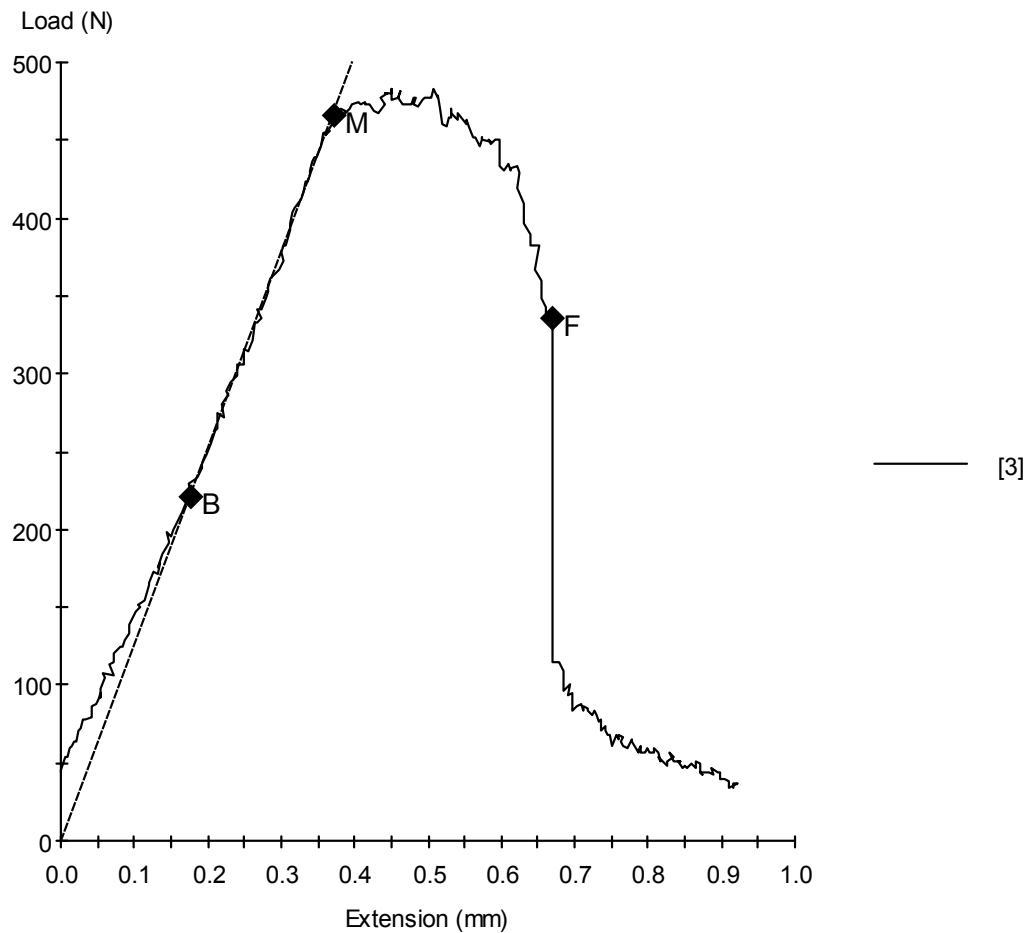
Tagged: False

**Specimen Results:**

Name	Value	Units
Thickness	50.000	mm
Width	25.000	mm
Area	1250	mm <sup>2</sup>
Peak Load	276	N
Peak Stress	0.22	MPa
Break Load	205	N
Break Stress	0.16	MPa
Elongation At Break	0.658	mm
Stress At Offset Yield	****	MPa
Load At Offset Yield	****	N

12/05/2009

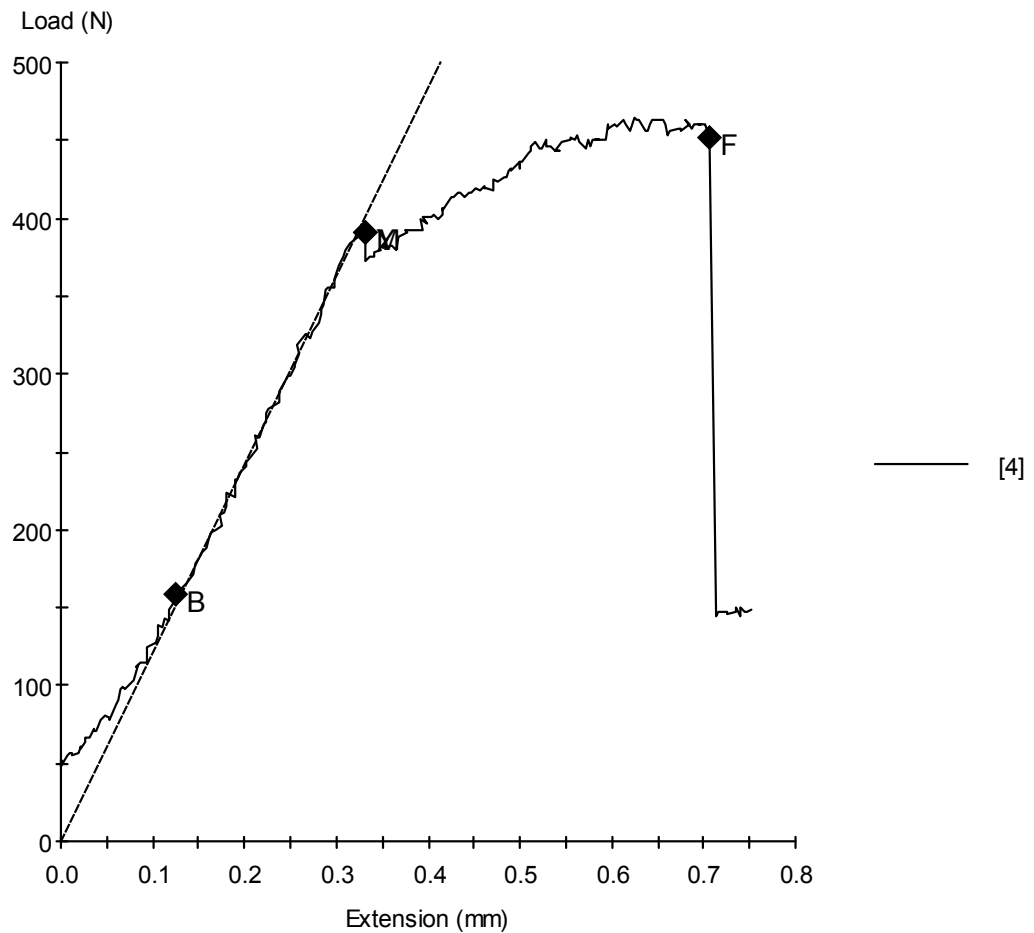
Sample ID: mustapha-30%-3.mss  
Specimen Number: 3  
Tagged: False

**Specimen Results:**

Name	Value	Units
Thickness	50.000	mm
Width	25.000	mm
Area	1250	mm <sup>2</sup>
Peak Load	483	N
Peak Stress	0.39	MPa
Break Load	335	N
Break Stress	0.27	MPa
Elongation At Break	0.668	mm
Stress At Offset Yield	0.379	MPa
Load At Offset Yield	473.342	N

12/05/2009

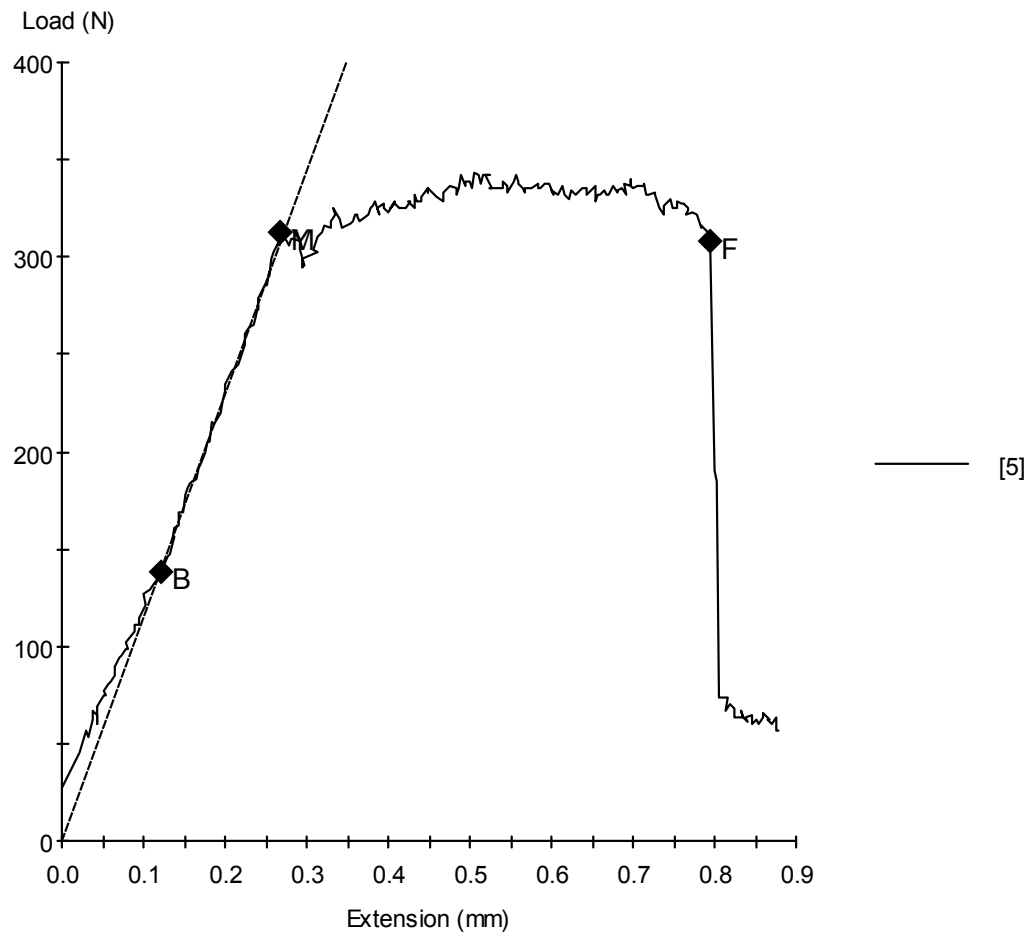
Sample ID: mustapha-30%-4.mss  
Specimen Number: 4  
Tagged: False

**Specimen Results:**

Name	Value	Units
Thickness	50.000	mm
Width	25.000	mm
Area	1250	mm <sup>2</sup>
Peak Load	465	N
Peak Stress	0.37	MPa
Break Load	452	N
Break Stress	0.36	MPa
Elongation At Break	0.706	mm
Stress At Offset Yield	0.333	MPa
Load At Offset Yield	416.272	N

12/05/2009

Sample ID: mustapha-30%-5.mss  
Specimen Number: 5  
Tagged: False

**Specimen Results:**

Name	Value	Units
Thickness	50.000	mm
Width	25.000	mm
Area	1250	mm <sup>2</sup>
Peak Load	343	N
Peak Stress	0.27	MPa
Break Load	308	N
Break Stress	0.25	MPa
Elongation At Break	0.795	mm
Stress At Offset Yield	0.258	MPa
Load At Offset Yield	322.275	N

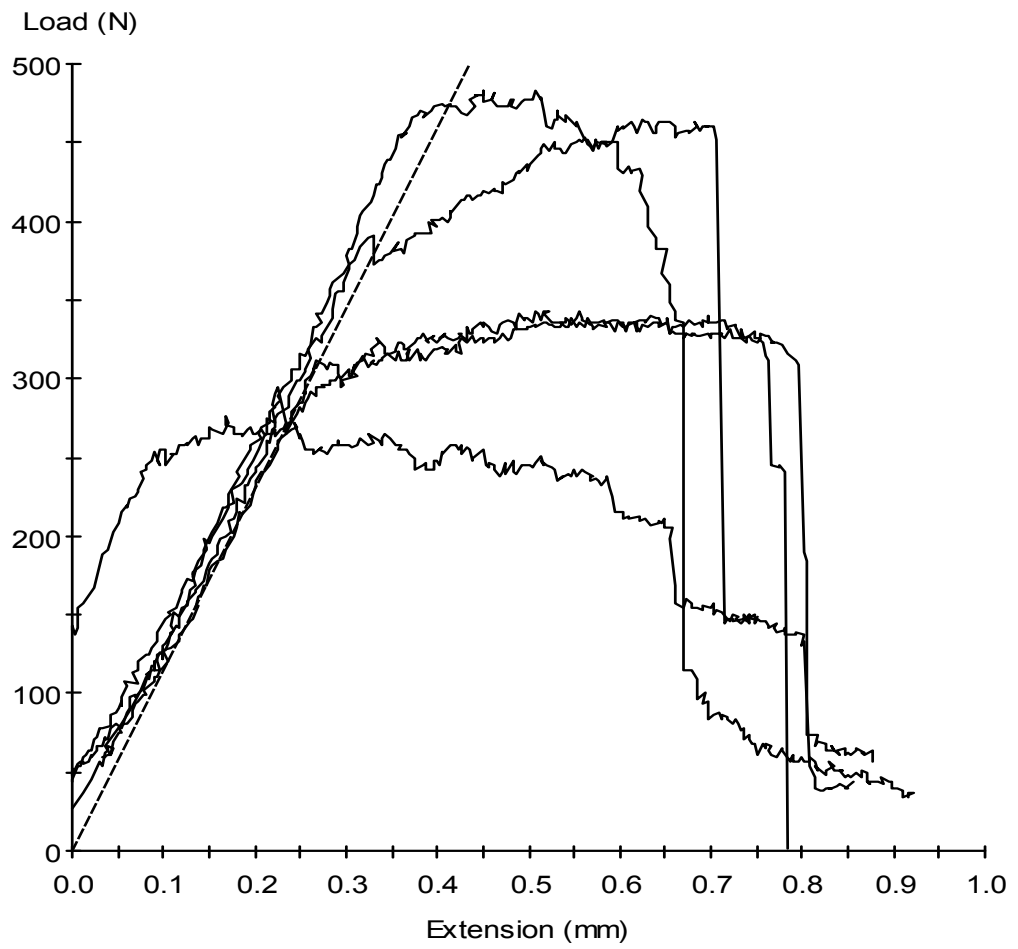
Test Date : 12/05/2009

Method : MMT fracture toughness Test .msm

**Specimen Results:**

Specimen #	Thickness mm	Width mm	Area mm <sup>2</sup>	Peak Load N	Peak Stress MPa	Break Load N	Break Stress MPa
1	50.000	25.000	1250	340	0.27	312	0.25
2	50.000	25.000	1250	276	0.22	205	0.16
3	50.000	25.000	1250	483	0.39	335	0.27
4	50.000	25.000	1250	465	0.37	452	0.36
5	50.000	25.000	1250	343	0.27	308	0.25
<b>Mean</b>	<b>50.000</b>	<b>25.000</b>	<b>1250</b>	<b>381</b>	<b>0.31</b>	<b>322</b>	<b>0.26</b>
<b>Std Dev</b>	<b>0.000</b>	<b>0.000</b>	<b>0</b>	<b>89</b>	<b>0.07</b>	<b>88</b>	<b>0.07</b>

Specimen #	Elongation At Break mm	Stress At Offset Yield MPa	Load At Offset Yield N				
1	0.763	0.252	315.561				
2	0.658	****	****				
3	0.668	0.379	473.342				
4	0.706	0.333	416.272				
5	0.795	0.258	322.275				
<b>Mean</b>	<b>0.718</b>	<b>0.305</b>	<b>381.863</b>				
<b>Std Dev</b>	<b>0.060</b>	<b>0.061</b>	<b>76.374</b>				

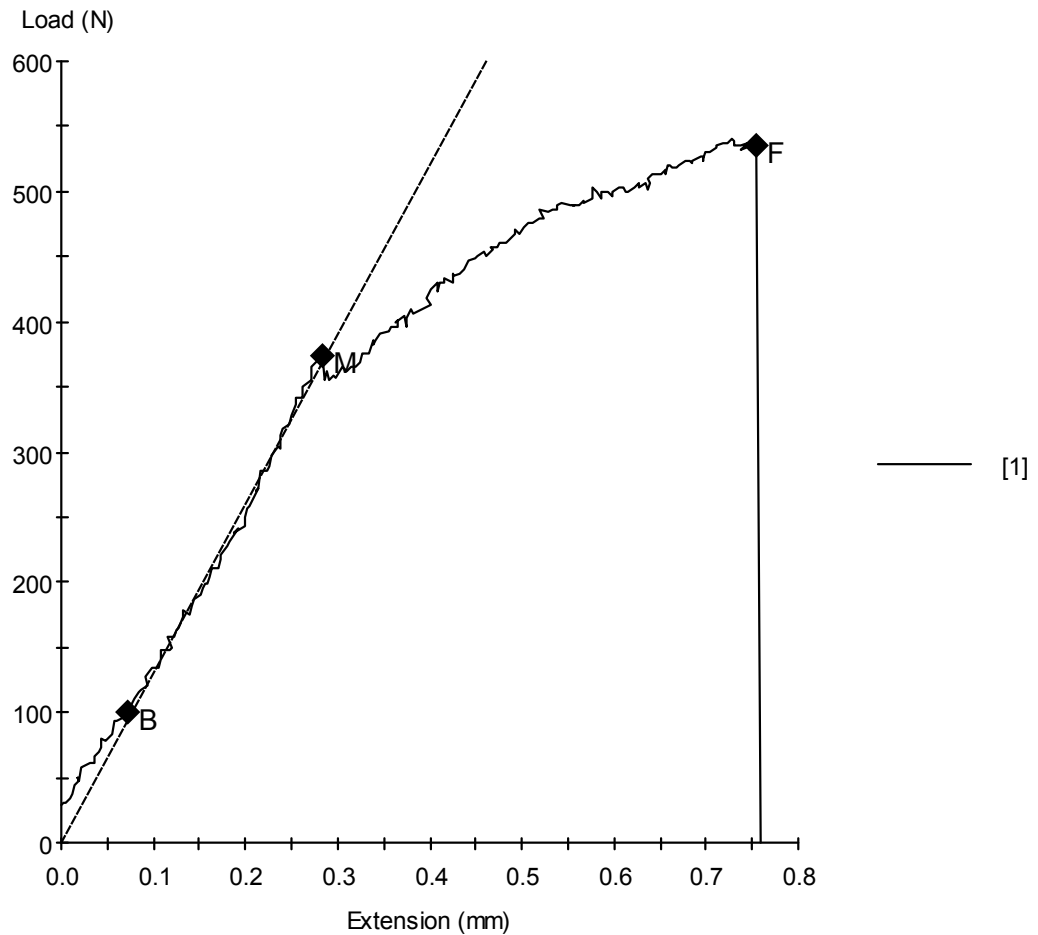


# MTS 810 Testing System Data

## **35% by Weight of Filler**

12/05/2009

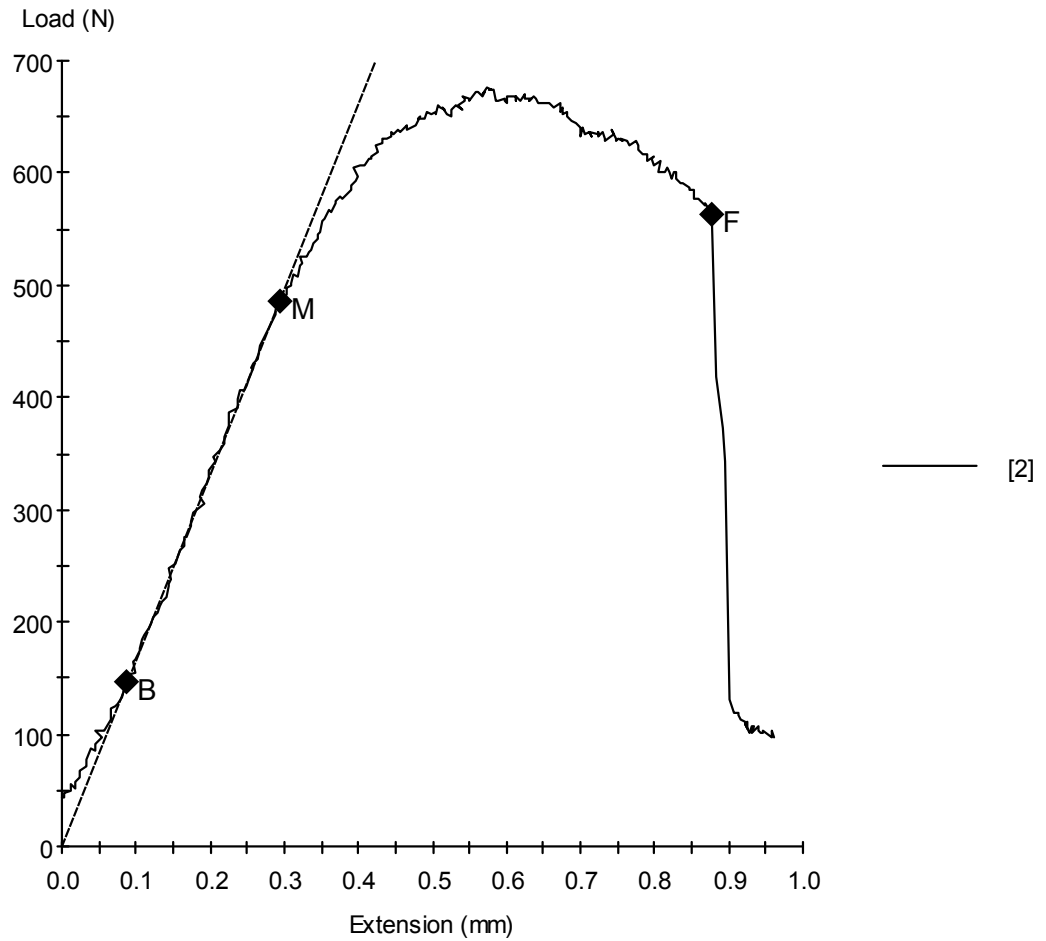
Sample ID: mustapha-35%-1.mss  
Specimen Number: 1  
Tagged: False

**Specimen Results:**

Name	Value	Units
Thickness	50.000	mm
Width	25.000	mm
Area	1250	mm <sup>2</sup>
Peak Load	540	N
Peak Stress	0.43	MPa
Break Load	535	N
Break Stress	0.43	MPa
Elongation At Break	0.753	mm
Stress At Offset Yield	0.359	MPa
Load At Offset Yield	448.332	N

12/05/2009

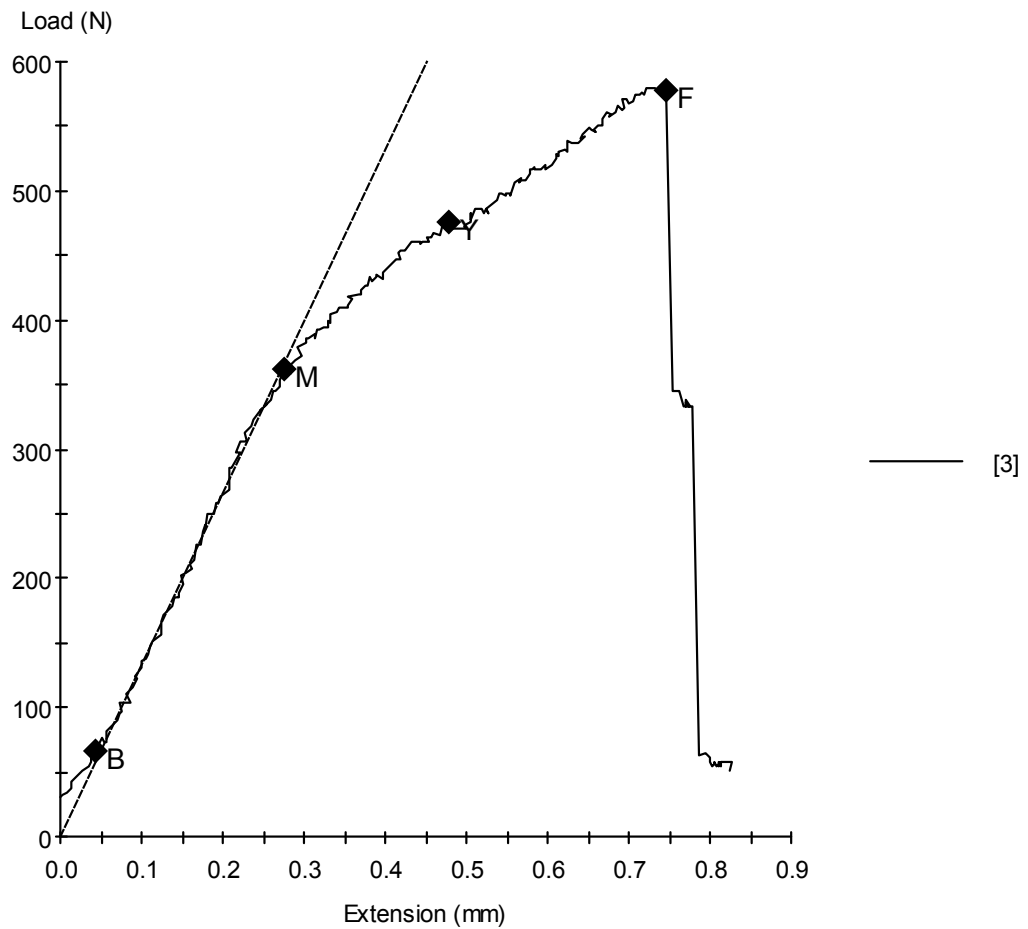
Sample ID: mustapha-35%-2.mss  
Specimen Number: 2  
Tagged: False

**Specimen Results:**

Name	Value	Units
Thickness	50.000	mm
Width	25.000	mm
Area	1250	mm <sup>2</sup>
Peak Load	675	N
Peak Stress	0.54	MPa
Break Load	564	N
Break Stress	0.45	MPa
Elongation At Break	0.878	mm
Stress At Offset Yield	0.522	MPa
Load At Offset Yield	653.111	N

12/05/2009

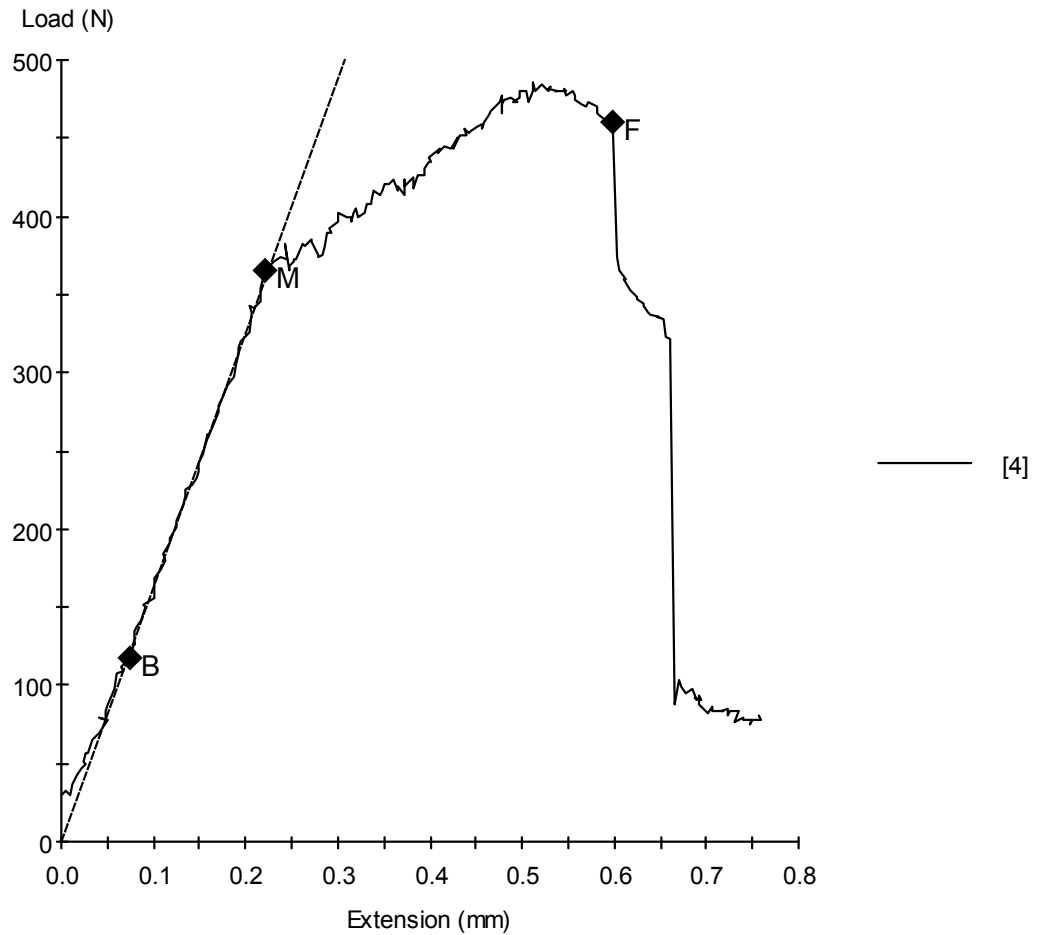
Sample ID: mustapha-35%-3.mss  
Specimen Number: 3  
Tagged: False

**Specimen Results:**

Name	Value	Units
Thickness	50.000	mm
Width	25.000	mm
Area	1250	mm <sup>2</sup>
Peak Load	579	N
Peak Stress	0.46	MPa
Break Load	578	N
Break Stress	0.46	MPa
Elongation At Break	0.745	mm
Stress At Offset Yield	0.368	MPa
Load At Offset Yield	459.914	N

12/05/2009

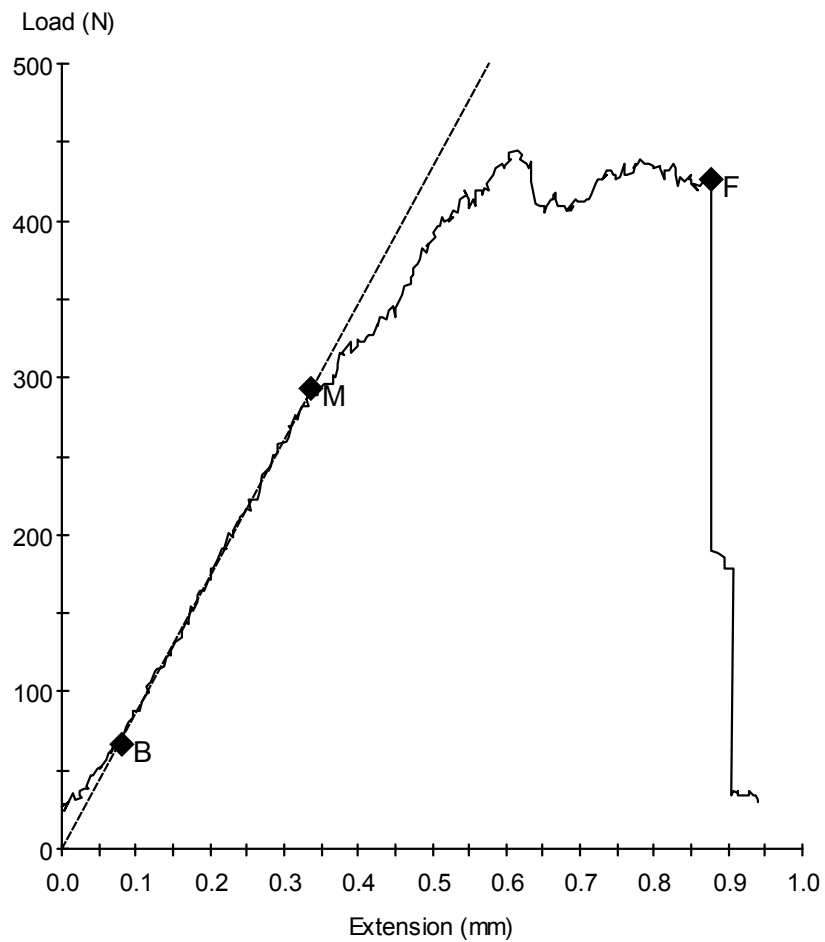
Sample ID: mustapha-35%-4.mss  
Specimen Number: 4  
Tagged: False

**Specimen Results:**

Name	Value	Units
Thickness	50.000	mm
Width	25.000	mm
Area	1250	mm <sup>2</sup>
Peak Load	485	N
Peak Stress	0.39	MPa
Break Load	460	N
Break Stress	0.37	MPa
Elongation At Break	0.597	mm
Stress At Offset Yield	0.334	MPa
Load At Offset Yield	416.944	N

12/05/2009

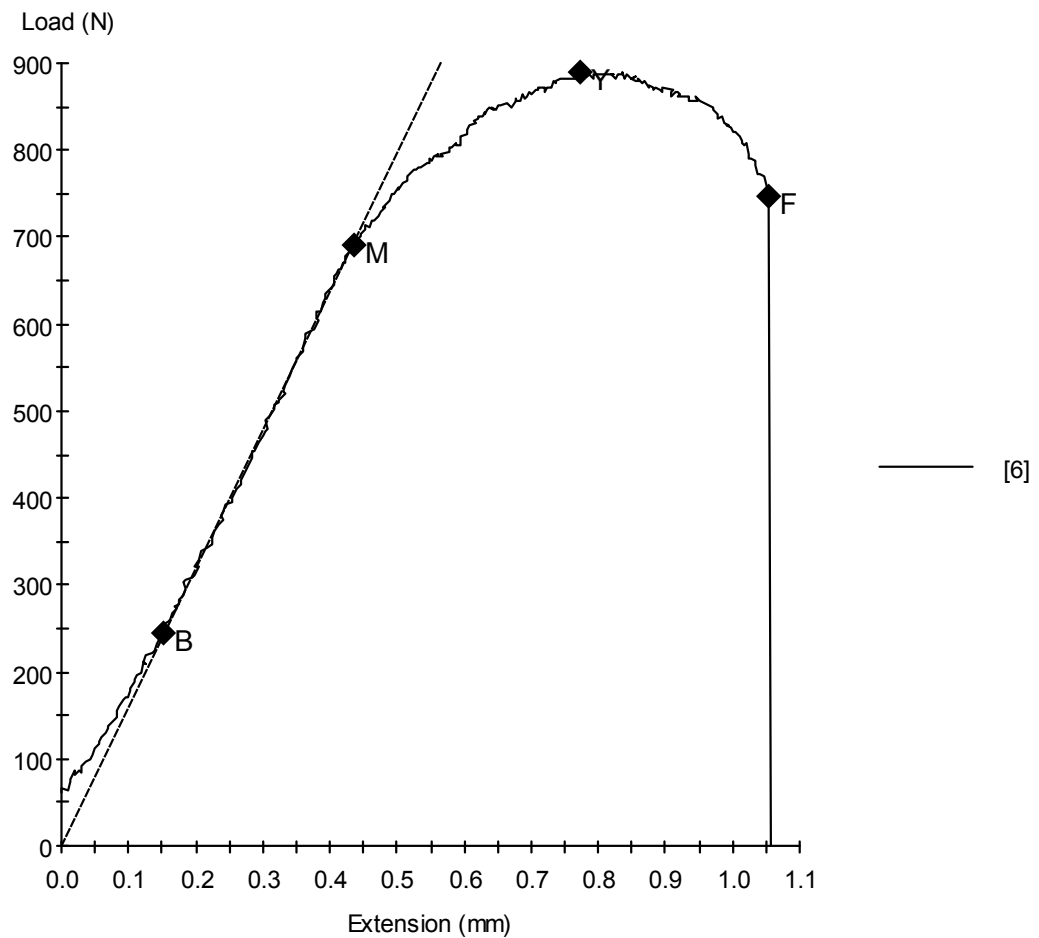
Sample ID: mustapha-35%-5.mss  
Specimen Number: 5  
Tagged: False

**Specimen Results:**

Name	Value	Units
Thickness	50.000	mm
Width	25.000	mm
Area	1250	mm <sup>2</sup>
Peak Load	445	N
Peak Stress	0.36	MPa
Break Load	426	N
Break Stress	0.34	MPa
Elongation At Break	0.876	mm
Stress At Offset Yield	0.351	MPa
Load At Offset Yield	438.932	N

12/05/2009

Sample ID: mustapha-35%-6.mss  
Specimen Number: 6  
Tagged: False

**Specimen Results:**

Name	Value	Units
Thickness	50.000	mm
Width	25.000	mm
Area	1250	mm <sup>2</sup>
Peak Load	891	N
Peak Stress	0.71	MPa
Break Load	747	N
Break Stress	0.60	MPa
Elongation At Break	1.054	mm
Stress At Offset Yield	0.671	MPa
Load At Offset Yield	838.588	N

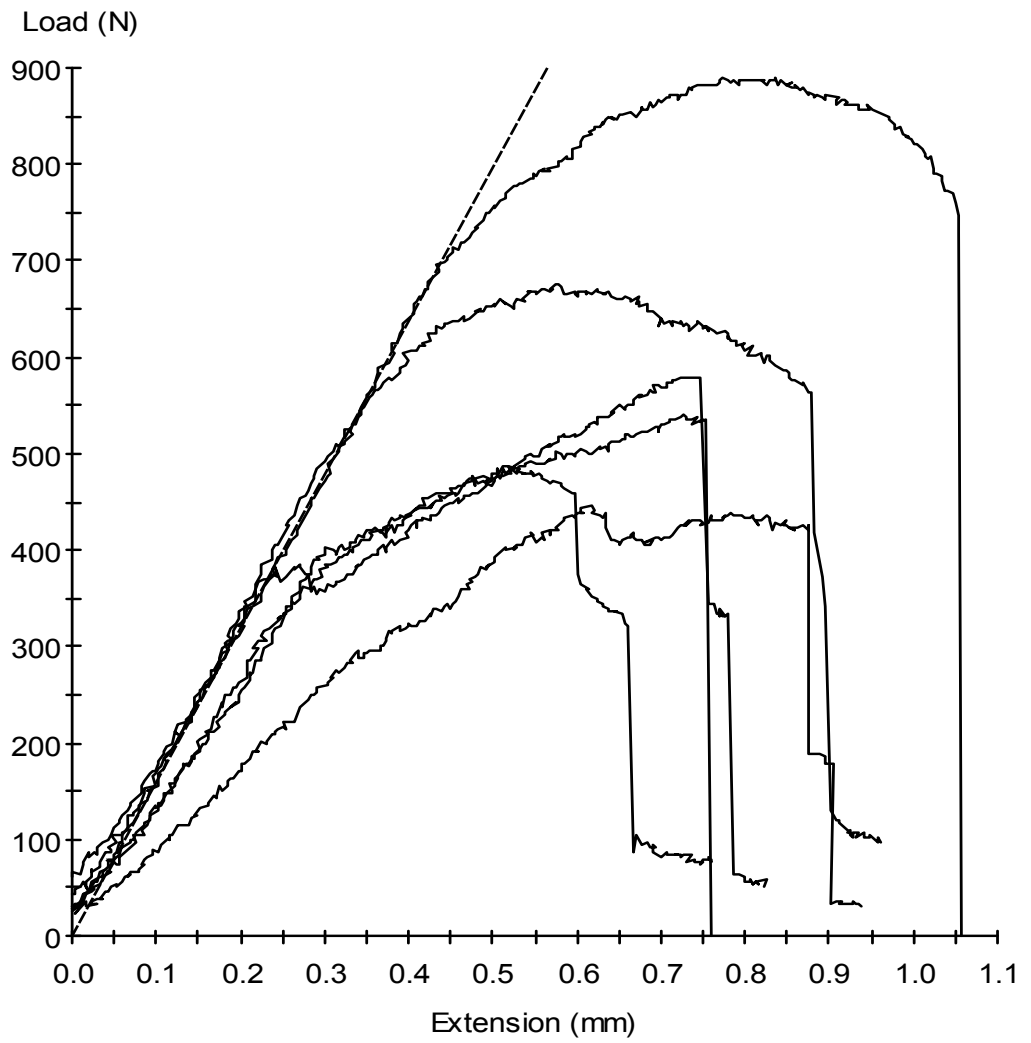
Test Date : 12/05/2009

Method : MMT fracture toughness Test .msm

**Specimen Results:**

Specimen #	Thickness mm	Width mm	Area mm <sup>2</sup>	Peak Load N	Peak Stress MPa	Break Load N	Break Stress MPa
1	50.000	25.000	1250	540	0.43	535	0.43
2	50.000	25.000	1250	675	0.54	564	0.45
3	50.000	25.000	1250	579	0.46	578	0.46
4	50.000	25.000	1250	485	0.39	460	0.37
5	50.000	25.000	1250	445	0.36	426	0.34
6	50.000	25.000	1250	891	0.71	747	0.60
<b>Mean</b>	<b>50.000</b>	<b>25.000</b>	<b>1250</b>	<b>603</b>	<b>0.48</b>	<b>552</b>	<b>0.44</b>
<b>Std Dev</b>	<b>0.000</b>	<b>0.000</b>	<b>0</b>	<b>162</b>	<b>0.13</b>	<b>113</b>	<b>0.09</b>

Specimen #	Elongation At Break mm	Stress At Offset Yield MPa	Load At Offset Yield N				
1	0.753	0.359	448.332				
2	0.878	0.522	653.111				
3	0.745	0.368	459.914				
4	0.597	0.334	416.944				
5	0.876	0.351	438.932				
6	1.054	0.671	838.588				
<b>Mean</b>	<b>0.817</b>	<b>0.434</b>	<b>542.637</b>				
<b>Std Dev</b>	<b>0.156</b>	<b>0.135</b>	<b>168.571</b>				

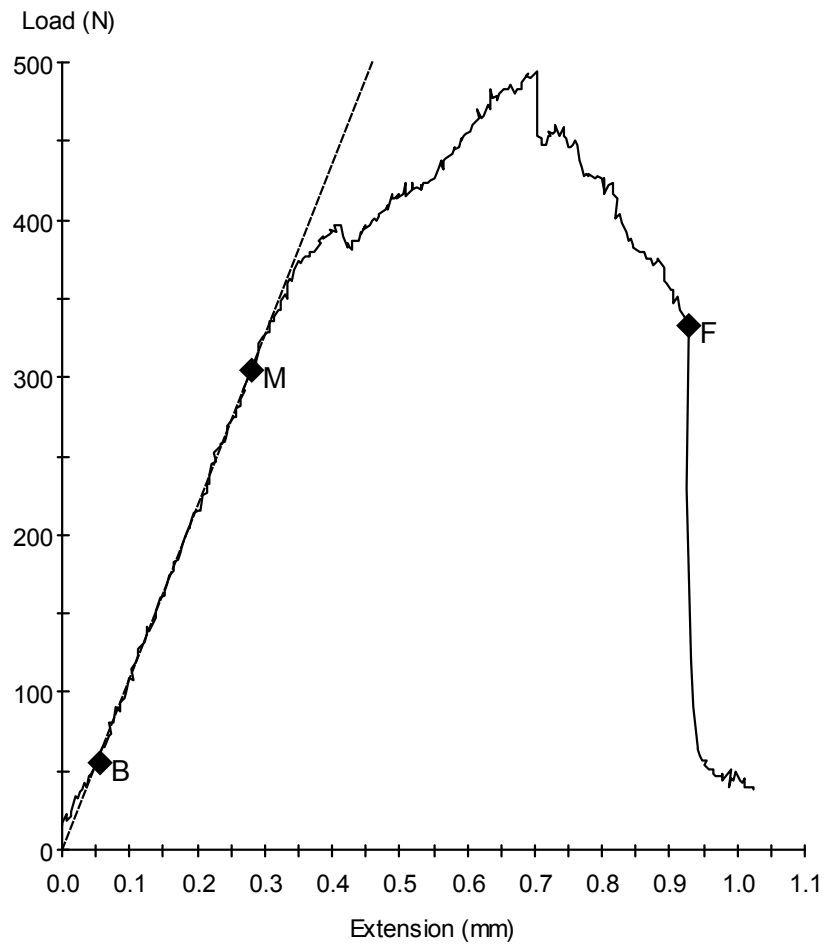


# MTS 810 Testing System Data

## **40% by Weight of Filler**

28/05/2009

Sample ID: mustapha-40%-1.mss  
Specimen Number: 1  
Tagged: False

**Specimen Results:**

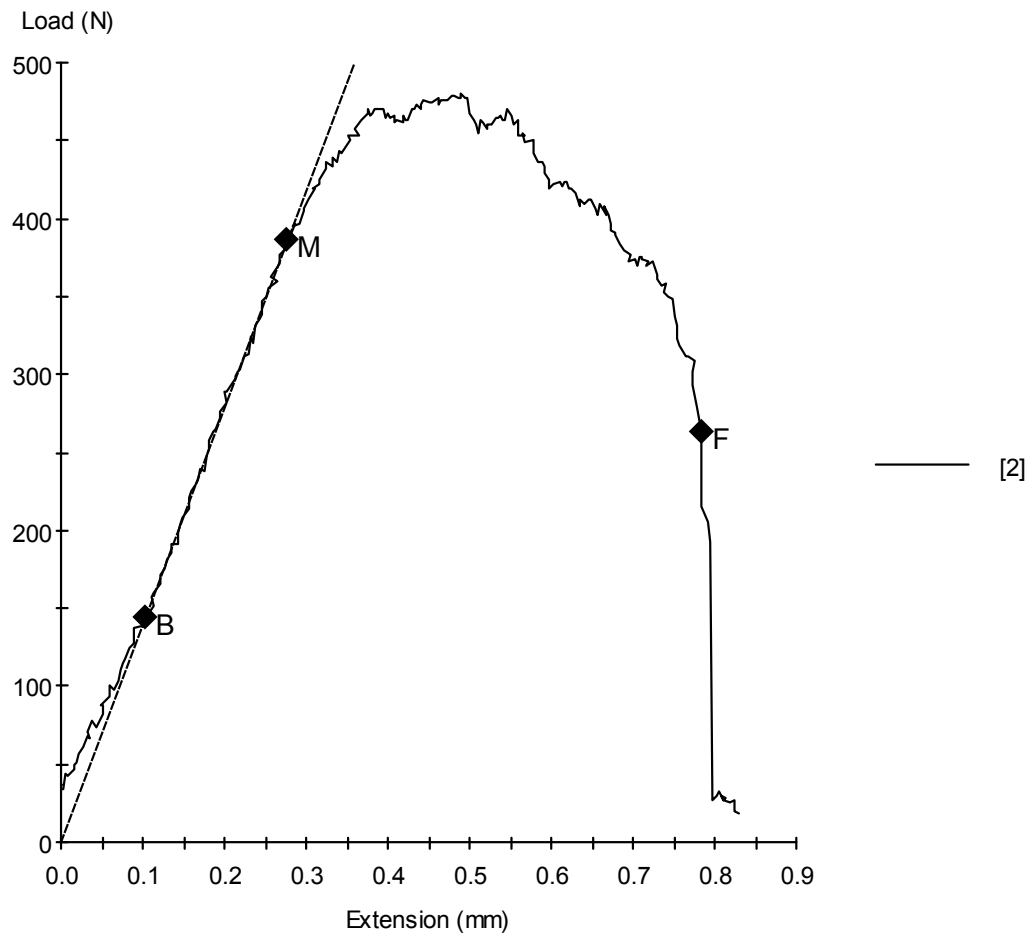
Name	Value	Units
Thickness	50.000	mm
Width	26.000	mm
Area	1300	mm <sup>2</sup>
Peak Load	494	N
Peak Stress	0.38	MPa
Break Load	332	N
Break Stress	0.26	MPa
Elongation At Break	0.927	mm
Stress At Offset Yield	0.313	MPa
Load At Offset Yield	406.873	N

28/05/2009

Sample ID: mustapha-40%-2.mss

Specimen Number: 2

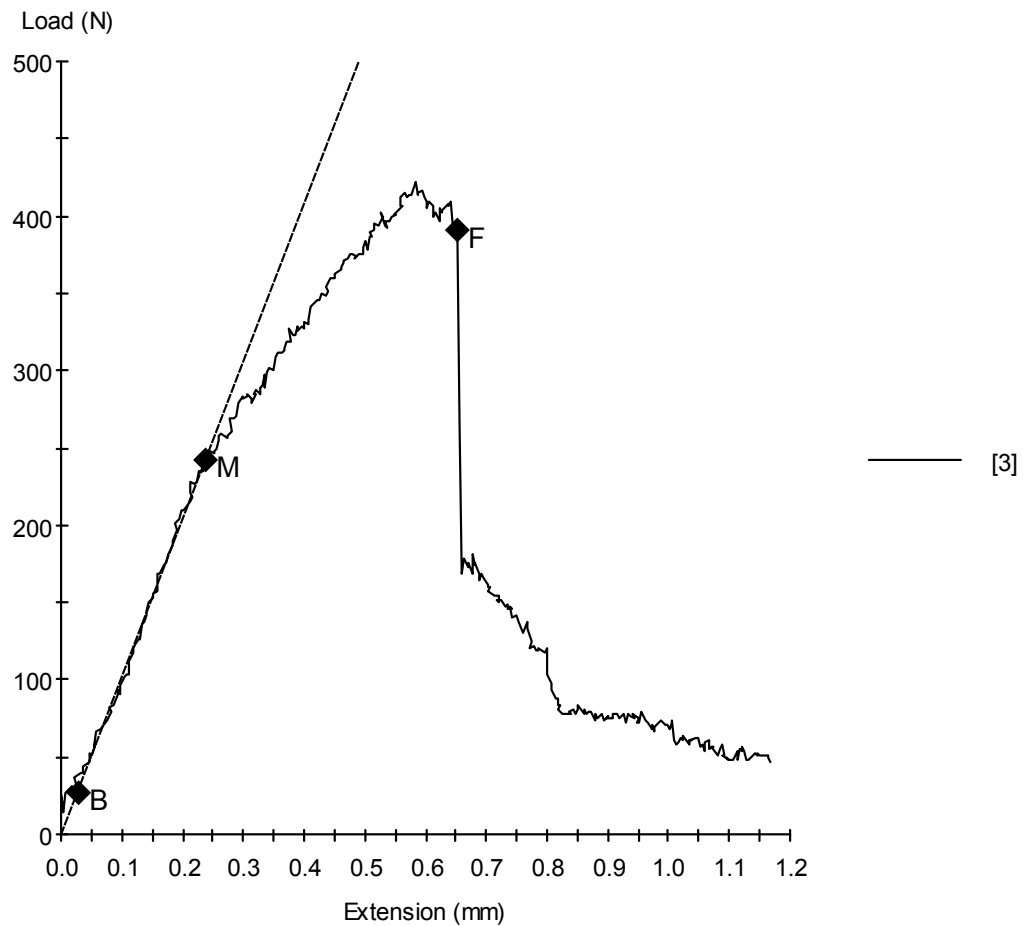
Tagged: False

**Specimen Results:**

Name	Value	Units
Thickness	50.000	mm
Width	26.000	mm
Area	1300	mm <sup>2</sup>
Peak Load	480	N
Peak Stress	0.37	MPa
Break Load	264	N
Break Stress	0.20	MPa
Elongation At Break	0.784	mm
Stress At Offset Yield	0.362	MPa
Load At Offset Yield	469.985	N

28/05/2009

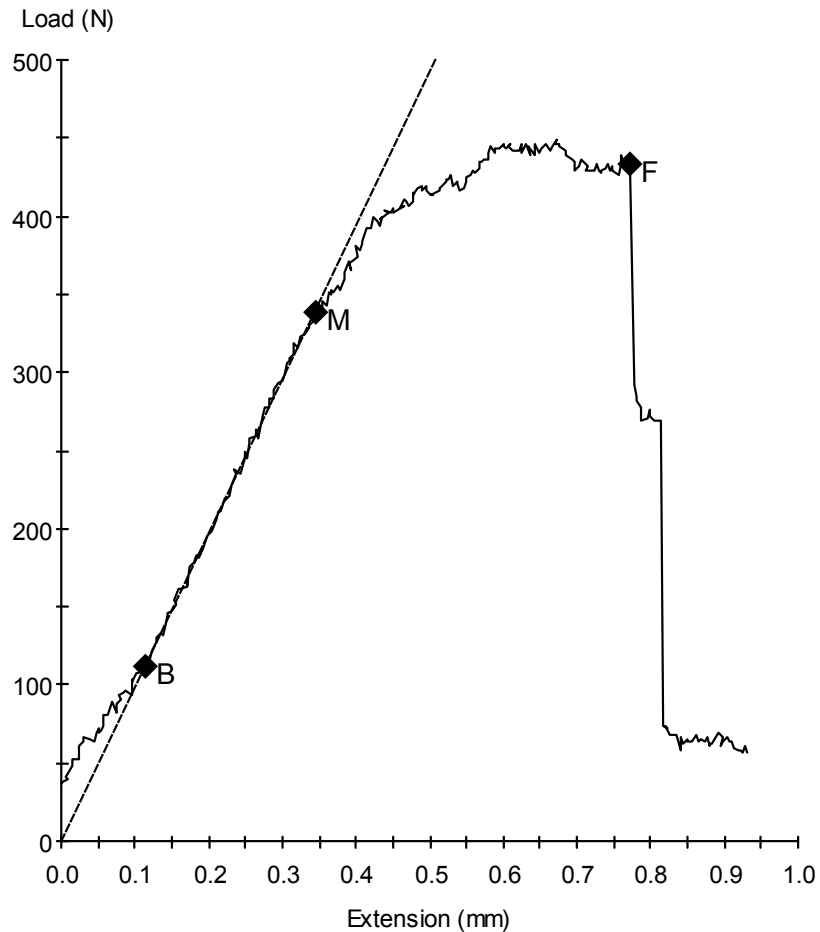
Sample ID: mustapha-40%-3.mss  
Specimen Number: 3  
Tagged: False

**Specimen Results:**

Name	Value	Units
Thickness	50.000	mm
Width	26.000	mm
Area	1300	mm <sup>2</sup>
Peak Load	422	N
Peak Stress	0.32	MPa
Break Load	391	N
Break Stress	0.30	MPa
Elongation At Break	0.652	mm
Stress At Offset Yield	0.281	MPa
Load At Offset Yield	365.917	N

28/05/2009

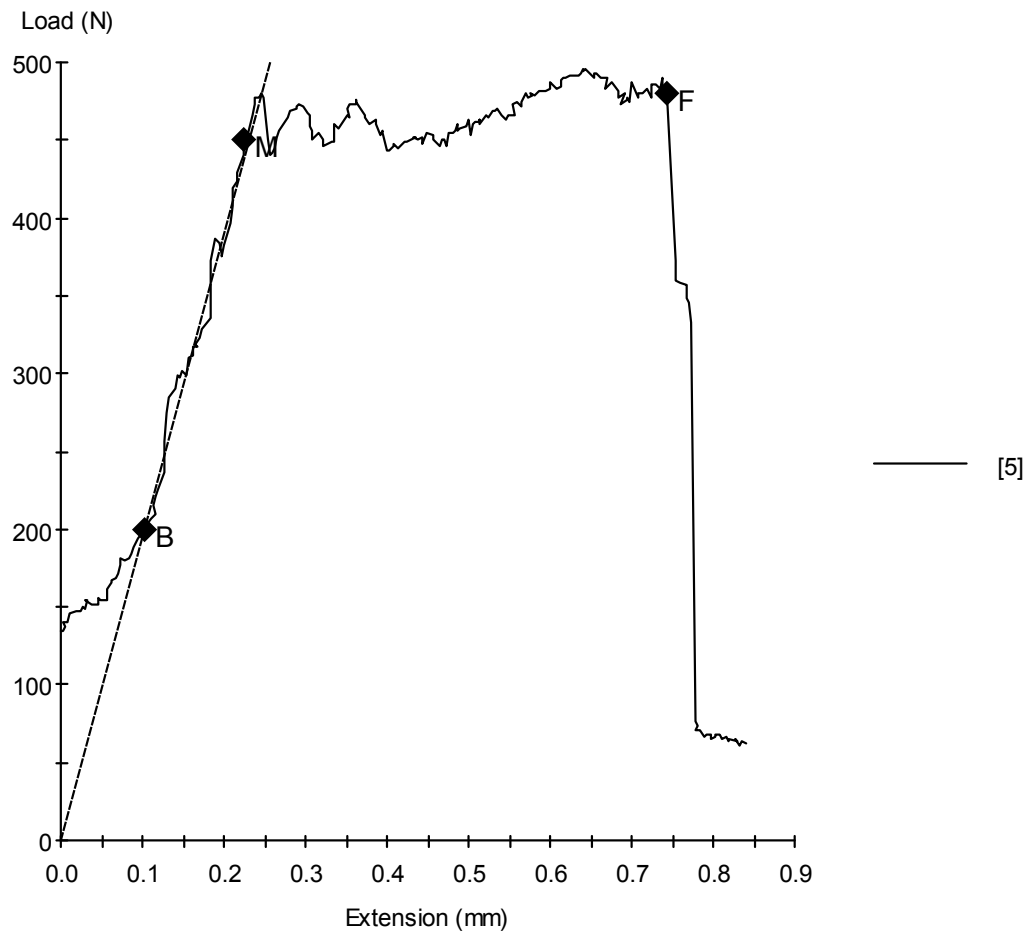
Sample ID: mustapha-40%-4.mss  
Specimen Number: 4  
Tagged: False

**Specimen Results:**

Name	Value	Units
Thickness	50.000	mm
Width	26.000	mm
Area	1300	mm <sup>2</sup>
Peak Load	449	N
Peak Stress	0.35	MPa
Break Load	433	N
Break Stress	0.33	MPa
Elongation At Break	0.771	mm
Stress At Offset Yield	0.323	MPa
Load At Offset Yield	419.630	N

28/05/2009

Sample ID: mustapha-40%-5.mss  
Specimen Number: 5  
Tagged: False

**Specimen Results:**

Name	Value	Units
Thickness	50.000	mm
Width	26.000	mm
Area	1300	mm <sup>2</sup>
Peak Load	495	N
Peak Stress	0.38	MPa
Break Load	480	N
Break Stress	0.37	MPa
Elongation At Break	0.744	mm
Stress At Offset Yield	0.345	MPa
Load At Offset Yield	448.500	N

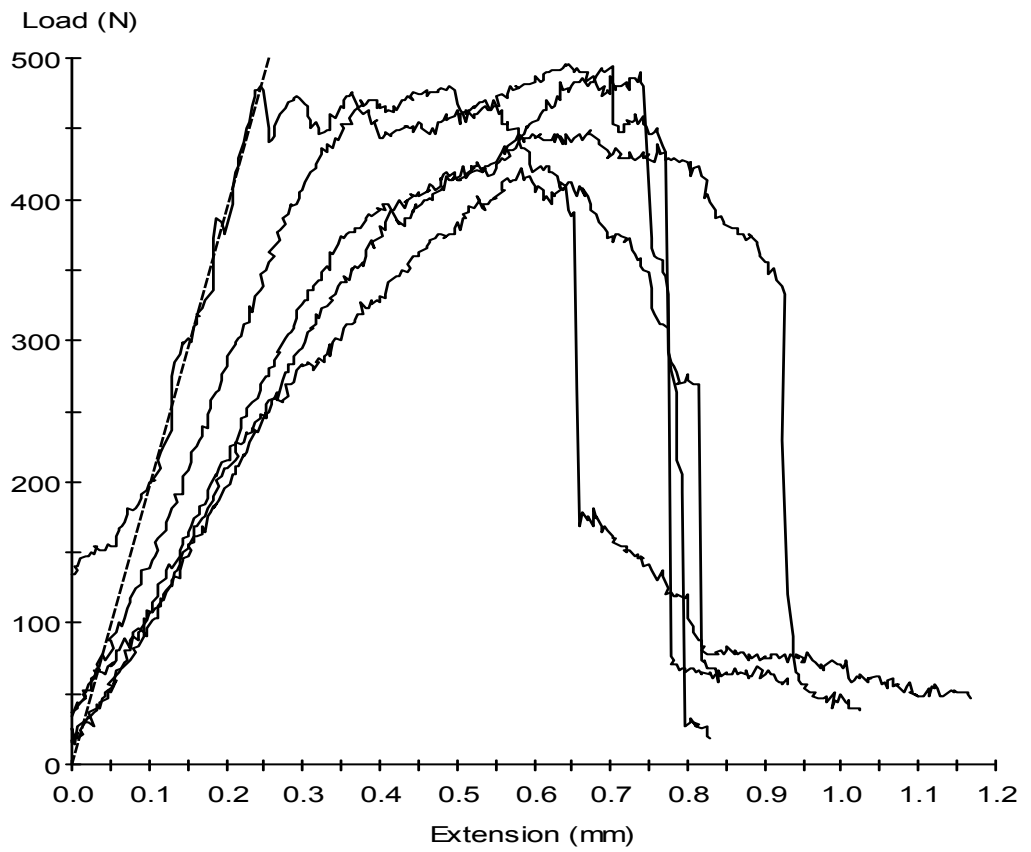
Test Date : 28/05/2009

Method : MMT fracture toughness Test .msm

**Specimen Results:**

Specimen #	Thickness mm	Width mm	Area mm <sup>2</sup>	Peak Load N	Peak Stress MPa	Break Load N	Break Stress MPa
1	50.000	26.000	1300	494	0.38	332	0.26
2	50.000	26.000	1300	480	0.37	264	0.20
3	50.000	26.000	1300	422	0.32	391	0.30
4	50.000	26.000	1300	449	0.35	433	0.33
5	50.000	26.000	1300	495	0.38	480	0.37
<b>Mean</b>	<b>50.000</b>	<b>26.000</b>	<b>1300</b>	<b>468</b>	<b>0.36</b>	<b>380</b>	<b>0.29</b>
<b>Std Dev</b>	<b>0.000</b>	<b>0.000</b>	<b>0</b>	<b>32</b>	<b>0.02</b>	<b>85</b>	<b>0.07</b>

Specimen #	Elongation At Break mm	Stress At Offset Yield MPa	Load At Offset Yield N				
1	0.927	0.313	406.873				
2	0.784	0.362	469.985				
3	0.652	0.281	365.917				
4	0.771	0.323	419.630				
5	0.744	0.345	448.500				
<b>Mean</b>	<b>0.776</b>	<b>0.325</b>	<b>422.181</b>				
<b>Std Dev</b>	<b>0.099</b>	<b>0.031</b>	<b>39.951</b>				



## Appendix G – LCR Loss Tangent Measurements

All the measured electrical properties of the composites are listed in this appendix.

The LCR meter used to obtain the measurements showed huge fluctuation in the reading at 120 Hz. Therefore, 4 reading were taken for the dissipation factor “D” and then the average value of these reading was presented in the result section. The variations in the reading indicate that the electrical properties measured at 120 Hz are not very accurate.

**Note that the dissipation factor “D” is equal to the loss tangent or  $\tan \delta$**

The electrical properties measured are:

- Impedance “Z”
- Admittance “Y”
- Phase angle “ $\theta$ ”
- Resistance “R”
- Equivalent series inductance “Ls”
- Equivalent parallel inductance “Lp”
- Equivalent series capacitance “Cs”
- Equivalent parallel capacitance “Cp”
- **dissipation factor “D”**
- Conductance “G”
- Reactance “X”
- Susceptance “B”

**5% by weight of VE/CACO<sub>3</sub> (Ambient cured)**

Meas/Freq	100 Hz	120 Hz	1 kHz	10 kHz	20 kHz	100 kHz
<b>Z/θ</b>	+29.97 MΩ -88.88°	+25.5 MΩ -88.5°	+3.0243 MΩ -89.69°	+304.29 kΩ -89.67°	+ 152.48 kΩ -89.61°	+30.726 kΩ -89.53°
<b>Y/θ</b>	+0.0334 μS -88.88°	+0.0390 μS +88.5°	+0.3307 μS +89.69°	+3.2864 μS +89.67°	+6.5583 μS +89.61°	+32.546 μS +89.53°
<b>R/X</b>	+575.0 kΩ -29.97 MΩ	+478.0 kΩ -25.8 MΩ	+16.399 kΩ -3.024 MΩ	+1.7530 kΩ -304.28 kΩ	+1.0319 kΩ -152.48 kΩ	+252.30 kΩ -30.724 kΩ
<b>G/B</b>	+0.0006 μS +0.0333 μS	+0.0003 μS +0.0387 μS	+0.0018 μS +0.3306 μS	+0.0189 μS +3.2864 μS	+0.0444 μS +6.5581 μS	+0.2670 μS +32.546 μS
<b>Cp/D</b>	+0.0531 nF +0.0190	+0.0522 nF +0.0233	+52.62 pF +0.0054	+52.305 pF +0.0058	+52.186 pF +0.0068	+51.80 pF +0.0082
<b>Cs/D</b>	+0.0531 nF +0.0192	+0.0526 nF +0.0107	+52.62 pF +0.0054	+52.305 pF +0.0058	+52.191 pF +0.0068	+51.80 pF +0.0082
<b>Lp/D</b>	-47.72 kH +0.0190	-34.557 kH +0.0101	-481.32 H +0.0054	-4.8428 H +0.0058	-1.2134 H +0.0068	-48.902 mH +0.0082
<b>Ls/D</b>	-47.68 kH +0.0190	-34.184 kH +0.0102	-48.344 H +0.0054	-4.8427 H +0.0058	-1.2134 H +0.0068	-48.899 mH +0.0082

**5% by weight of VE/CACO<sub>3</sub> (Ambient cured Plus Oven Post-cured)**

Meas/Freq	100 Hz	120 Hz	1 kHz	10 kHz	20 kHz	100 kHz
<b>Z/θ</b>	+27.471 MΩ -89.10°	+20.9 MΩ -93.72°	+2.7629 MΩ -89.77°	+277.56 kΩ -89.71°	+139.05 kΩ -89.63°	+28.018 kΩ -89.50°
<b>Y/θ</b>	+0.0364 μS +89.12°	+0.0480 μS +93.49°	+0.3619 μS +89.77°	+3.6028 μS +89.71°	+7.1916 μS +89.71°	+35.691 μS +89.50°
<b>R/X</b>	+434.19 kΩ -27.478 MΩ	-1.0415 MΩ -20.821 MΩ	+10.905 kΩ -2.7628 MΩ	+1.404 kΩ -277.56 kΩ	+890.72 Ω -139.04 kΩ	+246.37 Ω -28.017 kΩ
<b>G/B</b>	+0.0006 μS +0.0364 μS	-0.0029 μS +0.0475 μS	+0.0014 μS +0.3619 μS	+0.0183 μS +3.6027 μS	+0.0461 μS +7.1916 μS	+0.3139 μS +35.69 μS
<b>Cp/D</b>	+0.0579 nF +0.0157	+0.0629 nF -0.0122	+57.60 pF +0.0040	+57.339 pF +0.0051	+57.229 pF +0.0064	+56.80 pF +0.0088
<b>Cs/D</b>	+0.0579 nF +0.0151	+0.0635 nF -0.0110	+57.60 pF +0.0040	+57.340 pF +0.0051	+57.229 pF +0.0064	+56.81 pF +0.0088
<b>Lp/D</b>	-43.758 kH +0.0153	-28.23 kH -0.0121	-439.74 H +0.0040	-4.4177 H +0.0051	-1.1065 H +0.0064	-44.594 mH +0.0088
<b>Ls/D</b>	-43.751 kH +0.0151	-28.188 kH -0.0125	-439.72 H +0.0040	-4.4177 H +0.0051	-1.1065 H +0.0064	-44.591 mH +0.0088

**10% by weight of VE/CACO<sub>3</sub> (Ambient cured)**

Meas/Freq	100 Hz	120 Hz	1 kHz	10 kHz	20 kHz	100 kHz
<b>Z/θ</b>	+29.753 MΩ -88.83°	+26.409 MΩ -99.44°	+3.0103 MΩ -89.58°	+303.57 kΩ -89.59°	+152.19 kΩ -89.54°	+30.699 kΩ -89.45°
<b>Y/θ</b>	+0.0336 μS +88.83°	+0.0379 μS +99.04°	+0.3322 μS +89.58°	+3.2941 μS +89.59°	+6.5712 μS +89.54°	+32.574 μS -89.45°
<b>R/X</b>	+609.05 kΩ -29.760 MΩ	-3.98 MΩ -26.252 MΩ	+21.964 kΩ -3.0103 MΩ	+2.1477 kΩ -303.56 kΩ	+1.2130 kΩ -152.18 kΩ	+293.24 Ω -30.097 kΩ
<b>G/B</b>	+0.0007 μS +0.0336 μS	-0.0062 μS +0.0372 μS	+0.0024 μS +0.3322 μS	+0.0232 μS +3.2941 μS	+0.0525 μS +6.5707 μS	+0.3113 μS +32.573 μS
<b>Cp/D</b>	+0.0535 nF +0.0197	+0.0492 nF -0.1652	+52.87 pF +0.0072	+52.428 pF +0.0071	+57.288 pF +0.0080	+51.84 pF +0.0096
<b>Cs/D</b>	+0.0535 nF +0.0198	+0.0515 nF -0.1690	+52.88 pF +0.0072	+52.430 pF +0.0071	+52.291 pF +0.0080	+51.85 pF +0.0096
<b>Lp/D</b>	-47.354 kH +0.0197	-36.735 kH -0.1505	-479.09 H +0.0073	-4.8315 H +0.0071	-1.2111 H +0.0080	-48.860 mH +0.0096
<b>Ls/D</b>	-47.351 kH +0.0198	-34.662 kH -0.1621	-479.06 H +0.0072	-4.8313 H +0.0071	-1.2110 H +0.0080	-48.855 mH +0.0096

**10% by weight of VE/CACO<sub>3</sub> (Ambient cured Plus Oven Post-cured)**

Meas/Freq	100 Hz	120 Hz	1 kHz	10 kHz	20 kHz	100 kHz
<b>Z/θ</b>	+27.958 MΩ -89.16°	+25.986 MΩ -84.48°	+2.8116 MΩ -89.77°	+282.39 kΩ -89.73°	+141.44 kΩ -89.67°	+28.474 kΩ -89.55°
<b>Y/θ</b>	+0.0358 μS +89.14°	+0.0384 μS +84.48°	+0.3557 μS +89.77°	+3.5412 μS +89.73°	+7.0705 μS +89.66°	+35.119 μS -89.55°
<b>R/X</b>	+421.55 kΩ -27.946 MΩ	+2.5422 MΩ -25.437 MΩ	+11.133 kΩ -2.8115 MΩ	+1.3250 kΩ -282.38 kΩ	+819.33 Ω -141.44 kΩ	+222.71 Ω -28.473 kΩ
<b>G/B</b>	+0.0005 μS +0.0358 μS	+0.0040 μS +0.0388 μS	+0.0014 μS +0.3557 μS	+0.0166 μS +3.5412 μS	+0.0415 μS +7.0703 μS	+0.2746 μS +35.188 μS
<b>Cp/D</b>	+0.0569 nF +0.0148	+0.0513 nF +0.0122	+56.61 pF +0.0040	+56.361 pF +0.0047	+56.263 pF +0.0058	+55.898 pF +0.0078
<b>Cs/D</b>	+0.0570 nF +0.0148	+0.0522 nF +0.0125	+56.61 pF +0.0040	+56.362 pF +0.0047	+56.266 pF +0.0058	+55.90 pF +0.0078
<b>Lp/D</b>	-44.498 kH +0.0147	-34.291 kH +0.0126	-447.47 H +0.0040	-4.4943 H +0.0047	-1.1255 H +0.0058	-45.319 mH +0.0078
<b>Ls/D</b>	-44.481 kH +0.0147	-34.099 kH +0.0124	-447.45 H +0.0040	-4.4942 H +0.0047	-1.1255 H +0.0058	-45.317 mH +0.0078

**15% by weight of VE/CACO<sub>3</sub> (Ambient cured)**

Meas/Freq	100 Hz	120 Hz	1 kHz	10 kHz	20 kHz	100 kHz
<b>Z/θ</b>	+26.420 MΩ -88.91°	+22.729 MΩ -82.95°	+2.6766 MΩ -89.50°	+270.69 kΩ -89.51°	+135.82 kΩ -89.48°	+27.423 kΩ -89.43°
<b>Y/θ</b>	+0.0379 μS +88.91°	+0.0441 μS +82.94°	+0.3736 μS +89.50°	+3.6943 μS +89.52°	+7.3627 μS +89.48°	+36.466 μS +89.43°
<b>R/X</b>	+502.82 kΩ -26.409 MΩ	+3.7444 MΩ -22.671MΩ	+23.326 kΩ -2.676 MΩ	+2.2977 kΩ -270.68 kΩ	+1.2285 Ω -135.81 kΩ	+272.75 Ω -27.421 kΩ
<b>G/B</b>	+0.0007 μS +0.0378 μS	+0.0061 μS +0.0443 μS	+0.0032 μS +0.3736 μS	+0.0314 μS +3.6941 μS	+0.0668 μS +7.3624 μS	+0.3632 μS +36.464 μS
<b>Cp/D</b>	+0.0602 nF +0.0187	+0.0591 nF +0.0131	+59.46 pF +0.0087	+58.795 pF +0.0085	+58.590 pF +0.0090	+58.03 pF +0.0100
<b>Cs/D</b>	+0.0602 nF +0.0187	+0.0605 nF +0.0127	+59.47 pF +0.0087	+58.798 pF +0.0085	+58.589 pF +0.0090	+58.04 pF +0.0100
<b>Lp/D</b>	-42.070 kH +0.0187	-30.405 kH +0.0128	-426.01 H +0.0087	-4.3082 H +0.0085	-1.0809 H +0.0090	-43.647 mH +0.0100
<b>Ls/D</b>	-42.040 kH +0.0187	-30.076 kH +0.0130	-425.96 H +0.0087	-4.3080 H +0.0085	-1.0808 H +0.0090	-43.643 mH +0.0100

**15% by weight of VE/CACO<sub>3</sub> (Ambient cured Plus Oven Post-cured)**

Meas/Freq	100 Hz	120 Hz	1 kHz	10 kHz	20 kHz	100 kHz
<b>Z/θ</b>	+30.470 MΩ -88.92°	+27.195 MΩ -81.51°	+3.0741 MΩ -89.71°	+309.12 kΩ -89.69°	+154.87 kΩ -89.63°	+31.198 kΩ -89.53°
<b>Y/θ</b>	+0.0328 μS +88.92°	+0.0367 μS +81.58°	+0.3253 μS +89.71°	+3.2350 μS +89.69°	+6.4570 μS +89.63°	+32.053 μS +89.53°
<b>R/X</b>	+571.46 kΩ -30.484 MΩ	+4.009 MΩ -27.077 MΩ	+15.248 kΩ -3.0741 MΩ	+1.6759 kΩ -309.11 kΩ	+1.0019 kΩ -154.87 kΩ	+258.17 Ω -31.196 kΩ
<b>G/B</b>	+0.0006 μS +0.0328 μS	+0.0056 μS +0.0362 μS	+0.0016 μS +0.3253 μS	+0.0175 μS +3.2350 μS	+0.0420 μS +6.4570 μS	+0.2654 μS +32.053 μS
<b>Cp/D</b>	+0.0522 nF +0.0185	+0.0482 nF +0.0116	+51.77 pF +0.0050	+51.486 pF +0.0054	+51.382 pF +0.0065	+51.02 pF +0.0083
<b>Cs/D</b>	+0.0522 nF +0.0185	+0.0496 nF +0.0115	+51.77 pF +0.0050	+51.488 pF +0.0054	+51.384 pF +0.0065	+51.02 pF +0.0083
<b>Lp/D</b>	-48.520 kH +0.0185	-36.886 kH +0.0118	-489.26 H +0.0050	-4.9198 H +0.0054	-1.2325 H +0.0065	-49.652 mH +0.0083
<b>Ls/D</b>	-48.508 kH +0.0182	-36.544 kH +0.0117	-489.25 H +0.005	-4.9196 H +0.0054	-1.2323 H +0.0065	-49.648 mH +0.0083